ANALYSIS OF SIX-PHASE SYNCHRONOUS MOTOR

Ph.D. THESIS

by

ARIF IQBAL

DEPARTMENT OF ELECTRICAL ENGINEERING
INDIAN INSTITUTE OF TECHNOLOGY ROORKEE
ROORKEE – 247667 (INDIA)

AUGUST, 2015

ANALYSIS OF SIX-PHASE SYNCHRONOUS MOTOR

A THESIS

Submitted in partial fulfilment of the requirements for the award of the degree

of

DOCTOR OF PHILOSOPHY

in

ELECTRICAL ENGINEERING

by

ARIF IQBAL

DEPARTMENT OF ELECTRICAL ENGINEERING
INDIAN INSTITUTE OF TECHNOLOGY ROORKEE
ROORKEE – 247667 (INDIA)

AUGUST, 2015

©INDIAN INSTITUTE OF TECHNOLOGY ROORKEE, ROORKEE-2015
ALL RIGHTS RESERVED

INDIAN INSTITUTE OF TECHNOLOGY ROORKEE
ROORKEE

CANDIDATE'S DECLARATION

I hereby certify that the work which is being presented in this thesis entitled "**ANALYSIS OF SIX-PHASE SYNCHRONOUS MOTOR"** in partial fulfilment of the requirements for the award of *the Degree of Doctor of Philosophy* and submitted in the Department of Electrical Engineering of Indian Institute of Technology Roorkee, Roorkee is an authentic record of my own work carried out during a period from July, 2010 to August, 2015 under the supervision of Dr. G.K. Singh, Professor and Dr. Vinay Pant, Assistant Professor, Department of Electrical Engineering, Indian Institute of Technology Roorkee.

The matter presented in this thesis has not been submitted by me for the award of any other degree of this or any other Institution.

(ARIF IQBAL)

This is to certify that the above statement made by the candidate is correct to the best of our knowledge.

(G.K. Singh)
Supervisor

(Vinay Pant)
Supervisor

Date:

The Ph.D. Viva-Voce Examination of ***Mr. Arif Iqbal***, Research Scholar, has been held on…….

Signature of Supervisors Chairman, SRC Signature of External Examiner

Head of the Department

Acknowledgement

I would like to express my deep gratitude to Dr. G.K. Singh and Dr. Vinay Pant for their excellent guidance, patience, caring, and providing me with a good atmosphere for doing research. Their advice on both research as well as on my career have been priceless. I would also like to thank my committee members, Dr. S.P. Yadav, Department of Mathematics, Dr. S. Das, and Dr. S.P. Srivastava, Department of Electrical Engineering, Indian Institute of Technology Roorkee, for serving as my committee members even in hardship. Further, I would like to thank all the teaching faculties for their timely advices towards the betterment of my research and career life.

I would like to thank Dr. S.P. Srivastava, Head, Department of Electrical Engineering, Indian Institute of Technology Roorkee, for providing me the required laboratory facilities during the work. Special thanks to Mr. Tula Ram, for their helping hands during experimental work. I would also like to express my appreciation and sincere gratitude to the Department of Electrical Engineering, Indian Institute of Technology Roorkee, its staff members and others, associated directly or indirectly with my research work.

I acknowledge my sincere gratitude to the Ministry of Human Resource and Development (MHRD), Govt. of India for it financial support during research work.

I would like to thank all my friends and elders, particularly, Mr. Derminder Singh for fruitful technical discussions during the work.

Above all, I am grateful to almighty, the most beneficent and merciful, who provides me the confidence and determination in accomplishing this work. Finally, I wish to express my deepest gratitude to my parents Late Md. Samiullah Ansari and Smt. Rukhsana Khatoon, brothers Asif and Asad Iqbal, and all my relatives for their encouragement and endless support throughout the work.

(Arif Iqbal)

Contents

Abstract

The area of multiphase (more than three phase) drive is well explored and remained in research focus during last two decades. This is because of the presence of several potential advantages when compared to its three phase counterpart; making it suitable for many applications like pumps, induced draft fans, ship propulsion, rolling mills, cement mills, paper and textile mills etc. Applications power range may vary from lower to higher where, both synchronous and induction motor are used in voltage source inverter fed drive. Such drives are still limited to the lower end of higher power application range. But, for the applications where power may vary in the range of multi MW, synchronous motor is employed, fed from current source inverter or cycloconverter. This is because of the limitation offered by lower power rating of power electronics switches and therefore, motivated the researchers towards multiphase system. In the new system of multiphase, power sharing by power electronics switches is substantially reduced. Hence, making it suitable for higher power applications.

Usually, the winding end terminals of ac motor are provided at terminal box, which can be connected either in star or delta. These existing motor windings can be reconfigured to a six phase winding structure, embedded in machine stator. The most usual winding configuration is the two sets of three phase winding which are physically displaced by 30^0 (asymmetrical six phase winding) such that each winding set can be fed from independent three phase source. The major advantage of asymmetrical winding configuration has been noted in the reduction in torque pulsation, but with increased stator current. This is due to the substantial reduction of lower order time harmonics (such as 5^{th}, 7^{th}, 17^{th}, 19^{th}…) as well as space harmonics (no harmonics less than 11^{th} order). Therefore, a smooth motor operation is obtained with less mechanical vibration and noise in rotor assembly. However, heating due to increased stator current can be conveniently handled with a suitable cooling arrangement in stationary part of machine.

Motor having the above six phase winding configuration offers yet more attractive features. Such drive system is very suitable for the applications where reliability is of prime importance. This is because it will start and continue to operate even during the supply outage to some phases without significant performance degradation. Infact, effect of supply outage to

few input phases will not be noticeable for motor having larger number of phases. Furthermore, a substantial reduction in phase current without increase in its voltage level was also noted at a particular output power. In this respect, power handling capability of six phase motor becomes ideally double, when compared to its three phase counterpart. But due to losses associated with actual machine operation it increases to 1.73 times, approximately. Thus increasing its power to weight ration. Hence, not only making it suitable of higher power applications but also in some other applications where space availability is extremely important (like aircraft).

The well developed general theory for the conventional three phase machine may be effectively extended for the modeling and analysis of six phase motor under balanced operating condition. A limited literature can be found in this regard, dealing with six phase synchronous motor. But for the motor operation under unbalanced condition (created due to fault at input terminals), the developed method of symmetrical component is usually adopted, during steady-state with sinusoidal excitation. This method is not suitable for evaluation of dynamic response, because of the non-existence of interaction between lost phase (due to fault condition) and remainder of machine winding, altering its dynamic behavior drastically. Another alternative approach is to carry out the analysis for unbalanced condition using Park's *dq0* variables, but has not been reported for six phase synchronous motor. Few authors have also developed the concept of space vector decomposition, applicable for unbalanced condition and has been reported for six phase induction motor only.

From a comprehensive literature survey, it was revealed that a very limited research activity has been carried out for six phase synchronous motor, as this field is still in its primitive stage. Therefore, the present work is dedicated for its extensive analysis of six phase synchronous motor in many aspects. Motivation for the selection of synchronous motor in this work is due to the existence of some important advantages when compared with other ac motors, particularly induction motor. Perhaps, the major advantage of a wound rotor (field excited) synchronous motor is its ease to control the operating power factor by just controlling its field excitation. Motor can be operated easily not only at lagging power factor, but also at unity as well as leading power factor, if required. This feature is not available with induction motor, until some complex scheme is employed. Secondly, speed of the synchronous motor is remain constant (synchronous speed) irrespective to the change in operating conditions. This is not the case with induction motor operation and requires some control scheme to keep the

speed constant (slightly less than synchronous speed). Furthermore, owing to the higher efficiency, use of synchronous motor is more economical. These factors together with its possibility to operate in leading power factor make it suitable to be used in load commutated inverter fed drive without employing the complex and expensive commutation circuitry. Hence, suited in higher power applications like electric ship propulsion, cement mills, rolling mills etc.

In the present work, an extensive exploration and analysis of six-phase synchronous motor has been reported in following aspects:

1: Initially, mathematical modeling together with its development of equivalent circuit has been carried out, wherein the effect of mutual coupling between two three-phase winding sets *abc* and *xyz* are considered, employing *dq0* approach. A detailed dynamic analysis of motor has been then carried out under sudden change in load torque, change in input voltage magnitude and field excitation. Motor operation was found to be stable with less swing in stator current and rotor speed.

2: Usually, any ac motor operates at steady-state at a particular output power. Therefore, steady-state analysis is extensively important in order to understand its operational behavior. It has been carried out in details for six-phase synchronous motor during its normal operation (input supply to both winding sets) as well as the operation with input supply to only one winding set. Analysis includes the development of mathematical model as well as phasor diagrams from which performance may be directly analyzed.

3: Fault analysis of motor drive system is an important step to develop a suitable protective scheme. The most frequent faults which are encountered at input terminals of machine are open-circuit and short-circuit. An exclusive analytical treatment together with its experimental validation has been carried out for open-circuit fault to explore the motor's redundancy characteristic followed by highlighting the machine operation both as motor as well as generator (motor-generator). It has been noted that open-circuit fault at few input terminals can be sustained without much performance degradation. Whereas, in the case of short-circuit fault, an abrupt increase in current was noted, irrespective to its nature (asymmetrical or symmetrical). This requires it to be cleared/isolated within prescribed time limit. The dynamic behavior of motor under such condition has been carried out by developing a suitable computer program in the work.

4: Stability of a machine is an important factor which is dependent directly or indirectly on many design factors and its operating conditions during steady-state. The present work reports a detailed small-signal stability analysis of a six-phase synchronous motor by developing a linearized mathematical model wherein the mutual leakage between both the stator winding sets *abc* and *xyz* is considered, using *dqo* approach. The developed linearized model was used to evaluate the system eigenvalues for its stability analysis under small disturbance/excursion during steady-state. An association between eigenvalue to the machine parameters has been established. It has been carried out by calculating eigenvalues by varying motor parameters within a particular range. Also, based on the variation of dominant eigenvalue, few stabilization technique is suggested, which can be considered during design stage. Further, a simple but effective stabilization technique (based on state feedback technique) has also been developed to ensure a stable operation at all operating region (both stable and unstable region). Finally, formulation of transfer function between input and output variables has also been carried out, where different stability plots (root locus, nyquist plot, bode plot) can be easily drawn.

5: Use of synchronous motor is suited in load commutated inverter (LCI) fed drive, used in higher power applications. The LCI drive has been investigated together with the development of a closed loop scheme for motor operation in self-controlled mode. The developed scheme ensures the motor operation at leading power factor at all load conditions. System dynamic simulation has been carried out for a step change in load torque.

6: Key analytical results have been experimentally investigated, as per the available facility in machine laboratory.

Research papers published/accepted in refereed journals

1: A. Iqbal, G.K. Singh and V. Pant, "Steady-state modeling and analysis of six-phase synchronous motor", System Science & Control Engineering, 2 (1), 2014.

2: A. Iqbal, G.K. Singh and V. Pant, "Stability analysis of asymmetrical six-phase synchronous motor", Turkish Journal of Electrical Engineering & Computer Sciences, (accepted, SCI journal).

3: A. Iqbal, G.K. Singh and V. Pant, "Some observation on no-load losses of asymmetrical six-phase synchronous machine", Turkish Journal of Electrical Engineering & Computer Sciences, (accepted, SCI journal).

In addition to the above, following two more papers are submitted to journals which are under review process:

4: Analysis of asymmetrical six-phase synchronous motor under fault condition.

5: Linearized modeling of asymmetrical six-phase synchronous motor for stable operation.

List of Symbols

Symbols are generally defined within text. Principal symbols used are listed below.

v_a, v_b, v_c	Phase voltage of winding set *abc*
v_x, v_y, v_z	Phase voltage of winding set *xyz*
i_a, i_b, i_c	Phase current of winding set *abc*
i_x, i_y, i_z	Phase current of winding set *xyz*
r_a, r_b, r_c	Resistance of each phase of winding set *abc*
r_x, r_y, r_z	Resistance of each phase of winding set *xyz*
L	Inductance matrix
L_{s11}	Inductance matrix of winding set *abc*
L_{s22}	Inductance matrix of winding set *xyz*
L_{rs1}	Mutual inductance matrix between rotor circuit and winding set *abc*
L_{rs2}	Mutual inductance matrix between rotor circuit and winding set *xyz*
L_{s12}	Mutual inductance matrix between both winding sets *abc* and *xyz*
v_{d1}, v_{q1}	*d-q* voltage of winding set *abc*
v_{d2}, v_{q2}	*d-q* voltage of winding set *xyz*
i_{d1}, i_{q1}	*d-q* current of winding set *abc*
v_{fr}	Field excitation voltage
i_{fr}	Field excitation current
v_{Kq}, v_{Kd}	Voltage along damper windings K_q and K_d respectively
i_{Kq}, i_{Kd}	Current along damper windings K_q and K_d, respectively
r_1, r_2	Stator resistance per phase of winding sets *abc* and *xyz*, respectively
x_{l1}, x_{l2}	Leakage reactance per phase of winding sets *abc* and *xyz*, respectively
x_{lKq}, x_{lKd}	Leakage reactance of damper windings K_q and K_d, respectively
x_{lfr}	Leakage reactance of field winding

x_{md}, x_{mq}	Magnetising inductance along *d-q* axes respectively
x_{lm}	Common mutual leakage reactance between winding sets *abc* and *xyz*
x_{ldq}	Cross mutual coupling reactance between *d-q* axes of stator windings
ψ_{d1}, ψ_{q1}	Flux linkage per second along *d-q* axes of stator winding *abc*
ψ_{d2}, ψ_{q2}	Flux linkage per second along *d-q* axes of stator winding *xyz*
ψ_{md}, ψ_{mq}	Magnetising flux linkage per second along *d-q* axes, respectively
$T_e,\ T_l$	Motor electromagnetic torque and load torque, respectively
ω_r, ω_b	Rotor speed and base speed, respectively
J	Moment of inertia

List of Tables

List of Figures

5.17 Root locus for the transfer function $\Delta Q(s)/\Delta E_{fr}(s)$

5.18 Steps to perform stability analysis of six-phase synchronous motor

6.1 Circuit diagram of LCI fed six-phase synchronous motor showing its (a) basic topology (b) rectifier control (c) inverter control

6.2 Phasor diagram of LCI-fed six-phase synchronous motor

6.3 Phase voltage and current waveforms of inverter feeding the motor showing (a) v_a (b) i_a (c) v_x (d) i_x

6.4 Phase voltage and current waveforms of three winding transformer feeding the rectifiers showing (a) v_a (b) i_a (c) v_x (d) i_x

6.5 Dynamic response of DC link current showing both the generated reference (a) i_{dc1}^* (b) i_{dc2}^* and actual (c) i_{dc1} (d) i_{dc2}

6.6 Motor currents in rotor reference frame showing (a) i_{q1} (c) i_{d1} (c) i_{q2} (d) i_{d2} (e) i_{fr}

6.7 Firing angles of both sets of rectifier-inverter circuitry showing (a) α_1 (b) α_2 (c) β_1 (d) β_2

6.8 Steady-state voltage and current waveforms of three winding transformer feeding the rectifiers showing (a) v_a (b) i_a (c) v_x (d) i_x

6.9 Steady-state Phase voltage and current waveforms of inverter feeding the motor showing (a) v_a (b) i_a (c) v_x (d) i_x

6.10 Motor current during steady-state showing (a) i_{q1} (c) i_{d1} (c) i_{q2} (d) i_{d2} (e) i_{fr}

6.11 Line voltage and current of inverter feeding the motor

7.1 Experimental set up showing (a) schematic diagram (b) general view (c) decoupled and (b) coupled test synchronous machine and DC machine

7.2 Terminal voltage and current of winding set *abc* and *xyz* (a) phase *a* (b) phase *b* (c) phase *c* (d) phase *x* (e) phase *y* (f) phase *z*

7.3 Steady state voltage and current of (a) phase *a* and (b) generated voltage of phase *x*

7.4 Plot of generated voltage (of winding set *xyz.*) with the variation in (a) load torque and (b) input voltage

7.5 Steady state phase voltage and current of healthy phases of winding set *abc*, (a) phase *b* (b) phase *c* and winding set *xyz* (c) phase *x* (d) phase *y* (e) phase *z* after the occurrence of single phase open circuit

7.6 Steady state phase voltage and current of healthy phases of winding set *abc* (a) current i_b and winding set *xyz* (b) current i_y , after the occurrence of double phase open circuit

7.7 Steady state phase voltage and current of healthy phases of winding set *abc* (a) current i_b and winding set *xyz* (b) current i_x, after the occurrence of double phase open circuit

7.8 Fixed losses of dc motor at different rotor speed associated with the synchronous speed of (a) 1100 rpm (b) 1000 rpm (c) 900 rpm (d) 800 rpm (e) 700 rpm (f) 600 rpm

7.9 Friction and windage losses of synchronous machine by experiment in section 7.5.2 (light bar) and by experiment in section 7.5.3 for 6 phase (black bar) and 3 phase (gray bar)

7.10 Experimental results of no load loss of synchronous machine in 3 phase and 6 phase winding configuration at different synchronous speed (a) 55 Hz. (b) 50 Hz. (c) 45 Hz. (d) 40 Hz. (e) 35 Hz.(f) 30 Hz.

7.11 No load losses at constant flux density (field current at 0.6 A) of test machine under its different synchronous speed

7.12 Separate evaluation of hysteresis loss and eddy current loss of test machine with its winding configuration of (a) six phase (b) three phase

7.13 Short circuit loss of test synchronous machine at different rotor speed

7.14 Stray loss at different synchronous speed

7.15 Field loss in excitation circuit

7.16 Efficiency curve of six-phase synchronous motor operation with input phase at 200 V

7.17 Efficiency curve of three-phase synchronous motor with input phase at 200 V

7.18 Efficiency curve of six-phase synchronous motor operation with input phase at 120 V

7.19 Efficiency curve of three-phase synchronous motor with input phase at 240 V

Chapter 1

Introduction

1.1 General

High power motor drive systems are extensively used in different applications such as pumps, fans, electric vehicles, ship propulsion, rolling mills, paper and textile mills etc. are just a few of many. In such applications, where power may be in the range of multi MW, it is usually preferred to use synchronous machine fed by current source inverter or cycloconverter. Although an extensive use of voltage source inverter (VSI) can be found in different applications, but it is limited to the lower end of higher power range. To enhance the power handling capability of VSI, sometime the technique of device grouping is adopted. In this technique, many semiconductor devices are connected either in series or parallel (may be the combination of both) to design a high power topological switch. But several severe problems are encountered in this technique particularly, the careful selection of power electronic switches, use of an additional auxiliary passive component to avoid the failure due to unbalanced condition among the switches etc. About a decade before, the development of multilevel inverter fed drive systems have appeared as a promising option in the field of higher power applications. Multilevel VSI operates with split-voltage dc bus, which results in substantial reduction in voltage stress on each power electronic switches.

As far as the power enhancement of motor is concerned, it is now a usual option to increase the number of phases more than the conventional three (multiphase machine). Infact, the winding of existing three phase motor can be easily reconfigured to a higher phase order. The most usual winding configuration of a six phase motor is the two sets of three phase winding physically displaced by 30^0 electrical apart, which are embedded in the same stator part. In such winding structure, input supply can be fed from two independent three phase sources (i.e. inverters). Therefore, for a constant power output, per phase current is reduced without increase in its voltage level. Hence, power handling capability increases substantially, as compared with its three phase counterpart.

The air gap distribution of ac machine contains unwanted harmonics, which are mainly constituted by phase belt harmonics. These harmonics result in torque pulsation together with

the stray load loss. The order of phase belt harmonic (k) is mathematically expressed as

$$k = 2qj \pm 1$$

where, j is any positive integer and q is number of phase belt per pole. This expression can be used to determine the lowest order of space harmonic with $j = 1$. The value of q is usually larger for a multiphase machine. Hence, for a six-phase motor with asymmetrical winding configuration (semi 12-phase) no harmonic will exsist below 11^{th} order. Therefor, short pitch of coils for elimination of 5^{th} and 7^{th} order harmonics is not required. The elimination of lower order space harmonics is clearly a major advantage, when compared with its three phase counterpart. Furthermore, the inculsion of asymmetric winding configuration for six-phase motor also results in the elimination of lower order time harmonics. Hence, torque pulsation is substantially reduced, leading to a smooth motor operation with less mechanical noise.

It is also believed that the six phase motor (multiphase motor in general) improves the overall reliability of drive system. This is because the loss of input supply to one or more phases will not prevent it from starting and will continue to run with satisfactory performance. This characteristic makes the motor suitable for the applications where reliability is of prime importance.

The generalized analytical approach can be extended for the analysis of multiphase (particularly six phase) motor by considering it as a set of magnetically coupled electrical circuit. But the complexity of system increases with the increase in number of windings. Furthermore, the presence of time varying coefficients (inductance terms) makes the system computationally more complex. In such system, it is better to incorporate a suitable transformation technique to achieve simplification in system analysis. Therefore, analysis is carried out in rotating reference frame, employing Park's transformation. A detailed discussion is presented in following chapters.

In the following section, development in the field of six phase synchronous motor (multiphase motor in general) has been surveyed highlighting new findings.

1.2 Literature survey

The concept of multiphase (more than three phase) machine was initially originated in late 1920's when larger power generation got hampered due to the limitations in circuit breaker interrupting capability. To overcome this situation, attention of scientists were diverted to the machine having double windings embedded in its stator. It was after this time, research

continued in the field of multiphase machine with steady but in slower way. A few older references [1-3] are available in this regard.

It was in 1969, where the concept of multiphase (more than three phase) penetrated in the field of motor drive system and a five phase voltage source inverter-fed induction motor was proposed [4]. Since then, the field of multiphase motor drive is remained in research focus and several interesting developments have been reported. Authors in [5] have pointed out the advantage of asymmetrical winding configuration of six-phase motor. It was shown that the machine torque characteristic having six-phase asymmetrical winding (two three phase windings displaced by 30 degree) improves substantially by the reduction of its torque pulsation, but results in increased stator current. Moreover, with asymmetrical winding configuration for six-phase motor, reduction of many time harmonics of lower order (such as 5^{th}, 7^{th},17^{th},19^{th} …) are prevented from the contribution to the airgap and torque pulsation, while contributing to supply input current [6]. Analysis of six-phase motor was later carried out in detail with different displacement angles by several authors [5-7, 10-12]. It was further suggested that the optimized angular displacement between winding sets is π/n for an even number of three-phase sets and $2\pi/n$ for an odd number of three-phase sets, where, n is the total number of machine phase. A detailed winding configuration of multiphase machine is given in references [6-7].

Usually, it is the end terminals, which are brought out of conventional three-phase ac machine, such that it can be connected either in star or delta fashion. In fact, the same machine winding can be easily reconfigured to a multiphase winding, as discussed in [6]. When a multiphase machine, particularly a six-phase motor with asymmetrical stator winding configuration, supplied by the independent two sets of three-phase source (using inverter circuitry), offers some more attractive features. Important of which is its increased power handling capability [7-9, 13-15]. In fact, motor in above configuration results in decreased phase current without increase in its voltage level for a constant output power, in comparison with its three-phase counterpart. Therefore, the motor in multiphase winding configuration is suitable for higher power applications, where power electronics switches of lower rating can be utilized. Theoretically, power rating of six-phase machine becomes doubled, when compared with three-phase machine. But experimentally, it was found to increase only by 1.73 times approximetely [16], due to saturation, insulation and other design factors associated during its

operating mode.

Together with the above advantages, multiphase motor drive is much suited for the applications where system reliability is of prime importance. This is because it works on the basic concept of parallel-redundancy technique [17]. Therefore, motor will start and continue to run with satisfactory performance, even with the loss of one or more input phase supply. The loss of supply to some of the input phases will create the unbalanced condition and is a major reason of performance degradation, explained in [18].

The developed general theory adopted for the analysis of conventional three-phase machine can be effectively extended for multiphase machine. Such analytical approach dealing with the mathematical modeling at a general level is available in [19]. However, the well adopted and simplified approach of mathematical modeling is by employing Park's transformation [19-20]. Few literatures are available that deals the mathematical modeling of multiphase (six-phase) synchronous machine [21-25] during balanced operating condition. But for the analysis under unbalanced operating condition (due to fault at input terminals), the well known approach of symmetrical component method may be used. In this approach, the three sequence network are identified and interconnected according to fault condition, which is then solved as a large equivalent network. This method can be successfully used for the analysis during steady-state with sinusoidal excitation. But the method is not suitable for evaluation of dynamic response of the machine. This is because of the non-existence of interaction between the lost phases and remainder of the machine windings which drastically alters the dynamic behavior of machine [7, 29]. Another alternative approach for the analysis of six-phase motor under unbalanced condition is by using the concept of space-vector decomposition discussed in detail by authors in [26-27]. Infact, analysis of unbalanced conditions created by terminal open circuit together with the development of post fault condition schemes is available in many references [28-33]. But the analysis of six-phase motor, particularly synchronous motor, under short circuit condition has not been reported so far.

During the exploration of progress made in the field of multiphase machine, it was noted that a large number of new findings have been reported for induction motor drives. But, as far as multiphase (six-phase) synchronous machine (particularly motor) is concerned, only a few literatures are available, as this is still in its primitive stage. A general modeling of six-phase synchronous machine is available in [21-23, 25]. The behavior of a six-phase

synchronous alternator equipped with two sets of three phase stator winding displaced by an arbitrary angle was analyzed by Fuchs and Rosenberg [21], where it has been concluded that the orthogonal transformation (*dq0*) eliminates partly the time-dependence of coefficients' of the system differential equations, and the phasor can be used for the analysis of steady-state behavior of generator with two stator windings. A detailed modeling of six-phase synchronous machine has been reported by Schiferl and Ong [22], where mutual coupling between the two sets of three-phase stator windings was considered. Steady-state operation of motor was also examined during the transformer and motor mode of power transfer. Authors in their companion paper [23] have also derived the expression of mutual leakage inductances, which can be used for different winding configurations of six-phase and proposed a scheme of a single machine uninterruptible power supply using a six-phase synchronous machine. Kataoka and Watanabe [24] have presented an important application of a double wound synchronous machine in a system of dc to ac conversion using a current source inverter, a position sensor and a control circuit. Authors have also derived an equivalent circuit to predict the system behavior during steady-state followed by a discussion to keep the output voltage and frequency constant. Along with the presentation of modeling and simulation of a high power drives using double star synchronous motor, effect of winding displacement angle on torque ripple and harmonic effects were highlighted by Terrien and Benkhoris [34]. Authors in ref. [35] have briefly presented the analysis of six-phase synchronous machine with emphasis of its redundancy property, operation during fault conditions, machine behavior when fed with non-sinusoidal voltage and sensitivity of the design parameters. However, to best of the authors' knowledge, no detailed investigation have been carried out about the steady-state and dynamic behavior of the machine under fault condition. In view of the above, there is strong motivation to undertake a systematic and through investigation about six-phase synchronous motor.

1.3 Author's Contributions

Due to a limited exploration and research activities in the field of six-phase synchronous motor, following attempts have been made to establish the contribution:

(1) Development of mathematical model of six-phase synchronous motor in rotor reference frame, followed by its dynamic analysis under different operating conditions.

(2) Steady-state analysis of six-phase synchronous motor. It includes the development a mathematical model and phasor diagram for motoring and motor-generator modes of operation.

(3) Analysis and exploration of motor behavior under fault conditions created by open-circuit and short-circuit at motor input terminals, considering almost all possible cases (asymmetrical and symmetrical).

(4) Steady-state stability analysis of six-phase synchronous motor. This includes the development of its linearized model, formulation of transfer function between required input and output variables, development of instability limits, stabilization scheme using state feedback technique in closed loop operation.

(5) Analysis of load commutated inverter (LCI) fed six-phase synchronous motor together with the development of a closed-loop scheme for its operation in self-controlled mode.

(6) Experimental investigation to validate the key analytical results.

Chapter 2

Mathematical Modeling and Dynamic Analysis of Six-Phase Synchronous Motor

2.1 Introduction

An electrical machine is a complex system that converts electrical energy to mechanical energy or vice versa, during its operation. It came into existence about more than a hundred years ago and research activities in this field appear to be never ending. In this context, mathematical modelling is an essential part of any system, which is required to understand its working characteristics and operating behavior, under different modes. Therefore, this chapter deals with a detailed mathematical modeling of a six-phase synchronous motor in rotor reference frame.

2.2 Mathematical Modeling

In the design of six-phase motor, it is a common strategy to split the stator winding into two through phase belt splitting, each of them supplied by separate three phase electrical source. The two sets of three phase windings namely *abc* and *xyz*, have the angular displacement of ξ = 30 degree, to have asymmetrical winding. This is because, with 30 degree space shift between the two three-phase winding sets and with the same electrical phase shift between the supply voltages, all the harmonics of order ($6n \pm 1$, where n = 1,3,5…) are eliminated from the airgap flux. Hence, the excitation voltage time harmonics such as 5^{th}, 7^{th}, 17^{th}, 19^{th}…etc. are prevented from the contribution to the air gap flux and torque pulsation, while they are contributing in the supply input current. This is due to the relatively small reluctance of these harmonics current paths. The shorted damper windings are K_q and K_d are along the quadrature and direct axis (field axis), respectively.

While going onwards for the motor equation, some of the important simplifying assumptions are made. These are as follows:

- Both the stator windings (*abc* and *xyz*) are symmetrical and have a perfect sinusoidal distribution along the air-gap,
- Space harmonics are neglected, flux and mmfs are sinusoidal in space,
- Saturation and hysteresis effects are neglected,
- No skin effect, i.e. winding resistance is not dependent on frequency.

A schematic representation of stator and rotor axes is shown in Fig. 2.1. Stator consists of two balanced three phase windings, *abc* and *xyz* which are physically displaced by ξ electrical degree. Rotor is equipped with the field winding f_r and a damper winding K_d along *d*-axis and a damper winding K_q along *q*-axis. By adopting the motor convention, voltage equations for stator and rotor windings can be written as

$$\begin{bmatrix} v_s \\ v_r \end{bmatrix} = \begin{bmatrix} r_s & 0 \\ 0 & r_r \end{bmatrix} \begin{bmatrix} i_s \\ i_r \end{bmatrix} + p \begin{bmatrix} \lambda_s \\ \lambda_r \end{bmatrix} \tag{2.1}$$

where,

$$\begin{bmatrix} \lambda_s \\ \lambda_r \end{bmatrix} = [L] \begin{bmatrix} i_s \\ i_r \end{bmatrix} \tag{2.2}$$

voltage and current vectors are defined as

$$v_s = \left[v_a, v_b, v_c, v_x, v_y, v_z\right]^T$$

$$v_r = \left[v_{Kq}, v_{Kd}, v_{fr}\right]^T$$

$$i_s = \left[i_a, i_b, i_c, i_x, i_y, i_z\right]^T$$

$$i_r = \left[i_{Kq}, i_{Kd}, i_{fr}\right]^T$$

and motor resistance and inductance matrices are defined by

$$r_s = diag\left[r_a, r_b, r_c, r_x, r_y, r_z\right]^T$$

$$r_r = diag\left[r_{Kq}, r_{Kd}, r_{fr}\right]^T$$

$$L = \begin{bmatrix} L_{s11} & L_{s12} & L_{s1r} \\ L_{s21} & L_{s22} & L_{s2r} \\ L_{rs1} & L_{rs2} & L_r \end{bmatrix}$$

where,

$$L_{s11} = \begin{bmatrix} L_{aa} & L_{ab} & L_{ac} \\ L_{ba} & L_{bb} & L_{bc} \\ L_{ca} & L_{cb} & L_{cc} \end{bmatrix}; \qquad L_{s22} = \begin{bmatrix} L_{xx} & L_{xy} & L_{xz} \\ L_{yx} & L_{yy} & L_{yz} \\ L_{zx} & L_{zy} & L_{zz} \end{bmatrix}$$

$$L_{s1r} = \begin{bmatrix} L_{aKq} & L_{bKd} & L_{cfr} \\ L_{bKq} & L_{cKd} & L_{afr} \\ L_{cKq} & L_{aKd} & L_{bfr} \end{bmatrix}; \qquad L_{s2r} = \begin{bmatrix} L_{xKq} & L_{yKd} & L_{zfr} \\ L_{yKq} & L_{zKd} & L_{xfr} \\ L_{zKq} & L_{xKd} & L_{yfr} \end{bmatrix}$$

$$L_{s12} = L_{s21} = \begin{bmatrix} L_{ax} & L_{ay} & L_{az} \\ L_{bx} & L_{by} & L_{bz} \\ L_{cx} & L_{cy} & L_{cz} \end{bmatrix}; \qquad L_r = \begin{bmatrix} L_{lKq} + L_{mKq} & 0 & 0 \\ 0 & L_{lKd} + L_{mKd} & L_{frKd} \\ 0 & L_{frKd} & L_{lfr} + L_{mfr} \end{bmatrix}$$

It should be noted that the subscripts 's' and 'r' indicate the variable for stator and rotor respectively, while the subscripts '1' and '2' refer the variable for stator winding *abc* and *xyz*, respectively. The sub-matrix L_{s11} and L_{s22} indicate the inductances of stator winding set *abc* and *xyz* respectively, whereas L_{s12} (and L_{s21}) indicate the mutual inductance between the winding sets *abc* and *xyz*. Moreover, each set of stator winding is assumed to be balanced and distributed symmetrically. Therefore the parameters (resistance and inductance) of each winding set will also be same. In this view, the resistance $r_a = r_b = r_c = r_1$ (for winding set *abc*) and $r_x = r_y = r_z = r_2$ (for winding set *xyz*). Such simplification can also be obtained for inductance terms as, $L_{aa} = L_{bb} = L_{cc}$ and $L_{xx} = L_{yy} = L_{zz}$ for winding sets *abc* and *xyz*. Also, the elements of mutual leakage inductances sub matrix is cyclic, therefore $L_{ax} = L_{by} = L_{cz}$, $L_{ay} = L_{bz} = L_{cx}$ and $L_{az} = L_{bx} = L_{cy}$. Each elements of the above inductance matrices are explained in Appendix I.

The voltage and electromagnetic torque equation when written in machine variables results in the sets of non-linear differential equations [36]. Non-linearity is introduced due to the presence of inductance term, which is the function of rotor position and is time dependent. In order to achieve simplified equations and constant inductance terms, reference frame theory is applied, and all the sets of equations will be written in rotor reference frame (Park's equation). The equations of voltages and flux linkage per second of a six-phase synchronous motor in Park's variables are [22, 25]:

2.2.1 Voltage equation:

$$v_{q1} = r_1 i_{q1} + \frac{\omega_r}{\omega_b}\psi_{d1} + \frac{p}{\omega_b}\psi_{q1} \tag{2.3}$$

$$v_{d1} = r_1 i_{d1} - \frac{\omega_r}{\omega_b}\psi_{q1} + \frac{p}{\omega_b}\psi_{d1} \tag{2.4}$$

$$v_{q2} = r_2 i_{q2} + \frac{\omega_r}{\omega_b}\psi_{d2} + \frac{p}{\omega_b}\psi_{q2} \tag{2.5}$$

$$v_{d2} = r_2 i_{d2} - \frac{\omega_r}{\omega_b}\psi_{q2} + \frac{p}{\omega_b}\psi_{d2} \tag{2.6}$$

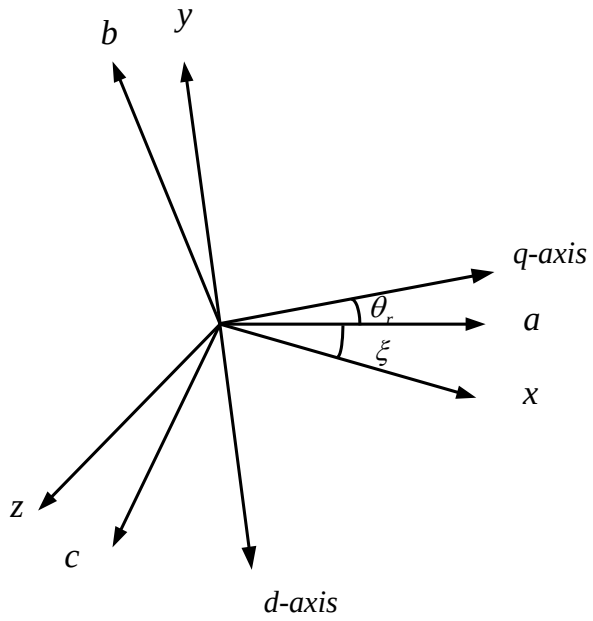

Fig. 2.1: Stator and rotor axes of six phase motor.

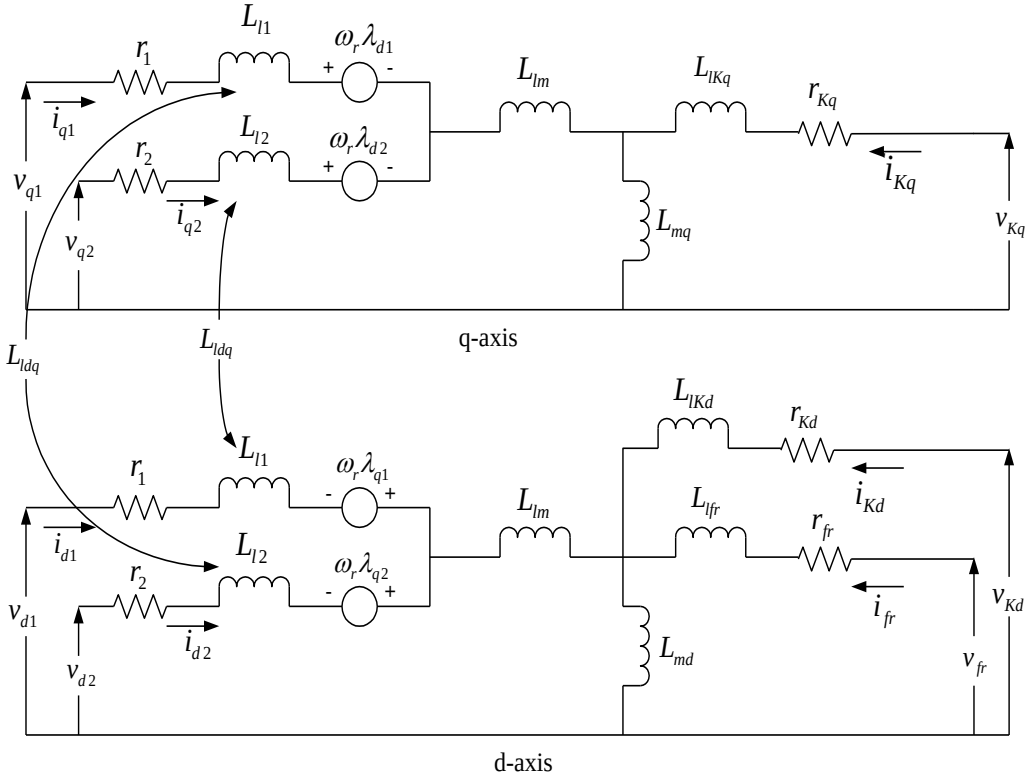

Fig. 2.2: An equivalent circuit of a six phase synchronous machine (motor).

$$v_{Kq} = r_{Kq} i_{Kq} + \frac{p}{\omega_b} \psi_{Kq} \tag{2.7}$$

$$v_{Kd} = r_{Kd} i_{Kd} + \frac{p}{\omega_b} \psi_{Kd} \tag{2.8}$$

$$v_{fr} = \frac{x_{md}}{r_{fr}} \left(r_{fr} i_{fr} + \frac{p}{\omega_b} \psi_{fr} \right) \tag{2.9}$$

where, all the symbols stands at their usual meaning. ω_r and ω_b are the rotor speed (also the speed of rotating reference frame) and base speed respectively. p denotes the differentiation function w.r.t. time.

2.2.2 Equations of Flux linkage per second:

$$\psi_{q1} = x_{l1} i_{q1} + x_{lm} \left(i_{q1} + i_{q2} \right) - x_{ldq} i_{d2} + \psi_{mq} \tag{2.10}$$

$$\psi_{d1} = x_{l1} i_{d1} + x_{lm} (i_{d1} + i_{d2}) + x_{ldq} i_{q2} + \psi_{md} \tag{2.11}$$

$$\psi_{q2} = x_{l2} i_{q2} + x_{lm} \left(i_{q1} + i_{q2} \right) + x_{ldq} i_{d1} + \psi_{mq} \tag{2.12}$$

$$\psi_{d2} = x_{l2} i_{d2} + x_{lm} (i_{d1} + i_{d2}) - x_{ldq} i_{q1} + \psi_{md} \tag{2.13}$$

$$\psi_{Kq} = x_{lKq} i_{Kq} + \psi_{mq} \tag{2.14}$$

$$\psi_{Kd} = x_{lKd} i_{Kq} + \psi_{md} \tag{2.15}$$

$$\psi_{fr} = x_{lfr} i_{fr} + \psi_{md} \tag{2.16}$$

where,

$$\psi_{mq} = x_{mq} (i_{q1} + i_{q2} + i_{Kq}) \tag{2.17}$$

$$\psi_{md} = x_{md} (i_{d1} + i_{d2} + i_{Kd} + i_{fr}) \tag{2.18}$$

The rotor circuit parameters are referred to one of the stator winding (*abc* winding set). These voltage and flux linkage equations suggest the equivalent circuit as shown in Fig. 2.2, where $L_{lm}$and L_{ldq} are known as common mutual leakage inductance and cross mutual coupling inductance between *d* and *q*-axis of stator respectively given by:

$$x_{lm} = x_{lax} \cos(\xi) + x_{lay} \cos(\xi + 2\pi/3) + x_{laz} \cos(\xi - 2\pi/3) \tag{2.19}$$

$$x_{ldq} = x_{lax} \sin(\xi) + x_{lay} \sin(\xi + 2\pi/3) + x_{laz} \sin(\xi - 2\pi/3) \tag{2.20}$$

The common mutual leakage reactance x_{lm} accounts for the mutual coupling between the two sets of stator winding occupying the same slot by leakage flux. It depends on the winding pitch and displacement angle between the two stator winding sets, and has an important effect on the harmonic coupling between them. However, neglecting this parameter has no noticeable effect on transient effect except some changes in voltage harmonic distortion

[25]. Detailed discussion on finding the slot reactance is given in ref. [37]. Standard test procedures are available to determine various machine parameters in [38-48].

The detailed computer simulation of six-phase synchronous motor is based on the integral form of motor's voltage and torque equations with flux linkage per second and speed as state variable, winding currents as output variables, applied voltage and load torque as input variables. The voltage equations (2.3) - (2.9) together with the flux linkages equations (2.10) - (2.16) are firstly solved for the currents, which are then back substituted in the voltage equations. These mathematical manipulations yields the following integral equations:

$$\psi_{q1} = \frac{\omega_b}{p}\{v_{q1} - \frac{\omega_r}{\omega_b}\psi_{d1} - \frac{r_1}{X_b}\left[(x_{l2} + x_{lm})\psi_{q1} - x_{lm}\psi_{q2} - x_{l2}\psi_{mq} + x_{ldq}(\psi_{d2} - \psi_{md})\right]\} \tag{2.21}$$

$$\psi_{d1} = \frac{\omega_b}{p}\{v_{d1} + \frac{\omega_r}{\omega_b}\psi_{q1} - \frac{r_1}{X_b}\left[(x_{l2} + x_{lm})\psi_{d1} - x_{lm}\psi_{d2} - x_{l2}\psi_{md} - x_{ldq}\left(\psi_{q2} - \psi_{mq}\right)\right]\} \tag{2.22}$$

$$\psi_{q2} = \frac{\omega_b}{p}\{v_{q2} - \frac{\omega_r}{\omega_b}\psi_{d2} - \frac{r_1}{X_b}\left[(x_{l1} + x_{lm})\psi_{q2} - x_{lm}\psi_{q1} - x_{l1}\psi_{mq} - x_{ldq}(\psi_{d1} - \psi_{md})\right]\} \tag{2.23}$$

$$\psi_{d2} = \frac{\omega_b}{p}\{v_{d2} + \frac{\omega_r}{\omega_b}\psi_{q2} + \frac{r_1}{X_b}\left[(x_{l1} + x_{lm})\psi_{d2} - x_{lm}\psi_{d1} - x_{l1}\psi_{md} + x_{ldq}\left(\psi_{q2} - \psi_{mq}\right)\right]\} \tag{2.24}$$

$$\psi_{Kq} = \{v_{kq} - \frac{r_{Kq}}{x_{lKq}}\left[\psi_{Kq} - \psi_{mq}\right]\} \tag{2.25}$$

$$\psi_{Kd} = \{v_{kd} - \frac{r_{Kd}}{x_{lKd}}[\psi_{Kd} - \psi_{md}]\} \tag{2.26}$$

$$\psi_{fr} = \{\frac{v_{fr}x_{md}}{r_{fr}} - \frac{r_{fr}}{x_{lfr}}\left[\psi_{fr} - \psi_{md}\right]\} \tag{2.27}$$

Current can be expressed in terms of flux as:

$$i_{q1} = \frac{1}{x_b}[(x_{l2} + x_{lm})\psi_{q1} - x_{lm}\psi_{q2} - x_{l2}\psi_{mq} + x_{ldq}(\psi_{d2} - \psi_{md})] \tag{2.28}$$

$$i_{d1} = \frac{1}{x_b}[(x_{l2} + x_{lm})\psi_{d1} - x_{lm}\psi_{d2} - x_{l2}\psi_{md} - x_{ldq}\left(\psi_{q2} - \psi_{mq}\right)] \tag{2.29}$$

$$i_{q2} = \frac{1}{x_b}[(x_{l1} + x_{lm})\psi_{q2} - x_{lm}\psi_{q1} - x_{l1}\psi_{mq} - x_{ldq}(\psi_{d1} - \psi_{md})] \tag{2.30}$$

$$i_{d1} = \frac{1}{x_b}[(x_{l1} + x_{lm})\psi_{d2} - x_{lm}\psi_{d2} - x_{l1}\psi_{md} + x_{ldq}\left(\psi_{q1} - \psi_{mq}\right)] \tag{2.31}$$

$$i_{Kq} = \frac{1}{x_{lKq}}[\psi_{Kq} - \psi_{mq}] \tag{2.32}$$

$$i_{Kd} = \frac{1}{x_{lKd}}[\psi_{Kd} - \psi_{md}] \tag{2.33}$$

$$i_{fr} = \frac{1}{x_{lfr}}[\psi_{fr} - \psi_{md}] \tag{2.34}$$

ψ_{mq} and ψ_{md} can be expressed in the term of state variables as

$$\psi_{mq} = x_{aq}\left[\frac{x_{l2}\psi_{q1}+x_{l1}\psi_{q2}+x_{ldq}(\psi_{d2}-\psi_{d1})}{x_b} + \frac{\psi_{Kq}}{x_{lKq}}\right] \tag{2.35}$$

$$\psi_{md} = x_{ad}\left[\frac{x_{l2}\psi_{d1}+x_{l1}\psi_{d2}+x_{ldq}(\psi_{q1}-\psi_{q2})}{x_b} + \frac{\psi_{Kd}}{x_{lKd}} + \frac{\psi_{fr}}{x_{lfr}}\right] \tag{2.36}$$

where,

$$x_{aq} = \left[\frac{1}{x_{mq}} + \frac{1}{x_{lKq}} + \frac{x_{l1}+x_{l2}}{x_b}\right]^{-1} \tag{2.37}$$

$$x_{ad} = \left[\frac{1}{x_{md}} + \frac{1}{x_{lKd}} + \frac{1}{x_{lfr}} + \frac{x_{l1}+x_{l2}}{x_b}\right]^{-1} \tag{2.38}$$

$$x_b = x_{l1}x_{l2} + (x_{l1} + x_{l2})x_{lm} - x_{ldq}^2 \tag{2.39}$$

The electromagnetic torque (T_e) and rotor dynamic equations for *P*- pole, six-phase synchronous motor can be expressed as:

$$T_e = T_{e1} + T_{e2} \tag{2.40}$$

where,

$$T_{e1} = k(i_{q1}\psi_{d1} - i_{d1}\psi_{q1}) \tag{2.41}$$

is torque due to the first set of winding, and

$$T_{e2} = k(i_{q2}\psi_{d2} - i_{d2}\psi_{q2})\ ;\ k = \frac{3}{2}\frac{P}{2}\frac{1}{\omega_b} \tag{2.42}$$

is torque due to the second set of winding.

$$\frac{\omega_r}{\omega_b} = \frac{1}{p}\left[\frac{1}{\omega_b}\ \frac{P}{2}\ \frac{1}{J}(T_e - T_l)\right] \tag{2.43}$$

where, T_e is the electromagnetic torque, which is positive for motor, T_l is the load torque and *J* is the moment of inertia of rotor assembly.

Block diagram showing the computer simulation of a six-phase synchronous motor is shown in Fig. 2.3. Use of motor equations during computation steps are indicated by its numbers. Input voltages v_{abcs} and v_{xyzs} in stationary phase coordinate are transformed directly to v_{dq0s}^{r} and $v_{dq0s}^{r-\xi}$, i.e. in rotor reference frame by using the transformation matrix [20, 22] K_s^r and $K_s^{r-\xi}$, associated with each stator winding sets *abc* and *xyz*. The voltages applied to the damper windings are not shown because the windings are always short- circuited and voltages are zero.

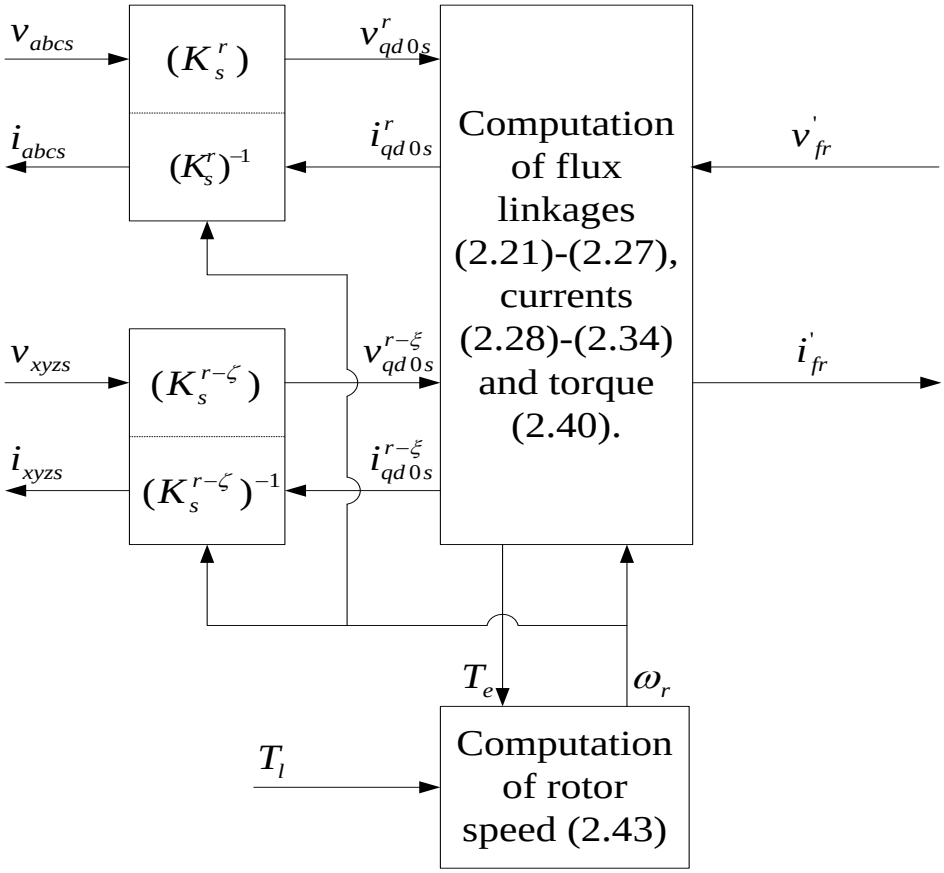

Fig. 2.3: Simulation of a six-phase synchronous motor in rotor reference frame in block diagram form.

2.3 Dynamic Analysis of Six-Phase Synchronous Motor

Dynamic analysis of any electrical system is of prime importance to understand its operating characteristic under different conditions changing suddenly. Therefore, the mathematical model developed in previous section has been effectively used to analyze the behavior of six-phase synchronous motor under sudden change in its operating conditions. Sudden changes considered are the change in load torque, field excitation and input voltage levels, in the following sections.

2.3.1 Change in load torque:

Considering the practical importance of motor operation at different load torque, dynamic performance of six-phase synchronous motor has been presented. For this purpose, a set of differential equations that describe the synchronous motor operation were simulated in Matlab/Simulink environment. Simulation steps of motor in rotor reference frame are depicted

in Fig. 2.3.

Simulation has been carried out for a motor of 3.7 kW, 6 poles, whose parameters are mentioned in Appendix II. Computer traces shown in Fig. 2.4 and Fig. 2.5, illustrate the dynamic behavior of six-phase synchronous motor due to a step change in load torque from zero to 50 percentage of rated/base torque at time t = 5 sec. and further increase in load torque by 50 percent (i.e. at full load) at time t = 15 sec. It is assumed that the input voltage and frequency is constant irrespective of the change in load torque. Input phase voltage was maintained constant at 220 V, 50 Hz. operating at 0.85 power factor (lagging). Initially, motor is operating with zero load torque, i.e. at no load condition at synchronous speed. At time t = 5 sec., a step increase in load torque was applied. This resulted in the decrease in rotor speed immediately following the step increase in load torque as shown in Fig. 2.4 (b), where the load angle *delta* increases (in magnitude). The rotor speed continues to decrease till the accelerating torque on the rotor vanishes. It can be noted from Fig. 2.4 that the speed decreases to approximately 104.3 rad/sec. at the time when T_e equal to T_l. At this time, accelerating torque is zero, the rotor is running below synchronous speed; hence, load angle *delta* and thus motor torque T_e will keep on increasing. Increase in torque T_e results in an increase in the output power of the machine that causes the rotor to accelerate towards synchronous speed. Hence, due to rotor inertia, it will continue to accelerate above synchronous speed and consequently load angle *delta* begin to decrease (in magnitude), with decrease in motor torque T_e. In this way, damped oscillation of motor variable continues and settles to a new-steady state value.

Due to the increase in motor load torque, increase in the stator phase current can be noted in Fig. 2.5, which is required to meet the increased output. The increase in stator current is associated with the increase in active output power of the motor, while maintaining its operation at constant power factor (i.e. constant reactive power). Hence, the change in *q*-axis component of stator current (active component of current changes from 2.05 A to 4.23 A, approximately) has been depicted in Fig. 2.6, with no change in its *d*-axis component of stator current (reactive component of current), of both the winding sets *abc* and *xyz*.

Variation of motor torque T_e with load angle *delta* has been plotted in Fig. 2.7. Dynamic characteristic of torque-angle shows a larger variation in T_e at a particular load angle *delta* and settles to its steady-state value after all transients have subsides. Therefore, the dynamic response is considerably different from its steady-state characteristic.

2.3.2 Change in field excitation:

Perhaps the major advantage of a wound rotor (field excited) synchronous motor over other types of ac motors is its ease to control the operating power factor from field excitation. Operation of the motor at required power factor (lagging, unity or leading) can easily be obtained by just controlling its field excitation, which has been simulated in this section. Motor operation with sudden change in its field excitation has been discussed.

The field excitation has been changed from its operation at lagging power factor of 0.8 to unity power factor at time t = 10 sec. to the leading power factor of 0.8 at time t = 15 sec. The variation of operating power factor (by changing the field excitation) is associated with the change in its reactive power while maintaining its active power constant, as shown in Fig. 2.8. Therefore, the variation in *d*-axis component of stator current, i_{d1} and i_{d2} (reactive component changed from 1.39 A to -0.10 A at time t = 10 sec. to -1.5 A at t = 15 sec.) can be noted in Fig. 2.9 (b) and Fig. 2.9 (d) respectively, with almost no variation in *q*-axis component of the stator current (active component). This results in overall change in stator current as shown in Fig. 2.10. Stator current was found to be minimum during motor operation at unity power factor. This is because of considerable reduction in *d*-axis component of the stator current. It can be further noted that following the step change in field excitation, variation in motor torque, rotor speed and load angle is negligible after settling to its steady-state, as indicated in Fig. 2.11. Plot of torque-angle characteristic is also shown in Fig. 2.12.

2.3.3 Change in input voltage:

From the practical viewpoint, there is always a variation in input voltage of the synchronous motor, because of a continuous variation in the loads connected to utility grid. Therefore, the motor dynamic behavior has been observed under such condition of input voltage variation. This condition was simulated for the change in input phase voltage at time t = 10 sec., such that the voltage was decreased to 180 V. Since the variation of voltage level of any electrical system is associated with the change of its reactive power component, therefore, *d* - axis component of the stator current was found to be changed from 1.13 A to 1.31 A, after the settlement of all transient, as shown in Fig. 2.13 (b) and Fig. 2.13 (d). A small variation in active component was also noted (*q* - axis component of stator current changed from 2.05 A to 2.55 A) in Fig. 2.13 (a) and Fig. 2.13 (c). This is because the output power of machine is constant, and is the

product of its voltage and current. Hence, the change in input voltage level (both *d* and *q*-axis component of voltage is changed) also results in small variation of *q* axis component of stator current. Therefore, decrease in input voltage level leads to the overall increase in motor current from 2.35 A to 2.87 A as shown in Fig. 2.14. Effect of voltage variation in input voltage was also found on the transient production in motor torque T_e, resulting the swing in rotor speed and load angle *delta*, as shown in Fig. 2.15. It was noted that the value of load angle *delta* is also dependent on voltage input and magnitude increases from 2.9 to 4.4 electrical degree. This variation is due to the small change in *q*-axis component (active component) of input voltage supplied to stator winding sets. Torque-angle characteristic is shown in Fig. 2.16.

2.4 Motor performance with different displacement angle between winding sets

In this section, the effect of displacement angle (between stator winding sets *abc* and *xyz*) on motor performance has been simulated under load variation (load increased to 50 % of rated/base torque at time t = 5 sec.). Three cases of displacement angle ξ (at 0^0, 30^0 and 60^0) are considered. Therefore, the same phase shift (in electrical degree) between two sets of balanced three phase input supply is required. For this purpose switching of inverter gate pulses must be synchronized to ensure the required phase shift between the independent three-phase supply. Inverter used during simulation was a simple six-step in nature. (six-step voltage source inverter). In all the cases considered, both dynamic and steady-state (during load) characteristic are plotted and explained below:

Nature of the input voltage will differ (by 0^0, 30^0 and 60^0) as per the angular difference ξ between both the winding sets *abc* and *xyz*. Input voltage (phase voltages v_a and v_x are shown) to each set of stator winding is shown in Fig. 2.17, Fig. 2.24 and Fig. 2.31 for value of ξ at 0^0, 30^0 and 60^0, respectively. Presence of harmonics in the stator current was found to be dependent on the value of displacement angle ξ. For the displacement angle of 0^0 and 60^0, magnitude of current harmonics was found to be 17 A approximately, as shown in Fig. 2.18 and Fig. 2.32, respectively. But it increases to a larger value of 83.3 A at displacement angle of 30^0 as shown in Fig. 2.25. This increase in machine current is mainly attributed due to the *d*-axis current component (reactive component) with small dependency on *q*-axis component (active component) of stator current, as shown in Fig. 2.19, Fig. 2.26, and Fig. 2.33 for value of ξ at 0^0, 30^0 and 60^0, respectively. Stator currents both in stationary as well as rotor reference

frame during steady-state (at 50 percent of motor load) are also shown in a parallel way in order to visualize it more clearly for different value of ξ.

It is worthwhile to note here that in case of synchronous motor operation with symmetrical stator winding configuration ($\xi = 0^0, 60^0$), there exist a magnetic interlocking between the stator and rotor field. Moreover, the salient structure of rotor will align itself along the path of least reluctance. Therefore, during steady-state, a small airgap *x*, exists between rotor and stator field, as shown in Fig. 2.38 (a). But, during the motor operation with asymmetrical six-phase winding configuration ($\xi = 30^0$), the rotor aligns itself along the resultant stator field attributed by the winding sets *abc* and *xyz*, as depicted in Fig. 2.38 (b). Rotor axis in this position will have the airgap x', w.r.t. magnetic axis of the individual winding sets *abc* and *xyz*. The airgap x' (for asymmetrical six-phase operation) is clearly greater than *x* (for symmetrical six-phase operation). Therefore, to establish the required flux level in airgap, magnetizing current and hence, the stator current and its harmonics increase. Larger magnitude of current harmonics ($\xi = 30^0$) will result in the unwanted losses, and therefore, heating of the machine stator. The pattern of harmonic variation in motor torque T_e was found to be reversed. Magnitude of torque ripples for displacement angle ξ equal to 0^0 and 60^0 was found to be almost equal, 81 Nm. as shown in Fig. 2.23 and Fig. 2.37. But a considerable reduction in torque harmonic ripples (57 Nm.) was noted for the displacement angle of 30^0, as shown in Fig. 2.30. This reduction in torque harmonics results in a smooth operation of the machine with very less noise and mechanical vibration in rotor assembly. Although, heating of stator will increase (due to increased current harmonics), but cooling of the stationary part i.e. stator of machine can be conveniently handled.

2.5 Conclusion

In this chapter a simple but effective mathematical model of six-phase synchronous motor has been developed, considering the effect of mutual leakage reactance between the two sets of three-phase stator winding *abc* and *xyz*, in rotor reference frame. The developed mathematical model was effectively simulated under different operating conditions to explore the detailed dynamic characteristics of six-phase synchronous motor. These conditions include the change in load torque, field excitation and its input voltage levels which was then followed by its investigation of operating behavior for different displacement angle (0^0, 30^0 and 60^0)

between both the stator winding sets *abc* and *xyz*, in a well elaborated way.

Motor dynamic performance was found to be satisfactory as the developed motor torque T_e was supplying the load with less swing in stator current and rotor speed. These swings were found to be still smaller for the change in field excitation and input voltage magnitude, and finally settle to its steady-state. Hence, a stable operation was noted.

A great performance improvement was observed for 30^0 phase displacement between both the stator winding sets *abc* and *xyz*, when supplied by six-step voltage source inverter. Although the magnitude of stator current was found to increase, but a substantial decrease in motor torque harmonics was also observed. Hence, a smooth motor operation is achieved with less mechanical noise and vibration in the machine. Increase in stator current leads to increased heating of stationary stator, but it can be easily handled by a suitable cooling arrangement.

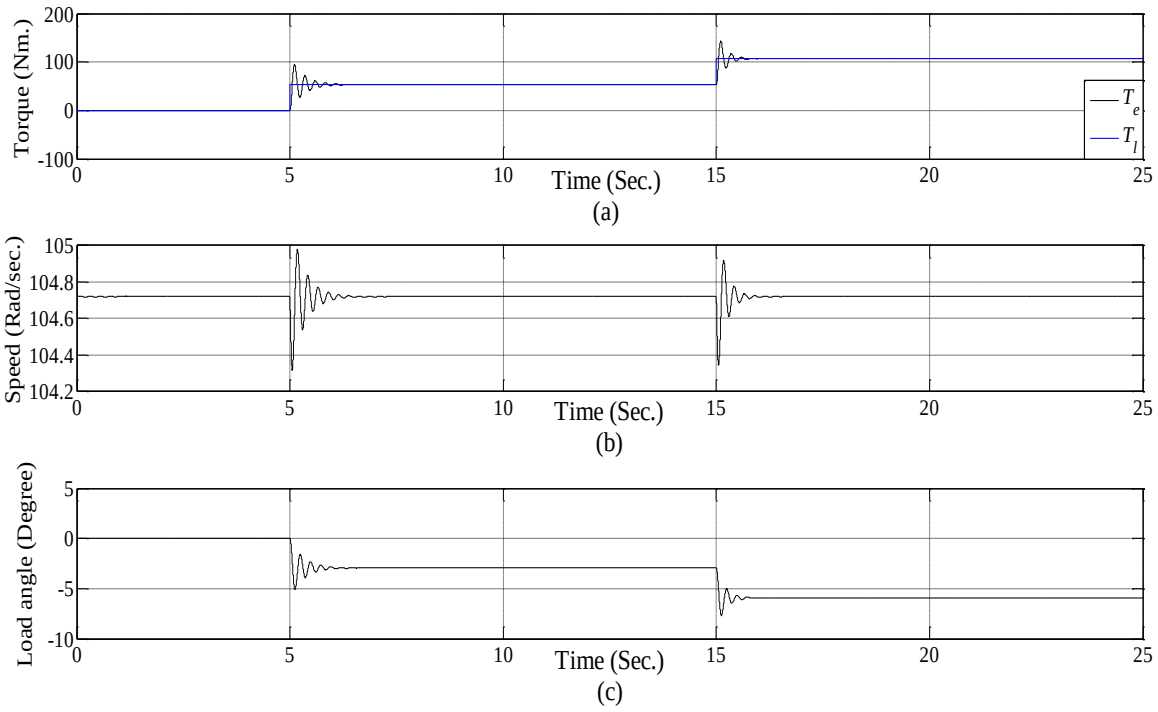

Fig. 2.4: Dynamic response of motor following the change in load torque showing (a) motor torque T_e (b) rotor speed ω_r (c) load angle, *delta*.

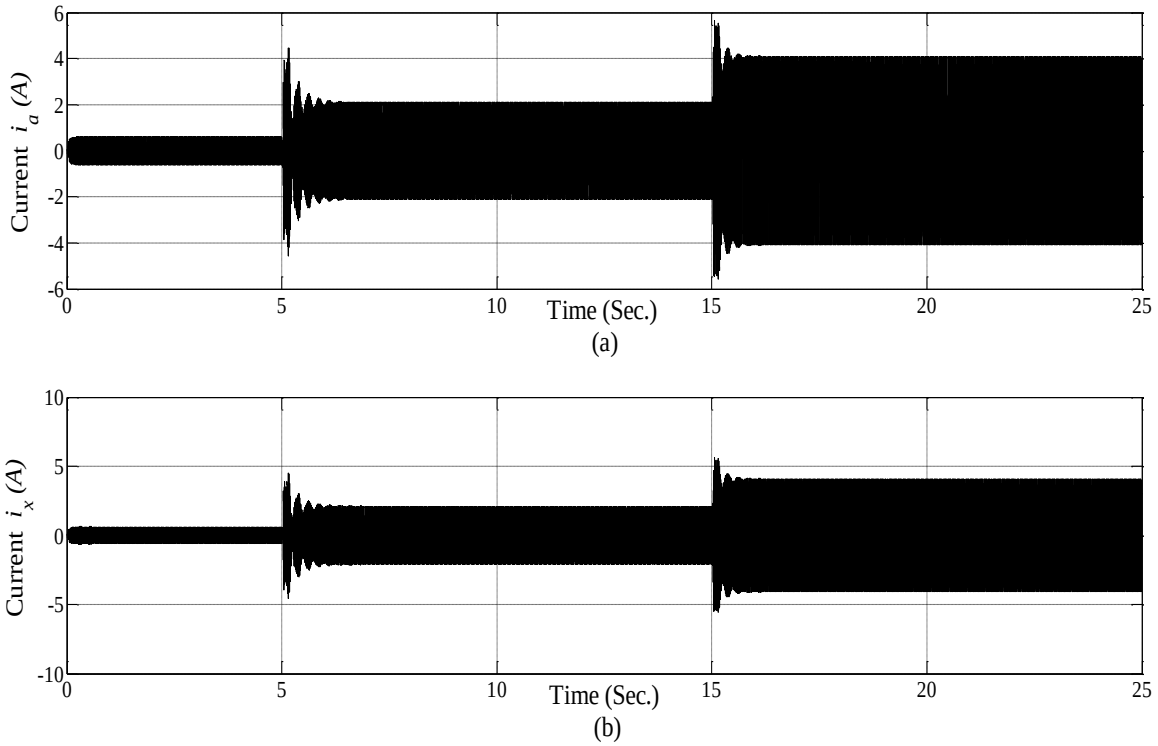

Fig. 2.5: Dynamic response of motor following the change in load torque showing stator currents (a) i_a (b) i_x.

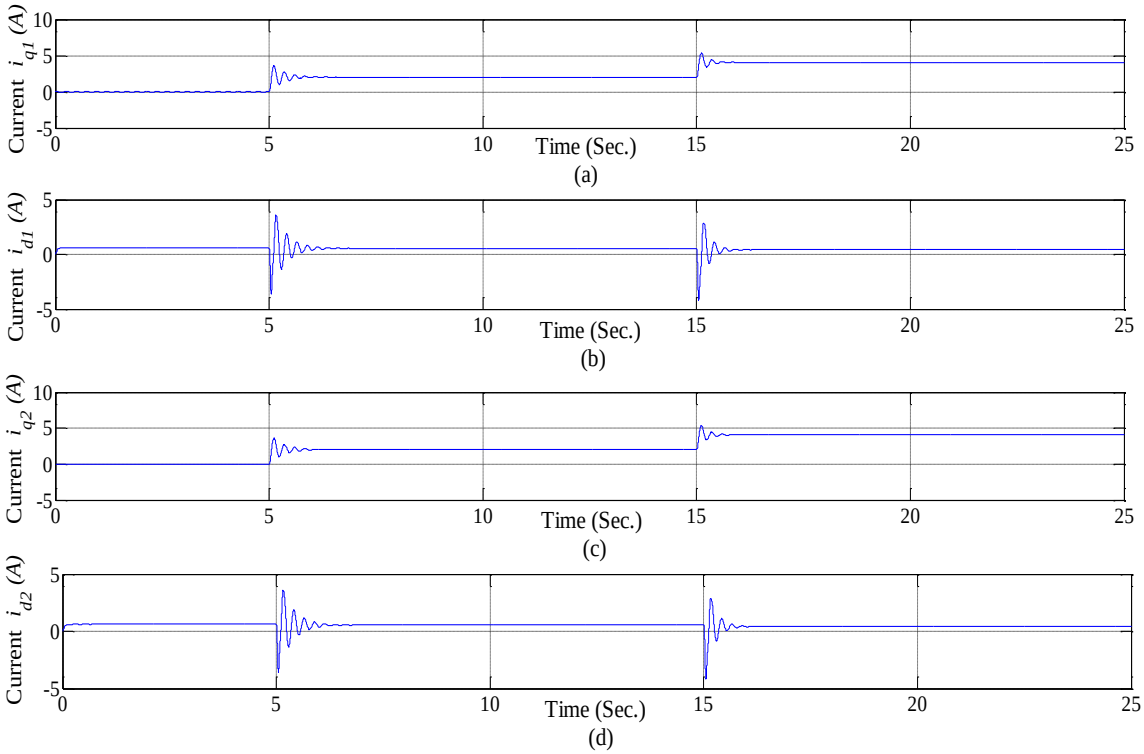

Fig. 2.6: Dynamic response of motor following the change in load torque showing stator currents (a) i_{q1} (b) i_{d1} (c) i_{q2} (d) $i_{d2.}$

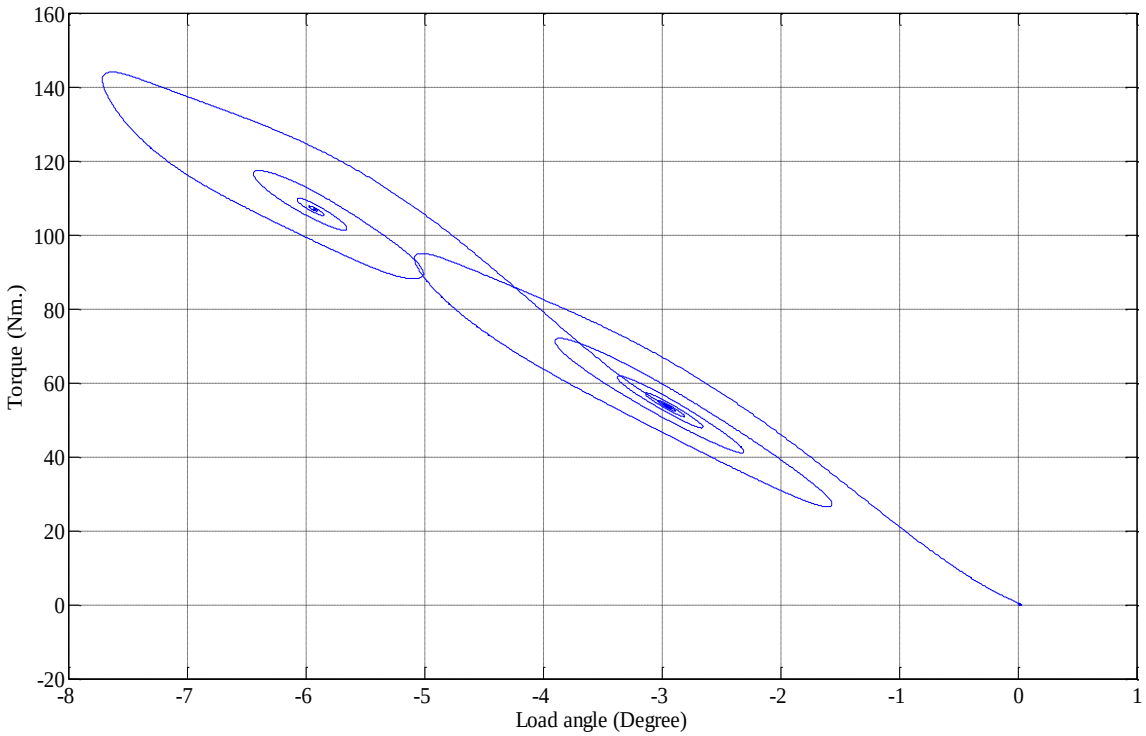

Fig. 2.7: Torque-angle characteristic during change in load torque.

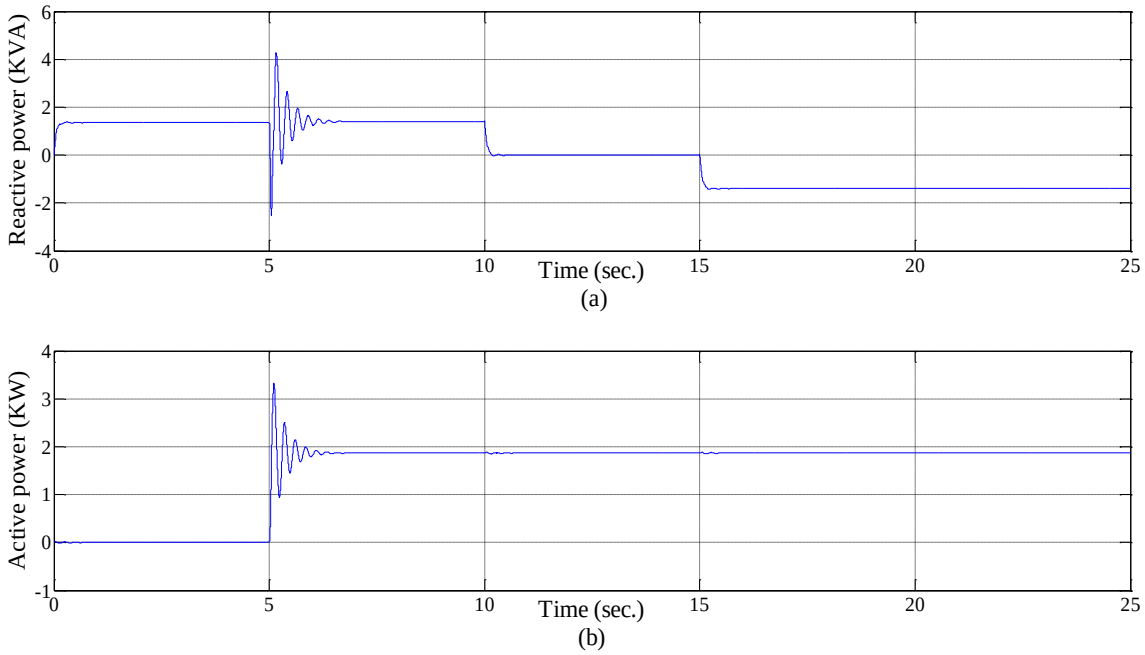

Fig. 2.8: Dynamic response of motor during change in field excitation showing (a) reactive power and (b) active power.

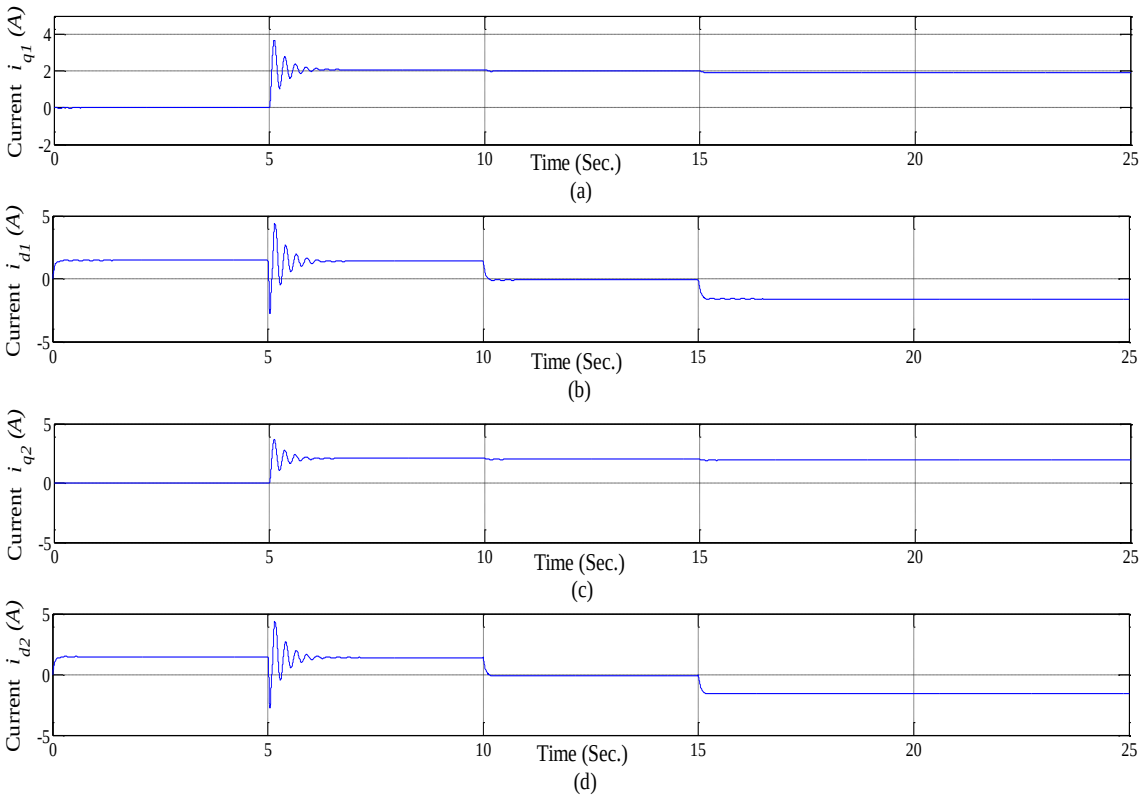

Fig. 2.9: Dynamic response of motor during change in field excitation showing stator currents (a) i_{q1} (b) i_{d1} (c) i_{q2} (d) $i_{d2.}$

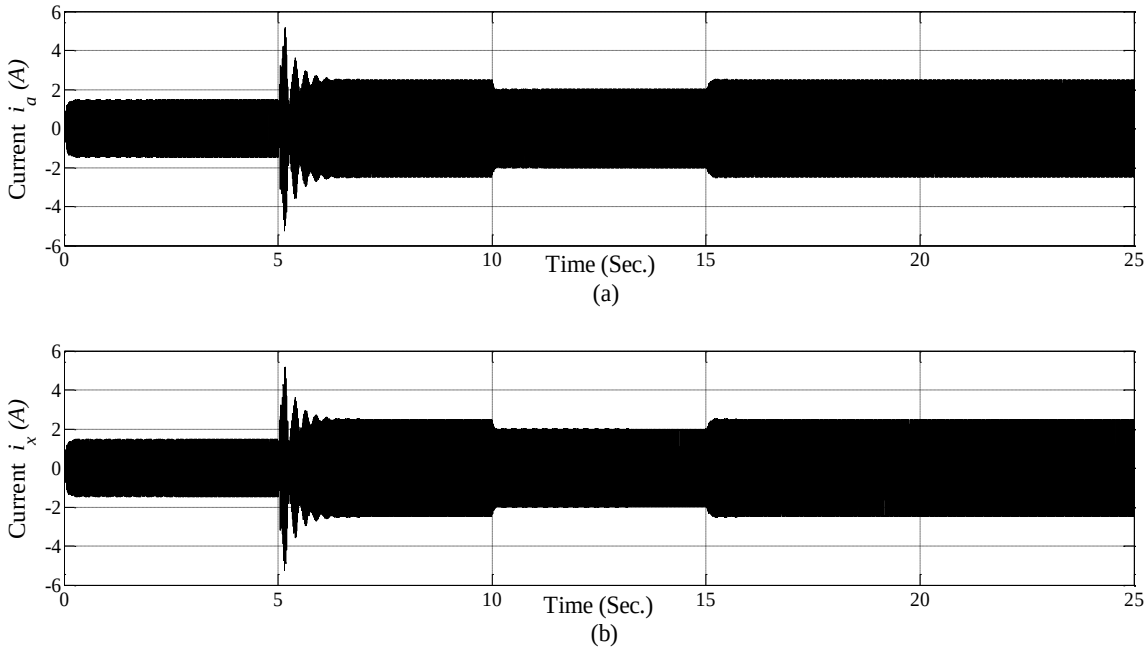

Fig. 2.10: Dynamic response of motor during change in field excitation showing stator currents (a) i_a (b) i_x.

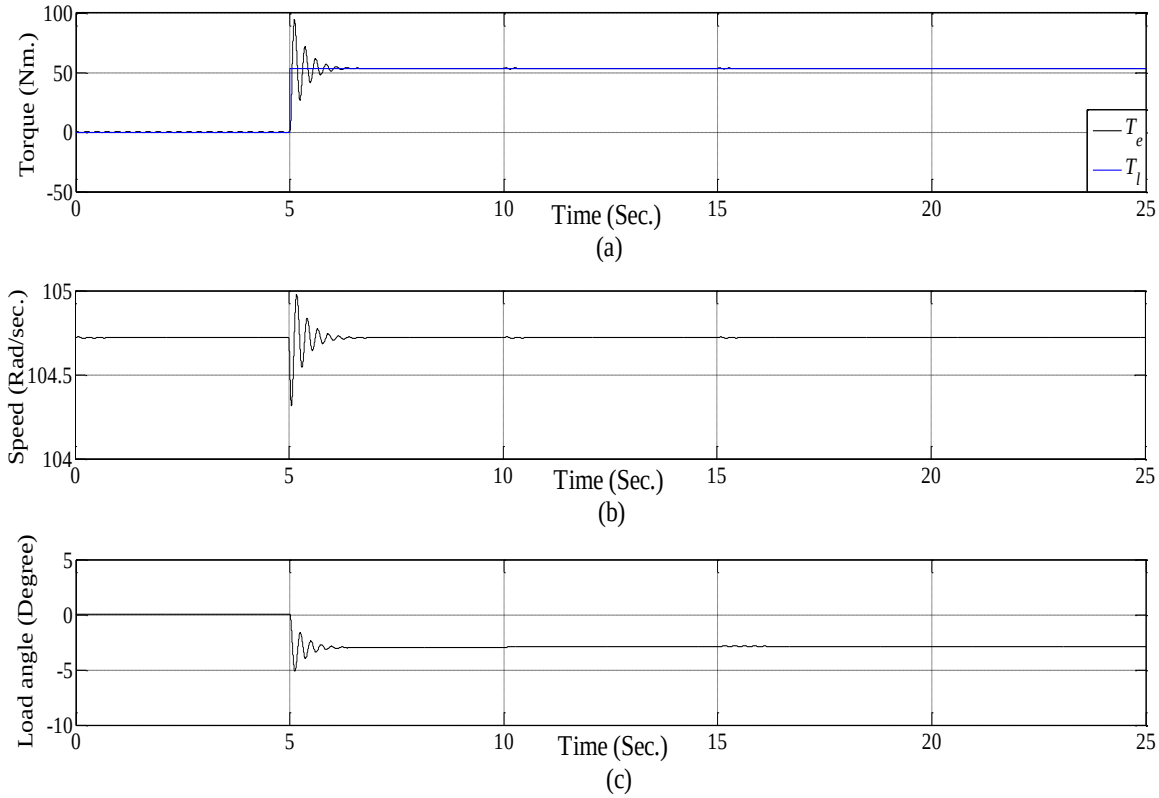

Fig. 2.11: Dynamic response of motor during change in field excitation showing (a) motor torque T_e (b) rotor speed ω_r (c) load angle, *delta*.

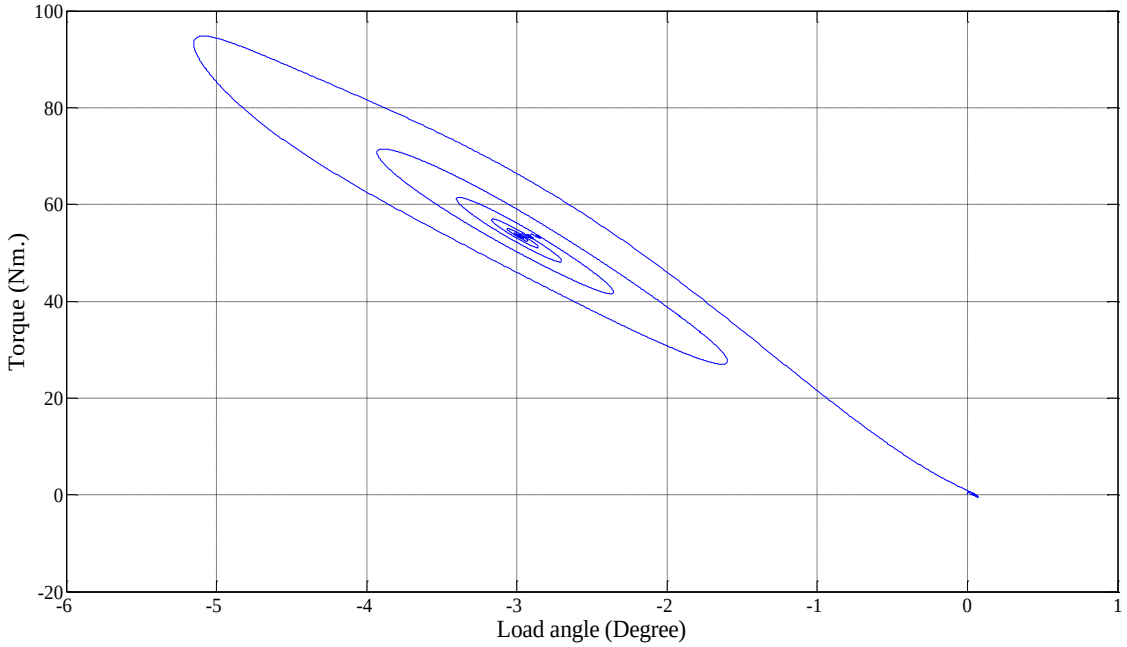

Fig. 2.12: Torque-angle characteristic during change in field excitation.

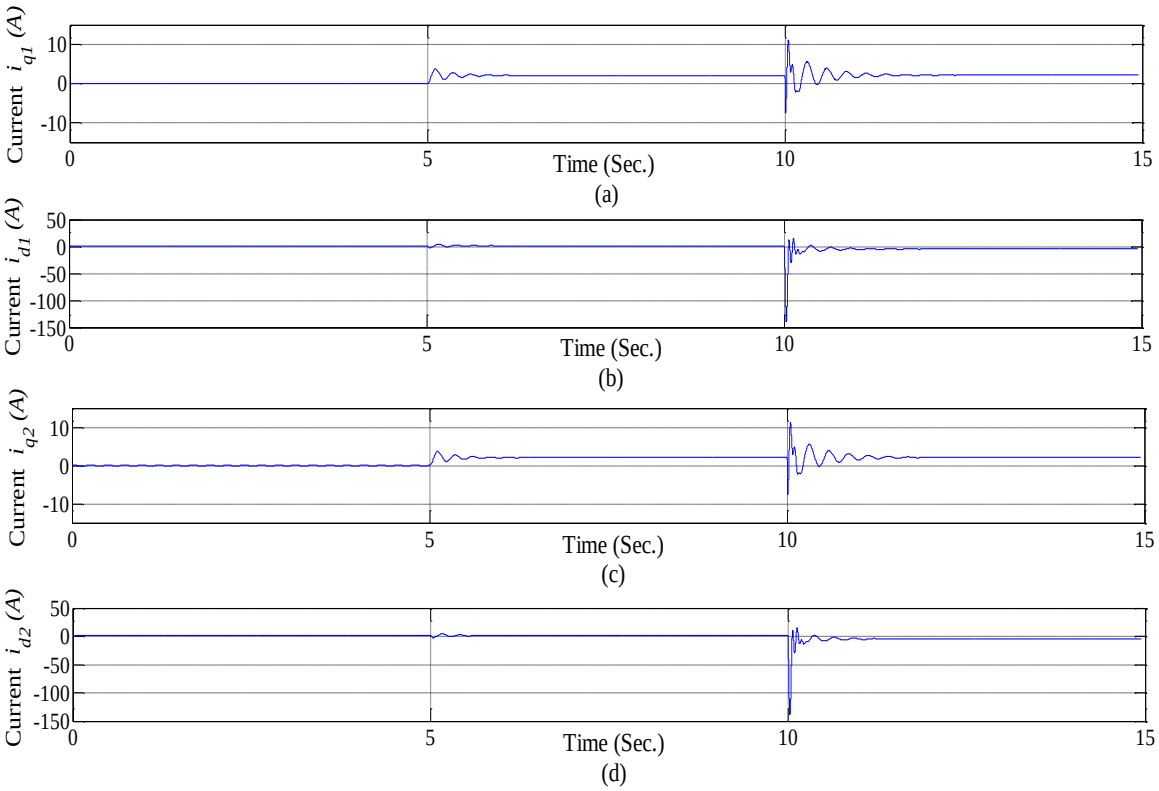

Fig. 2.13: Dynamic response of motor during change in input voltage showing stator currents (a) i_{q1} (b) i_{d1} (c) i_{q2} (d) i_{d2}.

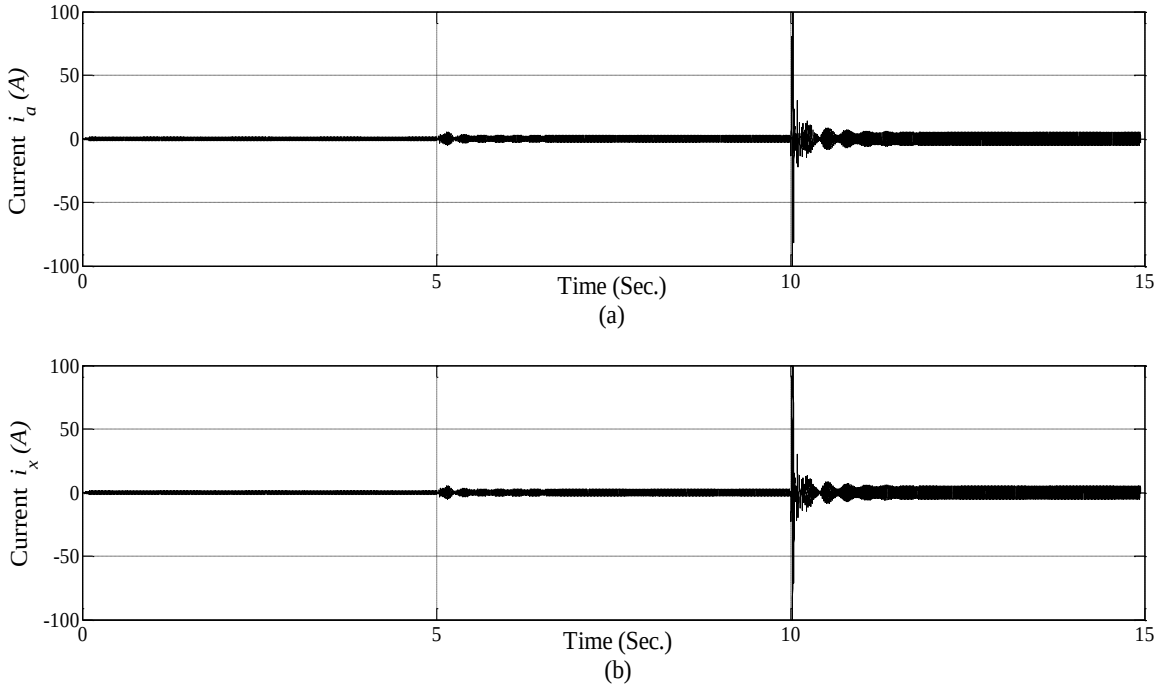

Fig. 2.14: Dynamic response of motor during change in input voltage showing stator currents (a) i_a (b) i_x.

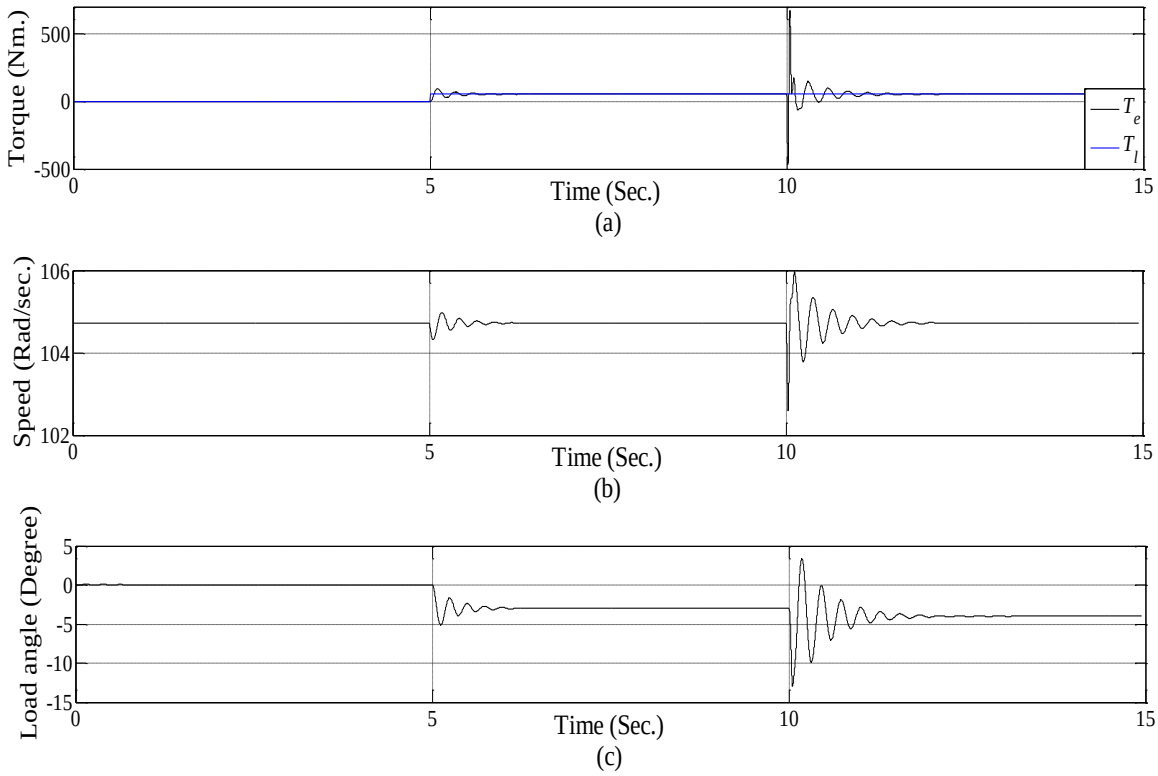

Fig. 2.15: Dynamic response of motor during change in input voltage showing (a) motor torque T_e (b) rotor speed ω_r (c) load angle, *delta*.

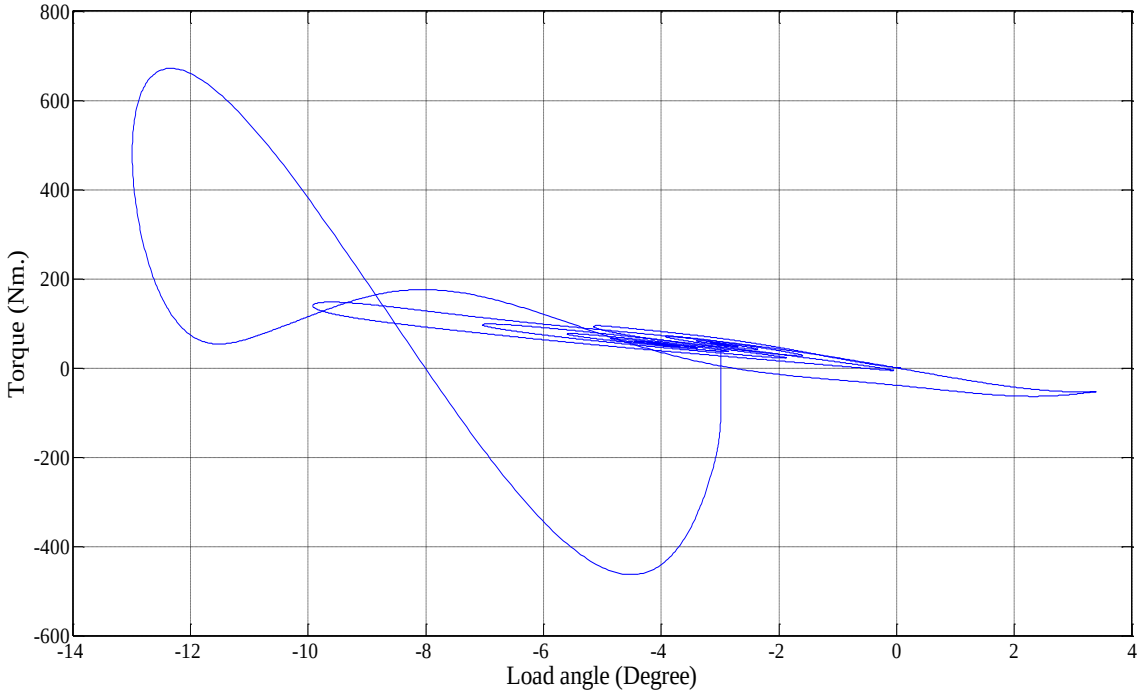

Fig. 2.16: Torque-angle characteristic during change in input voltage.

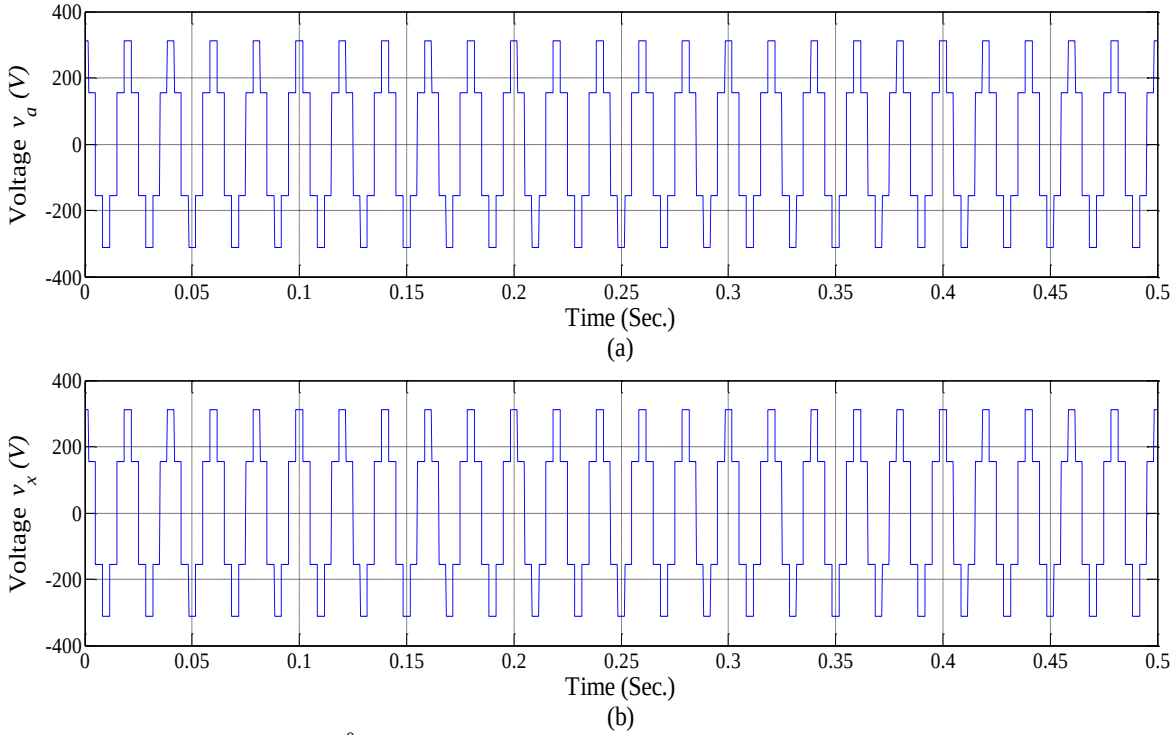

Fig. 2.17: Input phase voltage with 0^0 displacement between stator winding sets showing (a) v_a (b) v_x.

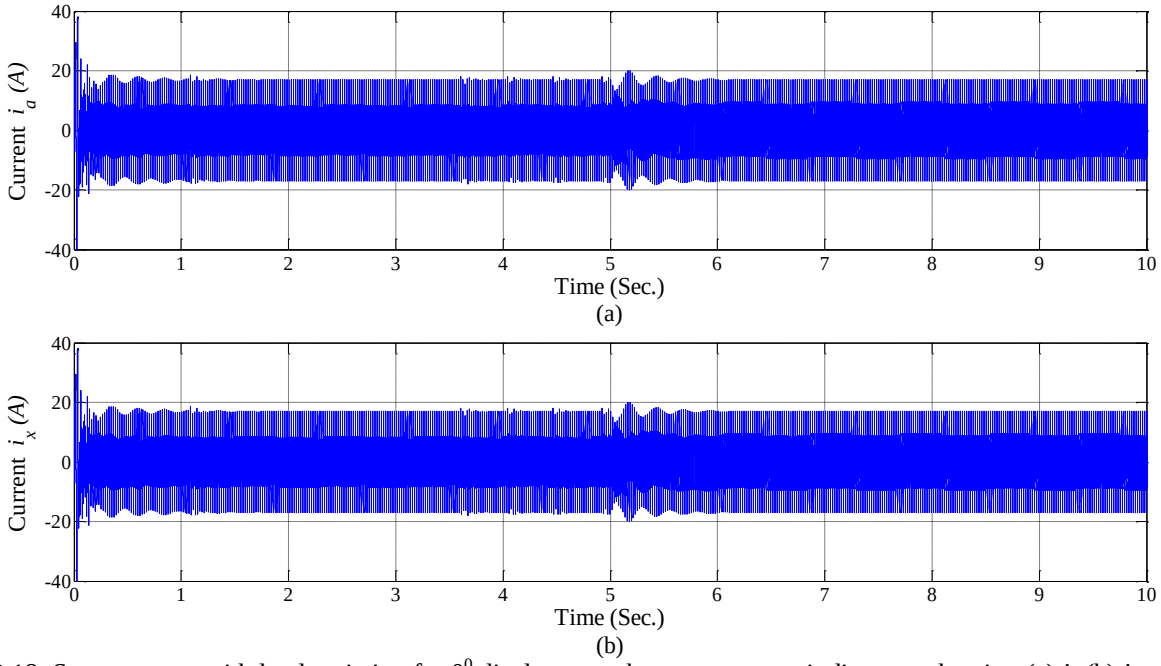

Fig. 2.18: Stator current with load variation for 0^0 displacement between stator winding sets showing (a) i_a (b) i_x.

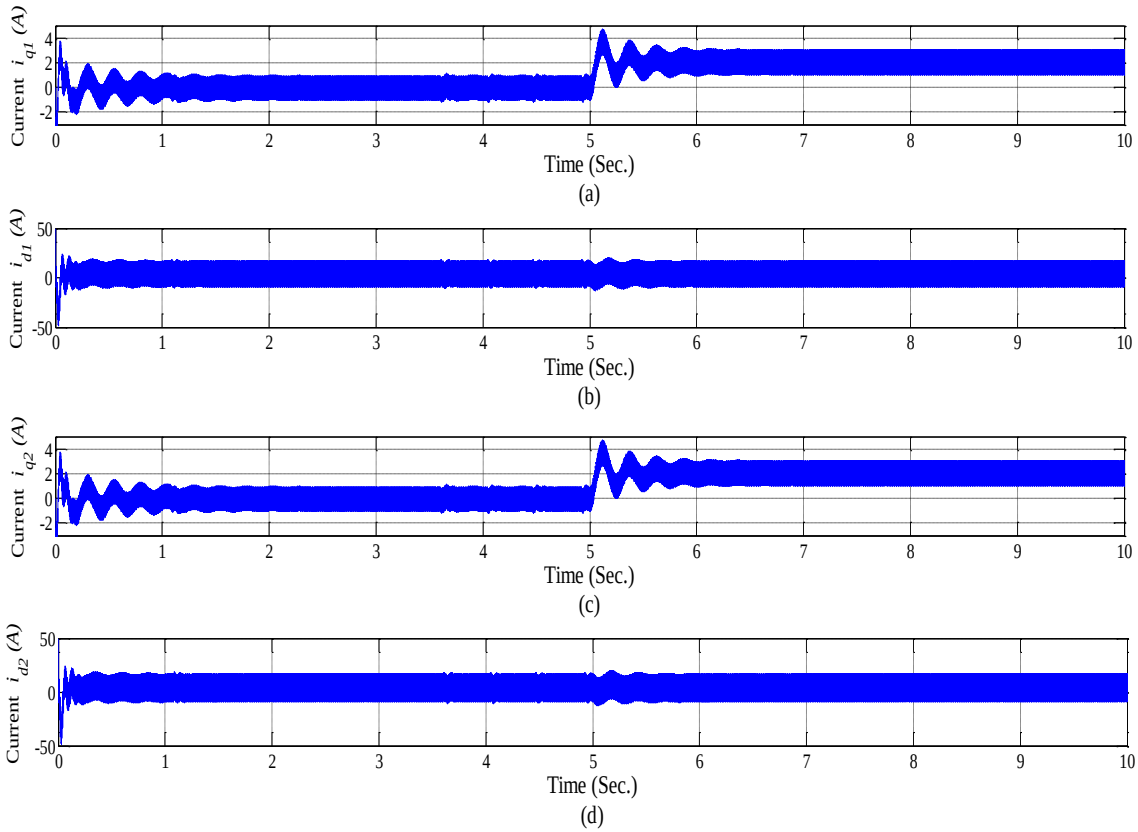

Fig. 2.19: Dynamic response of motor with load variation for 0^0 displacement between stator winding sets showing stator currents (a) i_{q1} (b) i_{d1} (c) i_{q2} (d) $i_{d2.}$

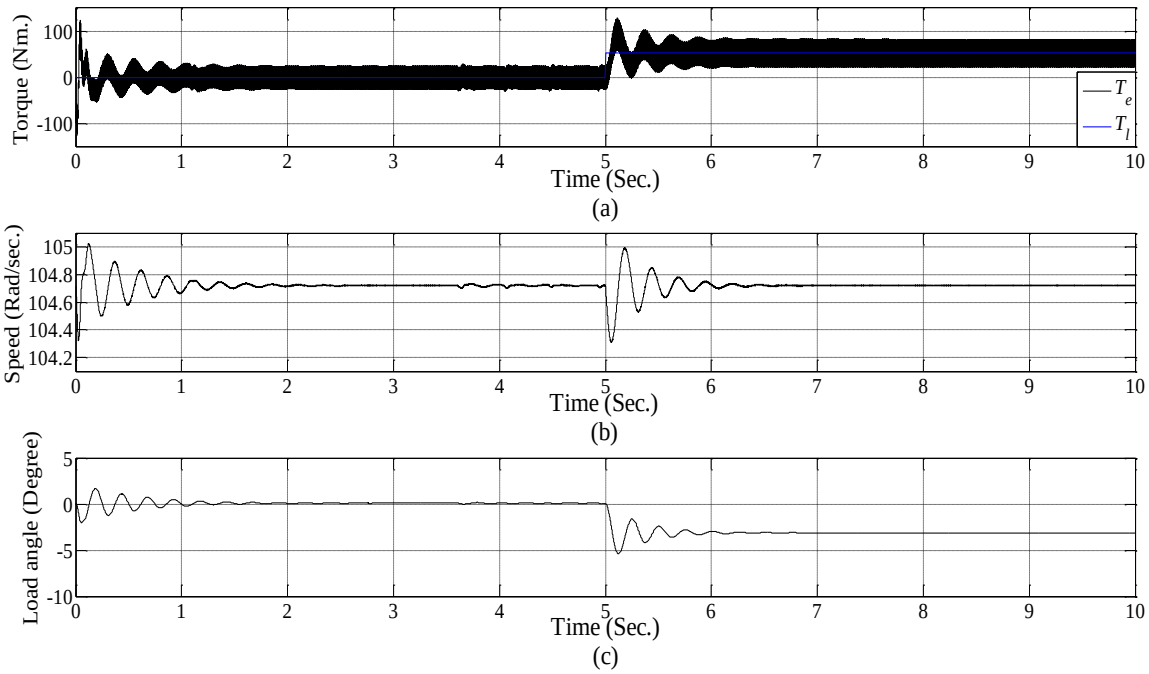

Fig. 2.20: Dynamic response of motor during load variation with 0^0 displacement between stator winding sets showing (a) motor torque T_e (b) rotor speed ω_r (c) load angle, *delta.*

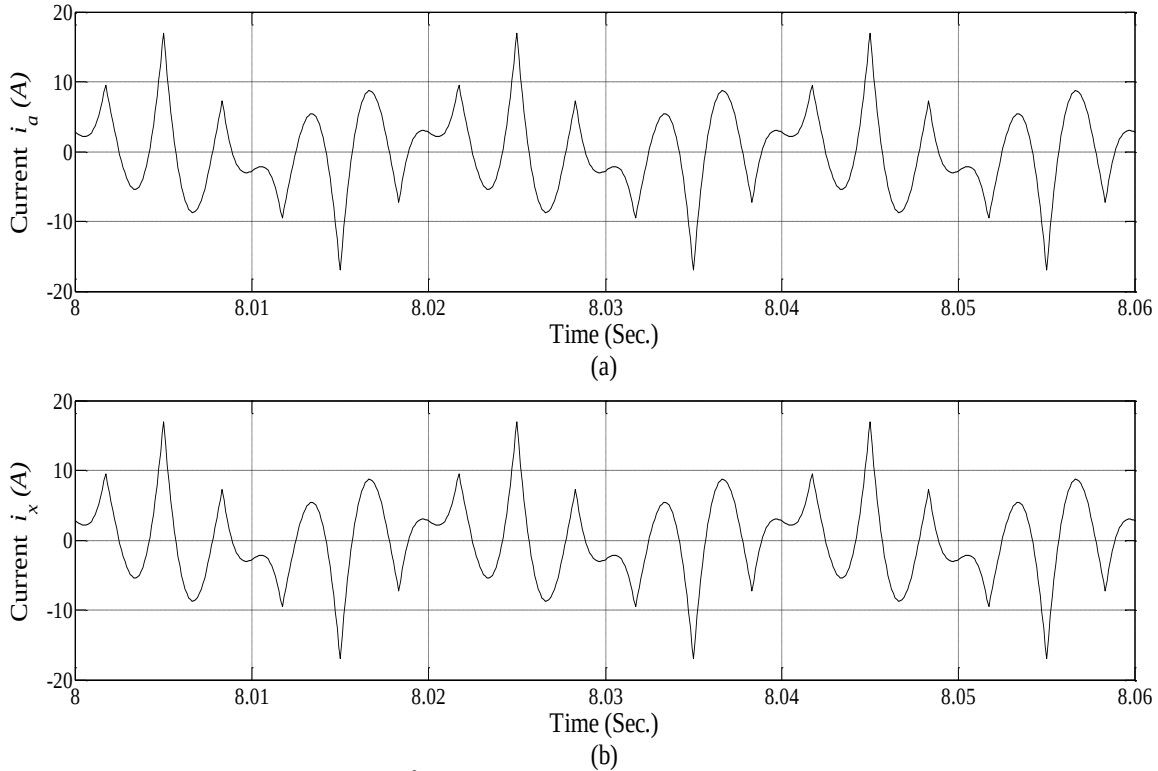

Fig. 2.21: Steady-state phase current with 0^0 displacement between stator winding sets showing (a) i_a (b) i_x.

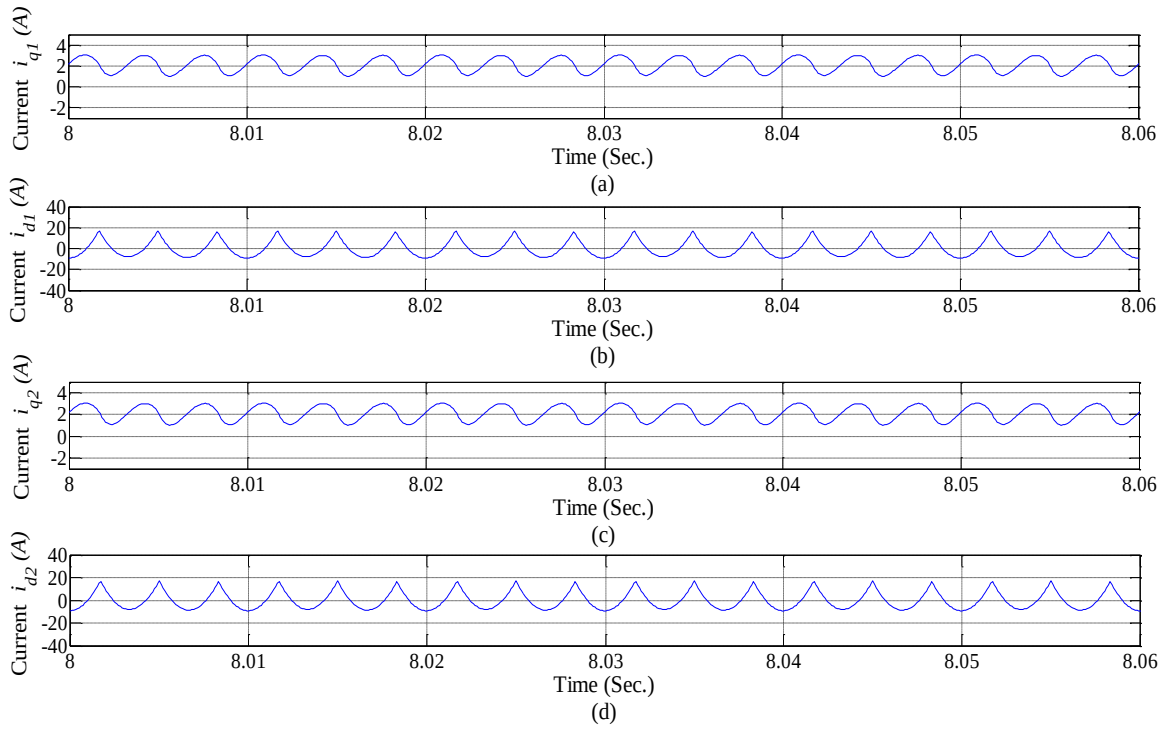

Fig. 2.22: Steady-state phase current with 0^0 displacement between stator winding sets showing (a) i_{q1} (b) i_{d1} (c) i_{q2} (d) $i_{d2.}$

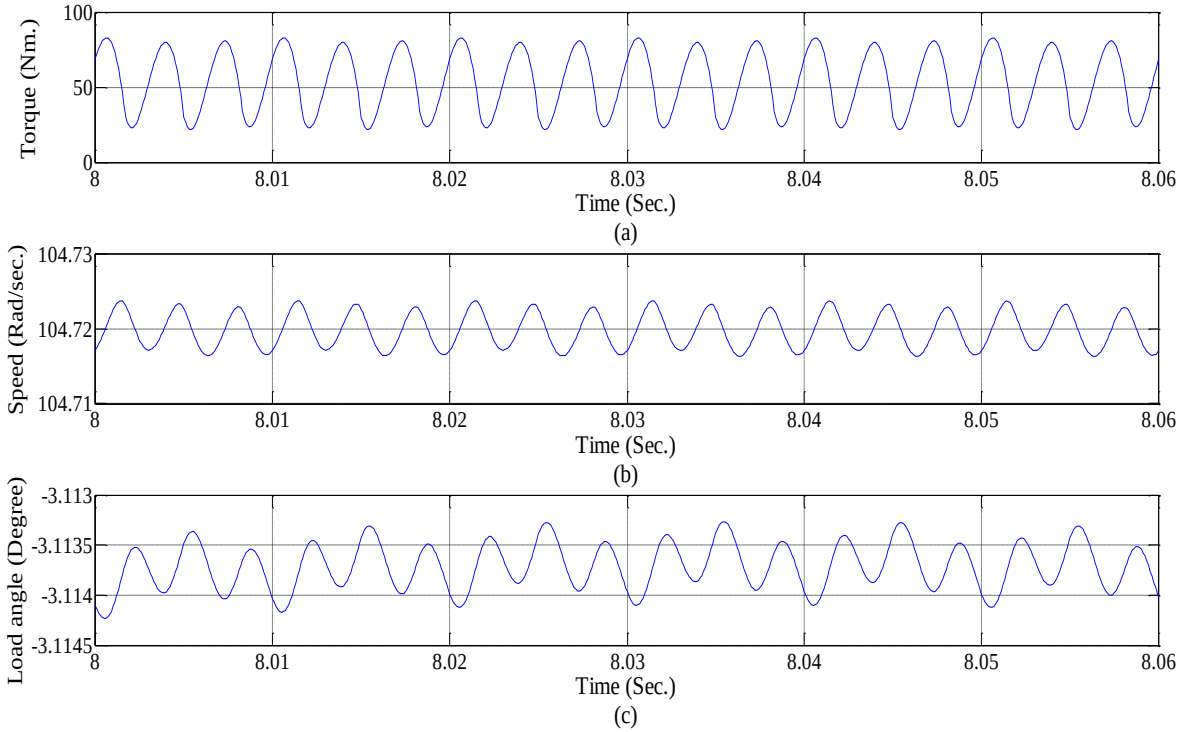

Fig. 2.23: Steady-state motor response with 0^0 displacement between stator winding sets showing (a) motor torque T_e (b) rotor speed ω_r (c) load angle, *delta*.

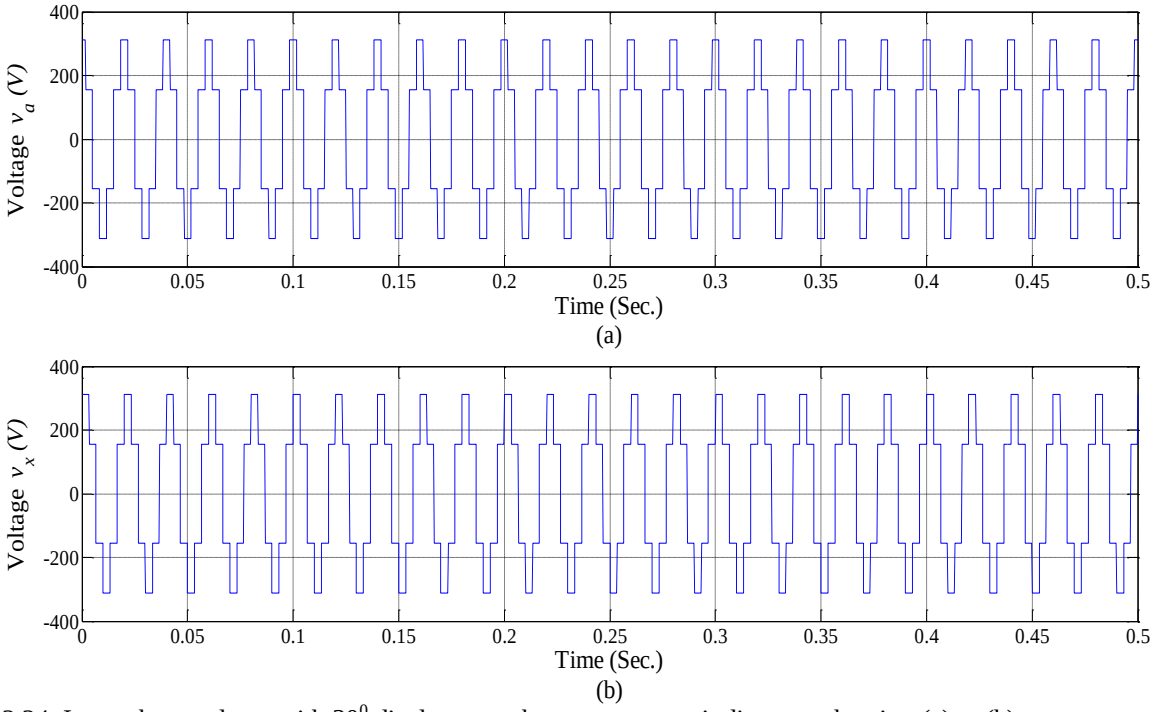

Fig. 2.24: Input phase voltage with 30^0 displacement between stator winding sets showing (a) v_a (b) v_x.

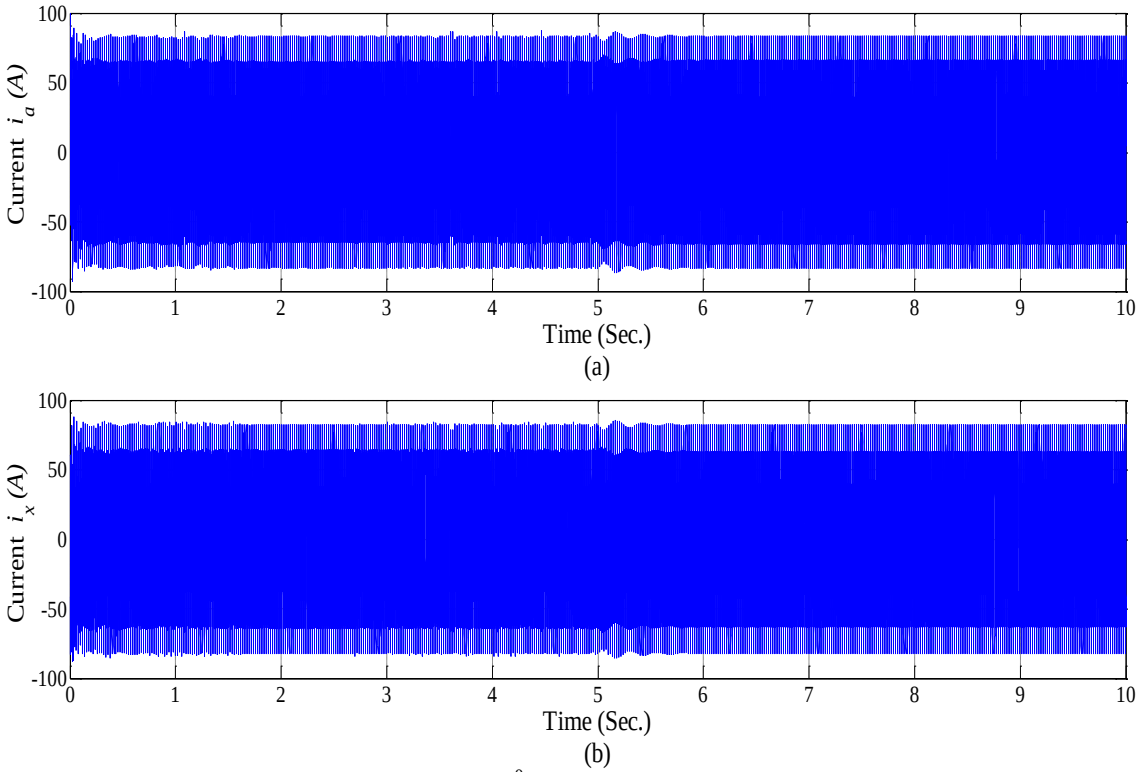

Fig. 2.25: Stator current during load variation with 30^0 displacement between stator winding sets showing (a) i_a (b) i_x.

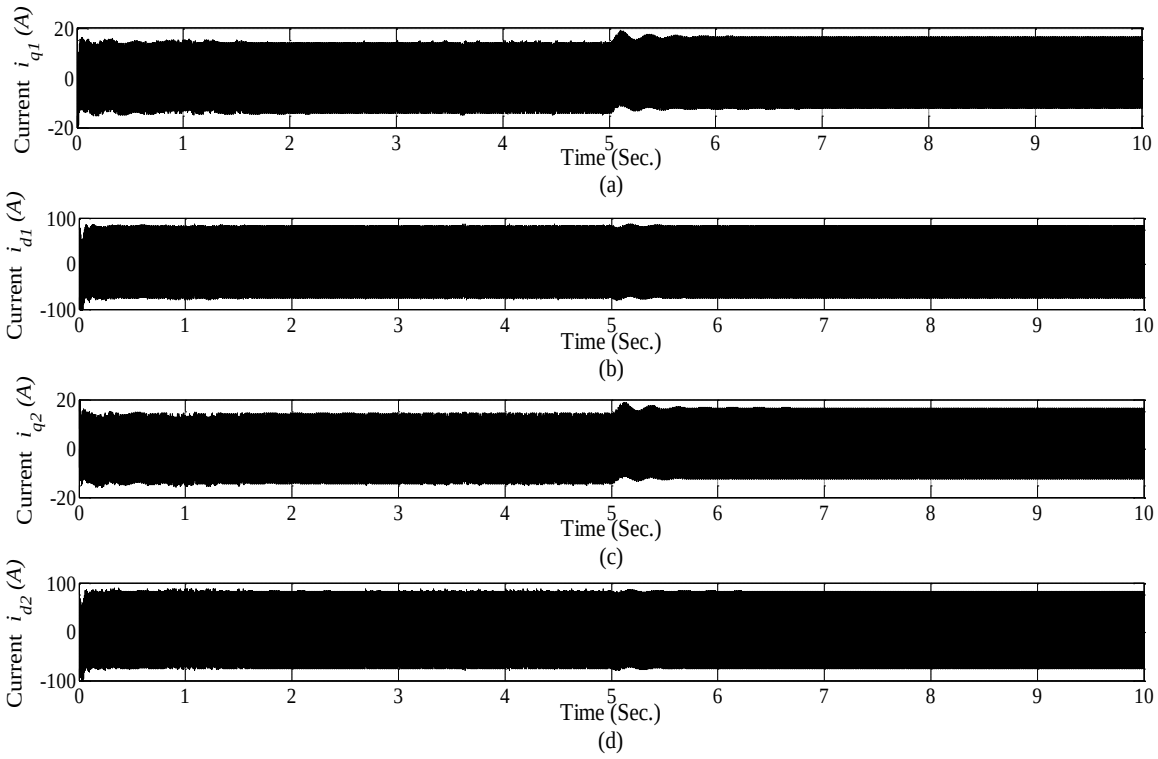

Fig. 2.26: Dynamic response of motor during load variation with 30^0 displacement between stator winding sets showing stator currents (a) i_{q1} (b) i_{d1} (c) i_{q2} (d) i_{d2}.

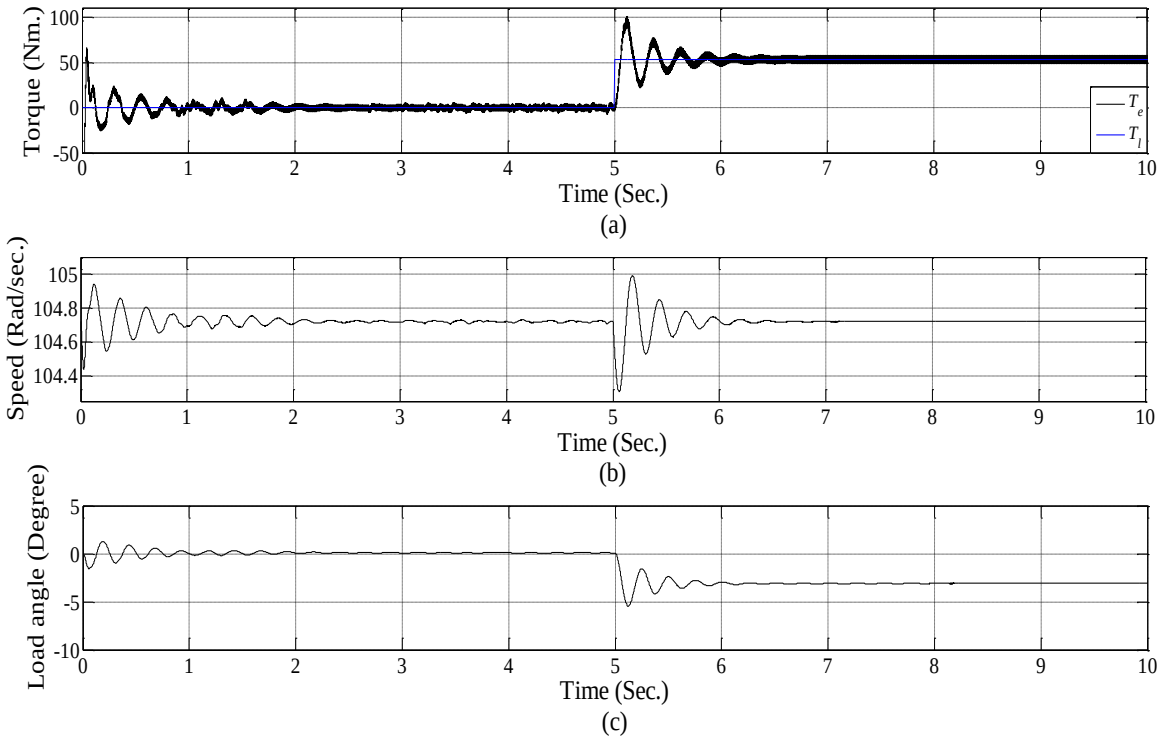

Fig. 2.27: Dynamic response of motor during load variation with 30^0 displacement between stator winding sets showing (a) motor torque T_e (b) rotor speed ω_r (c) load angle, *delta*.

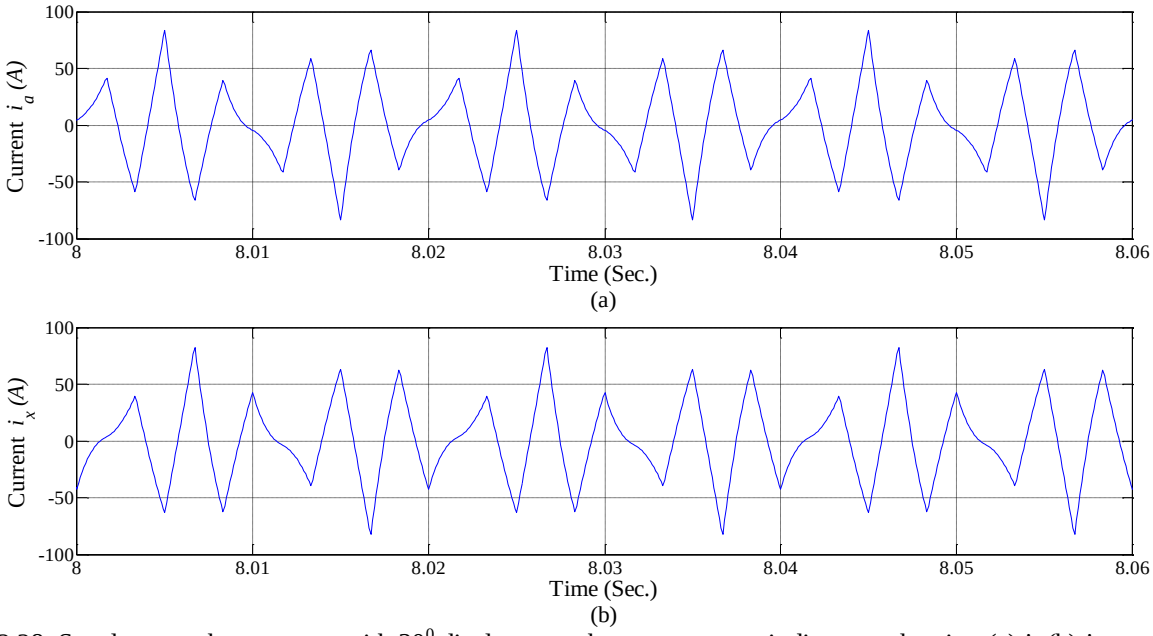

Fig. 2.28: Steady-state phase current with 30^0 displacement between stator winding sets showing (a) i_a (b) i_x.

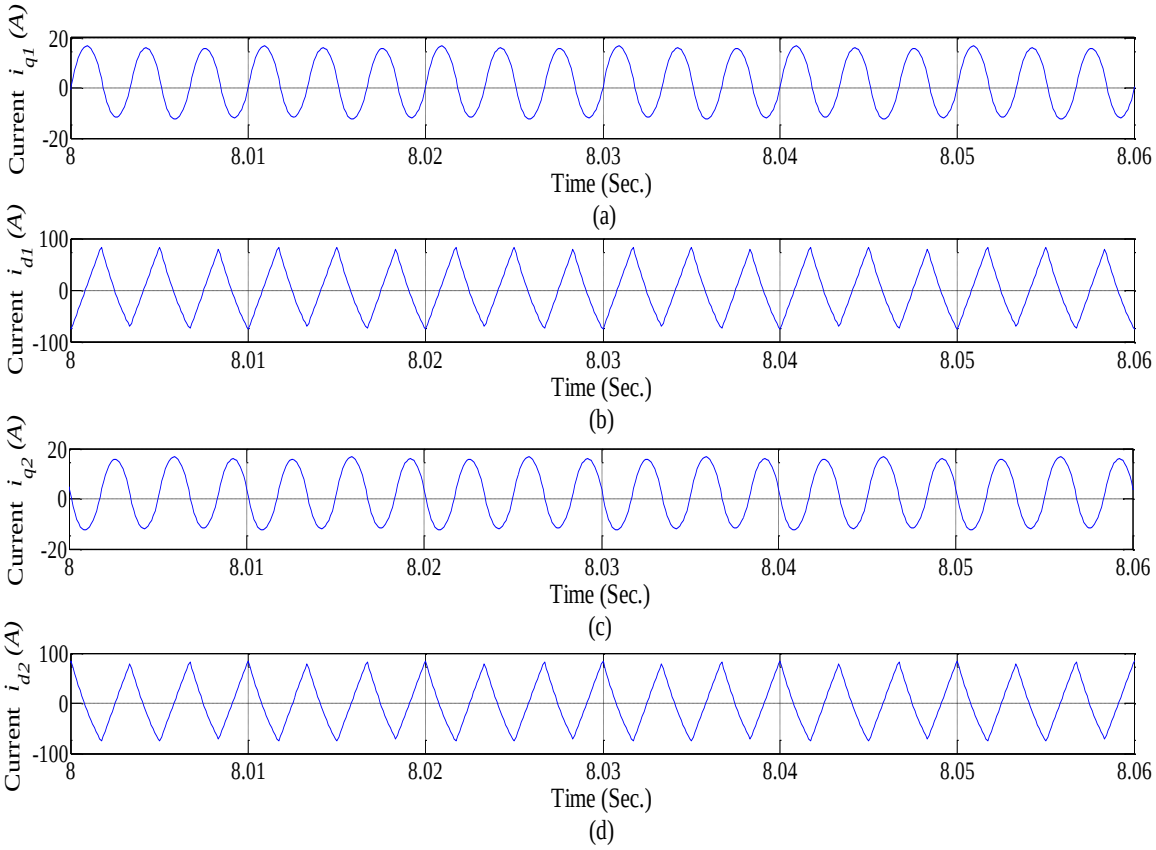

Fig. 2.29: Steady-state phase current with 30^0 displacement between stator winding sets showing (a) i_{q1} (b) i_{d1} (c) i_{q2} (d) $i_{d2.}$

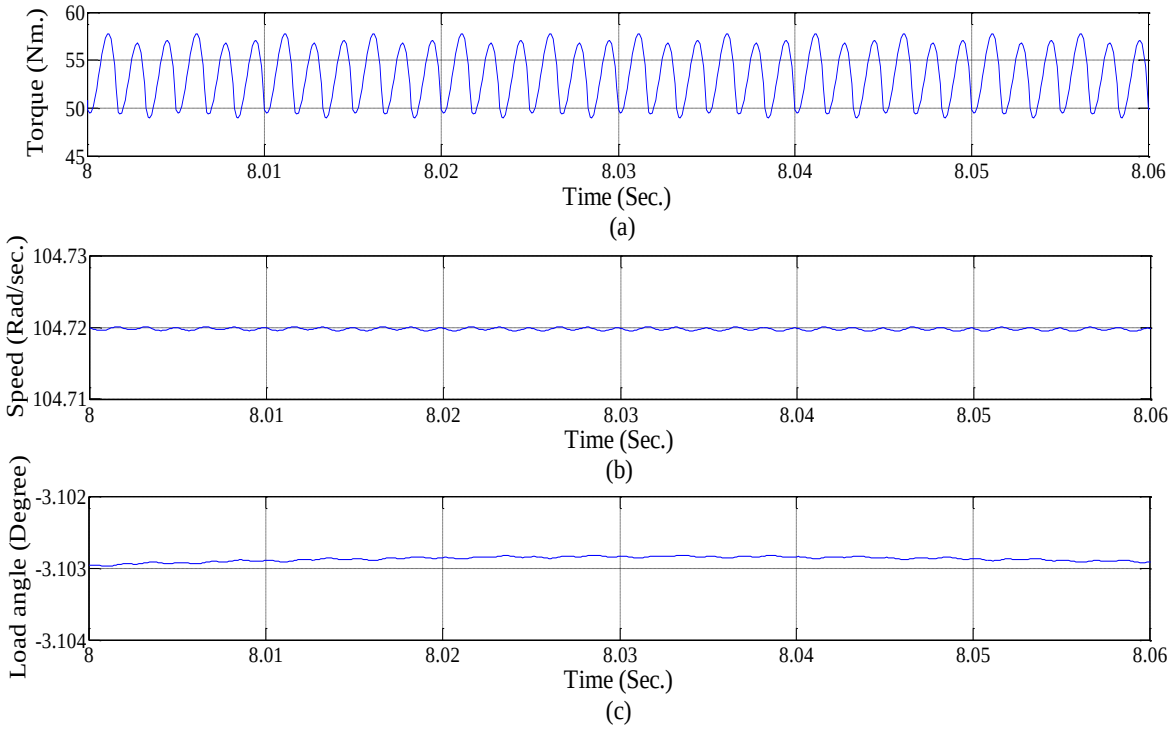

Fig. 2.30: Steady-state motor response with 30^0 displacement between stator winding sets showing (a) motor torque T_e (b) rotor speed ω_r (c) load angle, *delta*.

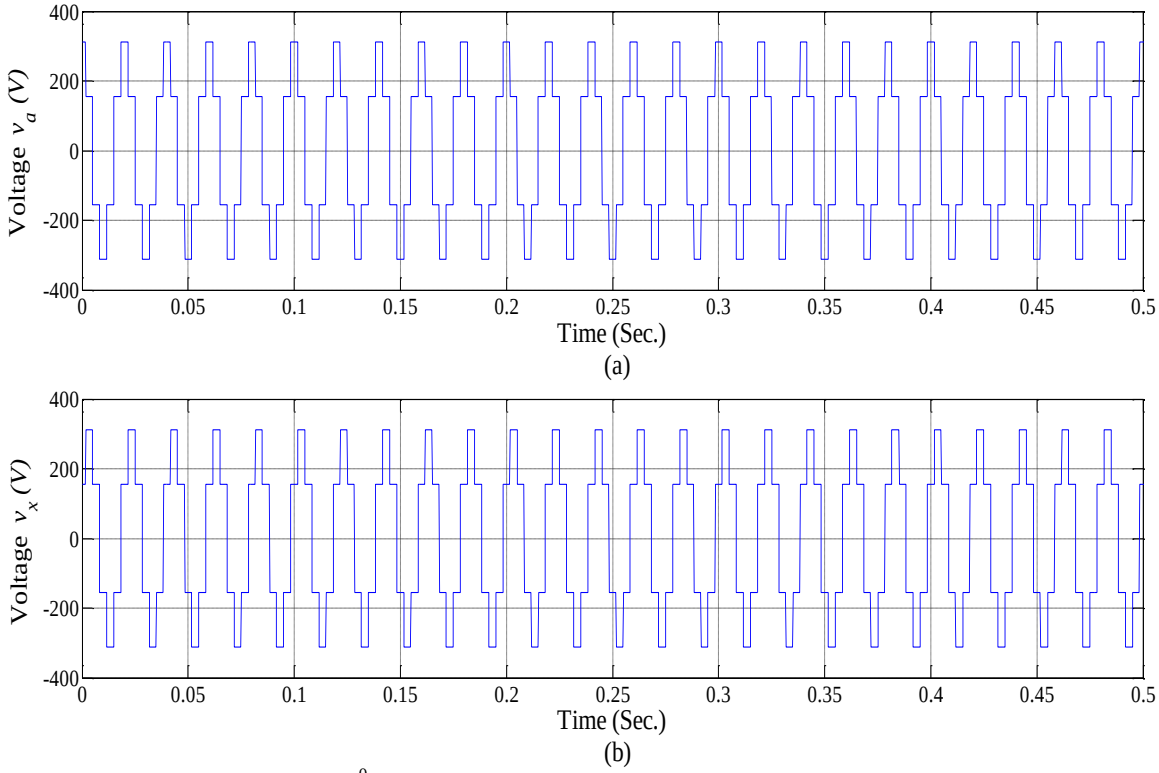

Fig. 2.31: Input phase voltage with 60^0 displacement between stator winding sets showing (a) v_a (b) v_x.

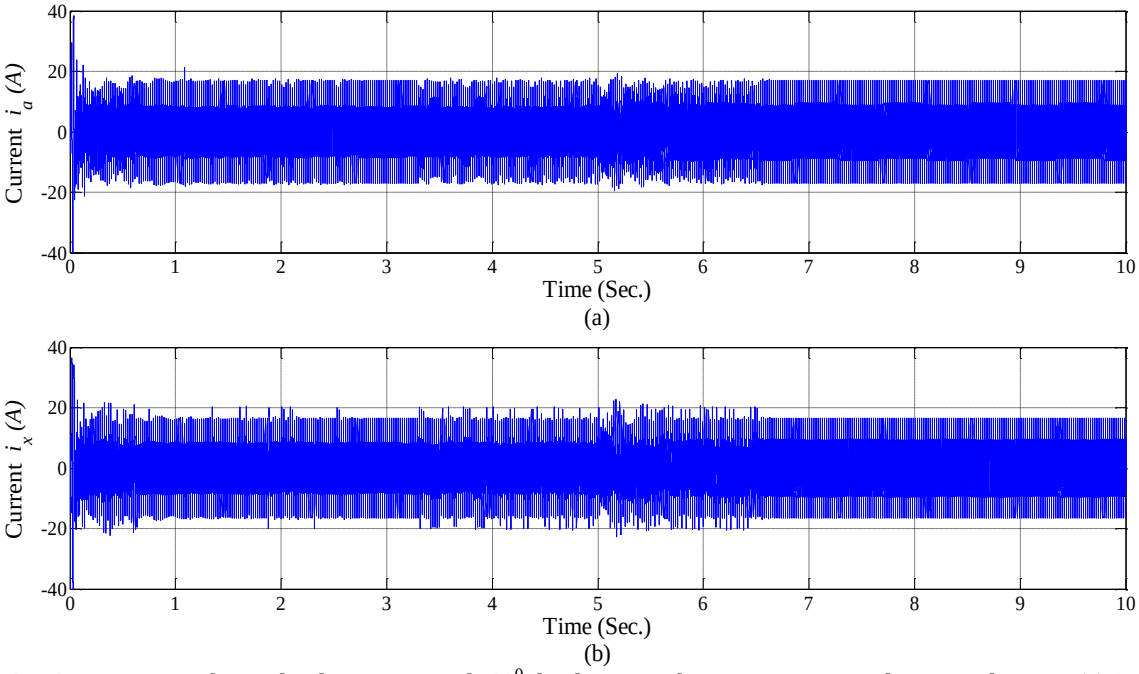

Fig. 2.32: Stator current during load variation with 60^0 displacement between stator winding sets showing (a) i_a (b) i_x.

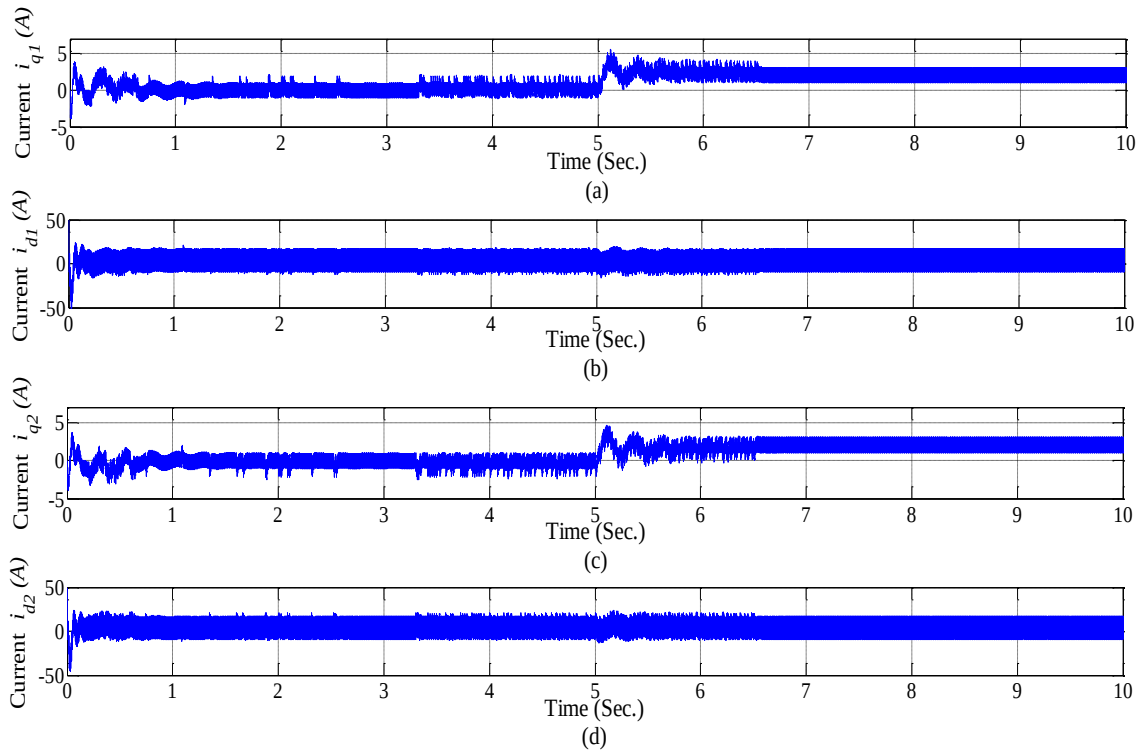

Fig. 2.33: Dynamic response of motor during load variation with 60^0 displacement between stator winding sets showing stator currents (a) i_{q1} (b) i_{d1} (c) i_{q2} (d) i_{d2}.

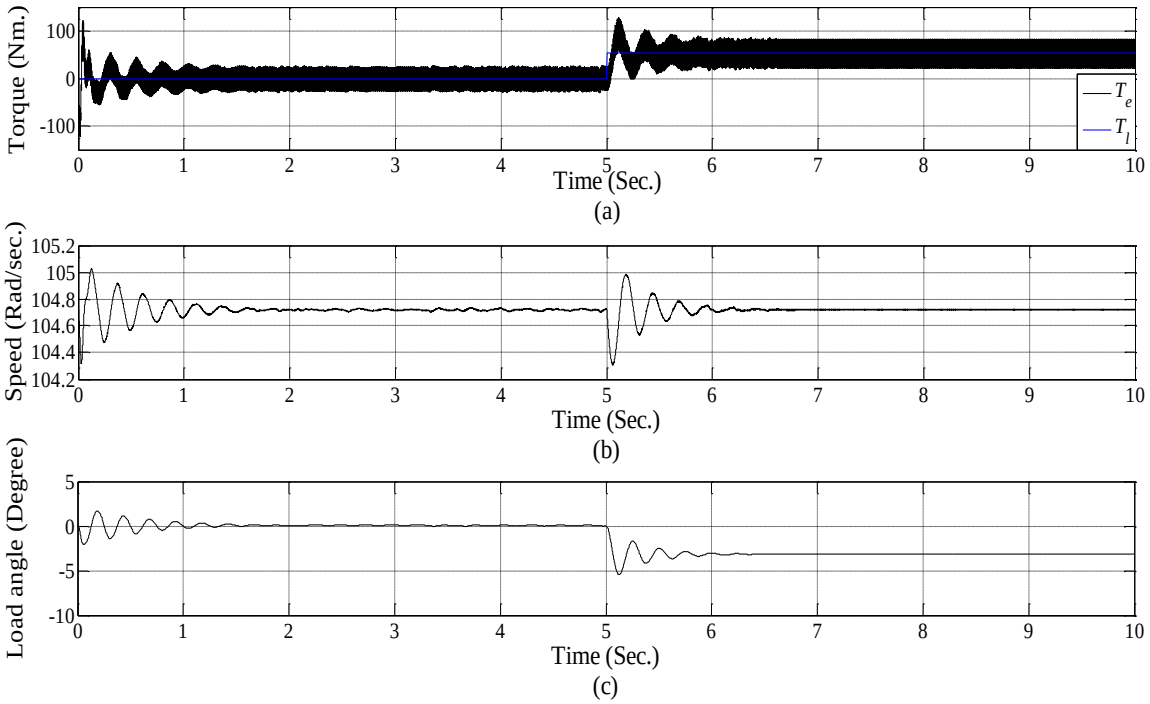

Fig. 2.34: Dynamic response of motor during load variation with 60^0 displacement between stator winding sets showing (a) motor torque T_e (b) rotor speed ω_r (c) load angle, *delta*.

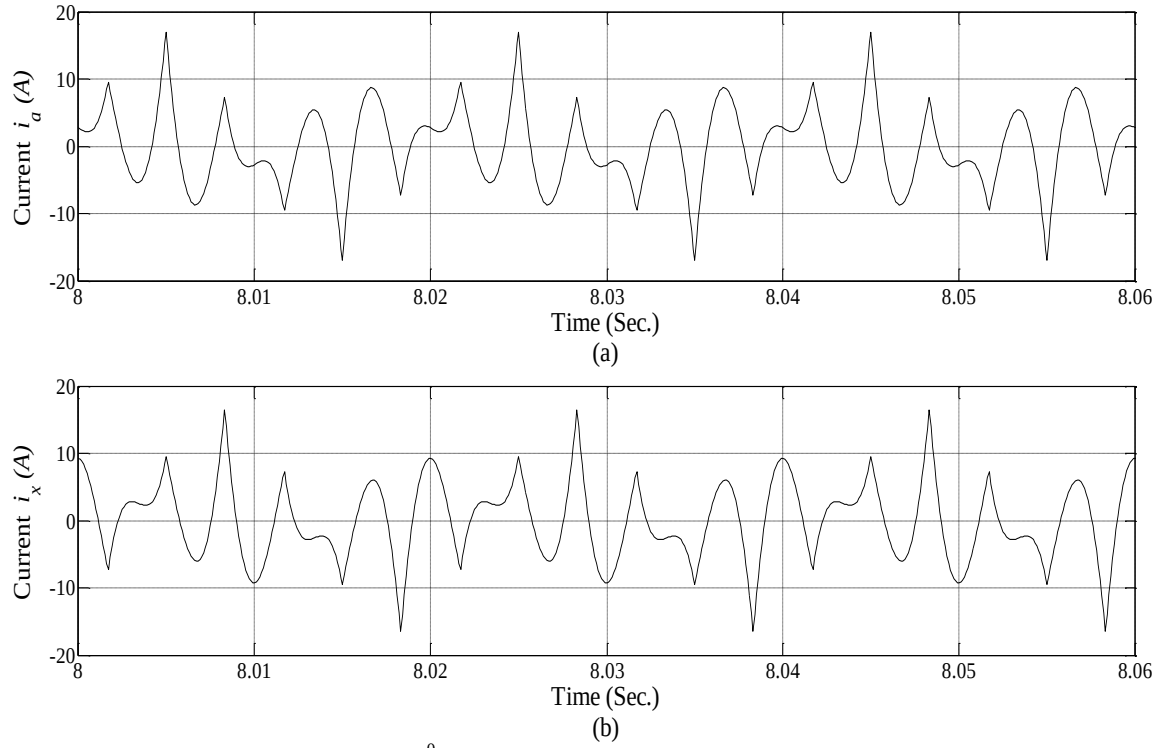

Fig. 2.35: Steady-state phase current with 60^0 displacement between stator winding sets showing (a) i_a (b) i_x.

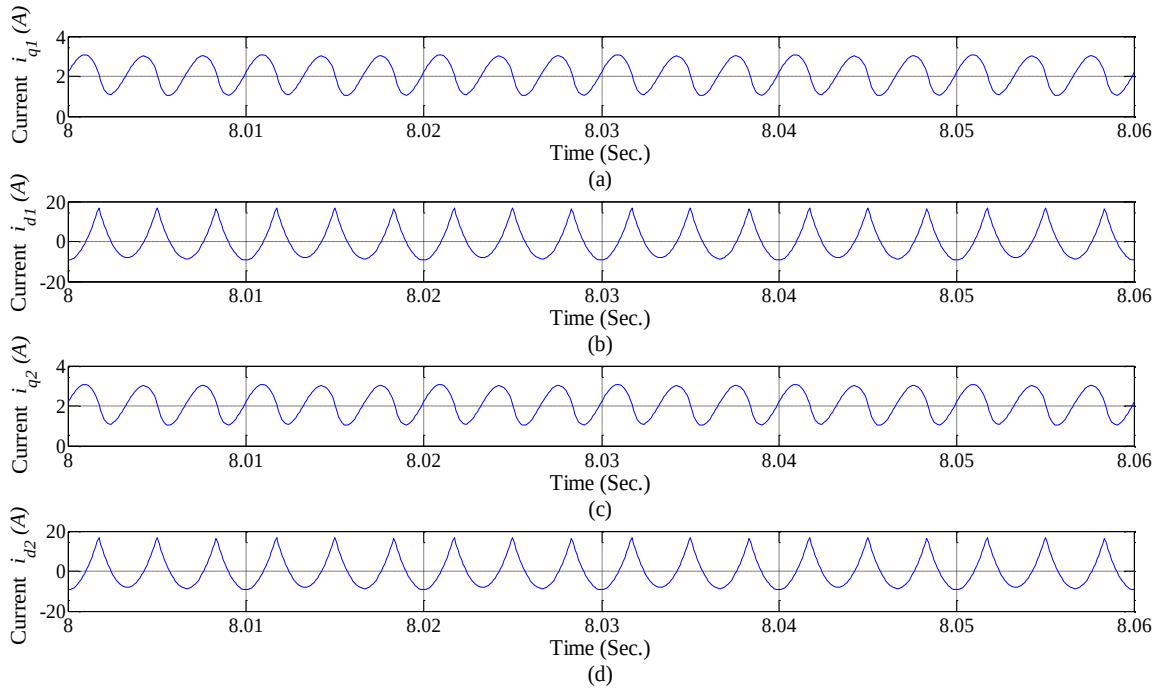

Fig. 2.36: Steady-state phase current with 60^0 displacement between stator winding sets showing (a) i_{q1} (b) i_{d1} (c) i_{q2} (d) $i_{d2.}$

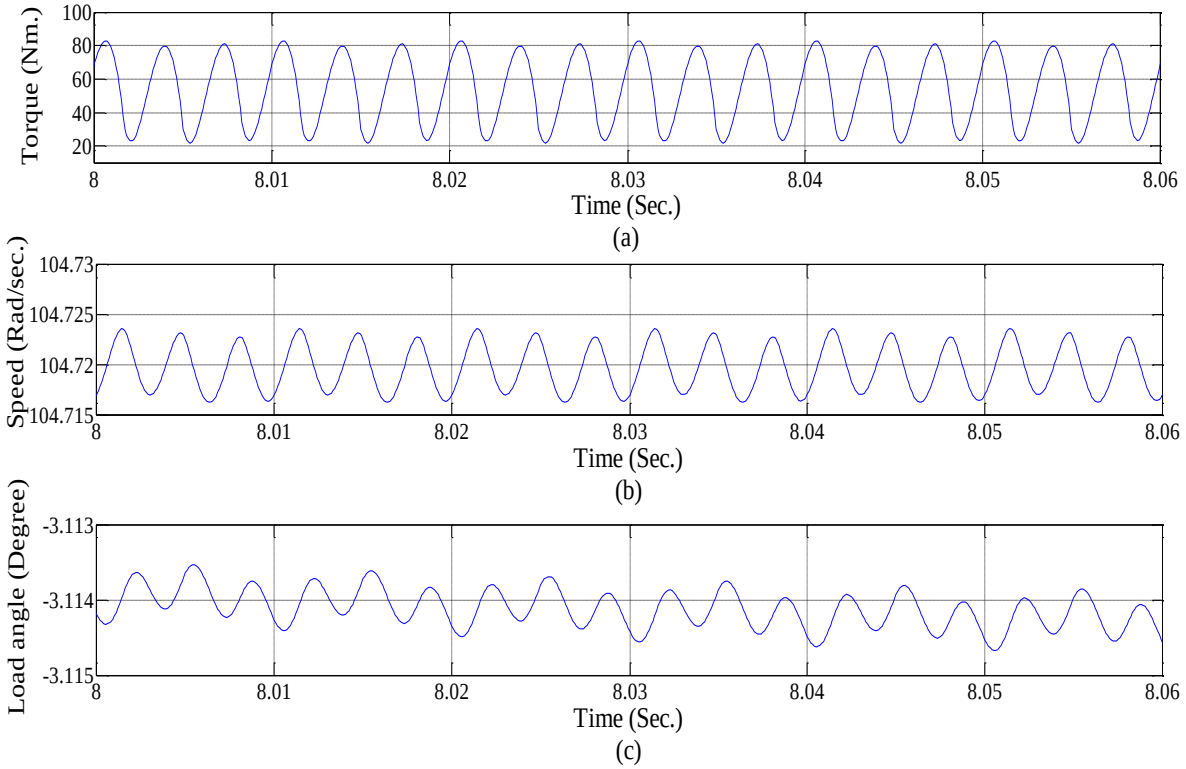

Fig. 2.37: Steady-state motor response with 60^0 displacement between stator winding sets showing (a) motor torque T_e (b) rotor speed ω_r (c) load angle, *delta*.

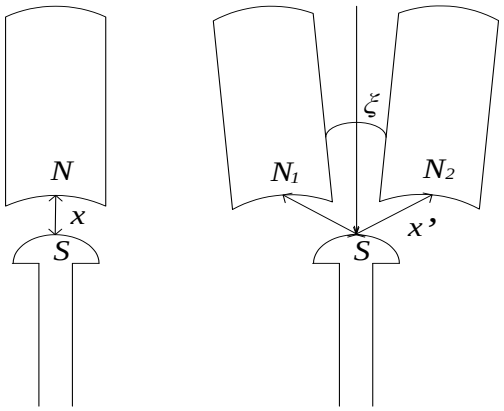

(a) (b)

Fig. 2.38: Effective airgap distance in machine operation with (a) symmetrical winding ($\xi = 0^0, 60^0$) and (b) asymmetrical ($\xi = 30^0$) winding configuration of six phase.

Chapter 3

Steady-state Modeling and Analysis of Six-phase Synchronous Motor

3.1 Introduction

Steady-state analysis is needed for a better understanding of the operational behavior of six-phase synchronous motor under different operating conditions. It will be advantageous to examine its describing equations followed by the development of phasor diagram. While performing the dynamic simulation of motor, these steady-state equations can also be used for the calculation of steady-state initial values to initialize the dynamic simulation. Also, knowledge of steady-state behavior is indispensable for checking correctness of the simulation results. The steady-state analysis of six-phase synchronous motor is not yet reported to best of the authors' knowledge. Therefore, the main contribution of this chapter is to explore the steady-state operation of six-phase synchronous motor during its normal operating condition as well as the operation with input supply in only one set of three-phase stator winding (motor-generator mode). Initially, a mathematical model of six-phase synchronous motor has been developed, followed by the development of its phasor diagram in steady-state operating condition, from which performance of the motor may be directly analyzed. Mathematical treatment has been carried out through the Park's (*dq0*) transformation.

3.2 Mathematical Modeling during steady-state

It is convenient to use the park's equations for the derivation of steady-state equations, though several other approaches may be used to describe the balanced steady-state operation of synchronous machine. In this mode of operation, the rotor rotates at synchronous speed, i.e. the relative speed between the armature field and rotor field is zero. Hence, the time rate change of flux linkage is zero with no current in the short-circuited damper windings. This fact has been incorporated by dropping the differential terms in voltage equations 2.3 to 2.9 in chapter 2. These equations can then be written as

$$V_{q1} = r_1 I_{q1} + \frac{\omega_e}{\omega_b}(x_{l1} + x_{lm} + x_{md}) I_{d1} + \frac{\omega_e}{\omega_b}(x_{lm} + x_{md}) I_{d2} + \frac{\omega_e}{\omega_b} x_{ldq} I_{q2} + E_{fr} \quad (3.1)$$

$$V_{d1} = r_1 I_{d1} - \frac{\omega_e}{\omega_b}\left(x_{l1} + x_{lm} + x_{mq}\right) I_{q1} - \frac{\omega_e}{\omega_b}\left(x_{lm} + x_{mq}\right) I_{q2} + \frac{\omega_e}{\omega_b} x_{ldq} I_{d2} \quad (3.2)$$

$$V_{q2} = r_2 I_{q2} + \frac{\omega_e}{\omega_b}(x_{l2} + x_{lm} + x_{md}) I_{d2} + \frac{\omega_e}{\omega_b}(x_{lm} + x_{md}) I_{d1} - \frac{\omega_e}{\omega_b} x_{ldq} I_{q1} + E_{fr} \quad (3.3)$$

$$V_{d2} = r_2 I_{d2} - \frac{\omega_e}{\omega_b}\left(x_{l2} + x_{lm} + x_{mq}\right) I_{q2} - \frac{\omega_e}{\omega_b}\left(x_{lm} + x_{mq}\right) I_{q1} - \frac{\omega_e}{\omega_b} x_{ldq} I_{d1} \quad (3.4)$$

$$E_{fr} = \frac{\omega_e}{\omega_b} x_{md} I_{fr} \quad (3.5)$$

Steady-state analysis has been carried out under the assumption that each of the stator winding sets *abc* and *xyz* are supplied by a balanced set of three-phase voltage sources such that the phase voltage can be written as:

$$v_a = \sqrt{2} V_1 cos\omega_e t \quad (3.6)$$

$$v_x = \sqrt{2} V_2 cos(\omega_e t - \alpha) \quad (3.7)$$

and phase current can be written as

$$i_a = \sqrt{2} I_1 cos(\omega_e t - \emptyset_1) \quad (3.8)$$

$$i_x = \sqrt{2} I_2 cos(\omega_e t - \emptyset_2 - \alpha) \quad (3.9)$$

where,

V_1 = rms value of the phase voltage of winding set *abc*

I_1 = rms value of the phase current of winding set *abc*

V_2 = rms value of the phase voltage of winding set *xyz*

I_2 = rms value of the phase current of winding set *xyz*

$\emptyset_1$ = power factor angle of winding set *abc*

$\emptyset_2$ = power factor angle of winding set *xyz*

α = phase difference between the phase voltage of *a* and *x*.

In rotor reference frame, *d-q* components of stator voltages become constant and can be written as

$$V_{q1} = V_1 cos\delta \quad (3.10)$$

$$V_{d1} = V_1 sin\delta \quad (3.11)$$

$$V_{q2} = V_2 cos(\delta - \xi - \alpha) \quad (3.12)$$

$$V_{d2} = V_2 sin(\delta - \xi - \alpha) \quad (3.13)$$

Above voltages can be related to synchronously rotating voltage phasor $\boldsymbol{V_a}$ and $\boldsymbol{V_x}$ as

$$\boldsymbol{V_a} e^{-j\delta} = V_{q1} - jV_{d1} \tag{3.14}$$

$$\boldsymbol{V_x} e^{-j(\delta-\xi)} = V_{q2} - jV_{d2} \tag{3.15}$$

Similar relation can be written for stator current as

$$\boldsymbol{I_a} e^{-j\delta} = I_{q1} - jI_{d1} \tag{3.16}$$

$$\boldsymbol{I_x} e^{-j(\delta-\xi)} = I_{q2} - jI_{d2} \tag{3.17}$$

Substitution of equation 3.1 and equation 3.2 in equation 3.14, followed by the mathematical simplification yields the voltage equation in phasor form as

$$\boldsymbol{V_a} = \left[r_1 + j\frac{\omega_e}{\omega_b}\left(x_{l1} + x_{lm} + x_{mq}\right)\right]\boldsymbol{I_a} + \frac{\omega_e}{\omega_b}\left[x_{ldq} + j\left(x_{lm} + x_{mq}\right)\right]\boldsymbol{I_x} e^{j\xi} + \boldsymbol{E_q} \tag{3.18}$$

Similarly for other winding set, *xyz* yields

$$\boldsymbol{V_x} e^{j\xi} = \left[r_2 + j\frac{\omega_e}{\omega_b}\left(x_{l2} + x_{lm} + x_{mq}\right)\right]\boldsymbol{I_x} e^{j\xi} + \frac{\omega_e}{\omega_b}\left[-x_{ldq} + j\left(x_{lm} + x_{mq}\right)\right]\boldsymbol{I_a} + \boldsymbol{E_q} \tag{3.19}$$

where,

$$\boldsymbol{E_q} = \left[\frac{\omega_e}{\omega_b}\left(x_{md} - x_{mq}\right)(I_{d1} + I_{d2}) + E_{fr}\right] e^{j\delta} \tag{3.20}$$

is the voltage phasor along q-axis and field voltage is given by

$$E_{fr} = \frac{\omega_e}{\omega_b} x_{md} I_{fr} \tag{3.21}$$

The above voltage phasors can be used to draw equivalent circuit as well as phasor diagram as depicted in Fig. 3.1 and Fig. 3.2. In order to retain generality of the operation of two winding sets *abc* and *xyz*, voltage drops and power factor angle are shown to be different for two sets. While evaluating the performance indices during steady-state, these values are taken to be equal for both the winding sets. This is because power sharing by each stator winding set is equal.

Three modes of operation can be illustrated, based on three operating conditions:

(1) $\boldsymbol{E_q} = \boldsymbol{V_a} (= \boldsymbol{V_x} e^{j\xi})$: First condition appears during no-load condition, if friction and windage losses along with ohmic drop of stator windings are neglected, then input currents to the stator windings will be zero, i.e. $\boldsymbol{I_a} = \boldsymbol{I_x} e^{j\xi} = 0$. In this mode of operation, motor will run at synchronous speed without absorbing energy from the electrical system. This operation is referred as "floating on the line". The operation is practically not possible because motor will absorb a small amount of energy associated with ohmic and friction and windage losses.

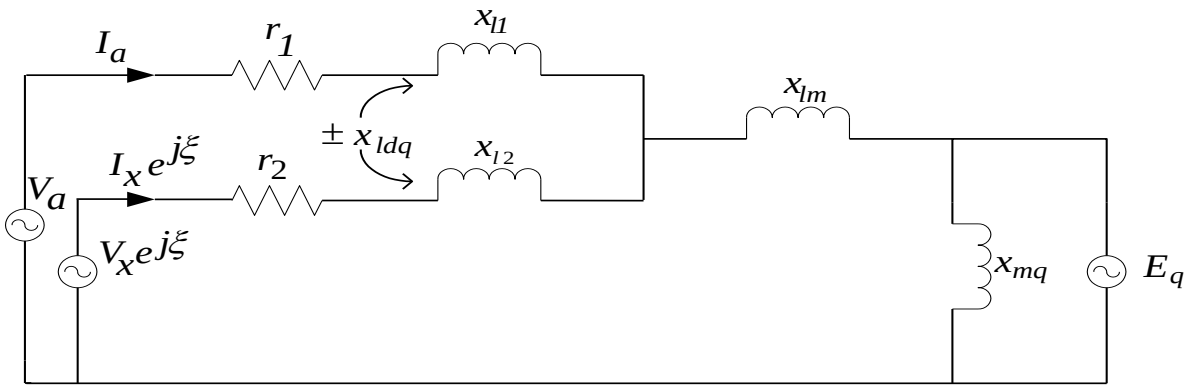

Fig. 3.1: Steady-state equivalent circuit of six-phase synchronous motor.

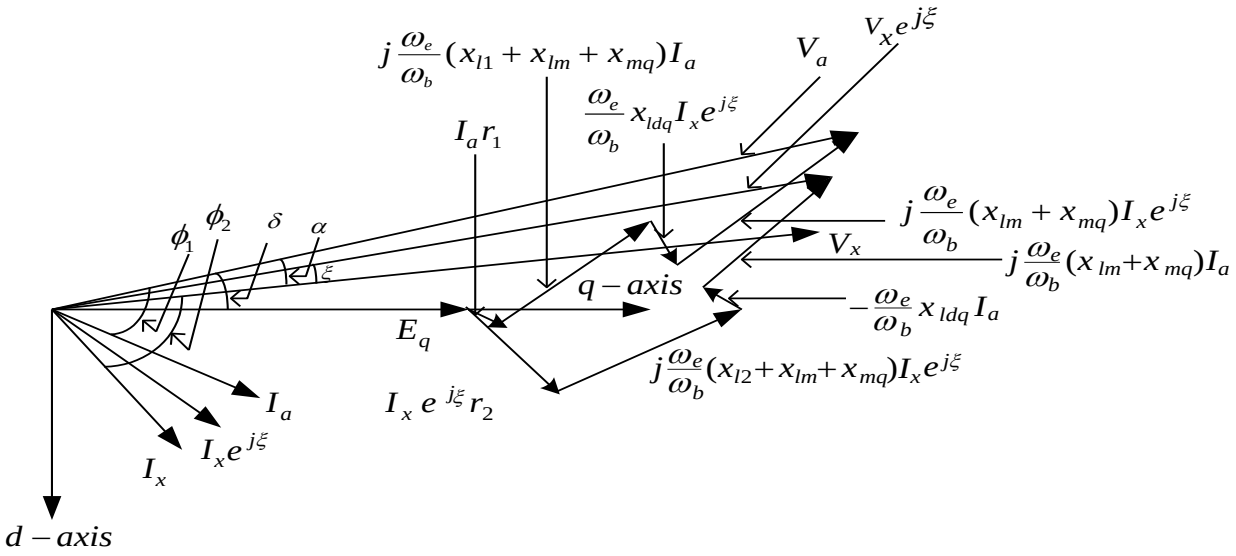

(a)

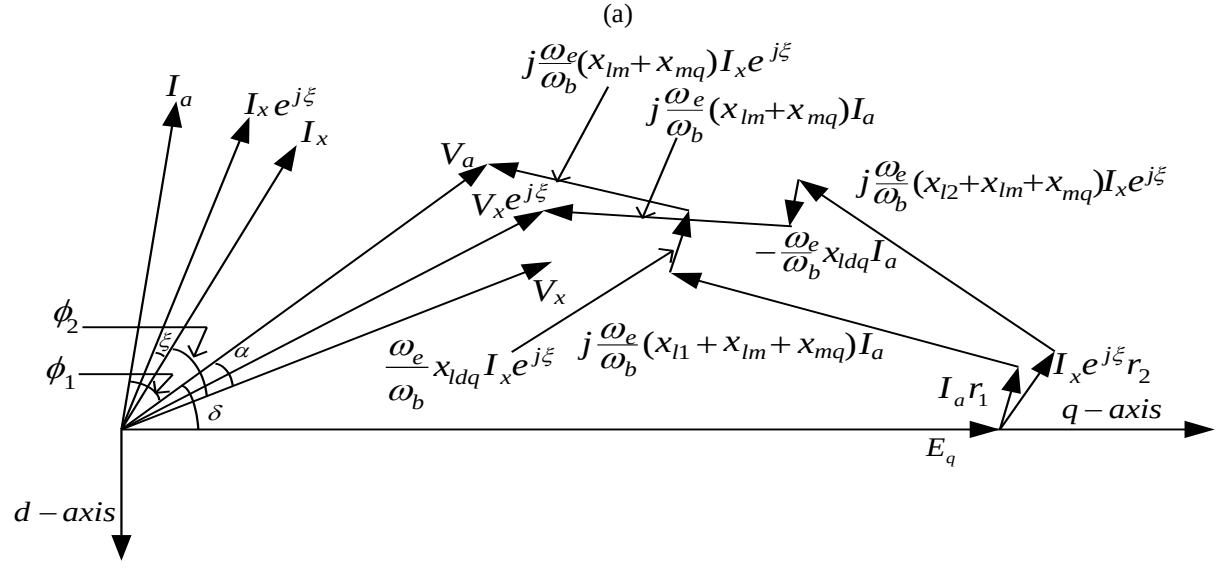

(b)

Fig. 3.2: Phasor diagram of six-phase synchronous motor at (a) lagging power factor (b) leading power factor.

(2) $\boldsymbol{E_q} < \boldsymbol{V_a}(and\, \boldsymbol{V_x} e^{j\xi})$: During this mode of operation, $\boldsymbol{I_a}\,(and\, \boldsymbol{I_x} e^{j\xi})$ is lagging $\boldsymbol{V_a}(and\, \boldsymbol{V_x} e^{j\xi})$, therefore, motor will absorb reactive power, hence appears as an inductor to system. (3) $\boldsymbol{E_q} > \boldsymbol{V_a}(and\, \boldsymbol{V_x} e^{j\xi})$: During this mode of operation, $\boldsymbol{I_a}\,(and\, \boldsymbol{I_x} e^{j\xi})$ is leading $\boldsymbol{V_a}(and\, \boldsymbol{V_x} e^{j\xi})$, hence appears as a capacitor supplying reactive power to the system.

3.2.1 Power and Torque Expression:

The total complex power of both sets of stator windings *abc* and *xyz* is given by

$$S = P + jQ \tag{3.22}$$

where, P and Q are the active and reactive power component of motor respectively. These powers can be expressed as

$$P = (\tfrac{3}{2})\{(V_{q1}I_{q1} + V_{d1}I_{d1}) + (V_{q2}I_{q2} + V_{d2}I_{d2})\} \tag{3.23}$$

$$Q = (\tfrac{3}{2})\{(V_{q1}I_{d1} - V_{d1}I_{q1}) + (V_{q2}I_{d2} - V_{d2}I_{q2})\} \tag{3.24}$$

Electromagnetic power developed by the motor is obtained by subtracting from the input power, the losses in stator, which is just the copper loss of stator windings in the model. This can be easily obtained by putting the value of *d-q* voltages from equations 3.1 to 3.4 in equation 3.24. Suitable mathematical simplification then yields,

$$P = copper\ loss + P_{em} \tag{3.25}$$

where,

$$copper\ loss = r_1(I_{q1}^2 + I_{d1}^2) + r_2(I_{q2}^2 + I_{d2}^2) \tag{3.26}$$

is the stator winding copper loss.

$$P_{em} = E_{fr}(I_{q1} + I_{q2}) + (x_{md} - x_{mq})(i_{d1}i_{q1} + i_{d2}i_{q2}) + (x_{md} - x_{mq})(i_{d1}i_{q2} + i_{q1}i_{d2}) \tag{3.27}$$

is the developed electromagnetic power by the motor.

Electromagnetic torque expression is obtained by dividing the electromagnetic power by the actual rotor speed. Therefore, electromagnetic torque is given by

$$T_{em} = \frac{P_{em}}{\omega_r} = \left(\frac{P}{2\omega_b}\right)\{E_{fr}(I_{q1} + I_{q2}) + (x_{md} - x_{mq})(i_{d1}i_{q1} + i_{d2}i_{q2}) + (x_{md} - x_{mq})(i_{d1}i_{q2} + i_{q1}i_{d2})\} \tag{3.28}$$

Above equation of torque is valid for steady-state operation, neglecting the stator resistance. However, in variable-speed drive system at low frequencies, stator resistance must be considered while evaluating the torque.

Torque expression permits a quantitative description of the nature of steady-state electromagnetic torque of six-phase synchronous motor. The first term on the right hand side of equation 3.28 is due to the interaction of magnetic system produced by the currents flowing in both the winding sets *abc* and *xyz*, and the magnetic system produced by the current flowing in the field winding. Second and third terms are due to the saliency of rotor. Second term is named as "self-reluctance torque", which is the sum of reluctance torques produced by the two sets of stator windings operating independently. Third term is named as "mutual-reluctance torque", which is produced due to the mutual coupling between two sets of stator windings. The torque produced due to the interaction of stator and field currents is the dominant torque. The reluctance torque is generally a relatively small part of the total torque of a synchronous motor. It is worthwhile to mention here that the reluctance torque (self and mutual-reluctance torque) vanishes in cylindrical rotor synchronous motor because $x_{md} = x_{mq}$.

The above analytical approach can be easily extended to other type of multiphase machines with multiple three-phase winding sets $(N = n/3)$ having angular displacement of ξ, where *N* is an integer representing the number of winding sets, and takes the value 1 and 2 for 6-phase; 1, 2 and 3 for 9-phase; 1, 2, 3 and 4 for 12-phase; 1, 2, 3 and *n*/3 for *n*-phase.

3.2.2 Supply in one set of winding only

Apart from the above discussed cases of steady-state operation of motor with two sets of stator windings *abc* and *xyz*, case of complete outage of supply in one winding set *xyz* is also considered here. As there is only one set of three phase supply connected to winding set *abc*, six-phase synchronous motor in this case will act as a three-phase synchronous motor. Analytical results can be obtained by putting $i_{q2} = i_{d2} = 0$, i.e $I_x = 0$ in above discussed model of six-phase synchronous motor. As there is a coupling between the winding sets *abc* and *xyz* due to sharing of same stator slots by coil sides of *abc* and *xyz* winding, therefore, a voltage will be generated in winding set *xyz* due to transformer action. Hence, six-phase synchronous machine in this mode will both act as a motor as well as a generator (motor-generator mode).

The developed model of the machine can be applied easily to evaluate the motor performance under steady-state condition with input in both sets of stator windings as well as

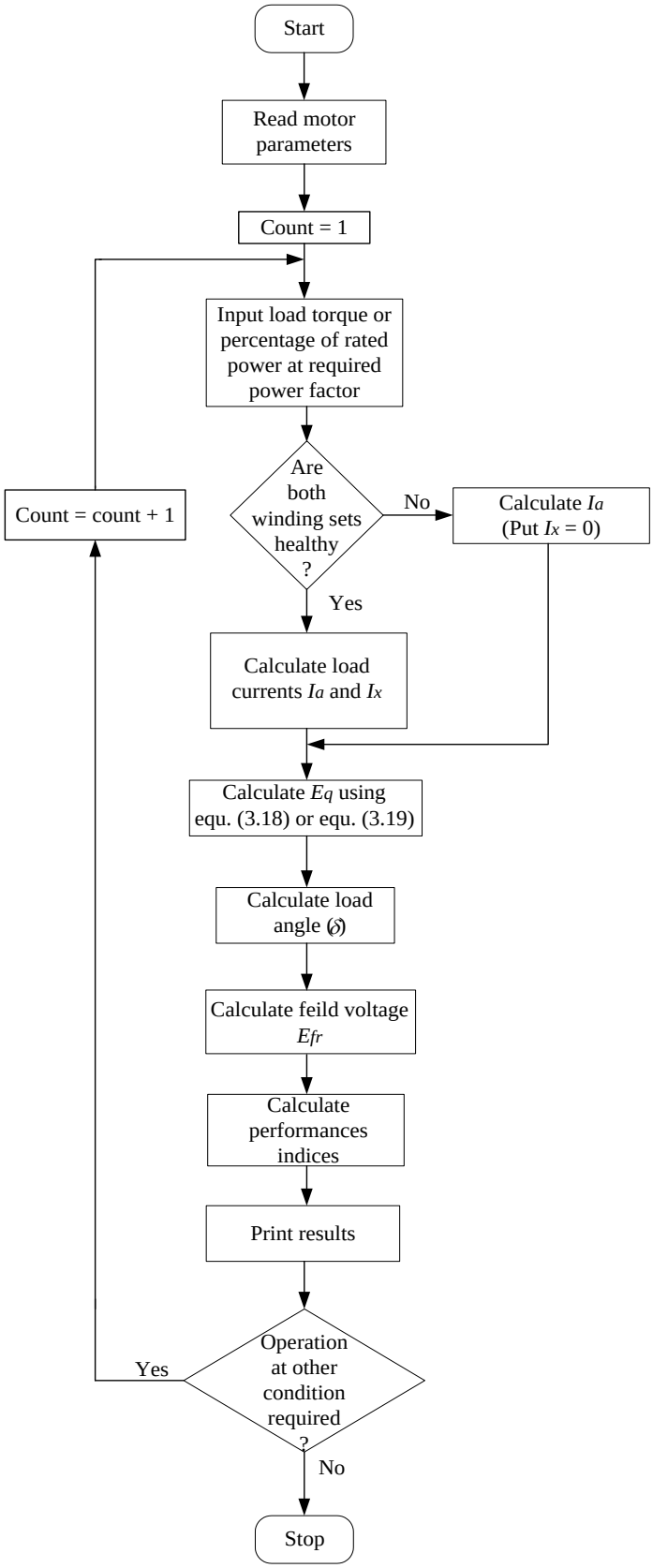

Fig. 3.3: Flow chart for evaluating the motor performance during steady-state.

input in only one set of stator winding. A unified and simplified step for these operating conditions is shown in the flow chart in Fig. 3.3.

3.3 Simulation Results

Mathematical model developed for the operation of six-phase synchronous motor at steady-state condition in previous section has been investigated via simulation in Matlab/Simulink environment. A motor of 3.7 kW with its parameters given in Appendix II has been simulated for 50 percentage of base/rated torque, operating at power factor of 0.85 (lagging). Input phase voltage of both the winding sets *abc* and *xyz* has been maintained constant at 160 V where the input phase current was found to be 2.29 A in each winding set. The steady-state phase voltage-current waveforms of phases *a* and *x* are shown in Fig. 3.4. Under this condition, calculated active power and reactive power was found to be 1865 W and 1155.8 VAr respectively, with the load angle δ equal to -5.76 degree. Induced field voltage and current has been maintained at 206.73 V and 33.53 A respectively.

Simulation results for various other operating conditions during steady-state are shown in Fig. 3.5. Fig. 3.5 (a) shows the operating properties at different load condition (i.e. at different load torque) operating at a power factor of 0.85 (lagging). As expected, motor current as well as load angle δ (only numerical value shown) proportionately increases with the increase of output load torque. Fig 3.5 (b) shows the operating properties at different operating power factor (shown by different phase angle) operating at 50 percent of base/rated torque. Variation in current and load angle δ can be noted at different phase angles (i.e. at different power factor). The variation of current is basically due to the variation of reactive component of power, since motor is operating at constant active power to deliver a constant load. Under this condition, variation of load angle, δ can also be noted and it decreases when motor operating mode moves from lagging to leading power factor. Simulation results at different operating conditions (different load torque with constant power factor and constant load torque with different power factor) have also been shown in Table 3.1 and Table 3.2. Some more results are given in chapter 7 with its experimental validation to give more insight into the motor operation at different input voltage and load torque.

3.4.1 Inclusion of supply asymmetry

For the purpose of simplicity and better understanding, it has been assumed that the input supply in the above analysis is perfectly ideal. Practically, this may not be the case as there is a continuous change of input supply voltage (in magnitude and/or phase) due to the variation of other loads connected to the supply lines, resulting in an unbalance flow of current in motor. This phenomenon has been identified in a number of available references [18, 49-51] for multiphase motor. It has been found that the multiphase motor is more sensitive to the supply asymmetries than the machine asymmetry [18, 51]. Therefore, supply asymmetries have also been incorporated in simulation results similar to actual motor operation in the following sections.

Following to the inclusion of supply asymmetry with operation of motor at 50 percent of base/rated torque approximately, the input current in each phase of six-phase synchronous motor was found to be different. The magnitude of input currents was found to be 3.20 A, 3.35 A, 2.87 A and 2.83 A, 2.35 A, 2.45 A in the phases of winding sets *abc* and *xyz* respectively, as shown in Fig. 3.6. Supply voltage at input motor phases was taken as 160 V, with the variation similar to that of experimental operating condition, as shown in chapter 7. It has to be noted that motor torque is supplying the load, accompanied by the production of harmonics, which varies between the peak value of 56.24 Nm and 53.56 Nm. Variation of instantaneous torque can further be noted in rotor speed, as depicted in Fig. 3.7 (b).

3.4.2 Supply in one winding set (abc) only

Simulation was carried out for the supply in winding set *abc* only, assuming a complete outage of supply in winding set *xyz*. Therefore, the output power will have to be supplied by winding set *abc* only, resulting in the increase of its current magnitude to 5.45 A approximately. Since machine in this mode is giving the output power both in the form of mechanical (to supply the load torque) as well as electrical (voltage generated in winding set *xyz*) power, therefore, the machine is acting both as motor and generator at a time (motor-generator mode). Generation of voltage in winding set *xyz* will take place due to the transformer action, generated phase voltage was found to be 159.94 V approximately for each phase. Computer traces of generated phase voltage V_x and voltage-current of phase '*a*' are shown in Fig. 3.8. Harmonic production in this mode of operation was found to decrease

considerably as compared to above. It is due to the inherent filtering provided by the six-phase machine. Such inherent filtering characteristic capability helps to reduce the external filtering requirement. Reduction in harmonic is also due to the reduced sensitivity of motor (with three phase winding configuration) towards supply asymmetries; hence, resulting in the flow of relatively more balanced three-phase current into the motor, though with an increased magnitude.

3.5 Conclusion

A simple steady-state mathematical model of an asymmetrical six-phase synchronous motor is presented, where the effect of common mutual leakage reactance between the two sets of three-phase stator winding has been considered. A unified and simplified approach has been adopted for digital simulation, considering the operation at two operating conditions at input terminals i.e. the input supply at both two three phase of stator winding, and at only one set of three-phase stator winding. This shows the additional possibilities offered by using six-phase synchronous motor compared to its three-phase counterpart which indicates its redundancy characteristic making it suitable for the application where reliability is of prime importance. Furthermore, there is a possibility of generation of voltage at one of the three-phase winding set, when other winding set is supplied by three-phase electrical source. Hence, a single machine acts as motor as well as generator making it suitable for some special applications. Also, a general methodology of the steady-state analysis using the approach of Park's (*dq0*) transformation, which can be easily extended to other type of multiphase machine under different operating conditions.

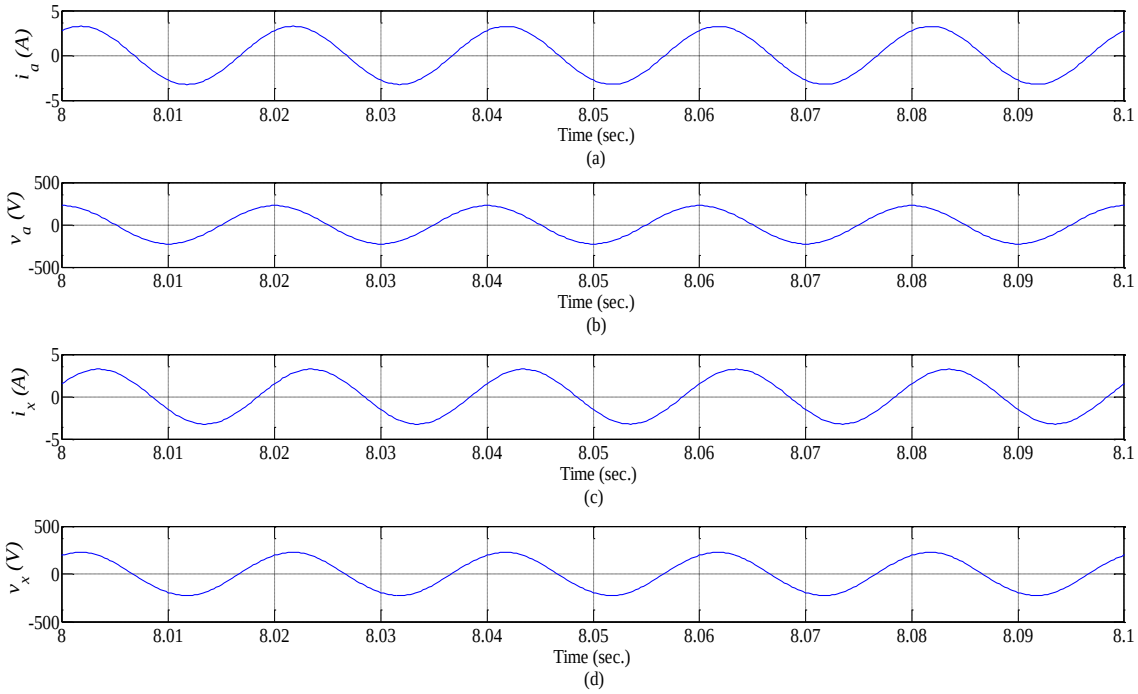

Fig. 3.4: Steady-state voltage and current of phases *a* and *x* of six-phase synchronous motor.

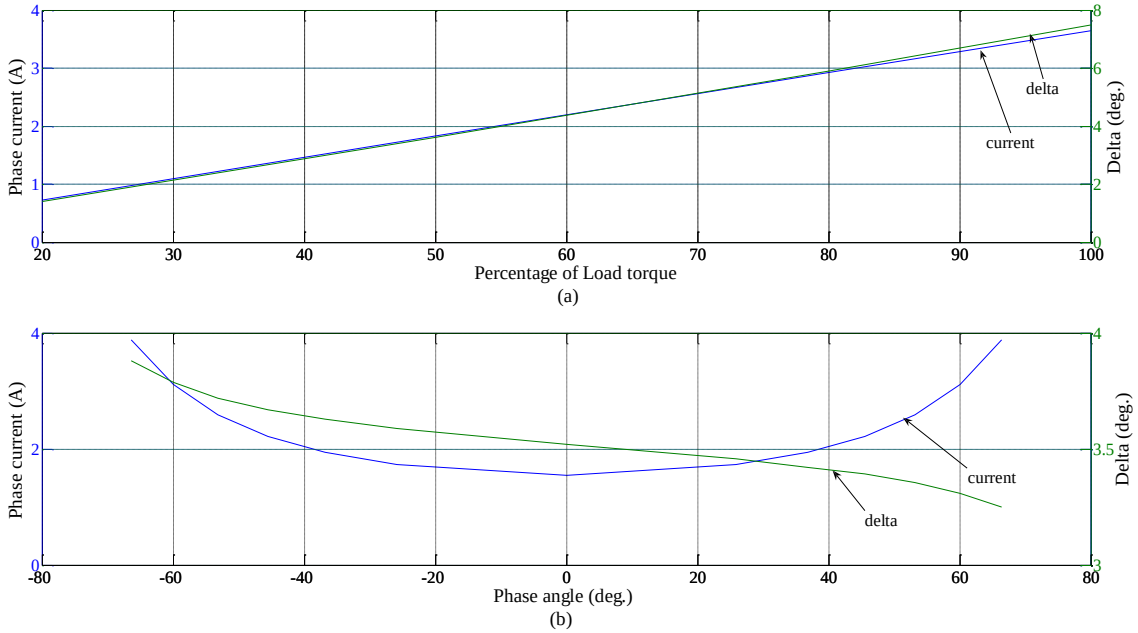

Fig. 3.5: Steady-state operation of six-phase synchronous motor at different operating conditions (a) different load torque (b) different power factor (shown by phase angle).

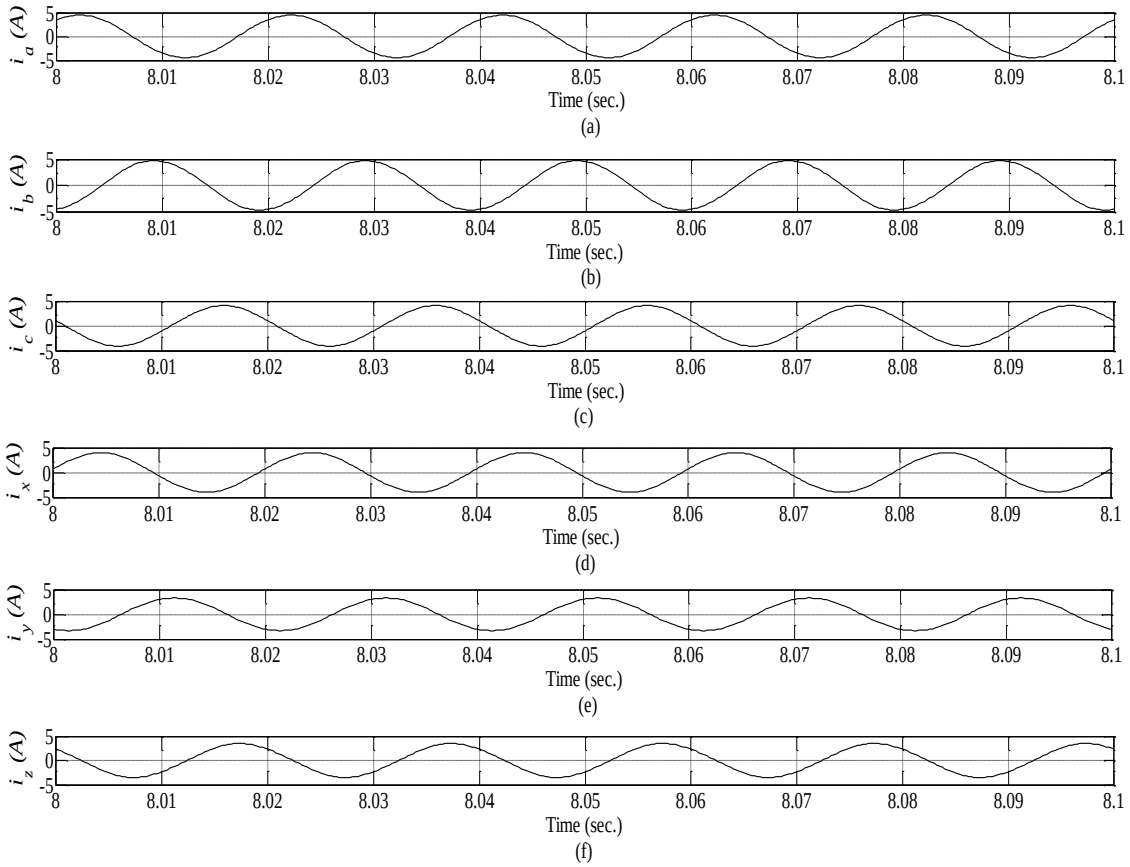

Fig. 3.6: Steady-state phase current of winding sets *abc* and *xyz* fed by unsymmetrical supply (a) i_a (b) i_b (c) i_c (d) i_x (e) i_y (f) i_z .

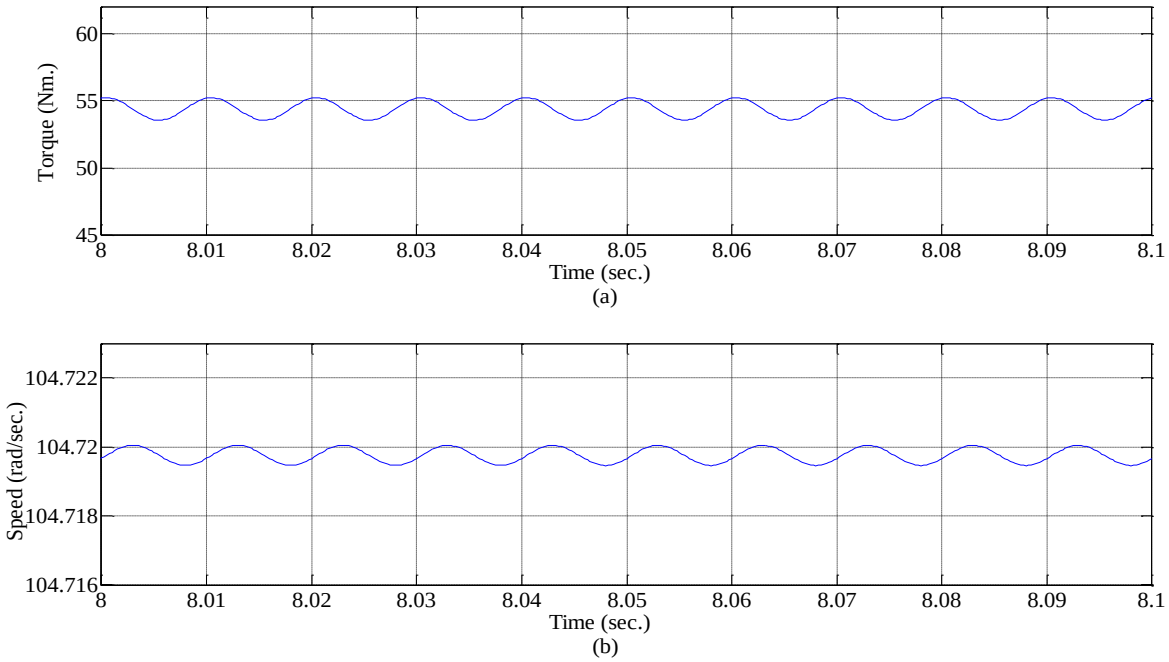

Fig. 3.7: Steady-state motor response under asymmetrical operation (a) motor torque T_e (b) rotor speed.

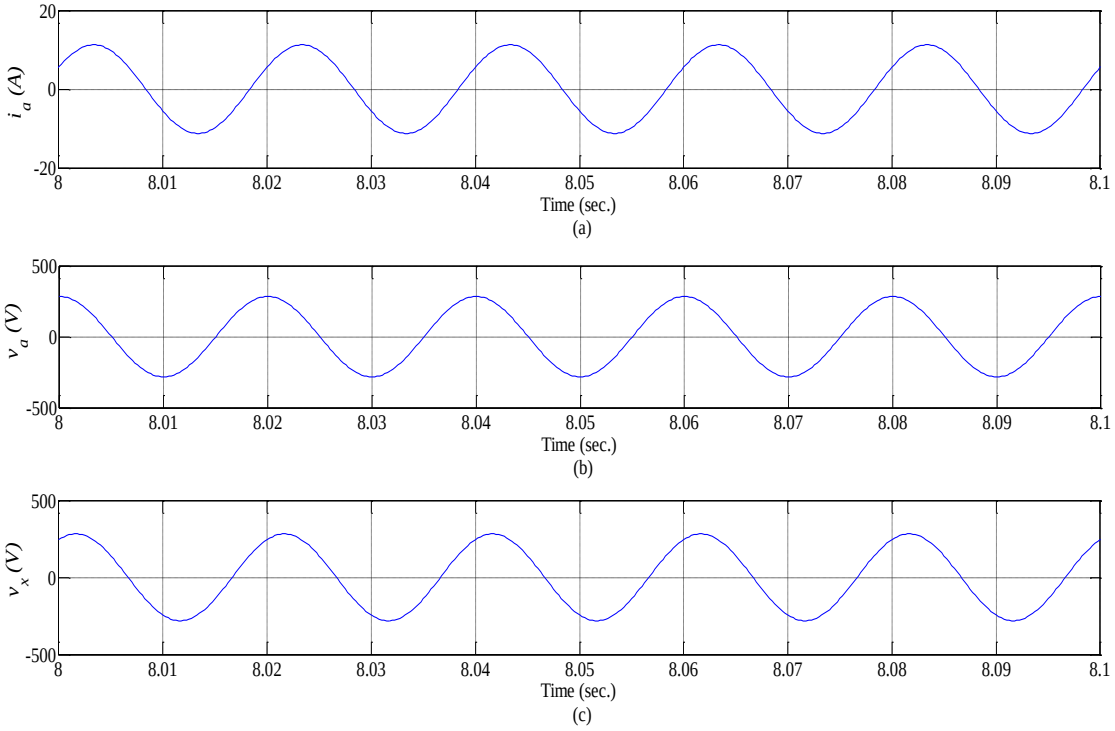

Fig. 3.8: Steady-state phase voltage and current of six-phase synchronous motor with supply in *abc* winding.

Table 3.1: Steady-state performance calculation under different loads at 0.85 power factor (lagging)

Percentage of Base Torque	**Active power (W)**	**Reactive power (VAr)**	**Phase current (Amp.)**	**Field voltage, E_{fr} (V)**	**Load Angle, δ (degree)**	**Field current I_{fr} (Amp.)**
20	746	462.32	0.91	217.96	-2.22	35.31
50	1865	1155.80	2.28	206.97	-5.76	33.52
80	2984	1849.30	3.65	197.93	-9.54	32.06
100	3730	2311.60	4.57	193.10	-12.19	31.28

Table 3.2: Steady-state performance calculation under different power factor at 50 percentage load with input phase voltage of 160 V

Power factor	**Active power (W)**	**Reactive power (VAr)**	**Phase current (Amp.)**	**Field voltage, E_{fr} (V)**	**Load Angle, δ (degree)**	**Field current I_{fr} (Amp.)**
0.4 (lagging)	1865	4273.3	4.85	150.34	-6.67	24.35
0.8 (lagging)	1865	1398.8	2.43	202.55	-5.82	32.81
1.0 (unity)	1865	0.00	1.94	228.01	-5.49	36.93
0.8 (leading)	1865	-1398.8	2.43	253.49	-5.21	41.06
0.4 (leading)	1865	-4273.3	4.85	305.93	-4.74	49.55

Chapter 4

Fault Analysis of Six-Phase Synchronous Motor

4.1 Introduction

Phase redundancy is an important property of multiphase motor which make it suitable for the applications where reliability is of prime importance [7, 13-14, 25]. The applications like automotive, aerospace and nuclear are a few of many, wherein multiphase ac motor are more and more being used as a substitute of traditional three phase motor. This is because a loss of supply in one or more phases does not prevent the motor from starting and it continues to run with a satisfactory operating performance though with reduced efficiency [7, 13-14]. Existence of such fault condition can be caused by mechanical failure of a motor terminal, or by an electrical failure in one of the inverter legs (if supplied by inverter). For the purpose to have a satisfactory performance level of multiphase motor under such conditions, it has to be explored and analyzed extensively. The most commonly used analytical tool for the analysis of unbalanced operation of electric machines has been the well-known symmetrical component method [7, 29]. In this approach, the three sequence networks are identified and interconnected according to the fault condition, which is then solved as one large equivalent network. Although, it can be used successfully in the steady-state analysis for sinusoidal excitation; however, as far as the dynamic of machine is concerned, the method losses its utility due to non-existence of interaction between the lost phases and remainder of the machine windings which drastically alters the dynamic behavior of the machine [7]. Another alternative approach for above conditions is to carry out the analysis using Park's *dq0* variables. Simulation and analysis of a synchronous machine with an open phase, employing *dq0* variables was reported in various available literatures [17, 27, 29, 52-54]. Along with the well known advantage of the elimination of time-varying inductances in voltage equations, this approach also eliminates the computational stability problem, and the matrix inversion is not required [53]. This approach can, however, be extended to the analysis of multiphase synchronous motor with one or more phases opened.

Therefore, this chapter presents the open-circuit analysis of six-phase synchronous motor on a mathematical basis under different conditions to explore its performance. A mathematical model has been developed for the analysis of motor behavior during open circuit condition in single phase and double phases, through *dq0* approach. Motor behavior under such operating conditions was also experimentally analyzed (in chapter 7) under steady state operating condition, including the operation of motor with the complete outage of input supply to one set of winding. Operation of motor in generating mode is also examined.

In addition to open circuit fault, critical condition created by short circuit at machine input terminals has also been considered. This is because short circuit condition during machine operation is always considered as a serious situation, as it results in an abrupt increase in its current to several times the rated value. This may further result in a permanent machine outage, if not cleared within the prescribed time. Therefore, machine behavior under short circuit conditions will have to explored and analyzed extensively, before a suitable protection scheme can be applied in conjugation with such condition. Short circuit analysis of synchronous machine is a complex task under different operating modes (asymmetrical/symmetrical). The early researchers preferred the method of computer simulation in classical wound-field synchronous machine [55-56]. As far as analytical approach is concerned, most of the authors adopted the well-known symmetrical component method. Using this concept machine acting as a synchronous generator has been extensively analyzed [57-60], whereas synchronous machine operating as motor has been considered in a few literatures [61-62]. Another alternative approach to carry out the analysis during short circuit condition is by employing Park's (*dq0*) transformation, and few literature [55, 62-64] can be found in this regard. As far as the short circuit analysis of six-phase synchronous motor is concerned, it has not been reported so far. Therefore, the following section also deals with a detailed short circuit analysis of a six-phase synchronous motor by using an accurate computer simulation for different cases (both asymmetrical and asymmetrical).

4.2 Mathematical Equations during open circuit

It is assumed that the stator winding sets *abc* and *xyz* (having separate neutral points *n*1 and *n*2) are supplied by the two sets of balanced three-phase voltage sources v_{ag}, v_{bg}, v_{cg} and v_{xg}, v_{yg}, v_{zg} respectively. Condition of open circuit may occur at one or more supply phases to

the motor input terminal. Hence, different cases are possible for open circuit or open conductor fault study. In order to explore the redundancy characteristic and performance of motor under such condition, mathematical equations have to be determined, which are valid under such condition. For the purpose of mathematical modelling of motor during open circuit conditions, two cases are considered: open circuit fault at single phase at one winding set and single phase at both the three phase winding set from each input phase of the two three phase input terminals, as discussed in following sections:

4.2.1 Case 1: Single phase open circuit

Initially, occurrence of open conductor fault is assumed to take place at phase *a*, so that its terminal current is zero (i.e. $i_a = 0$). Terminal voltages, which force the current i_a to remain zero are given by

$$v_a = \frac{p}{\omega_b}\psi_a \tag{4.1}$$

$$v_b = v_{bg} - v_{n1g} \tag{4.2}$$

$$v_c = v_{cg} - v_{n1g} \tag{4.3}$$

Flux and current (which is zero) expression for phase *a* in the term of *d* and *q* variables can be written as

$$\psi_a = \psi_{q1}\, cos\theta_r + \psi_{d1}\, sin\theta_r \tag{4.4}$$

$$0 = i_{q1}\, cos\theta_r + i_{d1}\, sin\theta_r \tag{4.5}$$

From equations 2.10 and 2.11, i_{q1} and i_{d1} can be expressed as

$$i_{q1} = \frac{1}{x_{l1}}\left(\psi_{q1} - \psi_{mq} - A + C\right) \tag{4.6}$$

$$i_{d1} = \frac{1}{x_{l1}}(\psi_{d1} - \psi_{md} - B - D) \tag{4.7}$$

where, $A = x_{lm}\left(i_{q1} + i_{q2}\right)$; $B = x_{lm}(i_{d1} + i_{d2})$; $C = x_{ldq} i_{d2}$; $D = x_{ldq} i_{q2}$.

Substitution of i_{q1} and i_{d1} from equations 4.6 and 4.7 into equation 4.5 yields

$$\psi_{q1}\, cos\theta_r + \psi_{d1}\, sin\theta_r = \left(\psi_{mq} + A - C\right)cos\theta_r + (\psi_{md} + B + C)sin\theta_r \tag{4.8}$$

Comparing equation 4.4 and 4.8, it is found

$$\psi_a = \left(\psi_{mq} + A - C\right)cos\theta_r + (\psi_{md} + B + C)sin\theta_r \tag{4.9}$$

Above obtained flux equation can be substituted in equation 4.1 and rewriting the same in terms of state variables by substituting equations 2.35 and 2.36 (chapter 2) for ψ_{mq} and ψ_{md},

respectively. Therefore,

$$v_a = \frac{p}{\omega_b}\left[\left\{x_{aq}\left[\frac{x_{l2}\psi_{q1}+x_{l1}\psi_{q2}+x_{ldq}(\psi_{d2}-\psi_{d1})}{x_b}+\frac{\psi_{Kq}}{x_{lKq}}\right]+A-C\right\}cos\theta_r + \left\{x_{ad}\left[\frac{x_{l2}\psi_{d1}+x_{l1}\psi_{d2}+x_{ldq}(\psi_{q1}-\psi_{q2})}{x_b}+\frac{\psi_{Kd}}{x_{lKd}}+\frac{\psi_{fr}}{x_{lfr}}\right]+B+C\right\}sin\theta_r\right] \quad (4.10)$$

which is the phase voltage during stator current $i_a = 0$.

For a single three phase winding *abc*, phase voltage satisfy the condition,

$$v_a + v_b + v_c = 0 \quad (4.11)$$

Therefore, v_{n1g} can be written by using equations 4.2, 4.3 and 4.11 as

$$v_{n1g} = \frac{1}{2}\left(v_{bg} + v_{cg} + v_a\right) \quad (4.12)$$

Substitution of equation 4.12 for v_{n1g} in equations 4.2 and 4.3, followed by the Park transformation of voltages v_a, v_b and v_c yields

$$v_{q1} = v_a cos\theta_r + \frac{1}{\sqrt{3}}\left(v_{bg} - v_{cg}\right)sin\theta_r \quad (4.13)$$

$$v_{d1} = v_a sin\theta_r + \frac{1}{\sqrt{3}}\left(v_{bg} - v_{cg}\right)cos\theta_r \quad (4.14)$$

which is valid for all the operating conditions. During normal operation, phase voltage $v_a = v_{ag}$ in above equations, whereas during the open circuit condition at phase *a*, phase voltage v_a is given by equation 4.10.

4.2.2 Case 2: Double phase open circuit

It is assumed that the opening of two phases occur simultaneously, one from each of the two three phase supply to the motor input terminal. Here, it is assumed to occur at the phases *a* and *x*, such that currents i_a and i_x are both zero. Mathematical treatment of such condition can be easily expressed on the way similar to above case. Determination of phase *a* is completely obtained from the equations 4.10, 4.13 and 4.14. Analogous to the phase *a*, voltage expression during open circuit, for phase *x* can be determined as

$$v_x = \frac{p}{\omega_b}\left[\left\{x_{aq}\left[\frac{x_{l2}\psi_{q1}+x_{l1}\psi_{q2}+x_{ldq}(\psi_{d2}-\psi_{d1})}{x_b}+\frac{\psi_{Kq}}{x_{lKq}}\right]+A+E\right\}cos(\theta_r-\xi) + \left\{x_{ad}\left[\frac{x_{l2}\psi_{d1}+x_{l1}\psi_{d2}+x_{ldq}(\psi_{q1}-\psi_{q2})}{x_b}+\frac{\psi_{Kd}}{x_{lKd}}+\frac{\psi_{fr}}{x_{lfr}}\right]+B-F\right\}sin(\theta_r-\xi)\right] \quad (4.15)$$

where, $E = x_{ldq}i_{d1}$; $F = x_{ldq}i_{q1}$

A general expression for winding set *xyz* in Parks variables is obtained as

$$v_{q2} = v_x cos(\theta_r - \xi) + \frac{1}{\sqrt{3}}(v_{yg} - v_{zg}) sin(\theta_r - \xi) \quad (4.16)$$

$$v_{d2} = v_x sin(\theta_r - \xi) + \frac{1}{\sqrt{3}}(v_{yg} - v_{zg}) cos(\theta_r - \xi) \quad (4.17)$$

Above obtained voltage equation is valid for all the operating conditions. During open circuit condition, phase voltage v_x will be given by equation 4.15, whereas in normal operating condition, $v_x = v_{xg}$. In order to evaluate the flux linkages ψ_{q1} and ψ_{d1}, it is required to substitute the value of phase voltage v_a in equation 4.13 and 4.14 from equation 4.10. The resulting equations are then substituted in equation 2.21 and 2.22 (chapter 2). Same parallel mathematical manipulation has to be done for winding set *xyz*, if double phase open circuit is considered. It will result in expression for ψ_{q1}, ψ_{d1} (and ψ_{q2}, ψ_{d2}) in terms of derivative of ψ_{q1}, ψ_{d1} (and ψ_{q2}, ψ_{d2}), making it necessary to perform numerical integration of derivative of the state variables. This task can be performed by digital simulation programmed with Runge-Kutta numerical integration subroutine. A unified and simplified step for evaluating the motor performance under normal and open circuit condition is shown in the form of flow chart in Fig. 4.1.

4.2.3 Case 3: Supply in one set of winding only

In addition to the above discussed cases of single and double fault open circuit cases, complete outage of supply in one winding set *xyz* is also considered here. Since, the availability of input supply exists for only one winding set *abc*; therefore the machine in this mode will act as a three-phase synchronous motor. Performance of the machine can be evaluated by substituting $i_{q2} = i_{d2} = 0$ in above developed model. It is important to emphasis that a voltage generation in the other winding set *xyz* will take place due to transformer action, because of a mutual coupling between the two winding sets *abc* and *xyz*, sharing the same stator slots by their coil sides. Hence, six-phase synchronous machine in this mode will act as a motor as well as a generator, both.

For simplicity and better understanding, it has been assumed that the different parameters of two winding sets *abc* and *xyz* are same. In actual machine, this may not be the case, leading the deviation of machine response from ideal behavior (asymmetrical six-phase). Secondly, asymmetrical operation is also due to unbalanced supply (i.e. difference in magnitude and /or phase), obtained through three-winding transformer fed to motor. Small

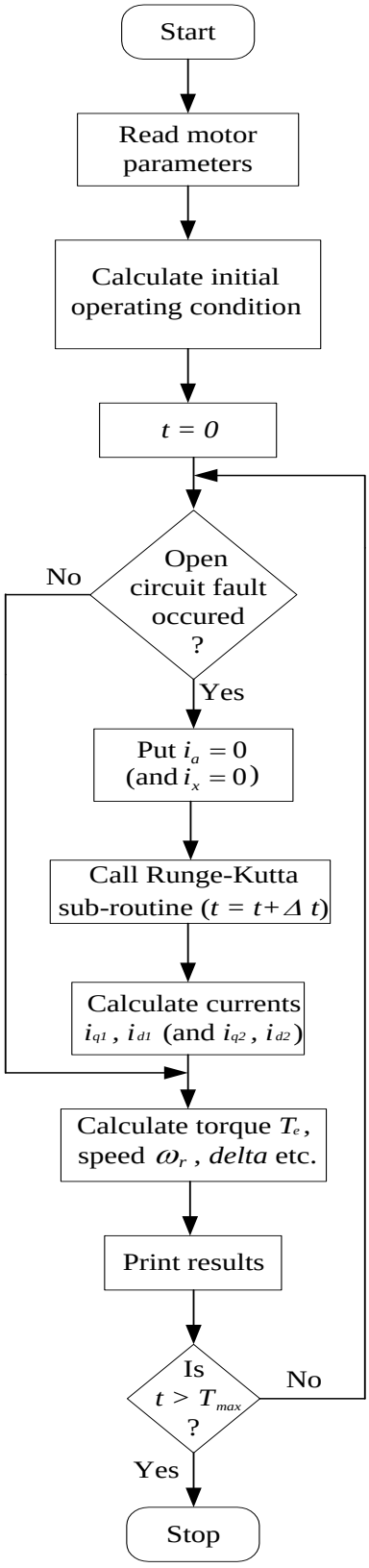

Fig. 4.1: Flow chart for evaluating the performance during open circuit.

error of input voltage will result in large error of input currents and different power factor for the two stator winding sets *abc* and *xyz*. It has been found that the machine is much more sensitive to the supply asymmetries than to the machine asymmetries [49-51]. Therefore, supply asymmetries have been incorporated in simulation, similar to the actual motor operation in the following sections. It is worthwhile to mention here that the above mathematical approach can be easily extended to other type of multiphase motors with multiple three-phase winding sets having a particular angular displacement ξ between them, for e.g. 6, 9, 12,…*n*-phases.

4.3 Simulation Results during open circuit conditions

Mathematical model developed for the operation of six-phase synchronous motor at open circuit condition in previous section was investigated via simulation in Matlab/Simulink environment. For the purpose to retain simplicity, it is necessary to note that the occurrence of open circuit condition takes place during steady state operation of the motor at a particular operating load. A motor of 3.7 kW (parameters given in Appendix II) was simulated for single and double phase open circuit condition, as explained below in following subsections. 4

4.3.1 Single phase open circuit

Before the occurrence of single phase open circuit, it was assumed and simulated for the steady state operating condition at 50% of motor base torque. Steady-state pre-fault phase current of each winding set *abc* and *xyz* was found to be 3.20 A, 3.35 A, 2.87 A and 2.83 A, 2.35 A, 2.45 A respectively. Supply voltage at input motor phases was taken as 160 V, with the variation similar to that of experimental operating condition. At time, $t = 8$ sec., open circuit condition was created by opening phase *a*, i.e. by nullifying the current of phase *a*. As soon as the phase current $i_a = 0$, a sudden increase in the phase current of winding set *xyz* was observed, followed by the decrease in remaining healthy phases of winding set *abc*. Increase in phase current of phases *x*, *y* and *z* was 53.89% (4.35 A), 106% (4.84 A i.e. almost double) and 12.65% (2.76 A) respectively, indicating a larger power shared by the winding set *xyz*. On the other hand, decrease in the phase current of phases *b* and *c* was 18.80% (2.72 A) and 5.22% (2.72 A) respectively, indicating a smaller power shared by the winding set *abc*. Both transient and steady state current of remaining healthy phases of winding sets *abc* and *xyz* are depicted in Fig. 4.2 and Fig. 4.3 respectively. Motor torque is supplying the load, accompanied by the

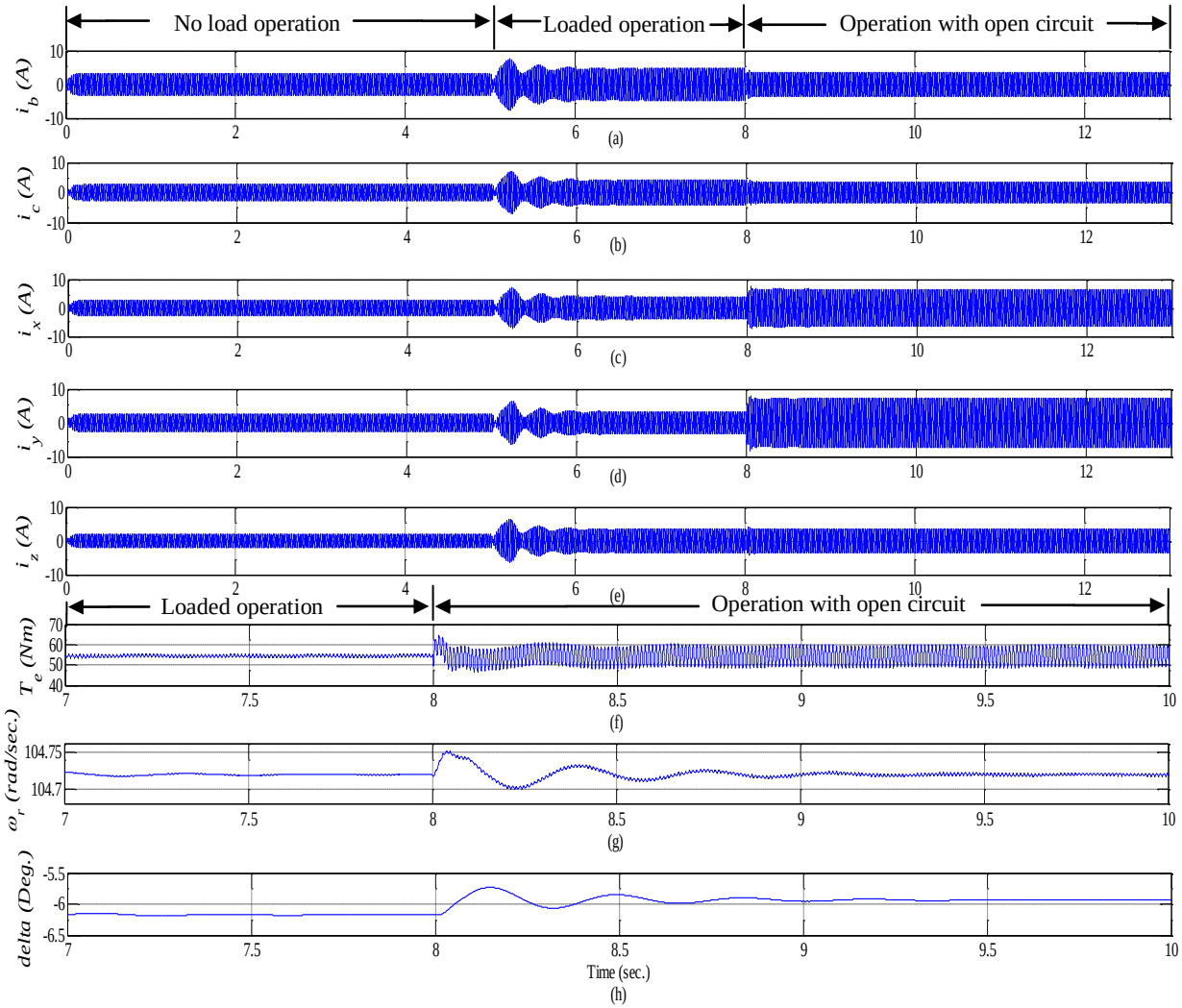

Fig. 4.2: Transient response of motor during pre and post-fault of single phase open circuit showing currents (a) i_b (b) i_c (c) i_x (d) i_y (e) i_z (f) Torque T_e (g) speed ω_r (h) load angle, *delta.*

production of harmonics which varies between the peak value of 59.66 Nm and 48.80 Nm. The effect of variation of instantaneous torque was noted in rotor speed and load angle, delta as shown in Fig. 4.2 (f)-(h).

4.3.2 Double phase open circuit

There may be the nine different cases of double phase open circuit condition, one phase from each winding set abc and xyz. To examine the motor behavior under the occurrence of double phase open circuit, two phases *a* and *x* were chosen in which open circuit condition was created at the same time, i.e. $t = 8$ sec., such that the currents $i_a = 0$ and $i_x = 0$. As expected, power shared by the healthy phases is increased, resulting in increase of its magnitude. Increase in the

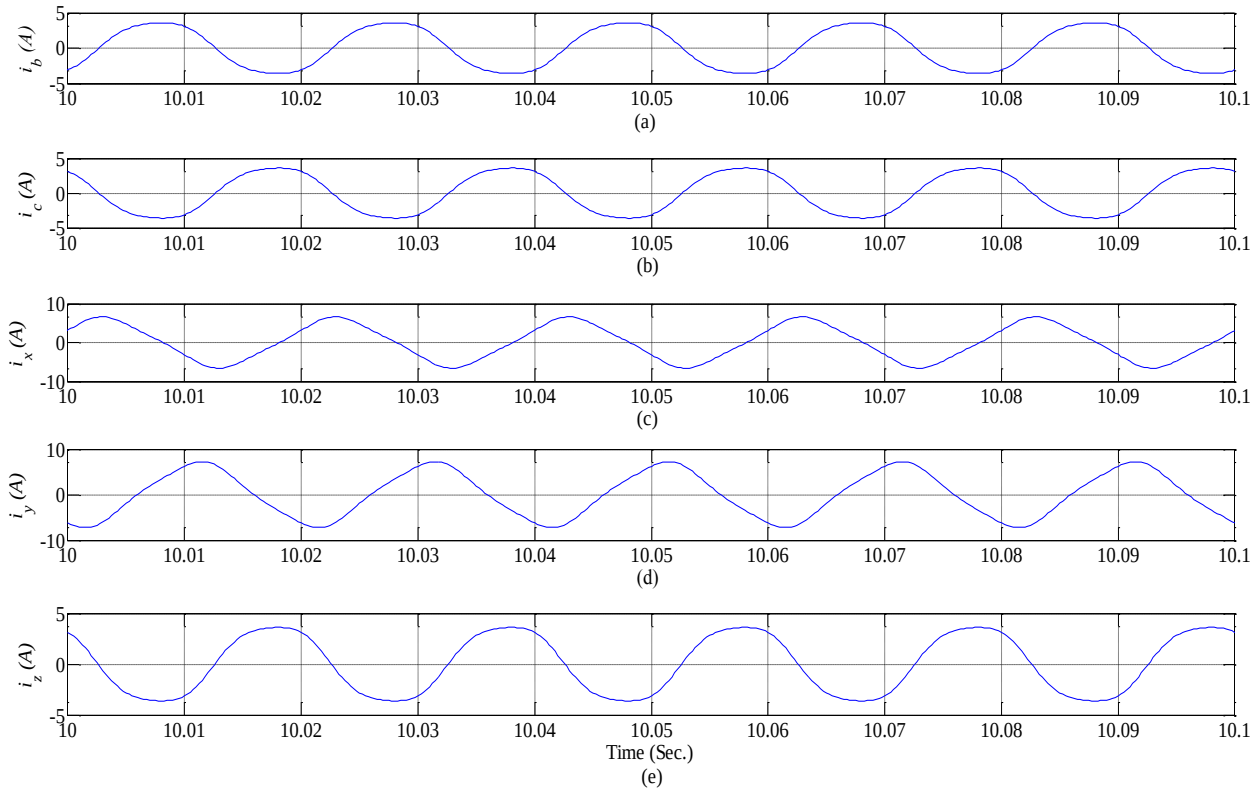

Fig 4.3: Steady-state phase current of remaining healthy phases of winding sets *abc* and *xyz* after the occurrence of single phase open circuit (a) i_b (b) i_c (c) i_x (d) i_y (e) i_z.

phase current of phase *b* and *c* was 15.82% (3.88 A) and 35.19% (3.88 A) respectively. Increase in phase current of phase *y* and *z* was 209.78% (7.28 A) and 197.14% (7.28 A i.e. almost three times) respectively, under safe current limit. Transient as well as steady state current of one healthy phase of winding sets *abc* and *xyz* are depicted in Fig. 4.4 and Fig. 4.5, respectively. Other healthy phase of each winding set will have the same magnitude, but will only have a phase shift of 180^0 electrical to satisfy the Kirchoff current law; and therefore, not shown in figure. Motor under this condition is still working satisfactory, though with increased harmonics content in the motor torque, which was found to be increased with its peak value variation between 26.08 Nm and 73.21 Nm. The harmonic variation in instantaneous torque is reflected in rotor speed and load angle, *delta* as shown in Fig. 4.4 (c)-(e). In another case, in which phase *a* and *y* were chosen for double phase open circuit at the same time $t = 8$ sec., such that the currents $i_a = 0$ and $i_y = 0$. It was observed that the nature of variation of phase current was same as that of previous case of phase *a* and *x*, though with the change in its magnitude. Increase of phase current of phase *b* and *c* was found to be 130.30% (7.60 A) and

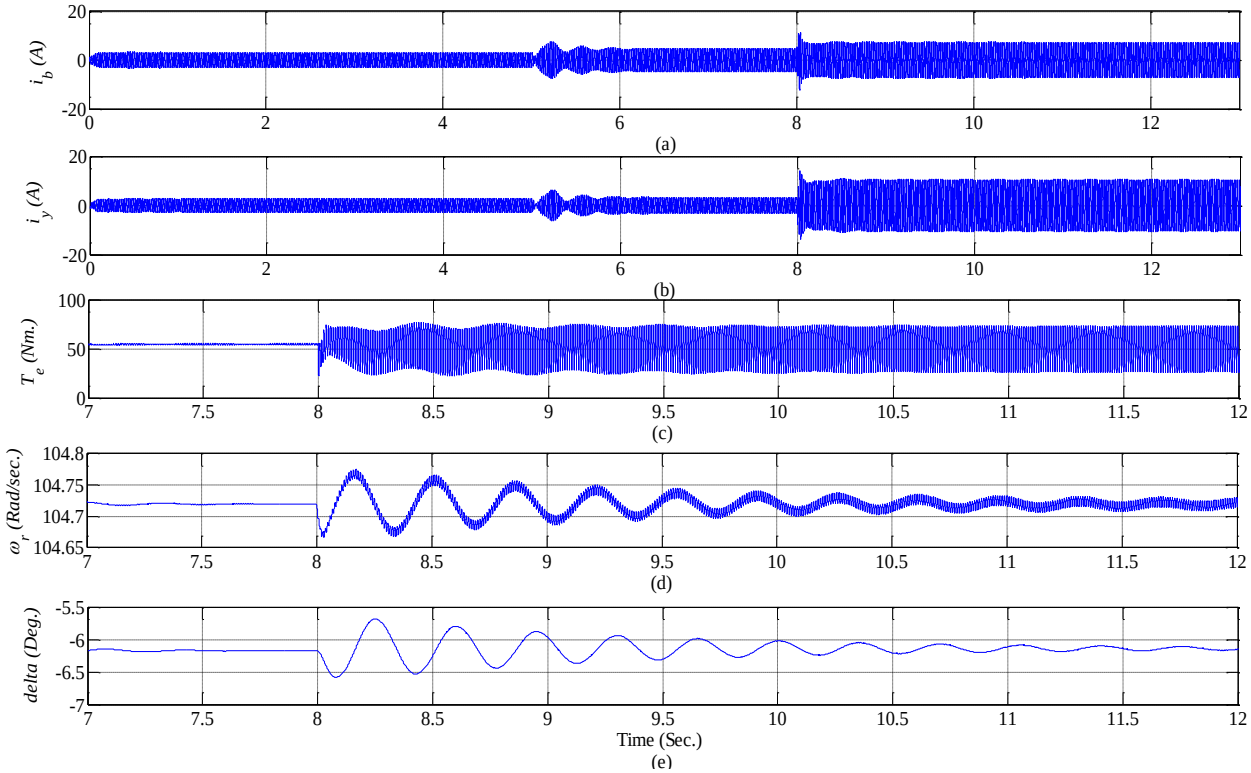

Fig. 4.4: Transient response of motor during pre and post-fault of double phase open circuit showing currents (a) i_b (b) i_y (c) Torque T_e (d) speed ω_r (e) load angle *delta*.

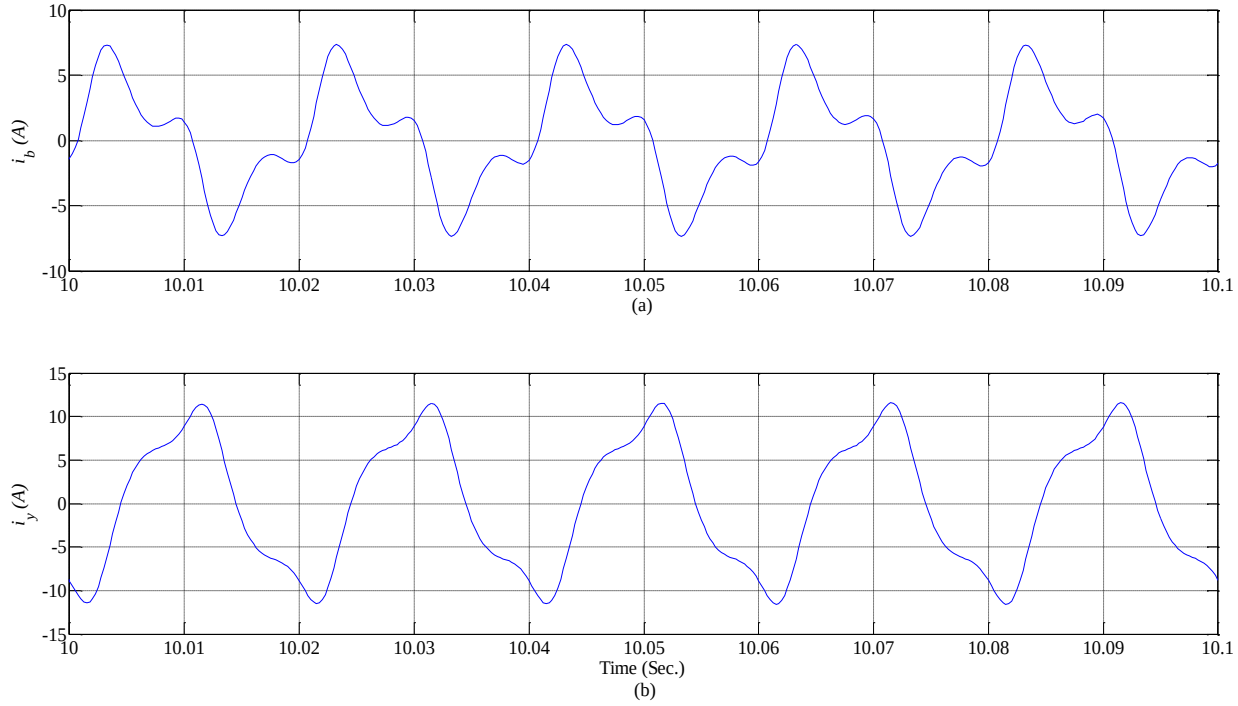

Fig. 4.5: Steady-state phase current of remaining healthy phases (a) i_b and (b) i_y, after the occurrence of double phase open circuit.

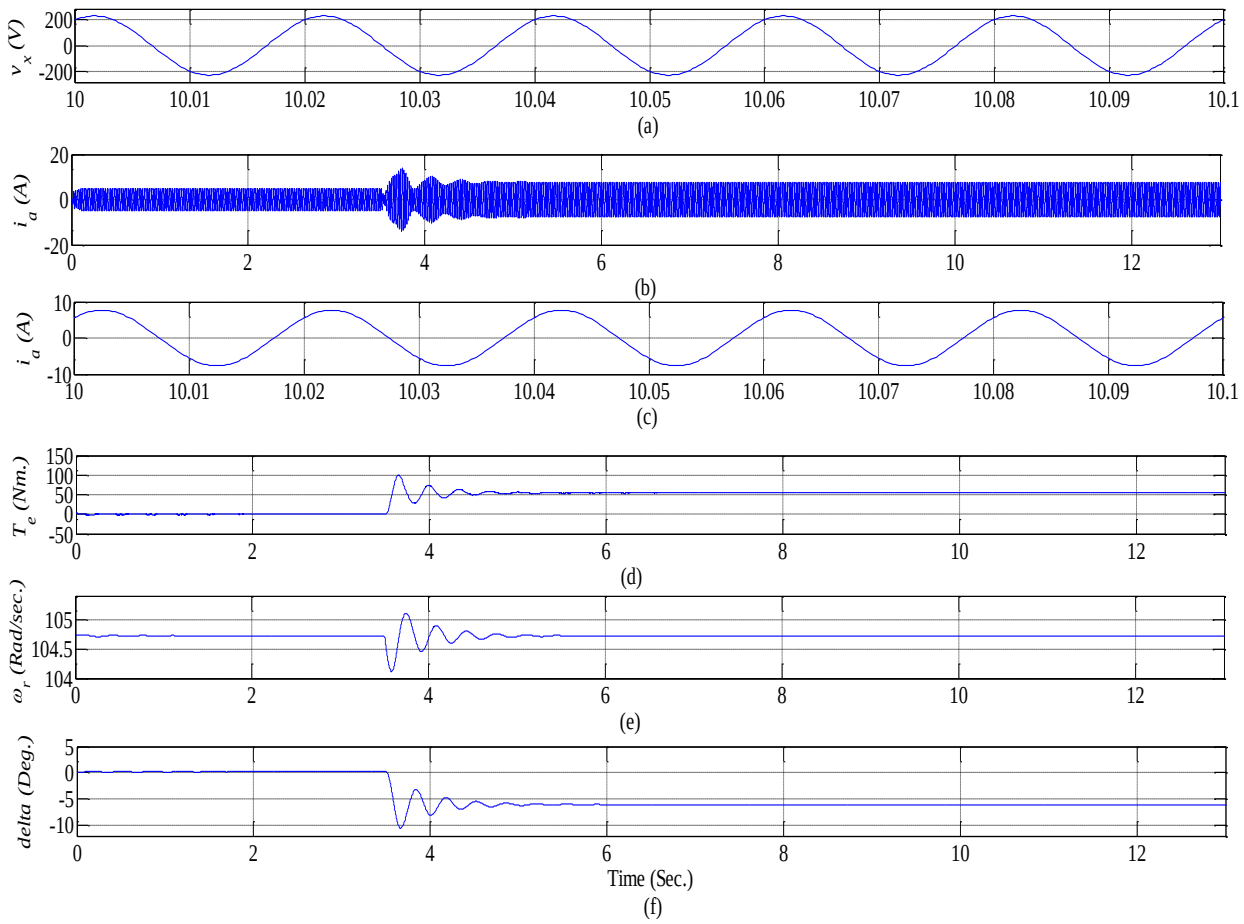

Fig. 4.6: Motor response (a) generated voltage v_x (b) torque T_e (c) speed ω_r (d) load angle *delta*, with input supply in winding set *abc* only.

162.34% (7.60 A) respectively. Similarly, increase of phase current of phase *x* and *y* was found to be 34.58% (3.61 A) and 50.42% (3.61 A) respectively.

4.3.3 Supply in one winding set (*abc*) only

With the assumption of a complete outage of input supply for winding set *xyz*, simulation was carried out for the supply in one winding set *abc* only. Therefore, the constant output power will have to be supplied by winding set *abc* only, so the magnitude of current was found to be increased by 5.45 A approximately, for each phase. It can be noted that output power of machine is both in the form of mechanical (to supply load torque) as well as the electrical (voltage generation in winding set *xyz*), hence working simultaneously as a motor and generator both at the same time. Voltage generation in winding set *xyz*, due to the transformer action was found to be 159.94 V approximately, for each phase. Waveform of generated voltage v_x and phase current i_a is shown in Fig. 4.6 (a) and Fig. 4.6 (b), respectively. In this mode, the

production of harmonics was found to be decreased considerably, when compared to the above cases of open circuit, reflected in the motor response. This is because of reduced sensitivity of the motor towards supply asymmetries, working with three phase winding configuration. Therefore, the flow of current into motor was found to be more balanced, but with an increased magnitude.

Motor operation with one or more phase opened has been discussed in above section. In these explanations supply asymmetry is considered. Exploration along with its experimental validation has been presented later in chapter 7. Furthermore, analytical results are also presented without considering the supply asymmetry, with its aim to have a better picture of current distribution during pre and post-fault conditions. This situation has been analysed at different motor load and input voltage levels in Table 4.1 and Table 4.2, respectively. It can be noted that an unbalanced flow of stator current was found in case of single phase open circuit (i.e. $i_a = 0$). Consequently, current in remaining healthy phase of winding set *abc* decreases, whereas it increases in winding set *xyz* in an irregular way. On the other hand, a balanced flow of current in each winding set *abc* and *xyz* can be noted for double phase open circuit fault (i.e. $i_a = i_x = 0$). During this condition, a slight variation in current magnitude in stator winding sets (*abc* and *xyz*) was observed. This is perhaps due to the existence of asymmetrical winding configuration of stator. It was also noted that at a particular open circuit fault, the pattern of current variation is same, when observed at different motor load and input voltage level. Change in operating condition (motor load or input voltage) only results in the variation of pre and post fault current magnitude.

4.4 Simulation results during Short circuit conditions

A flow chart of the developed simulation program during short circuit condition is shown in Fig. 4.7. Same is equally valid for all the cases of short circuit, irrespective of its nature (asymmetrical or symmetrical). Simplification and effectiveness of simulation program can be noted, as it uses the machine variables in rotor reference frame, i.e. Park's (*dq0*) variables.

4.4.1 Asymmetrical Short circuit

Most frequent occurrence of a short circuit at the input terminals of motor drive system is asymmetrical in nature, particularly the single line to ground (LG) fault. However, other causes

Table 4.1: Pre and post fault current during open-circuit at input motor terminals at different load with phase voltage of 160 V neglecting supply asymmetry

Motor load	**Operating modes**	**Motor phase current**					
		i_a	i_b	i_c	i_x	i_y	i_z
25 %	Normal	1.14	1.14	1.14	1.14	1.14	1.14
	Single phase OC	0	1.04	1.04	1.96	1.98	1.20
	Double phase OC	0	2.68	2.68	0	2.70	2.70
	Three phase supply only	2.27	2.27	2.27	0	0	0
50 %	Normal	2.29	2.29	2.29	2.29	2.29	2.29
	Single phase OC	0	2.08	2.08	3.93	3.96	2.40
	Double phase OC	0	5.28	5.28	0	5.46	5.46
	Three phase supply only	4.55	4.55	4.55	0	0	0

Table 4.2: Pre and post fault current during open-circuit at input motor terminals operating with different voltage levels at 50 % load neglecting supply asymmetry

Voltage level	**Operating modes**	**Motor phase current**					
		i_a	i_b	i_c	i_x	i_y	i_z
160	Normal	2.29	2.29	2.29	2.29	2.29	2.29
	Single phase OC	0	2.08	2.08	3.93	3.96	2.40
	Double phase OC	0	5.28	5.28	0	5.46	5.46
	Three phase supply only	4.55	4.55	4.55	0	0	0
200	Normal	1.83	1.83	1.83	1.83	1.83	1.83
	Single phase OC	0	1.66	1.66	3.14	3.17	1.92
	Double phase OC	0	4.21	4.21	0	4.35	4.35
	Three phase supply only	3.63	3.63	3.63	0	0	0

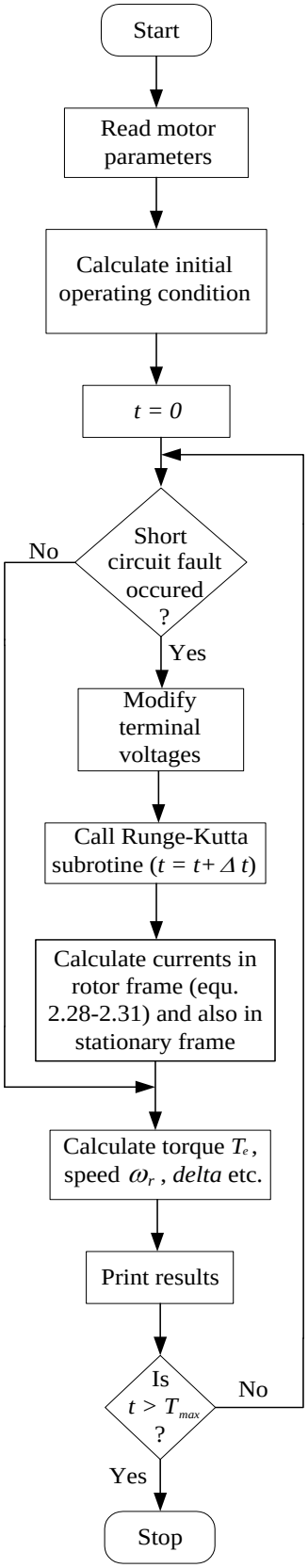

Fig. 4.7: Flow chart for evaluating the performance during short circuit.

include the short circuit among different input terminals of motor, e.g. line-line to ground (LLG) fault. Analysis of the asymmetrical short circuit is computationally complex [63], when dealing with the multiphase system. Therefore, it has been explored and studied by using a detailed dynamic simulation of six-phase synchronous motor (whose simulation steps are shown in Fig. 4.7) by modifying the input voltage for such conditions.

Simulation has been carried out for line to ground (LG) short circuit (most frequent case of short circuit), assuming it to take place at phase a by putting the value of its phase voltage equal to zero ($v_a = 0$). It has been assumed that the condition of short circuit prevails for a short duration (10 cycle i.e. 0.12 sec.). Short circuit occurs at time $t = 7$ sec. and motor current in all the phases has been depicted in Fig. 4.8, in stationary reference frame. Asymmetrical flow in each stator winding set can be noted from this figure. Moreover, due to the highly inductive nature of stator windings, a change in a phase current (hence a change in its magnetic flux) is equally compensated by opposite but equal change in the other winding set of corresponding phase. For example, after the occurrence of short circuit in phase a at time $t = 7$ sec., phase current i_a increases with negative magnitude of 266 A in its first swing in Fig. 4.8 (a). In order to maintain the constant flux, same change in current i_x of phase *x* may be noted in Fig. 4.8 (d). Similar variation in current can also be noted in other phases of both the winding sets *abc* and *xyz*. Since, motor output power is assumed to be constant; therefore, the variation in active component of current of a winding set is also compensated by current flowing in other winding set, as depicted in Fig. 4.9. Moreover, the transient offset in phase currents in winding sets *abc* and *xyz* in both stationary and rotor reference frame can also be noted, pulsating at 50 Hz. This transient offset was found to be reflected in instantaneous torque, decaying with 50 Hz. pulsation. Motor electromagnetic torque decreases and becomes less than the load torque. The rotor speed also decreases below the synchronous speed, which results in the increase (in magnitude) in load angle, *delta*. Rotor speed continues to decrease by 104.1 rad/sec. where the motor torque T_e becomes equal to load torque (T_l). At this time, the rotor is running below the synchronous speed and due to motor inertia the torque T_e will continue to increase along with the increase in load angle, *delta*. At the instant of reaching to synchronous speed, motor torque T_e will be greater than the load, resulting the rotor to accelerate towards synchronous speed. In this way, damped oscillation of rotor will continue till it settles to its steady state value, if allowed for a longer duration. The dynamic response of motor torque T_e, rotor speed ω_r and load angle *delta*

is shown in Fig. 4.10, whereas a torque - angle characteristic is shown in Fig. 4.11 in which switching sequence during short circuit has been shown by arrow mark.

As already mentioned that the occurrence of short circuit is usually followed by the open circuit/isolation of the faulted electrical circuit. Following to the occurrence of short circuit at an input terminal, open circuit of that phase was also simulated by putting its current to zero. It was simulated in phase *a* after the time of 0.2 sec. i.e. at time $t = 7.2$ sec. This also resulted in offset transient at 50 Hz. pulsation of stator current in remaining healthy phases in stationary as well as rotor reference frame is shown in Fig. 4.12 and Fig. 4.13, respectively. A much reduced current magnitude may be noted during transient period, when compared with short circuit current, and within a short duration (0.3 sec.) current settles to its new steady-state value. Rotor behavior during this condition is shown in Fig. 4.14 and dynamic torque-angle characteristic is shown in Fig. 4.15. A detailed explanation during open circuit at a single phase has already been presented in the previous section.

4.4.2 Symmetrical Short circuit:

Symmetrical short circuit at the motor input terminals result in a balanced flow of current in both the stator winding sets *abc* and *xyz*. This condition has been simulated at the input terminals of winding set *abc*, by putting its all phase voltages equal to zero i.e. $v_a = v_b = v_c = 0$. Initialization of short circuit was simulated at time $t = 7$ sec. and was cleared within 3 cycle i.e. 0.06 sec. If the fault was allowed to remain in the system for slight longer, problem of instability was noted, i.e. the motor could not return to its steady state at synchronous speed. Following the occurrence of symmetrical short circuit, the transient offset pulsating at 50 Hz in phase current of both winding sets *abc* and *xyz* can be noted in stationary reference frame as shown in Fig. 4.16. But transient offset was not observed when current was expressed in rotor reference frame as shown in Fig. 4.17. This is because of a tremendous increase of the magnitude of *d-q* component of stator current as compared to the magnitude of ripples in offset current in rotor reference frame. Also, symmetrical flow of current further decreases the magnitude of offset current ripples. Rotor behavior indicated by its speed and load angle variation along with the motor developed torque is shown in Fig. 4.18. Characteristic curve for torque-angle is shown in Fig. 4.19, where the arrow mark signifies the outgoing and returning of operating mode to its steady-state.

Furthermore, isolation of faulted element by open circuit of winding set *abc*, is now explored by putting the currents of all the phase equal to zero ($i_a = i_b = i_c = 0$), as shown in stationary as well as rotor reference frame in Fig. 4.20 and Fig. 4.21, respectively. After the open circuit/isolation of one stator winding set *abc*, motor will act as a three phase synchronous motor, with only input supply in winding set *xyz*. Response of machine in this mode (three phase synchronous motor) has been depicted in Fig. 4.22 and Fig. 4.23.

4.4.3 Discussion about short circuit

In the above presented simulation results of asymmetrical and symmetrical short circuit, utilization of detailed dynamic model was efficiently used. Frequently, it can be noted that in analytical approach [63-64], rotor speed is assumed to be constant during short circuit period. This is because the short circuit condition in electrical circuitry is allowed for a few cycle, resulting in the tremendous increase in machine current. This assumption facilitates to obtain a closed-form solution, which provides the insight performance of motor operation, not possible with above dynamic simulation [63]. The assumption of constant speed during the period of short circuit has been incorporated here by increasing the value of moment of inertia/inertia constant (say, 1000 times). The steady state value of phase current can then be easily determined under different short circuit conditions, whose correctness can be checked by the analytical approach, if required. Phase current magnitude with the variation of type of short circuit and change in input voltage levels is depicted in Table 4.3. A direct proportionality in the magnitude of phase current can be noted with input voltage level. Further, existence of asymmetry can also be observed due to the flow of unbalanced current of different magnitude of a particular winding set during asymmetrical short circuit condition (LG/LLG). Current magnitude in a winding set was found to increase with increase in the number of shorted terminals and is maximum for the case of LLLG (symmetrical) short circuit. It is also important to emphasize here that the symmetrical nature of current flow was found to be increased with the increase in number of shorted terminals and finally becomes symmetrical in nature during symmetrical short circuit LLLG.

Variation in the magnitude of phase current has been shown with the variation of motor load in Table 4.4. Current magnitude of a particular phase remains almost unaffected under different load conditions, but it changes for different short circuit cases, as discussed above.

It is important to have an insight on the nature of motor developed torque during asymmetrical and symmetrical short circuit cases. This has been shown in term of the variation of torque ripple magnitude with the variation of input voltage level and at different load in Fig. 4.24 (a) and Fig. 4.24 (b), respectively. The pattern of torque ripple variation was found to follow the same as that of winding current and is more dependent on the variation of voltage level than the variation of different load conditions. In these figures, *x*-axis denotes the type of short circuit case where integral value should be read as - 0: normal condition, 1: LG short circuit, 2: LLG short circuit, 3: symmetrical LLLG short circuit.

4.5 Post fault control scheme:

Operating performance during post-fault condition can be made better by increasing the number of phase [6], making multiphase ac motor suitable for fault tolerant drive system. It is worthwhile to mention here that depending upon the application, post-fault control scheme can be adopted for the system where high performance output can't be compromised during the occurrence of open circuit. Different post-fault control schemes have been reported for multiphase motor operation . Regardless to the type of control scheme, every scheme tries to maintain the airgap flux constant in post-fault condition by having a suitable combination of current in remaining healthy phases. Authors in ref. [28] have shown that by using a five-phase or seven-phase motor, it is possible to take advantage of additional degrees of freedom as a result of more phases, resulting in current combination so as to produce a smooth non-pulsating torque. An exclusive analysis of five-phase synchronous motor under asymmetrical fault condition is covered in ref. [65], wherein a synchronous frame current controller was designed which was shown to be superior than the conventional hysteresis current controller. Analysis of dual three-phase induction motor is available in literatures [27-33]. Zhao and Lipo [27] analysed the motor with asymmetrical winding structure, where the concept of space vector decomposition was utilised. A general model suitable for both healthy and faulty condition was given by Singh and Pant [29], whereas the possibility of different winding configuration during fault condition was addressed by Alberti and Bianchi [30]. Control of six-phase induction motor can equally be applied with six-phase synchronous motor. However, as far as control of six-phase synchronous motor is concerned it is still underway.

A block diagram showing a simple, effective and a self-explanatory post-fault control scheme, which can be easily implemented in six-phase synchronous motor is shown in Fig. 4.25.

The technique is actually an extension of the control of three-phase motor [66], where the connection of motor's star point is required at zero potential. Approach for a six-phase motor fed from two current-controlled inverter (for *abc* and *xyz* winding sets) suggests that the two remaining healthy phase current of a particular winding set should be phase shifted by 30^0 electrical away from the faulted phase and their magnitude should be increased by a factor of $\sqrt{3}$. A complete analysis and performance evaluation of the control scheme will be reported in future research work.

4.6 Conclusion:

A unified and simplified approach was adopted for digital simulation for different cases of open circuit fault at input terminals of six-phase synchronous motor using *dq0* variables. This approach can be extended for any type of multiphase machine, accompanying the open circuit fault at its one or more phases. This methodology has been adopted for the analysis of six-phase synchronous machine to explore the redundancy characteristic of motor, commonly used for higher power application. This includes the open conductor fault at one phase, two phases and three phases (complete outage of one set of input supply) of input terminal of motor. As the number of open conductor fault increases at input terminal of motor, power shared by the remaining healthy winding set/phases was found to be increased. It was observed analytically (and experimentally validated in chapter 7) that the motor continues to operate satisfactorily even during the outage of one or more input supply phases. Therefore, it can be concluded that in normal operation, fault in one of the two three phase winding set can even be sustained and motor continue to give a satisfactory operation. This characteristic is very important for the operation of motor where reliability is of prime importance. Also, the simultaneous operation of machine as a motor and as a generator, when one set of stator winding is supplied by one three-phase source only, is a very attractive property, making it suitable for some special application (like power supply of air conditioner in electric railway etc.).

A detailed simulation has been carried out for the different cases of short circuit (both asymmetrical and symmetrical) occurring at the motor input terminals, in a simplified way. The similar logical steps of simulation program, (shown in form of flow chart) can be efficiently used for any multiphase machine. In the above sections, two cases of asymmetrical short circuit (LG and LLG) have been simulated, which prevails for 10 cycles (i.e 0.12 sec.), resulting in an

unbalanced flow of current in both the stator winding sets *abc* and *xyz*. It was found that the motor operating under asymmetrical short circuit is more stable, whereas instability is noted if it operates for more than three cycles during symmetrical short circuit, but results in a balanced flow of stator current. In general, an excessive increase in the magnitude of stator current was noted which was maximum during symmetrical short circuit. The nature of variation in current magnitude is also reflected in the ripple magnitude of motor torque T_e, and found to be dependent on input voltage level of the motor. A small variation in torque ripple magnitude was noted with the change in motor load.

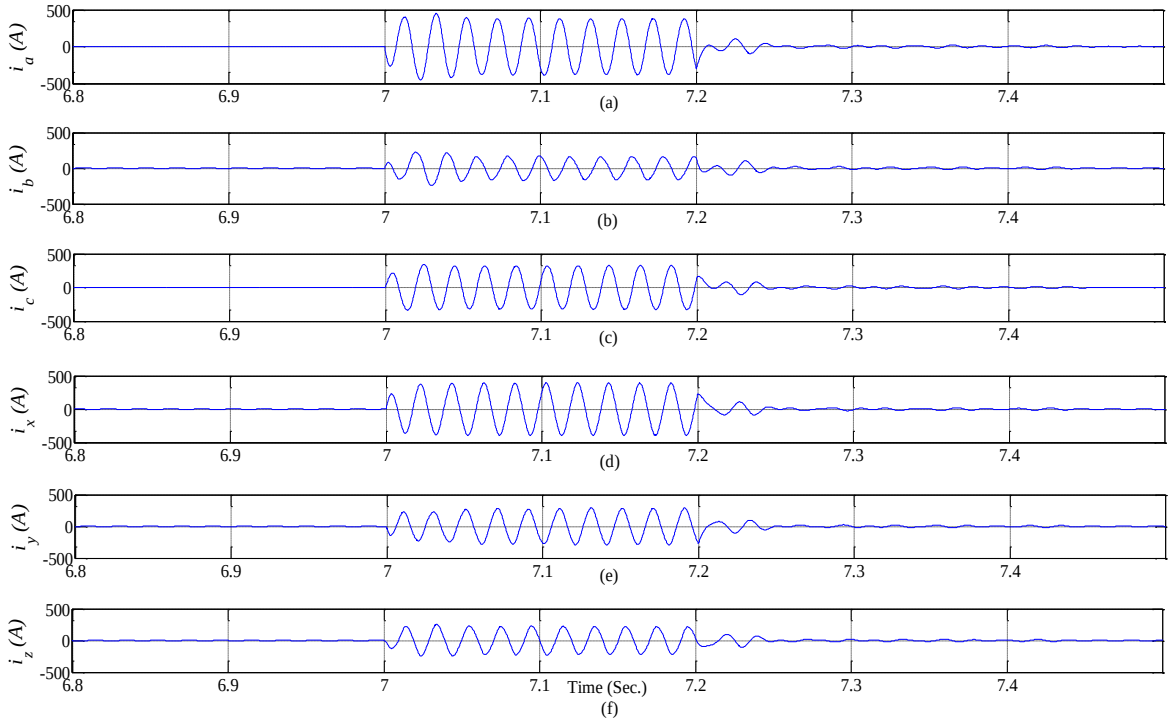

Fig. 4.8: Motor phase current (in stationary reference frame) during LG short circuit which is cleared within 0.2 sec. showing (a) i_a *(b)* i_b (c) i_c (d) i_x (e) i_y (f) i_z .

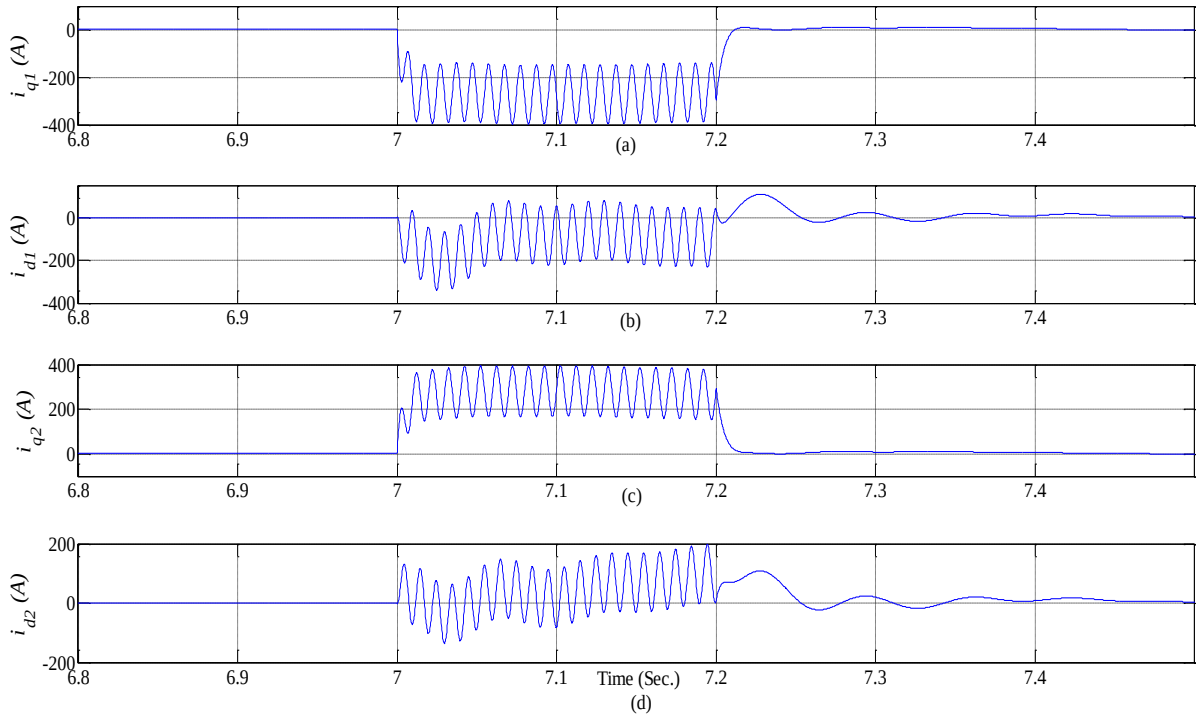

Fig. 4.9: *d-q* current component of both winding sets *abc* and *xyz* during LG short circuit which is cleared within 0.2 sec. showing (a) i_{q1} (b) i_{d1} (c) i_{q2} (d) i_{d2} .

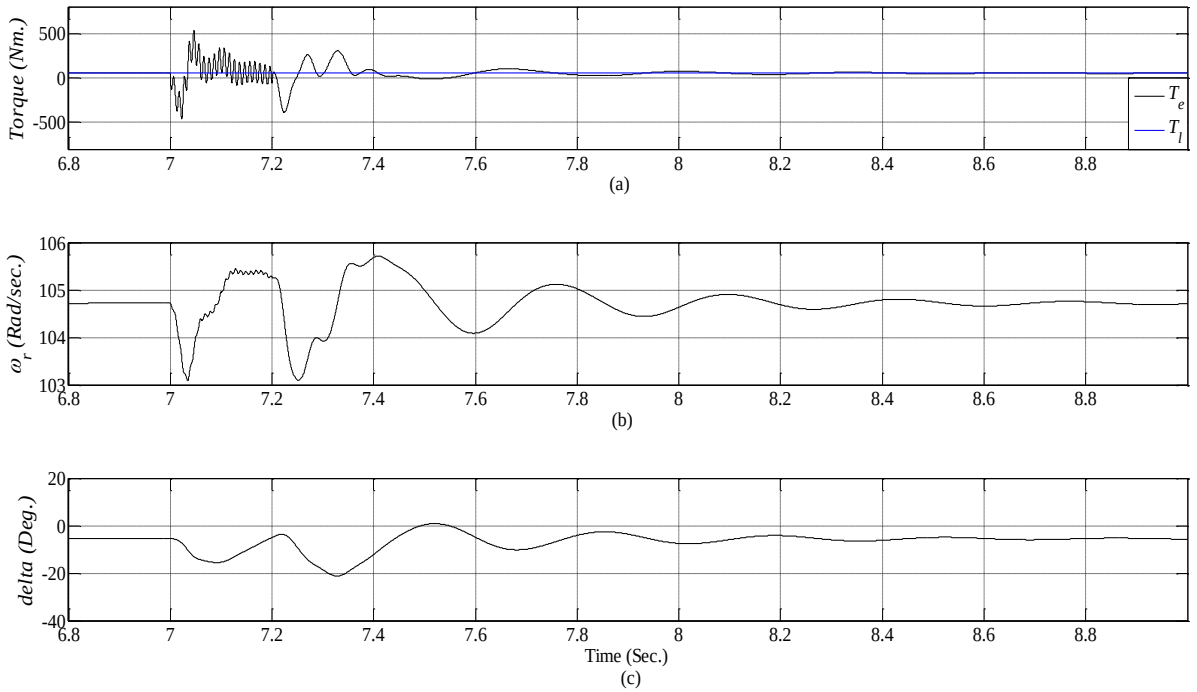

Fig. 4.10: Motor response during LG short circuit which is cleared within 0.2 sec. showing (a) Torque T_e (b) speed ω_r (c) load angle *delta*.

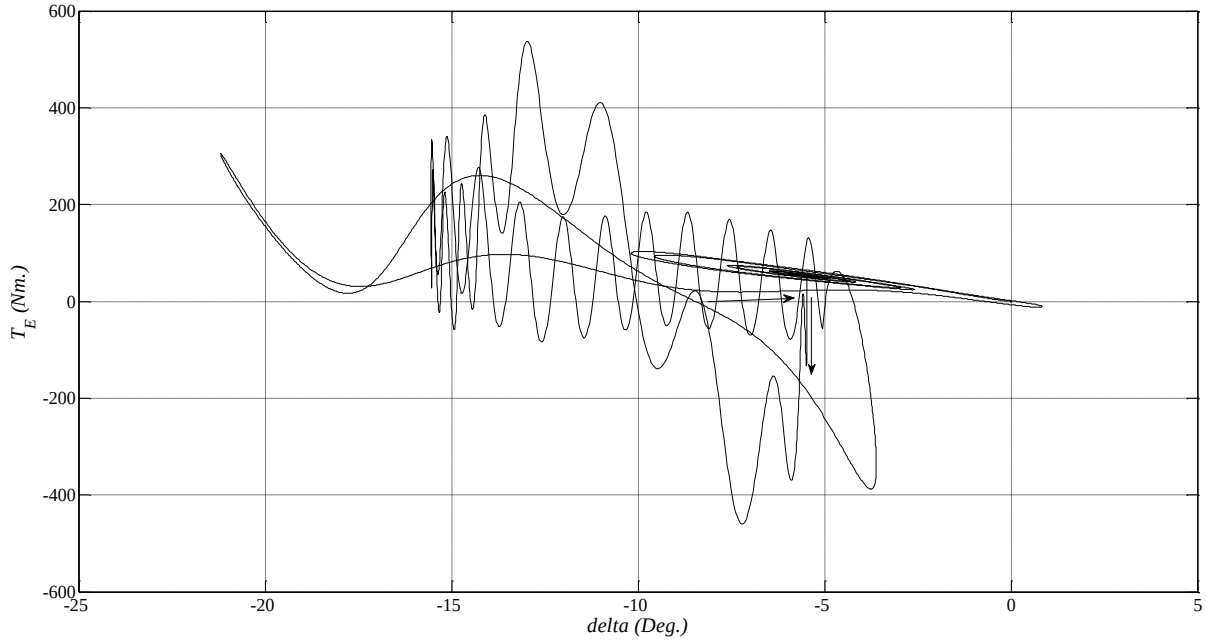

Fig. 4.11: Torque-angle characteristic during LG short circuit which is cleared within 0.2 sec.

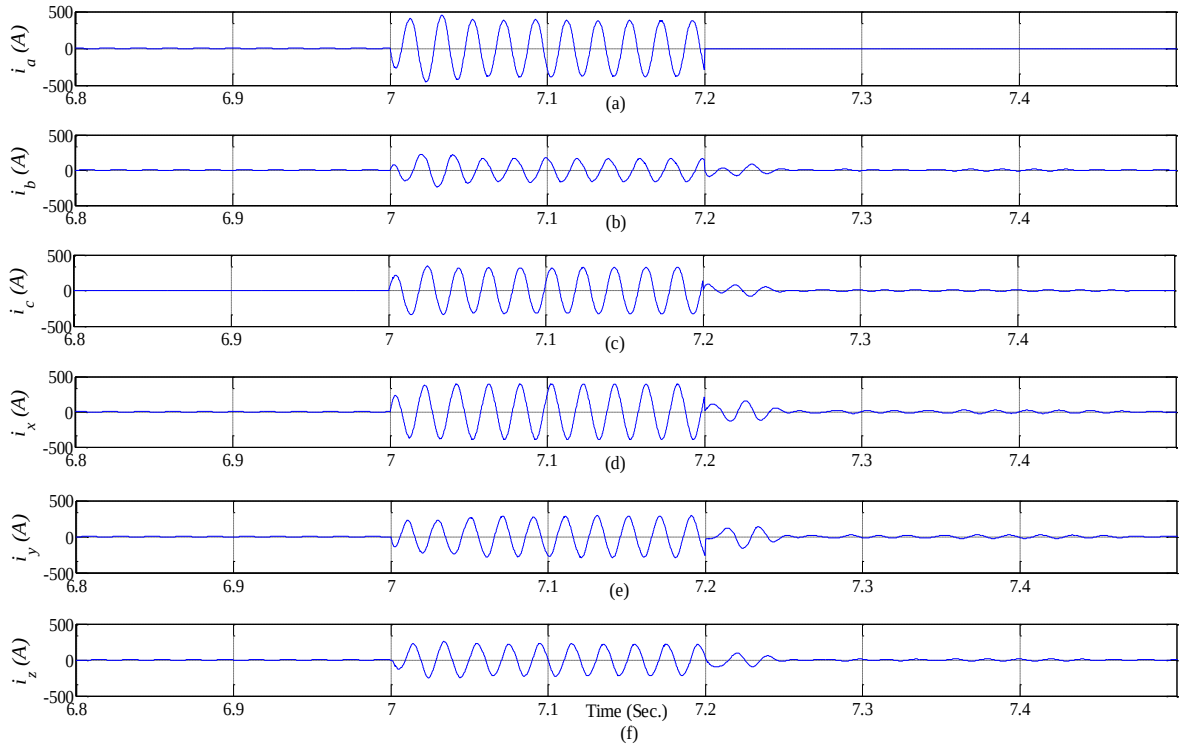

Fig. 4.12: Motor phase current (in stationary reference frame) during LG short circuit, followed by open-circuit showing (a) i_a *(b)* i_b (c) i_c (d) i_x (e) i_y (f) i_z .

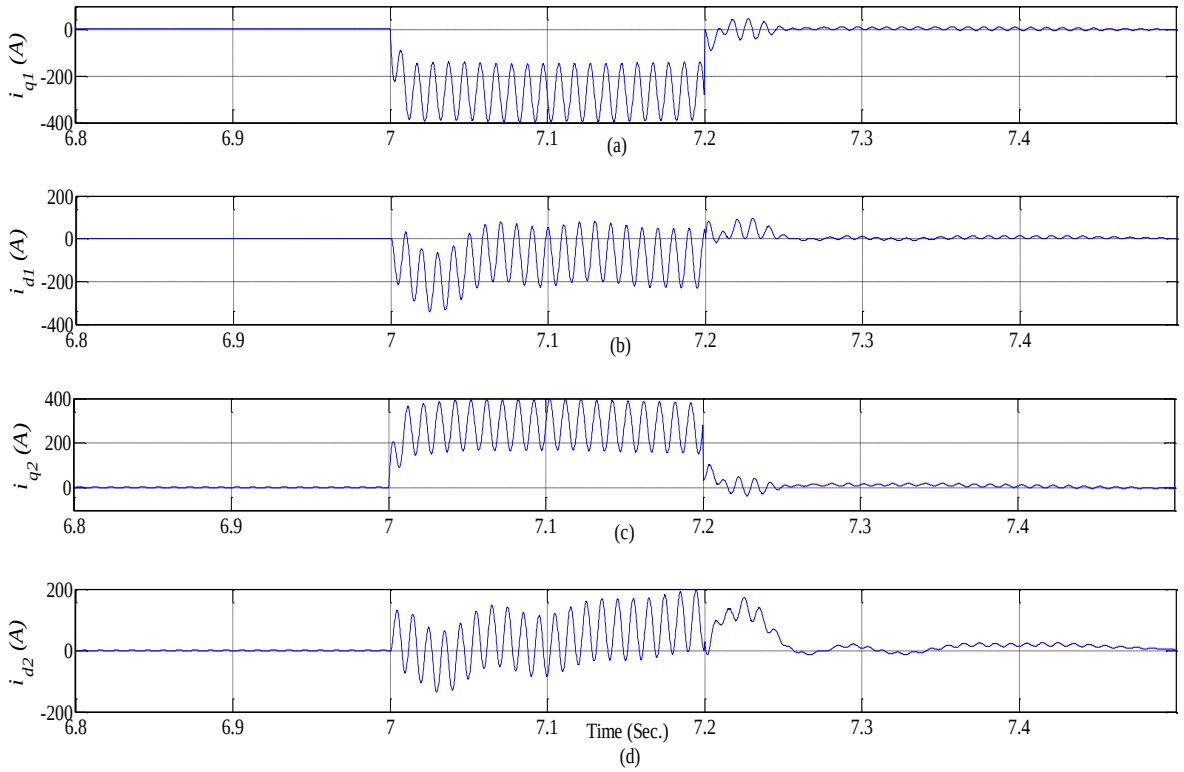

Fig. 4.13: *d-q* current component of both winding sets *abc* and *xyz* during LG short circuit , followed by open-circuit showing (a) i_{q1} (b) i_{d1} (c) i_{q2} (d) i_{d2} .

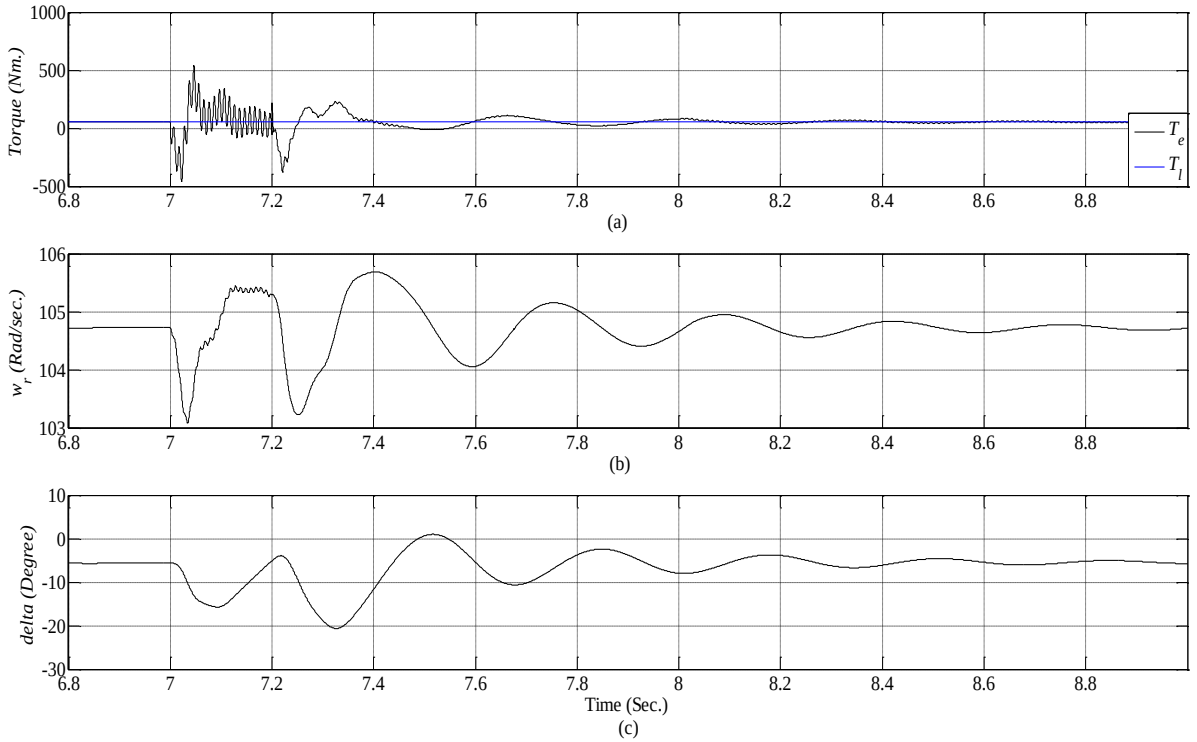

Fig. 4.14: Motor response during LG short circuit, followed by open-circuit showing (a) Torque T_e (b) speed ω_r (c) load angle *delta.*

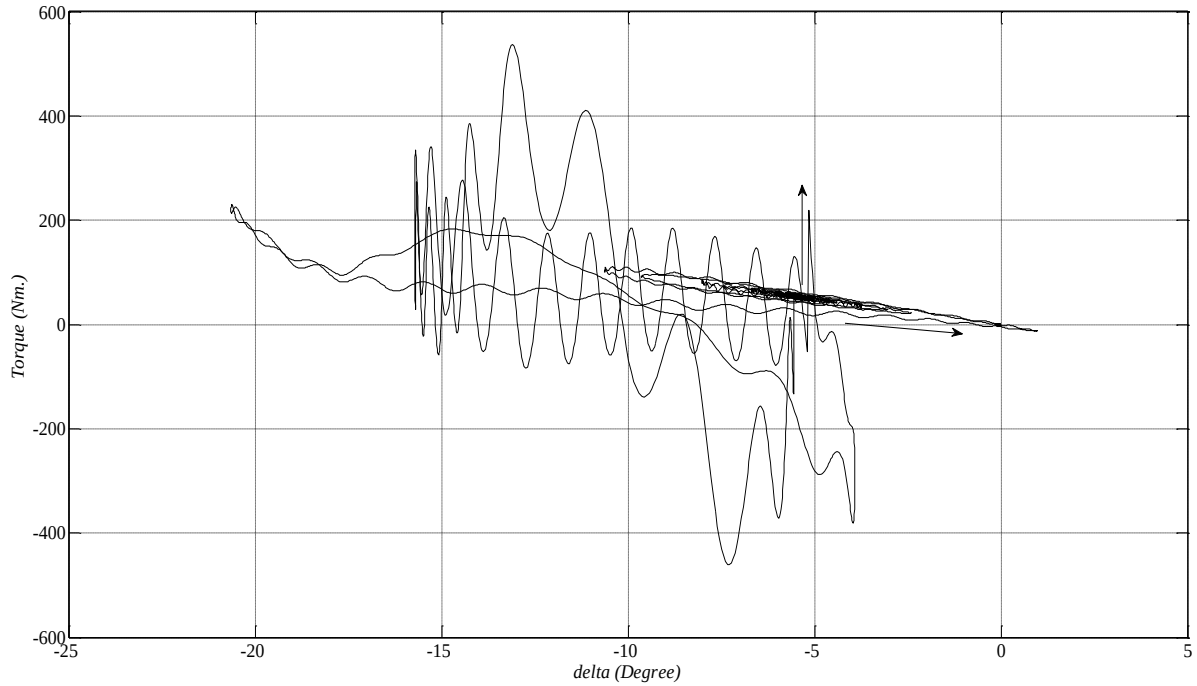

Fig. 4.15: Torque-angle characteristic during LG short circuit, followed by open-circuit.

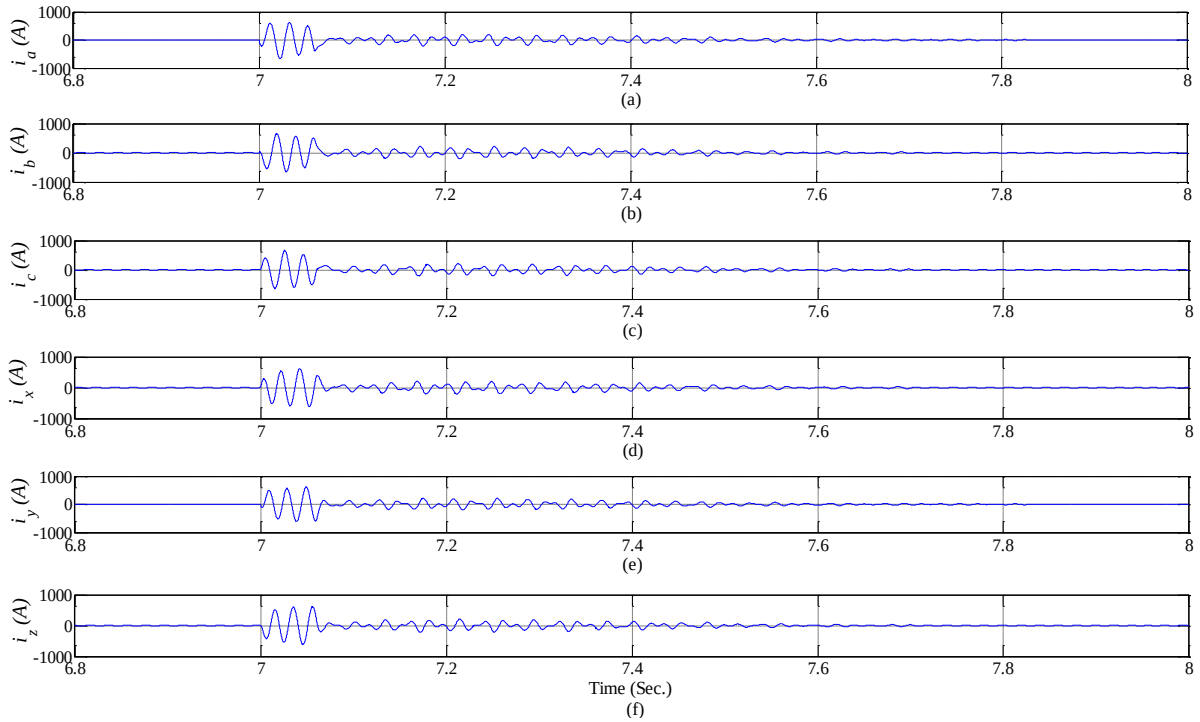

Fig. 4.16: Motor phase current (in stationary reference frame) during LLLG short circuit which is cleared within 0.06 sec. showing (a) i_a *(b)* i_b (c) i_c (d) i_x (e) i_y (f) i_z .

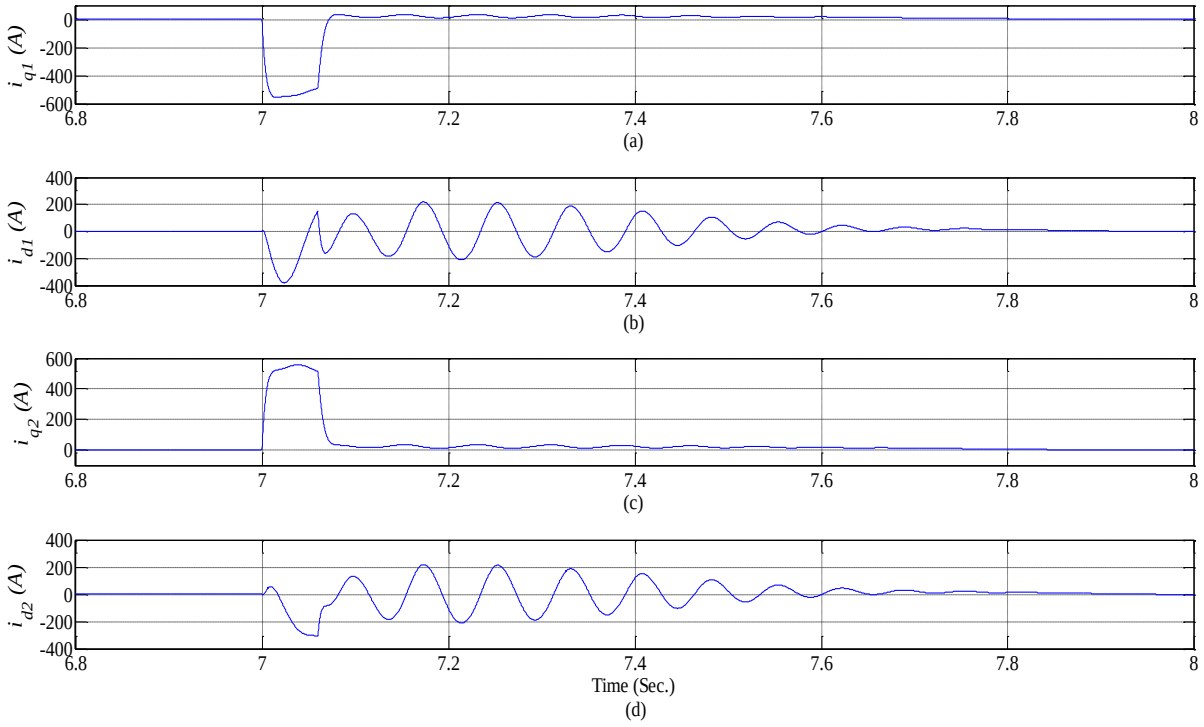

Fig. 4.17: *d-q* current component of both winding sets *abc* and *xyz* during LLLG short circuit which is cleared within 0.06 sec. showing (a) i_{q1} (b) i_{d1} (c) i_{q2} (d) i_{d2} .

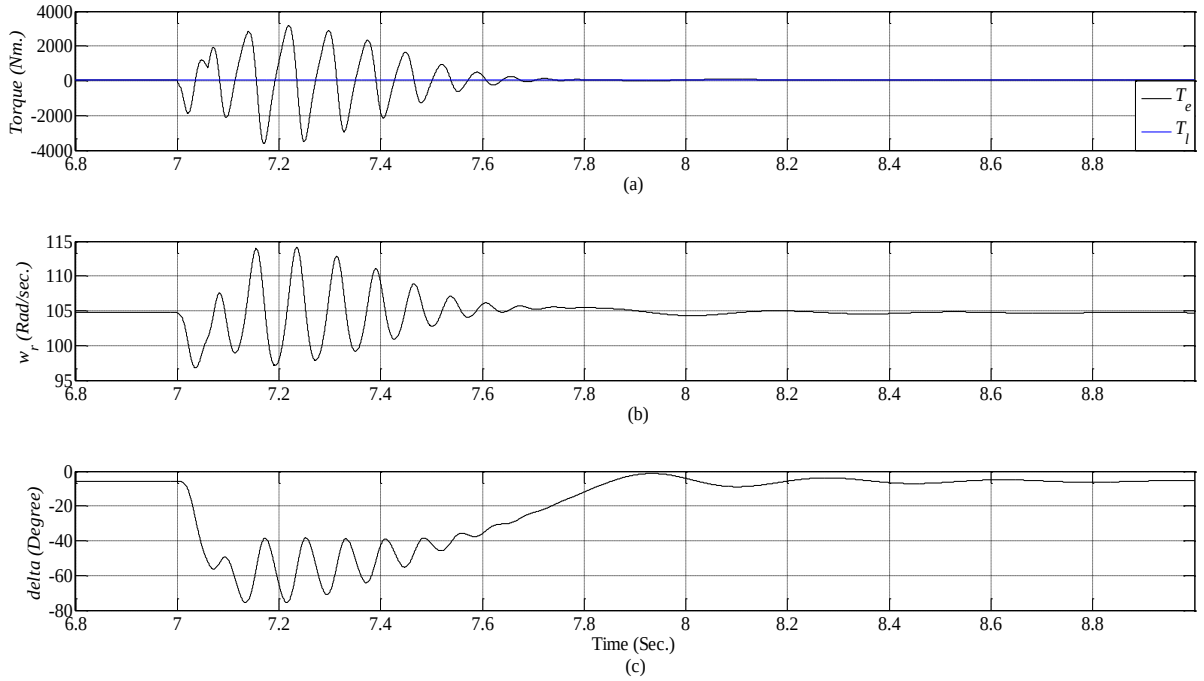

Fig. 4.18: Motor response during LLLG short circuit which is cleared within 0.06 sec. showing (a) Torque T_e (b) speed ω_r (c) load angle *delta.*

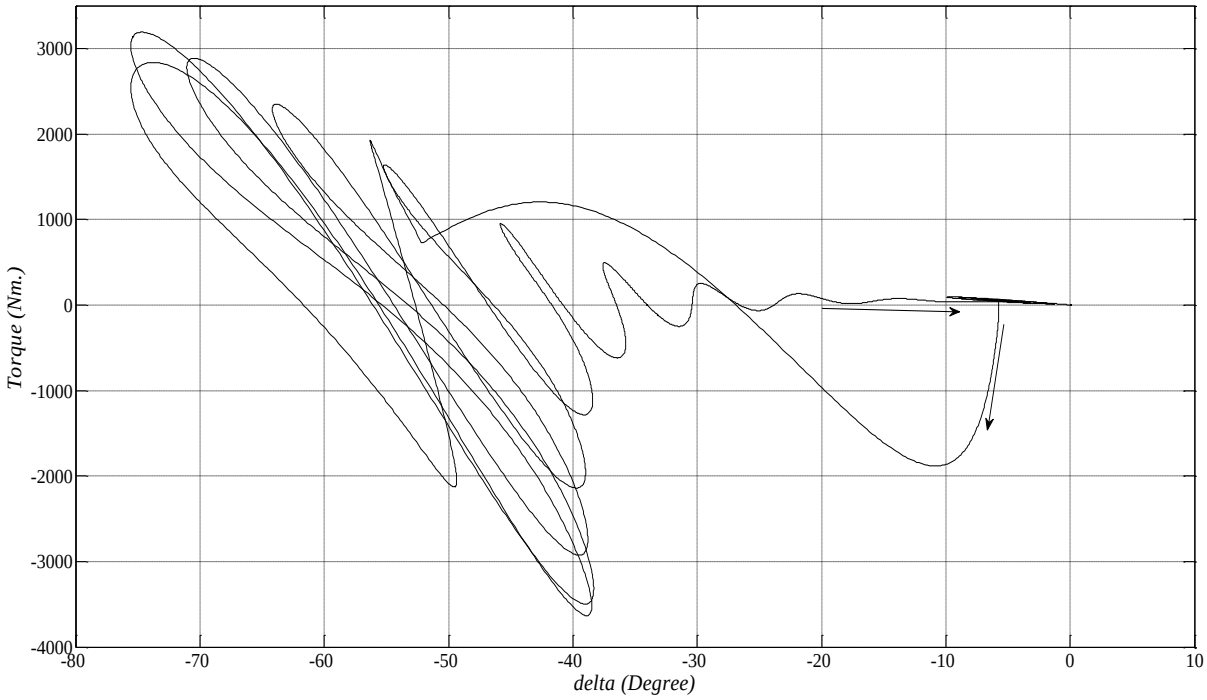

Fig. 4.19: Torque-angle characteristic during LLLG short circuit which is cleared within 0.06 sec.

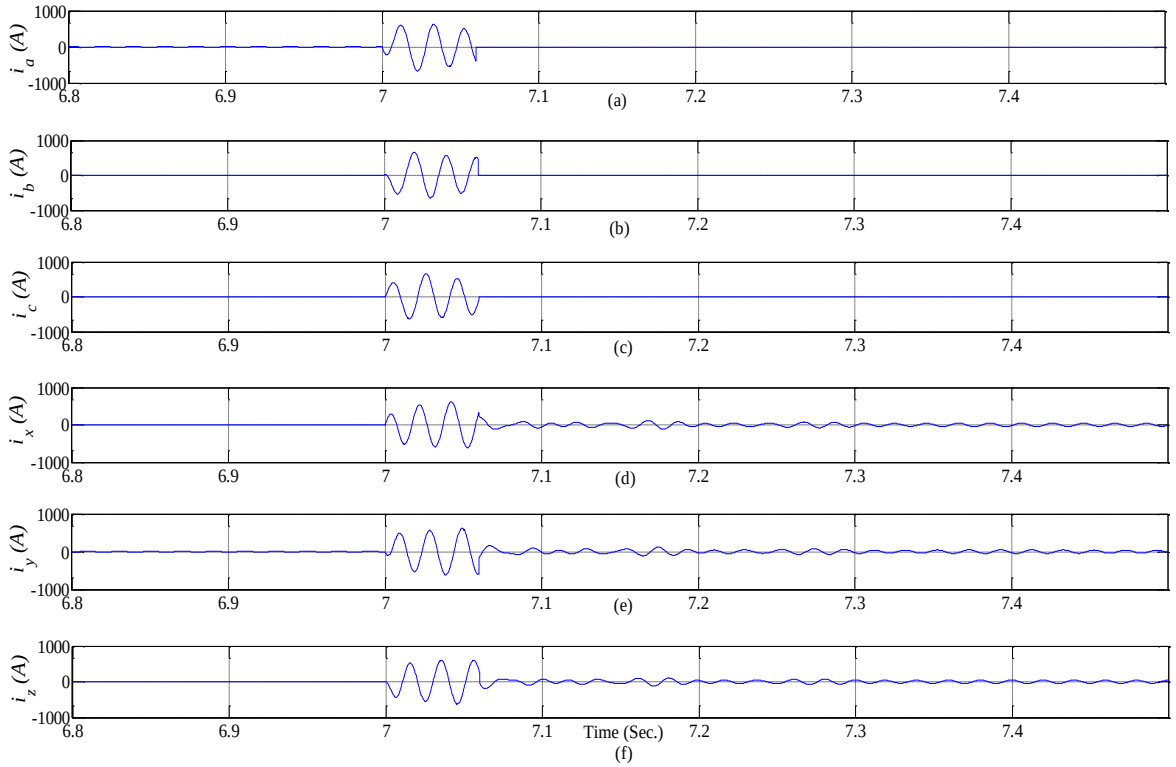

Fig. 4.20: Motor phase current (in stationary reference frame) during LLLG short circuit, followed by open- circuit showing (a) i_a *(b)* i_b (c) i_c (d) i_x (e) i_y (f) i_z .

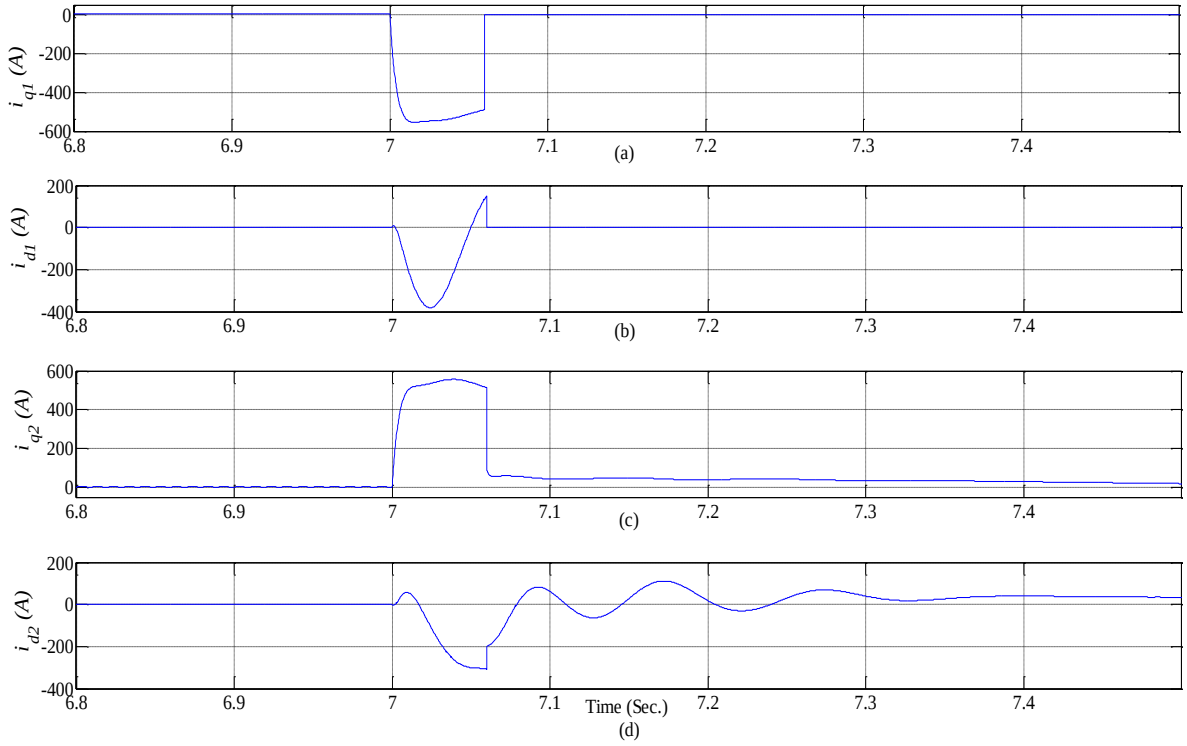

Fig. 4.21 *d-q* current component of both winding sets *abc* and *xyz* during LLLG short circuit, followed by open-circuit showing (a) i_{q1} (b) i_{d1} (c) i_{q2} (d) i_{d2}.

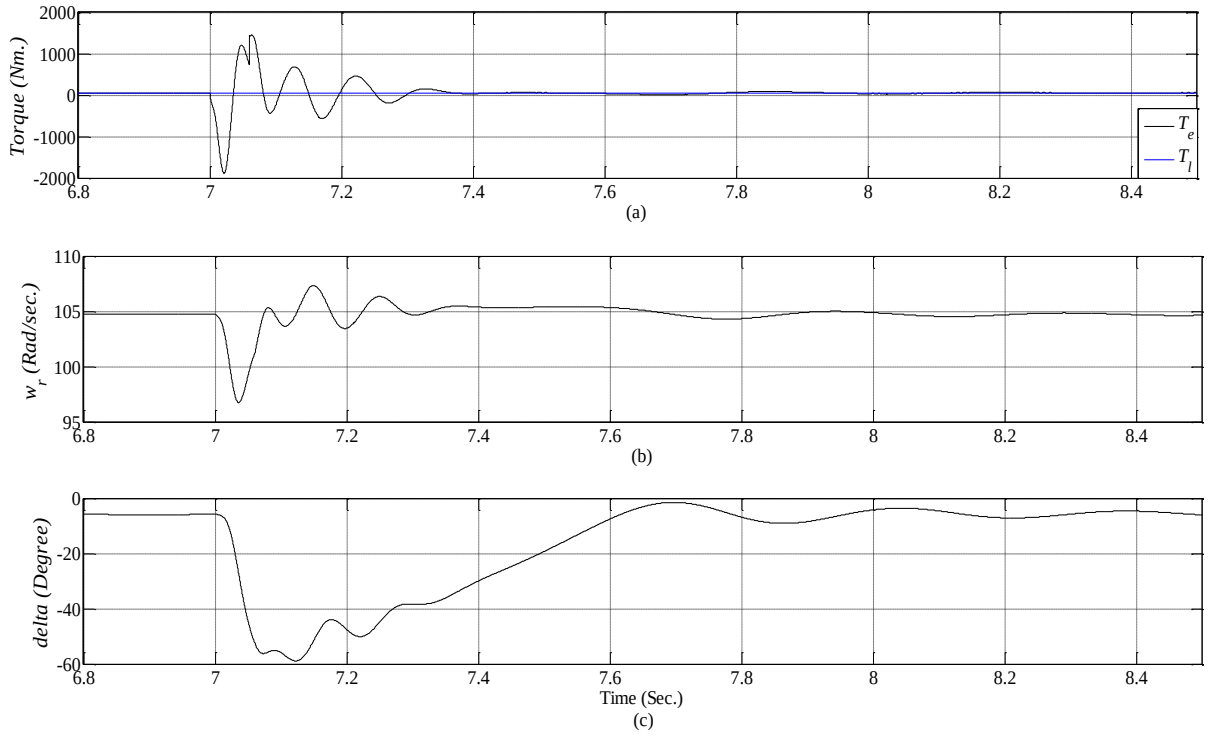

Fig. 4.22: Motor response during LG short circuit, followed by open-circuit showing (a) Torque T_e (b) speed ω_r (c) load angle *delta.*

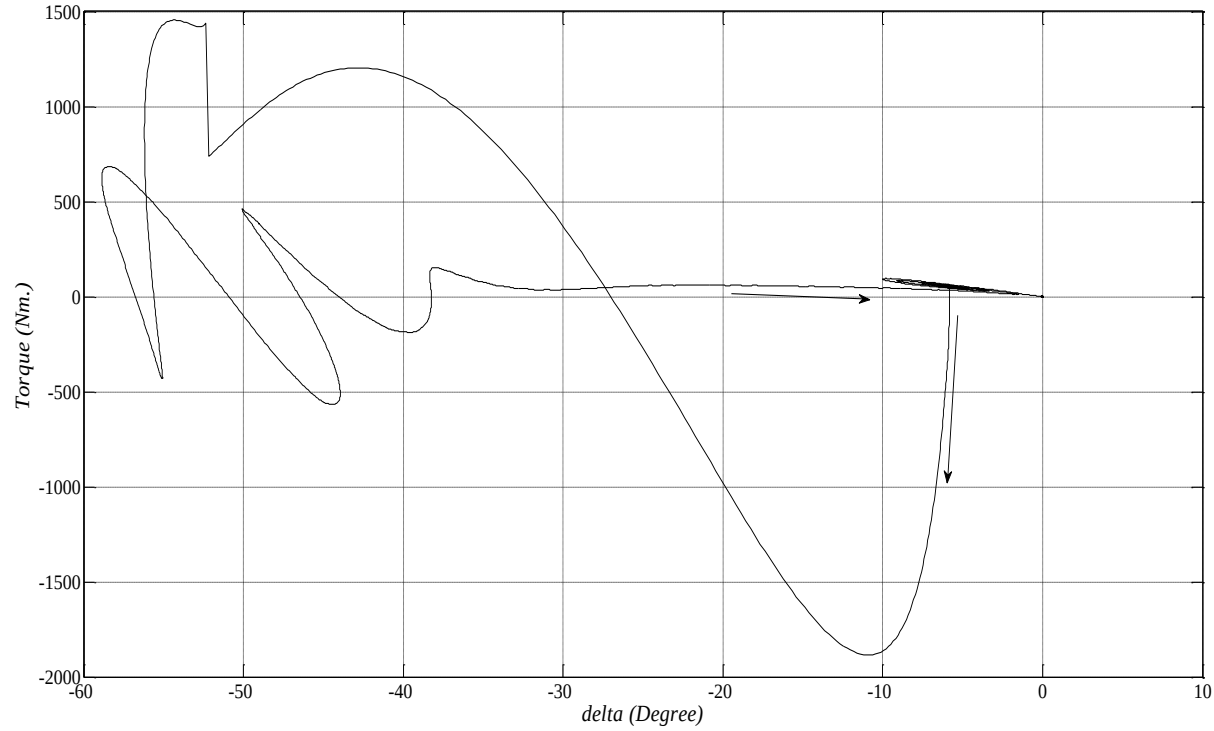

Fig. 4.23: Torque-angle characteristic during LG short circuit, followed by open-circuit.

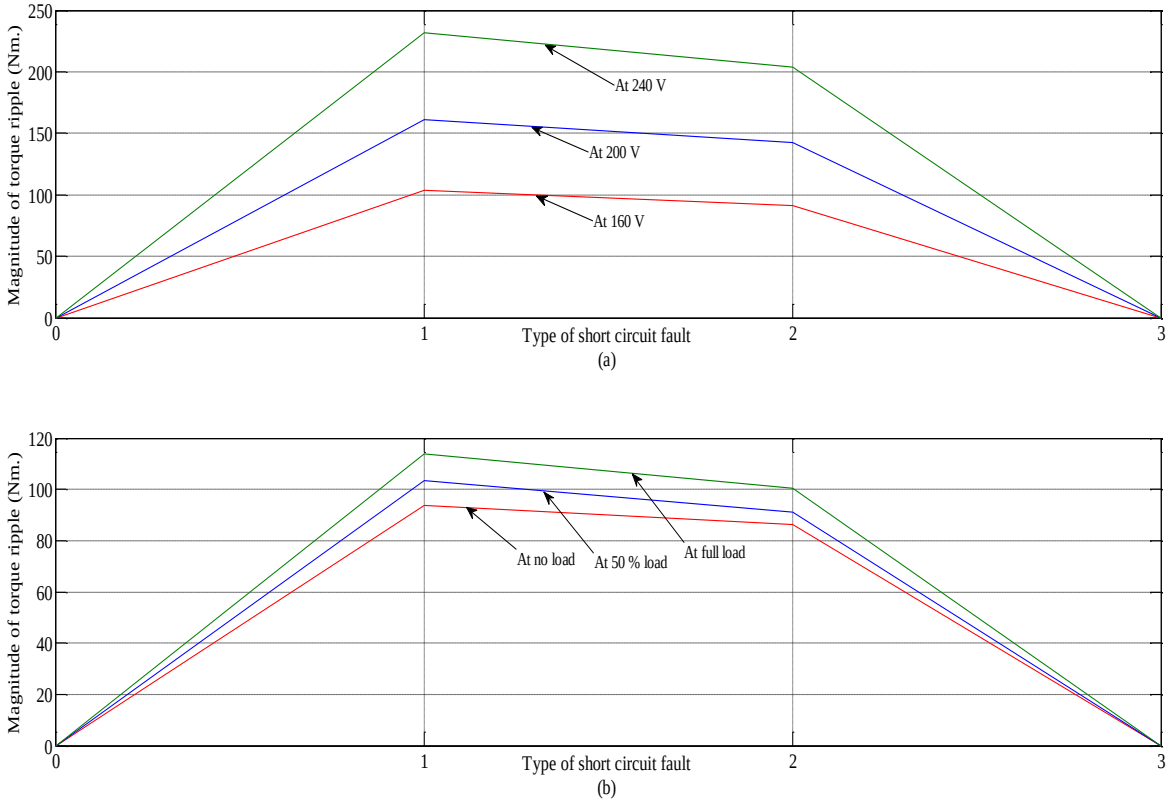

Fig. 4.24: Variation of torque ripple with the variation in (a) input voltage level (b) motor load.

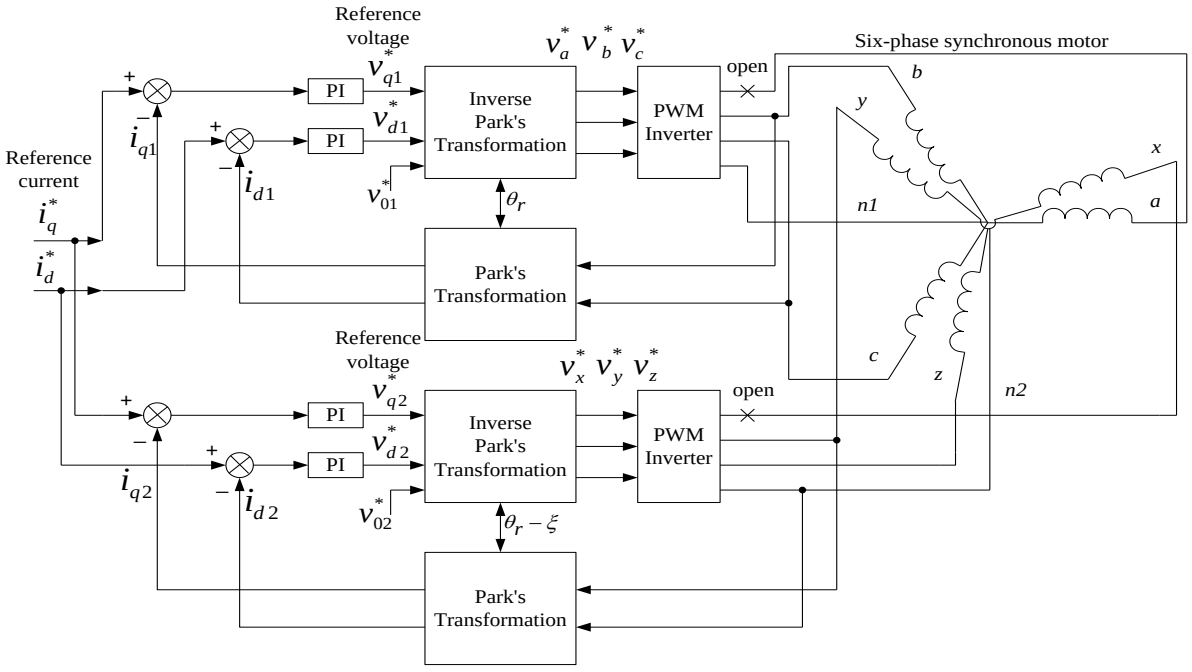

Fig. 4.25: Block diagram of post-fault control scheme.

Table 4.3: Effect on stator current at different input voltage levels during short-circuit fault

SC cases	i_a			i_b			i_c			i_x			i_y			i_z		
	160 V	200 V	240 V	160 V	200 V	240 V	160 V	200 V	240 V	160 V	200 V	240 V	160 V	200 V	240 V	160 V	200 V	240 V
LG	386.3	478.9	575.0	165.6	206.8	247.5	329.0	411.3	493.8	389.7	486.6	583.9	285.3	358.5	429.9	211.7	264.7	317.7
LLG	503.7	630.1	756.4	394.2	493.3	592.1	403.0	504.0	605.0	463.1	578.5	694.1	465.7	581.6	697.8	363.0	453.4	543.8
LLLG	565.5	707.1	848.9	565.5	707.1	848.9	565.5	707.1	848.9	558.9	698.4	838.2	558.9	698.4	838.2	558.9	698.4	838.2

Table 4.4: Effect on stator current at different load conditions during short-circuit fault

SC cases	i_a			i_b			i_c			i_x			i_y			i_z		
	No load	50 % load	Full load	No load	50 % load	Full load	No load	50 % load	Full load	No load	50 % load	Full load	No load	50 % load	Full load	No load	50 % load	Full load
LG	384.0	386.3	381.9	165.4	165.6	163.8	329.5	329.0	328.7	388.7	389.7	389.9	285.9	285.3	288.1	211.3	211.7	212.1
LLG	504.9	503.7	502.9	395.4	394.2	393.3	404.0	403.0	401.0	462.1	463.1	463.7	464.5	465.7	466.6	362.0	363.0	363.8
LLLG	566.4	565.5	564.8	566.4	565.5	564.8	566.4	565.5	564.8	558.1	558.9	559.6	558.1	558.9	559.6	558.1	558.9	559.6

Chapter 5

Stability analysis of six-phase synchronous motor

5.1 Introduction

Operation of any electrical machine during steady-state depends on many design factors that directly or indirectly affect the stability of machine. Stability of machine is an important factor, which is considered by the design engineers. Among the various aspects of stability, the small signal stability is an important one. It determines the stable operation of machine during small disturbance. This needs a comprehensive stability analysis of the machine to ensure a stable operation of the system. As far as stability of ac motor is concerned, very limited literature is available. Rogers [67] had indicated that the induction machine operation which gives an oscillatory response that is frequency dependent, and analyzed its stability using root locus technique. Stability of induction motor fed by variable frequency inverter was carried out in ref. [68], wherein the effect of harmonics was neglected, using Nyquist stability criteria [69] and root locus technique [70]. The technique of transfer function for the development of controlled current induction motor was carried out by Cornell and Lipo [71], whereas Macdonald and Sen [72] utilized a linearized small signal model of the current source inverter fed induction motor drive for stability analysis along with the formulation of transfer function for different control strategies. Tan and Richard [73] have calculated the eigenvalues for double-cage induction motor using a boundary layer model, whereas the Lyapnaov's first method using the placement of eigenvalues was carried out in detail for three-phase induction motor in ref. [74]. As far as the stability of synchronous machine is concerned, small signal stability analysis was carried out for reluctance-synchronous machine in ref. [75], and the variable frequency operation of synchronous machine in ref. [76] using Nyquist criteria technique, whereas the root locus study of synchronous machine was carried out in ref. [77].

From an extensive literature survey, it has been found that small signal stability of the system (particularly power system) has been carried out by using its eigenvalues, as reported in ref. [78-82]. However, some authors have also utilized the Hopf bifurcation technique [83-85] to access stability of the system. These analytical concepts can be effectively used for the

stability analysis of multiphase motor. In this regard, the only available literature is [86-87]. These works deal with the stability analysis of six-phase and five-phase induction motor, respectively. To the best of the knowledge of the authors, there is no available literature on stability analysis of multiphase synchronous motor. Therefore, this chapter deals the small signal stability analysis of six-phase synchronous motor. For this purpose, the eigenvalues criterion for small excursion behavior through the developed linearized version of machine equations has been used, followed by the establishment of eigenvalues association with motor parameters. Furthermore, determination of instability region is presented, under different parametric variation and working conditions. Results establish a preferable method for motor stabilization at its design stage as well as under normal working conditions. Formulation of transfer function is also presented, between the input and output variables, followed by the stability plots of root locus. Analysis has been carried out by employing *dq0* approach.

Optimal linear control employing state feedback technique [88] is more often used for the stabilization of power system [89-90]. In fact, much work has been done in this regard about two decades earlier. This is due to the development of modern control theory and computational technique with the state equations for a system at advanced level. Important power system element, i.e. synchronous generator has been extensively analyzed with this technique for stability purpose [89-94]. Performance of synchronous generator with derived linear optimal controller for a wide range of input disturbance was extensively evaluated by the authors in ref. [89, 91]. Rather than using all state variables, authors in ref. [95] pointed out to use only those state variables, which are physically available for measurement and evaluated the performance with different input disturbance and has been further analyzed in ref. [96-99]. While designing the optimal controller, evaluation of weighting matrix Q was addressed in ref. [89], employing the concept of sensitivity. Quite a few literatures are available for the synchronous motor operation employing this technique [100-101]. But as far as the multiphase synchronous motor is concerned, the application of this technique has not been reported so far. Therefore, this chapter also addresses a simple but effective control scheme, based on state feedback technique applicable for a six-phase synchronous motor to ensure the required stable operation in all the operating regions. Analysis has been carried out in MATLAB environment.

5.2 Linearization of Motor equations for stability analysis

A detailed mathematical modeling of six-phase synchronous motor has already been presented in chapter 2. The equations of voltages and flux linkage per second of a six-phase synchronous motor in Park's variables are given in section 2.2, which are the function of current and flux linkage per second. Since, current and flux linkage per second both are related to each other (as seen in equation 2.10- 2.18), one variable vector, either current or flux linkage per second can be taken as state variable. The choice of state variable is generally determined by the application [20]. Here, current has been selected as state variable. Treating the current as an independent variable, the flux linkage per second are replaced by the currents, and the voltage - current relation for the motor can be written in matrix form as:

$$[v] = [z][i] \tag{5.1}$$

where,

$$[v] = \left[v_{q1}, v_{d1}, v_{q2}, v_{d2}, v_{Kq}, v_{fr}, v_{Kd}\right]^T \tag{5.2}$$

$$[i] = \left[i_{q1}, i_{d1}, i_{q2}, i_{d2}, i_{Kq}, i_{fr}, i_{Kd}\right]^T \tag{5.3}$$

z

$$= \begin{bmatrix} r_1 + \frac{p}{\omega_b}(x_{l1} + x_{lm} + x_{mq}) & x_{l1} + x_{lm} + x_{md} & \frac{p}{\omega_b}(x_{lm} + x_{mq}) + x_{ldq} & -\frac{p}{\omega_b}x_{ldq} + (x_{lm} + x_{md}) & \frac{p}{\omega_b}x_{mq} & x_{md} & x_{md} \\ -(x_{l1} + x_{lm} + x_{mq}) & r_1 + \frac{p}{\omega_b}(x_{l1} + x_{lm} + x_{md}) & \frac{p}{\omega_b}x_{ldq} - (x_{lm} + x_{mq}) & \frac{p}{\omega_b}(x_{lm} + x_{md}) + x_{ldq} & -x_{mq} & \frac{p}{\omega_b}x_{md} & \frac{p}{\omega_b}x_{md} \\ \frac{p}{\omega_b}(x_{lm} + x_{mq}) - x_{ldq} & \frac{p}{\omega_b}x_{ldq} + (x_{lm} + x_{md}) & r_2 + \frac{p}{\omega_b}(x_{l2} + x_{lm} + x_{mq}) & x_{l2} + x_{md} + x_{lm} & \frac{p}{\omega_b}x_{mq} & x_{md} & x_{md} \\ -\frac{p}{\omega_b}x_{ldq} - (x_{lm} + x_{mq}) & \frac{p}{\omega_b}(x_{lm} + x_{md}) - x_{ldq} & -(x_{l1} + x_{lm} + x_{mq}) & r_2 + \frac{p}{\omega_b}(x_{l2} + x_{lm} + x_{md}) & -x_{mq} & \frac{p}{\omega_b}x_{md} & \frac{p}{\omega_b}x_{md} \\ \frac{p}{\omega_b}x_{mq} & 0 & \frac{p}{\omega_b}x_{mq} & 0 & r_{Kq} + \frac{p}{\omega_b}(x_{lKq} + x_{mq}) & 0 & 0 \\ 0 & \frac{p}{\omega_b}\frac{x_{md}^2}{r_{fr}} & 0 & \frac{p}{\omega_b}\frac{x_{md}^2}{r_{fr}} & \frac{x_{md}}{r_{fr}}\left\{r_{fr} + \frac{p}{\omega_b}(x_{lfr} + x_{md})\right\} & \frac{p}{\omega_b}\frac{x_{md}^2}{r_{fr}} & \\ 0 & \frac{p}{\omega_b}x_{md} & 0 & \frac{p}{\omega_b}x_{md} & 0 & \frac{p}{\omega_b}x_{md} & r_{Kd} + \frac{p}{\omega_b}(x_{lKd} + x_{md}) \end{bmatrix} \tag{5.4}$$

Developed motor electromagnetic torque is given by

$$T_e = \frac{3}{2}\frac{P}{2}\frac{1}{\omega_b}\begin{bmatrix} (i_{q1} + i_{q2})x_{md}(i_{d1} + i_{d2} + i_{Kd} + i_{fr}) \\ -(i_{d1} + i_{d2})x_{mq}(i_{q1} + i_{q2} + i_{Kq}) \end{bmatrix} \tag{5.5}$$

Relationship between torque and rotor speed is given by equation 5.6, whereas the expression of rotor angle (load angle) is given by equation 5.7.

$$T_e = \frac{P}{2J}\frac{\omega_r}{\omega_b} + T_l \tag{5.6}$$

$$\delta = \frac{\omega_b}{p}\left(\frac{\omega_r - \omega_e}{\omega_b}\right) \tag{5.7}$$

Relationship between the variables f_{qs}^{e} and f_{ds}^{e} in synchronously reference frame and variables f_{qs}^{r} and f_{ds}^{r} in rotor reference frame will be helpful in linearization process which is given by equation 5.8.

$$\begin{bmatrix} f_{kqs}^{r} \\ f_{kds}^{r} \end{bmatrix} = \begin{bmatrix} \cos\delta_k & -\sin\delta_k \\ \sin\delta_k & \cos\delta_k \end{bmatrix} \begin{bmatrix} f_{kqs}^{e} \\ f_{kds}^{e} \end{bmatrix} \tag{5.8}$$

where, $k = 1$ (for winding set *abc*) and 2 (for winding set *xyz*).

$\delta_1 = \delta_0$ (load angle)

$\delta_2 = \delta_0 - \gamma - \xi$

γ is the phase difference between phase *a* and *x* voltages and ξ is the phase shift between both the winding sets *abc* and *xyz*. Here, γ and ξ both are taken as 30 degree electrical.

The procedure of linearization for a small perturbation is carried out by using the well-known Taylor series expansion, wherein each variable *x* is replaced by its reference value plus a deviation ($x_0+\Delta x$). For example, consider an equation $z = xy$: this can be written as

$$z_0 + \Delta z = (x_0 + \Delta x)(y_0 + \Delta y)$$
$$= x_0 y_0 + y_0 \Delta x + x_0 \Delta y + \Delta x \Delta y$$

Terms in the reference level can be eliminated from both side of equation ($z_0 = x_0 y_0$). Also, the last term ($\Delta x \Delta y$) is neglected, considering that the deviations are very small, resulting in equation between the deviations with coefficient that can be considered constant over a limited region. Simplification incorporated in Taylor series expansion can be quantitatively included by the following restrictions imposed on motor equations:

(i) Under small perturbation, there is a little variation of flux levels, such that the inductances can be regarded as constant.

(ii) Under small perturbation, terms involving the product of two (or more) deviations can be neglected, being small with respect to other terms.

Linearization of the motor equations 5.1, 5.5, 5.6, 5.7 and 5.8 yields the set of equations which can be written in matrix form as:

$$\begin{bmatrix} \Delta v_{1qds} \\ \Delta v_{1qds} \\ \Delta v_{rr} \end{bmatrix} = \begin{bmatrix} W_1 & X_1 & Y_1 \\ X_2 & W_2 & Y_2 \\ Q_1 & Q_2 & S \end{bmatrix} \begin{bmatrix} \Delta i_{1qds} \\ \Delta i_{1qds} \\ \Delta i_{rr} \end{bmatrix} \tag{5.9}$$

where,

$$(x)^T = \left[(\Delta i_{1dqs})^T \ \ (\Delta i_{2dqs})^T \ \ (\Delta i_{rr})^T\right]$$
$$= \left[\Delta i_{q1}, \Delta i_{d1}, \Delta i_{q2}, \Delta i_{d2}, \Delta i_{Kq}, \Delta i_{fr}, \Delta i_{Kd}, \frac{\Delta\omega_r}{\omega_b}, \Delta\delta\right] \tag{5.10}$$

$$(u)^T = \left[(\Delta v_{1dqs})^T \ (\Delta v_{2dqs})^T \ (\Delta v_{rr})^T\right]$$
$$= \left[\Delta v_{q1}, \Delta v_{d1}, \Delta v_{q2}, \Delta v_{d2}, \Delta v_{Kq}, \Delta v_{fr}, \Delta v_{Kd}, \Delta T, 0\right] \quad (5.11)$$

Other elements of matrix are explained in the latter part of this section.

Since the driving force (input voltages) fed to synchronous motor is of constant amplitude and frequency (connected to infinite busbar) in synchronous reference frame; therefore, it will be advantageous to relate these variables in synchronously rotating reference frame to the variables in rotor reference frame. This has to be taken into account with the help of equation 5.8, which is non-linear. This equation will be linearized before incorporating it into a set of linear differential equations. Therefore, suitable approximation is taken, $cos\Delta\delta_k = 1$ and $sin\Delta\delta_k = \Delta\delta_k$. Such that linearization of equation 5.8 yields

$$\Delta f^r_{kdqs} = T_k \Delta f^e_{kdqs} + F^r \Delta\delta \quad (5.12)$$

Linearization of inverse transformation yields

$$\Delta f^e_{kdqs} = (T_k)^{-1} \Delta f^r_{kdqs} + F^e \Delta\delta \quad (5.13)$$

where,

F^r and F^e are the steady-state *d-q* operating indices in rotor and synchronously rotating reference frame respectively.

$$T_k = \begin{bmatrix} \cos\delta_k & -\sin\delta_k \\ \sin\delta_k & \cos\delta_k \end{bmatrix} \quad (5.14)$$

$$(T_k)^{-1} = \begin{bmatrix} \cos\delta_k & \sin\delta_k \\ -\sin\delta_k & \cos\delta_k \end{bmatrix} \quad (5.15)$$

Substitution of equations 5.12 and 5.13 into equation 5.9 yields

$$\begin{bmatrix} T_1\Delta v^e_{1dqs} \\ T_2\Delta v^e_{2dqs} \\ \Delta v_{rr} \end{bmatrix} = \begin{bmatrix} W_1 & X_1 & Y_1 \\ X_2 & W_2 & Y_2 \\ Q_1 & Q_2 & S \end{bmatrix} \begin{bmatrix} T_1\Delta i^e_{1dqs} \\ T_2\Delta i^e_{2dqs} \\ \Delta i_{rr} \end{bmatrix} \quad (5.16)$$

which can be further arranged and written as

$$\begin{bmatrix} \Delta v^e_{1dqs} \\ \Delta v^e_{2dqs} \\ \Delta v_{rr} \end{bmatrix} = \begin{bmatrix} (T_1)^{-1}W_1T_1 & (T_1)^{-1}X_1T_2 & (T_1)^{-1}Y_1 \\ (T_2)^{-1}X_2T_1 & (T_2)^{-1}W_2T_2 & (T_2)^{-1}Y_2 \\ Q_1T_1 & Q_2T_2 & S \end{bmatrix} \begin{bmatrix} \Delta i^e_{1dqs} \\ \Delta i^e_{2dqs} \\ \Delta i_{rr} \end{bmatrix} \quad (5.17)$$

Above equation can be expressed in following form

$$Epx = Fx + u \quad (5.18)$$

where,

$$(x)^T = \left[(\Delta i^e_{1qds})^T \ (\Delta i^e_{2qds})^T \ (\Delta i_{rr})^T\right]$$
$$= \left[\Delta i^e_{q1}, \Delta i^e_{d1}, \Delta i^e_{q2}, \Delta i^e_{d2}, \Delta i_{Kq}, \Delta i_{fr}, \Delta i_{Kd}, \frac{\Delta\omega_r}{\omega_b}, \Delta\delta\right] \quad (5.19)$$

$$(u)^T = \left[(\Delta v_{1qds}^e)^T \ (\Delta v_{2qds}^e)^T \ (\Delta v_{rr})^T\right]$$
$$= \left[\Delta v_{q1}^e, \Delta v_{d1}^e, \Delta v_{q2}^e, \Delta v_{d2}^e, \Delta v_{Kq}, \Delta v_{fr}, \Delta v_{Kd}, \Delta T, 0\right] \quad (5.20)$$

$$E = \begin{bmatrix} (T_1)^{-1}W_{1p}T_1 & (T_1)^{-1}X_{1p}T_2 & (T_1)^{-1}Y_{1p} \\ (T_2)^{-1}X_{2p}T_1 & (T_2)^{-1}W_{2p}T_2 & (T_2)^{-1}Y_{2p} \\ Q_{1p}T_1 & Q_{2p}T_2 & S_p \end{bmatrix} \quad (5.21)$$

$$F = -\begin{bmatrix} (T_1)^{-1}W_{1k}T_1 & (T_1)^{-1}X_{1k}T_2 & (T_1)^{-1}Y_{1k} \\ (T_2)^{-1}X_{2k}T_1 & (T_2)^{-1}W_{2k}T_2 & (T_2)^{-1}Y_{2k} \\ Q_{1k}T_1 & Q_{2k}T_2 & S_k \end{bmatrix} \quad (5.22)$$

In equation 5.18, coefficient matrix E is associated with the derivative part of the elements having subscript p. Similarly, the coefficient matrix F whose elements have subscript k are associated with the remaining terms of the linearized motor equations. Elements of the matrices E and F are defined as:

$$W_{1p} = \left(\frac{1}{\omega_b}\right)\begin{bmatrix} (x_{l1} + x_{lm} + x_{mq}) & 0 \\ 0 & (x_{l1} + x_{lm} + x_{md}) \end{bmatrix} \quad (5.23)$$

$$W_{2p} = \left(\frac{1}{\omega_b}\right)\begin{bmatrix} (x_{l2} + x_{lm} + x_{mq}) & 0 \\ 0 & (x_{l2} + x_{lm} + x_{md}) \end{bmatrix} \quad (5.24)$$

$$X_{1p} = \left(\frac{1}{\omega_b}\right)\begin{bmatrix} (x_{mq} + x_{lm}) & -x_{ldq} \\ x_{ldq} & (x_{md} + x_{lm}) \end{bmatrix} \quad (5.25)$$

$$X_{2p} = \left(\frac{1}{\omega_b}\right)\begin{bmatrix} (x_{mq} + x_{lm}) & x_{ldq} \\ -x_{ldq} & (x_{md} + x_{lm}) \end{bmatrix} \quad (5.26)$$

$$Q_{1p} = Q_{2p} = \left(\frac{1}{\omega_b}\right)\begin{bmatrix} x_{mq} & 0 \\ 0 & \frac{x_{md}^2}{r_{fr}} \\ 0 & x_{md} \\ 0 & 0 \\ 0 & 0 \end{bmatrix} \quad (5.27)$$

$$Y_{1p} = \left(\frac{1}{\omega_b}\right)\begin{bmatrix} x_{mq} & 0 & 0 & 0 & -(x_{l1} + x_{lm} + x_{mq})i_{d10} - (x_{mq} + x_{lm})i_{d20} \\ 0 & x_{md} & x_{md} & 0 & (x_{l1} + x_{lm} + x_{md})i_{q10} + (x_{md} + x_{lm})i_{q20} \end{bmatrix} \quad (5.28)$$

$$Y_{2p} = \left(\frac{1}{\omega_b}\right)\begin{bmatrix} x_{mq} & 0 & 0 & 0 & -(x_{l2} + x_{lm} + x_{mq})i_{d20} - (x_{mq} + x_{lm})i_{d10} \\ 0 & x_{md} & x_{md} & 0 & (x_{l2} + x_{lm} + x_{md})i_{q20} + (x_{md} + x_{lm})i_{q10} \end{bmatrix} \quad (5.29)$$

$$S_p = \left(\frac{1}{\omega_b}\right)\begin{bmatrix} (x_{lKq} + x_{mq}) & 0 & 0 & 0 & -(x_{mq}i_{d10} + x_{mq}i_{d20}) \\ 0 & \frac{x_{md}(x_{lfr} + x_{md})}{r_{fr}} & \frac{x_{md}^2}{r_{fr}} & 0 & \frac{x_{md}^2}{r_{fr}}(i_{q10} + i_{q20}) \\ 0 & x_{md} & (x_{lKd} + x_{md}) & 0 & x_{md}(i_{q10} + i_{q20}) \\ 0 & 0 & 0 & -\frac{2J\omega_b^2}{P} & 0 \\ 0 & 0 & 0 & 0 & -\omega_b \end{bmatrix} \quad (5.30)$$

$$W_{1k} = \begin{bmatrix} r_1 & (x_{l1} + x_{lm} + x_{md}) \\ -(x_{l1} + x_{lm} + x_{mq}) & r_1 \end{bmatrix} \tag{5.31}$$

$$W_{2k} = \begin{bmatrix} r_2 & (x_{l2} + x_{lm} + x_{md}) \\ -(x_{l2} + x_{lm} + x_{mq}) & r_2 \end{bmatrix} \tag{5.32}$$

$$X_{1k} = \begin{bmatrix} x_{ldq} & (x_{lm} + x_{md}) \\ -(x_{lm} + x_{mq}) & x_{ldq} \end{bmatrix} \tag{5.33}$$

$$X_{2k} = \begin{bmatrix} x_{ldq} & (x_{lm} + x_{md}) \\ -(x_{lm} + x_{mq}) & -x_{ldq} \end{bmatrix} \tag{5.34}$$

$$Q_{1k} = Q_{2k} =$$

$$\begin{bmatrix} 0 & 0 \\ 0 & 0 \\ 0 & 0 \\ (x_{md}(i_{d10} + i_{d20} + i_{fr0}) - x_{mq}(i_{d10} + i_{d20}))\, f_{qs} & (x_{md}(i_{q10} + i_{q20}) - x_{mq}(i_{q10} + i_{q20}))f_{qs} \end{bmatrix} \tag{5.35}$$

$$Y_{1k} =$$

$$\begin{bmatrix} 0 & x_{md} & x_{md} & \left(x_{l1} i_{d10} + x_{md}(i_{d10} + i_{d20} + i_{fr0})\right) & (-r_1 i_{d10} + (x_{l1} + x_{lm} + x_{md}) i_{q10} - x_{ldq} i_{d20} + (x_{md} + x_{lm}) i_{q20} + v_{d10} \\ -x_{mq} & 0 & 0 & -\left(x_{l1} i_{q10} + x_{mq}(i_{q10} + i_{q20})\right) & (r_1 i_{q10} + (x_{l1} + x_{lm} + x_{mq}) i_{d10} + (x_{mq} + x_{lm}) i_{d20} - v_{q10} \end{bmatrix} \tag{5.36}$$

$$Y_{2k} =$$

$$\begin{bmatrix} 0 & x_{md} & x_{md} & \left(x_{l2} i_{d20} + x_{md}(i_{d10} + i_{d20} + i_{fr0})\right) & (-r_2 i_{d20} + (x_{l2} + x_{lm} + x_{md}) i_{q20} + x_{ldq} i_{d10} + (x_{md} + x_{lm}) i_{q10} + v_{d20} \\ -x_{mq} & 0 & 0 & -\left(x_{l1} i_{q10} + x_{mq}(i_{q10} + i_{q20})\right) & (r_2 i_{q20} + (x_{l2} + x_{lm} + x_{mq}) i_{d20} + (x_{mq} + x_{lm}) i_{d10} - v_{q20} \end{bmatrix} \tag{5.37}$$

$$S_k = \begin{bmatrix} r_{Kq} & 0 & 0 & 0 & 0 \\ 0 & r_{fr}\left(\frac{x_{md}}{r_{fr}}\right) & 0 & 0 & 0 \\ 0 & 0 & r_{Kd} & 0 & 0 \\ -x_{mq}(i_{d10} + i_{d20}) f_{qs} & x_{md}(i_{q10} + i_{q20}) f_{qs} & x_{md}(i_{q10} + i_{q20}) f_{qs} & 0 & f_{qs}\, s_{45} \\ 0 & 0 & 0 & \omega_b & 0 \end{bmatrix} \tag{5.38}$$

where

$$s_{45} = -i_{d10}\left(x_{md}(i_{d10} + i_{d20} + i_{fr0}) - x_{mq}(i_{d10} + i_{d20})\right) + i_{q10}\left(x_{md}(i_{d10} + i_{d20}) - x_{mq}(i_{q10} + i_{q20})\right) - i_{d20}\left(x_{md}(i_{d10} + i_{d20} + i_{fr0}) - x_{mq}(i_{d10} + i_{d20})\right) + i_{q20}\left(x_{md}(i_{q10} + i_{q20}) - x_{mq}(i_{q10} + i_{q20})\right)$$

$$f_{qs} = 3P/4\omega_b$$

Variables with additional subscript '*0*' ($i_{d10},\ i_{d20},\ i_{fr0},\ i_{q10},\ i_{q20}$) show its value during steady-state operating condition. Equation 5.18 may be written in the fundamental form

$$px = Ax + Bu \tag{5.39}$$

where,

$$A = (E)^{-1}F \tag{5.40}$$

$$B = (E)^{-1} \tag{5.41}$$

It has to be noted that in the developed linearized model, effect of mutual leakage reactance has been considered. Results discussed in the following section is only for the asymmetrical motor (practical case where ξ = 30 degree electrical).

5.3 Stability analysis with eigenvalues

An effective but simple means of stability analysis under small disturbance is provided by the eigenvalues of a system characteristic equation, given by

$$\det(A - \lambda I) = 0 \tag{5.42}$$

where, *I* is the identity matrix and λ are the roots of the characteristic equation.

Eigenvalues may be either real or complex; when complex, they occur as conjugate pairs signifying a mode of oscillation of the state variables. System is said to be stable if all the real and/or real component of eigenvalues are negative. This is because a negative real part represents a damped oscillation to a finite value of system response and the roots with positive real part lead to an infinite output response indicating unstable system. Thus the absolute stability can be determined by examining the sign of real parts of the roots of a system characteristic equation, the location of the roots being in *s*-plan.

The state equation 5.39 of six-phase synchronous motor is described by nine state variables. Therefore, nine eigenvalues will be obtained, out of which there will be three complex conjugate pairs and remaining will be real. Since, dependency of eigenvalues on motor parameters are difficult to relate analytically [20, 86]; therefore, this dependency has been established by calculating the eigenvalues by varying the motor parameters with each parameter varied at a time within certain interval keeping the other parameters constant at its normal value. Calculation for motor eigenvalues has been carried out for the motor operating at the load torque of 50 percent, maintaining the phase voltage of *160 V* at power factor of *0.88* (lagging). Motor parameters are given in Appendix II.

5.3.1 Change in Stator parameters:

Variation of eigenvalues with the change in stator parameters are tabulated in Table 5.1 (a) for the change in stator resistance r_s and Table 5.1 (b) for the change in stator leakage reactance x_{ls} (assuming that stator resistance and leakage reactance are same for both the winding sets *abc* and *xyz*, i.e. $r_s = r_1 = r_2$ and $x_{ls} = x_{l1} = x_{l2}$). The complex conjugate pairs, which are getting affected by the change in stator parameters are termed as 'Stator eigenvalue' I and II, as shown in Tables where other eigenvalues almost remain unchanged. As the value of stator resistance of both the winding sets *abc* and *xyz* is increased, real part of both stator eigenvalue I and II becomes more negative, resulting the system to be more stable and lowers the time constant. Pattern of the variation of real part of stator eigenvalue I and II was found to be reversed and become less negative, as far as the variation of leakage reactance x_{ls} is concerned. Hence, taking the system towards instability. It has to be noted that for both the variation in stator parameters r_s, x_{ls} , there is no change in imaginary part of the stator eigenvalue I and small variation in stator eigenvalue II (close to base speed ω_b), indicating that the damped frequency of oscillation will be at base frequency, approximately.

5.3.2 Change in Field parameters:

Variation of the motor eigenvalues for the change in parameters of field circuit, i.e. field resistance r_{fr}, and field leakage reactance x_{lfr} , have been tabulated in Table 5.2 (a) and Table 5.2 (b), respectively. Since the real eigenvalues are associated with the decay of offset currents in the rotor circuit; therefore, they are associated with the inverse of effective time constant of these circuits. Field winding circuit has the largest time constant which gives rise to the smallest real eigenvalue. It has been confirmed by noting the variation in smallest real eigenvalue with the variation of field circuit parameters. As the field circuit resistance r_{fr} is increased (or decreased) upto 20 percentage of its normal value, variation in the real eigenvalue III was noted. This value becomes more negative (or less negative), moving the system towards more stable region, i.e. field offset current will decay more rapidly. This pattern of variation of real eigenvalue III was found to be reversed by having the variation in field leakage reactance x_{lfr} by the same percentage of amount, i.e. field offset current will decay less rapidly and system moves towards instability.

Table 5.1 (a): Variation of eigenvalue with the change in stator resistance

Value of stator resistance, r_s	Stator eigenvalue I	Stator eigenvalue II	Rotor eigenvalue	Real eigenvalue		
				I	II	III
0.1538	-91.6 ± j 104.7	-14.3 ± j 100.3	-11.5 ± j 58.2	-9135.9, -698.5, -16.3		
0.1629	-97.0 ± j 104.7	-15.2 ± j 100.0	-11.4 ± j 58.2	-9136.0, -699.1, -16.3		
0.1719	-102.4 ± j104.7	-16.1 ± j 99.7	-11.3 ± j 58.2	-9136.2, -699.7, -16.3		
0.1810*	-107.8 ± j 104.7	-16.9 ± j 99.4	-11.2 ± j 58.2	-9136.3, -700.3, -16.4		
0.1901	-113.2 ± j 104.7	-17.8 ± j 99.1	-11.1 ± j 58.3	-9136.5, -701.0, -16.4		
0.1991	-118.6 ± j 104.7	-18.7 ± j 98.8	-11.0 ± j 58.3	-9136.7, -701.6, -16.4		
0.2081	-124.0 ± j 104.7	-19.6 ± j 98.5	-10.9 ± j 58.3	-9136.8, -702.2, -16.5		

Table 5.1 (b): Variation of eigenvalue with the change in stator reactance

Value of stator leakage reactance, x_{ls}	Stator eigenvalue I	Stator eigenvalue II	Rotor eigenvalue	Real eigenvalue		
				I	II	III
0.1406	-134.8 ± j 104.7	-17.9 ± j 100.3	-11.3 ± j 58.6	-9192.3, -717.0, -17.3		
0.1582	-119.8 ± j 104.7	-17.7 ± j 99.2	-11.3 ± j 58.4	-9163.4, -708.5, -16.8		
0.1758*	-107.8 ± j 104.7	-16.9 ± j 99.4	-11.2 ± j 58.2	-9136.3, -700.3, -16.4		
0.1934	-98.0 ± j 104.7	-16.5 ± j 99.6	-11.2 ± j 58.1	-9110.9, -692.3, -16.0		
0.2110	-89.8 ± j 104.7	-16.1 ± j 99.8	-11.2 ± j 57.9	-9086.8, -684.6, -15.6		

Table 5.2 (a): Variation of eigenvalue with the change in field circuit resistance

Value of field resistance, r_{fr}	Stator eigenvalue I	Stator eigenvalue II	Rotor eigenvalue	Real eigenvalue		
				I	II	III
0.0448	-107.8 ± j 104.7	-17.1 ± j 100.0	-11.0 ± j 58.2	-9136.3, -700.3, -13.0		
0.0504	-107.8 ± j 104.7	-17.0 ± j 99.7	-11.1 ± j 58.2	-9136.3, -700.3, -14.7		
0.0560*	-107.8 ± j 104.7	-16.9 ± j 99.4	-11.2 ± j 58.2	-9136.3, -700.3, -16.4		
0.0616	-107.8 ± j 104.7	-16.8 ± j 99.1	-11.4 ± j 58.3	-9136.4, -700.3, -18.1		
0.0672	-107.8 ± j 104.7	-16.7 ± j 98.8	-11.5 ± j 58.3	-9136.4, -700.3, -19.8		

Table 5.2 (b): Variation of eigenvalue with the change in field circuit reactance

Value of field leakage reactance, x_{lfr}	Stator eigenvalue I	Stator eigenvalue II	Rotor eigenvalue	Real eigenvalue		
				I	II	III
0.1922	-107.8 ± j 104.7	-19.5 ± j 98.0	-11.3 ± j 59.0	-9158.5, -700.3, -19.1		
0.2162	-107.8 ± j 104.7	-18.1 ± j 99.7	-11.3 ± j 58.6	-9146.5, -700.3, -17.6		
0.24021*	-107.8 ± j 104.7	-16.9 ± j 99.4	-11.2 ± j 58.2	-9136.3, -700.3, -16.4		
0.2642	-107.8 ± j 104.7	-15.9 ± j 99.9	-11.2 ± j 58.0	-9127.6, -700.3, -15.3		
0.2883	-107.8 ± j 104.7	-15.0 ± j 100.3	-11.2 ± j 57.7	-9119.9, -700.3, -14.4		

Table 5.3 (a): Variation of eigenvalue with the change in damper winding Kd resistance

Value of damper winding resistance, r_{Kd}	Stator eigenvalue I	Stator eigenvalue II	Rotor eigenvalue	Real eigenvalue		
				I	II	III
112.56	-107.8 ± j 104.7	-16.9 ± j 99.4	-11.2 ± j 58.2	-7309.7, -700.3, -16.4		
126.63	-107.8 ± j 104.7	-16.9 ± j 99.4	-11.2 ± j 58.6	-8223.0, -700.3, -16.4		
140.70*	-107.8 ± j 104.7	-16.9 ± j 99.4	-11.2 ± j 58.2	-9136.3, -700.3, -16.4		
154.77	-107.8 ± j 104.7	-16.9 ± j 99.4	-11.2 ± j 58.2	-10050.0, -700.3, -16.4		
168.84	-107.8 ± j 104.7	-16.9 ± j 99.4	-11.2 ± j 58.2	-10963.0, -700.3, -16.4		

Table 5.3 (b): Variation of eigenvalue with the change in damper winding Kd reactance

Value of damper leakage reactance, x_{lKd}	Stator eigenvalue I	Stator eigenvalue II	Rotor eigenvalue	Real eigenvalue		
				I	II	III
1.2397	-107.8 ± j 104.7	-16.9 ± j 99.4	-11.2 ± j 58.2	-11309.0, -700.3, -16.4		
1.3946	-107.8 ± j 104.7	-16.9 ± j 99.4	-11.2 ± j 58.2	-10107.0, -700.3, -16.4		
1.5496*	-107.8 ± j 104.7	-16.9 ± j 99.4	-11.2 ± j 58.2	-9136.3, -700.3, -16.4		
1.7045	-107.8 ± j 104.7	-16.9 ± j 99.4	-11.2 ± j 58.2	-8335.7, -700.3, -16.4		
1.8595	-107.8 ± j 104.7	-16.9 ± j 99.4	-11.2 ± j 58.2	-7664.0, -700.3, -16.4		

Table 5.4 (a): Variation of eigenvalue with the change in damper winding Kq resistance

Value of damper winding resistance, r_{Kq}	Stator eigenvalue I	Stator eigenvalue II	Rotor eigenvalue	Real eigenvalue		
				I	II	III
4.0568	-107.8 ± j 104.7	-16.8 ± j 98.8	-14.4 ± j 58.5	-9136.3, -552.0, -16.3		
4.5639	-107.8 ± j 104.7	-16.9 ± j 99.1	-12.6 ± j 58.4	-9136.3, -626.6, -16.3		
5.071*	-107.8 ± j 104.7	-16.9 ± j 99.4	-11.2 ± j 58.2	-9136.3, -700.3, -16.4		
5.5781	-107.8 ± j 104.7	-17.0 ± j 99.6	-10.1 ± j 58.1	-9136.3, -773.6, -16.4		
6.0852	-107.8 ± j 104.7	-17.0 ± j 99.8	-9.2 ± j 58.1	-9136.3, -846.5, -16.4		

Table 5.4 (b): Variation of eigenvalue with the change in damper winding Kq reactance

Value of damper leakage reactance, x_{lKq}	Stator eigenvalue I	Stator eigenvalue II	Rotor eigenvalue	Real eigenvalue		
				I	II	III
0.5288	-107.8 ± j 104.7	-16.9 ± j 99.4	-11.2 ± j 58.1	-9136.3, -856.0, -16.4		
0.5949	-107.8 ± j 104.7	-16.9 ± j 99.4	-11.2 ± j 58.2	-9136.3, -770.6, -16.4		
0.6610*	-107.8 ± j 104.7	-16.9 ± j 99.4	-11.2 ± j 58.2	-9136.3, -700.3, -16.4		
0.7271	-107.8 ± j 104.7	-17.0 ± j 99.4	-11.3 ± j 58.3	-9136.3, -641.5, -16.4		
0.7932	-107.8 ± j 104.7	-17.0 ± j 99.4	-11.3 ± j 58.2	-9136.3, -591.5, -16.4		

Table 5.5: Variation of eigenvalue with the change in moment of inertia

Value of moment of inertia , J	Stator eigenvalue I	Stator eigenvalue II	Rotor eigenvalue	Real eigenvalue		
				I	II	III
0.4224	-107.8 ± j 104.7	-17.4 ± j 98.8	-13.7 ± j 65.6	-9136.3, -694.5, -16.3		
0.4752	-107.8 ± j 104.7	-17.1 ± j 99.2	-12.4 ± j 61.6	-9136.3, -697.8, -16.4		
0.5280*	-107.8 ± j 104.7	-16.9 ± j 99.4	-11.2 ± j 58.2	-9136.3, -700.3, -16.4		
0.7271	-107.8 ± j 104.7	-16.8 ± j 99.6	-10.3 ± j 55.4	-9136.3, -702.4, -16.4		
0.7932	-107.8 ± j 104.7	-16.7 ± j 99.7	-9.6 ± j 53.0	-9136.3, -704.2, -16.4		

Note: '*' indicates the normal value.

5.3.3 Change in Damper winding parameters:

Since, time constant of the damper winding K_d has the smallest value $(1.76 \times 10^{-4} sec.^{-1})$ than other rotor circuit; therefore, it will give rise to the largest real eigenvalue. This has been confirmed by having the variation in real eigenvalue I by changing the damper winding resistance r_{Kd} and leakage reactance x_{lKd} as tabulated in Table 5.3 (a) and Table 5.3 (b)

respectively. Value of real eigenvalue I becomes more negative for the change in resistance r_{Kd} from lower to higher (20 percentage of normal) value. Therefore, system will become more stable. However, the system moves towards instability for the variation of leakage reactance x_{lKd} from lower to higher value. It can be noted that other eigenvalues almost remain unaffected while changing the above parameters. The time constant of damper winding K_q was found to be $2.87 \times 10^{-3} sec.^{-1}$. This value is higher than the time constant of damper winding K_d but lower than the field circuit f_r. Therefore, it causes the variation of real eigenvalue II with the change in resistance r_{Kq} and leakage reactance x_{lKq}, as tabulated in Table 5.4 (a) and Table 5.4 (b) respectively. Variation of parameter of this damper winding also shows the same pattern of variation in eigenvalue II as discussed in above cases.

5.3.4 Change in Moment of Inertia:

The remaining eigenvalue has been termed as 'Rotor eigenvalue' of synchronous motor. It indicates the oscillatory behavior of motor, particularly referred as hunting or swing mode, i.e. primary mode of oscillation of rotor with respect to electrical angular velocity of electrical system. Oscillatory behavior of rotor is affected by the variation of moment of inertia, as tabulated in Table 5.5. It is to be noted that the frequency of rotor oscillation is decreased by varying the value of moment of inertia *J* from lower to higher (20 percentage of normal) value. Moreover, it also tends to move the system towards instability as the real component of eigenvalue is becoming less negative.

5.3.5 Effect of load variation:

The effect of load variation of eigenvalues has been graphically presented in Fig. 5.1. Solid line indicates the real component and dash line indicates the imaginary component of eigenvalue. Real component of both stator eigenvalue I and II are found to be numerically constant with imaginary component almost equal to base speed ω_b, i.e. stator eigenvalues are almost unaffected with the variation of load. Motor was found to become unstable at the load of 1.7 times the rated load/torque. This has been depicted by the rotor eigenvalue, where real component is becoming positive, associated with the increase in oscillation in rotor circuit, shown by imaginary component in Fig. 5.1 (c). Real eigenvalues remain negative with the increase and decrease in its magnitude for real eigenvalue II and III respectively.

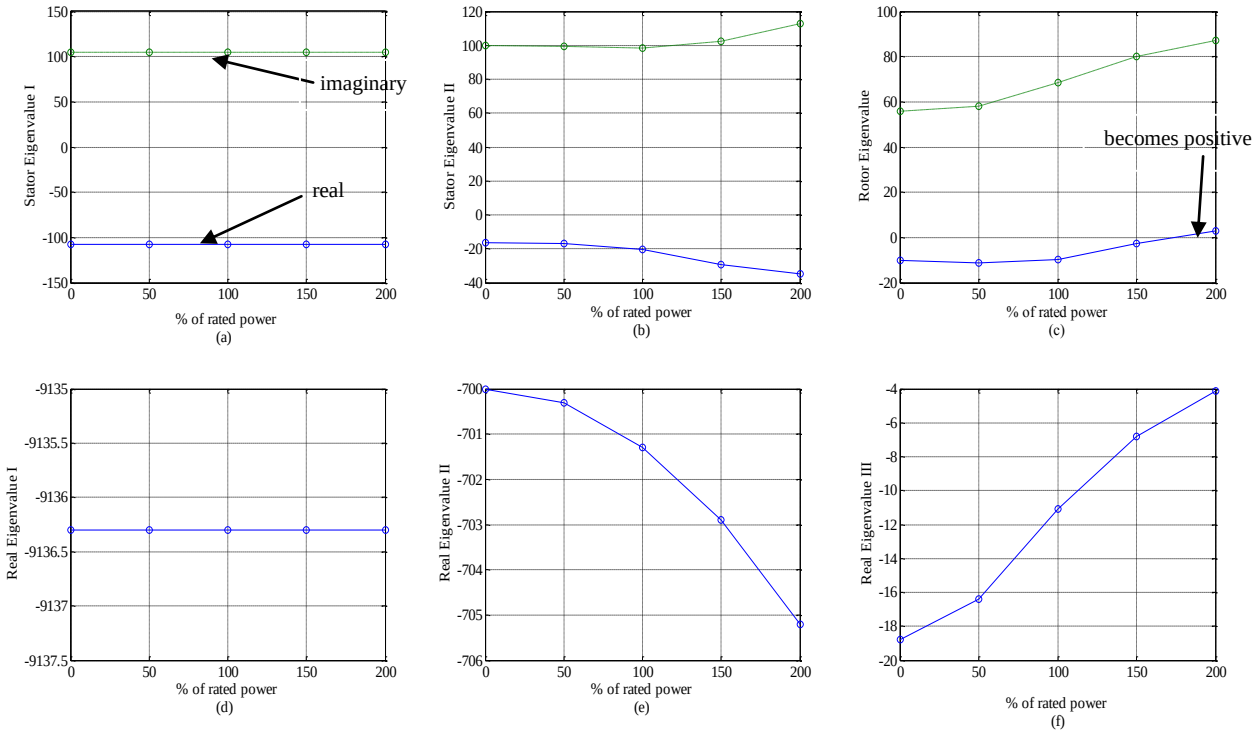

Fig. 5.1: Effect of load variation on motor's eigenvalues: (a) Stator eigenvalue I (b) Stator eigenvalue II (c) Rotor eigenvalue (d) Real eigenvalue I (e) Real eigenvalue II (f) Real eigenvalue III.

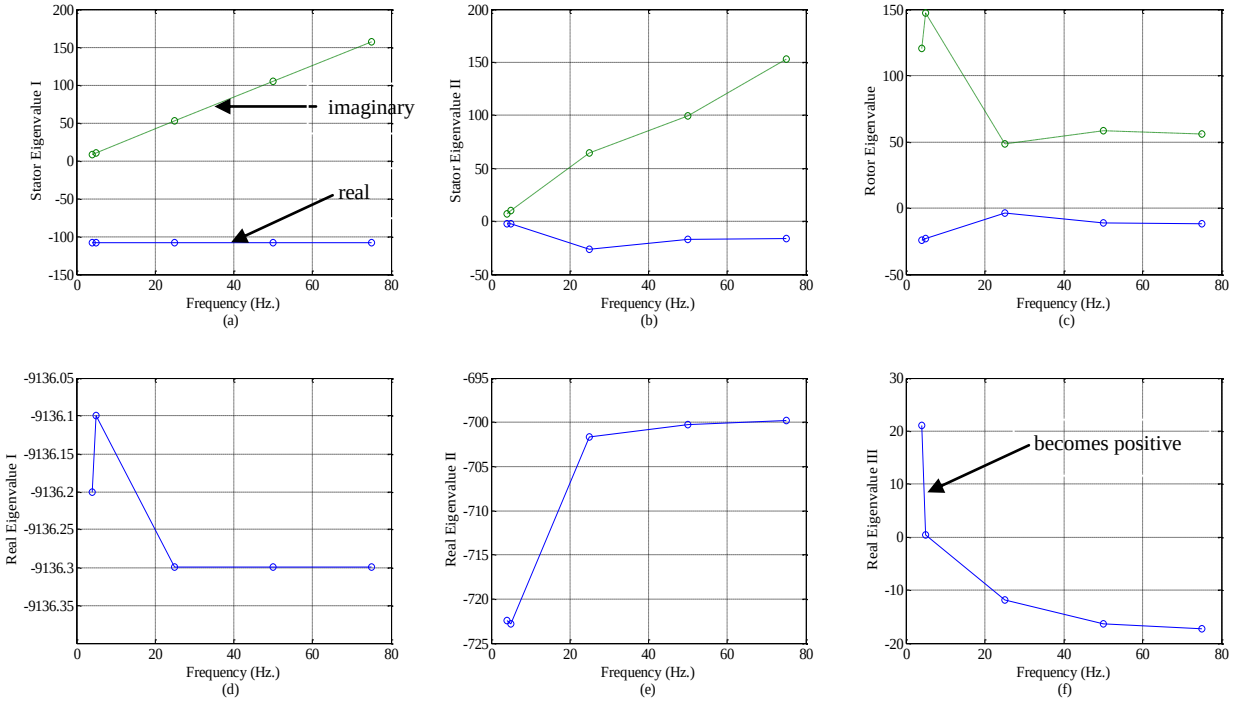

Fig. 5.2: Effect of frequency variation on motor's eigenvalues: (a) Stator eigenvalue I (b) Stator eigenvalue II (c) Rotor eigenvalue (d) Real eigenvalue I (e) Real eigenvalue II (f) Real eigenvalue III.

5.3.6 Effect of frequency/speed variation:

Frequency and voltage can be individually varied to study the stability of motor. Practically, this practice is not adopted. In fact, in variable speed system, the amplitude of applied voltages is varied in proportion with the frequency in order to avoid the saturation. Therefore, in this section, stability of the motor has been observed for the change in frequency and voltage of same ratio. The effect on motor eigenvalues with the change in frequency/speed is shown graphically in Fig. 5.2. Change in the eigenvalue, both real and imaginary components was found to have almost same variation patterns for both the stator eigenvalue I and II. Real component of rotor eigenvalue was also found to be almost same, irrespective with the change in frequency. But for lower value of frequency (less than 20 Hz.), imaginary component was found to increase, showing a larger frequency of oscillation in rotor circuit, whereas the magnitude of real eigen-value II was found to increase at lower frequency operation. Motor at very low frequency operation is becoming unstable. This is because the real eigenvalue III under very low frequency operation is becoming positive, as shown in Fig. 5.2 (f). This result is the same as discussed by the authors in [67, 69-71] for the operation of three-phase motor at very low frequency.

5.4 Determination of instability limits

Small signal stability is determined by the behavior of generated torque, and hence the rotor speed. For the system to be stable, the generated oscillatory torque, due to small disturbance/perturbation, will settle to its steady-state value, and hence speed will be at its constant value (synchronous speed). However, for an unstable system, the generated torque increases to a larger magnitude, resulting in the loss of rotor synchronism. Therefore, from the practical point of view, stability of motor operation is determined by the rotor behavior, followed by the application of small disturbance/perturbation. So, eigenvalue corresponding to rotor behavior was found to be dominant eigenvalue (eigenvalue near to positive s-plan). Calculation of motor eigenvalues has been carried out for motor operating at the load torque of 50 percent, maintaining the phase voltage of 120 V (for constant Volt/Hz ratio in six-phase winding configuration [102]) at a power factor of 0.95 (lagging), given in Table 5.6. Dominant eigenvalues has been used to determine the changes in instability limit of motor with the change

Table 5.6: Calculated eigenvalues of Six-phase synchronous motor

Nomenclature	Eigenvalues
Stator eigenvalue I	-107.8 ± 104.7
Stator eigenvalue II	-17.2 ± 99.8
Rotor eigenvalue	-7.6 ± 48.4
Real eigenvalue	-9136.3, -710.7, -13.0

in motor parameters (by 50 percent from its rated value). Effect on instability limit under various operating conditions is also discussed in the following sections.

It is worthwhile to mention here that the instability limit under different parametric variation has been plotted by considering the motor operation at different load torque and operating frequencies, in order to have an insight of motor operation under different operating conditions. Change in frequency has been made in proportion to the input voltage (constant Volt/Hz), so as to ensure a constant airgap flux in the machine. It was found that the two instability limits exist with normal operating frequency range. These limits are named as "instability limit 1" and "instability limit 2", discussed in following sections.

5.4.1 Change in Stator parameters:

Stability limit of motor for variation of stator resistance r_s and stator leakage reactance x_{ls} (assuming that stator resistance and leakage reactance are same for both the winding sets *abc* and *xyz*, i.e. $r_s = r_1 = r_2$ and $x_{ls} = x_{l1} = x_{l2}$) are shown in Fig. 5.3 (a) and Fig. 5.3 (b), respectively. Lower boundary of instability limit 1 is almost unaffected during the variation of both the parameters. However, its upper boundary was found to be dependent on these parameters. As resistance r_s is increased, the upper boundary of instability limit 1 was found to be shifted in upper portion, making the area of instability wider. Hence, region of instability increases with the increase in stator resistance r_s. This effect was found to be opposite with the variation of leakage reactance x_{ls}. Same effect was found on instability limit 2; however, no change was observed for variation of leakage reactance x_{ls} . Moreover, stability limit was found to be more dependent on the variation of resistance r_s, as depicted in Fig. 5.3. If required, stability of the motor can be increased (i.e. decreasing instability region) by increasing the value of leakage reactance externally, but it will affect the steady-state performance.

5.4.2 Change in Field parameters:

Change in the instability limit for the change in parameters of field circuit, i.e. field resistance

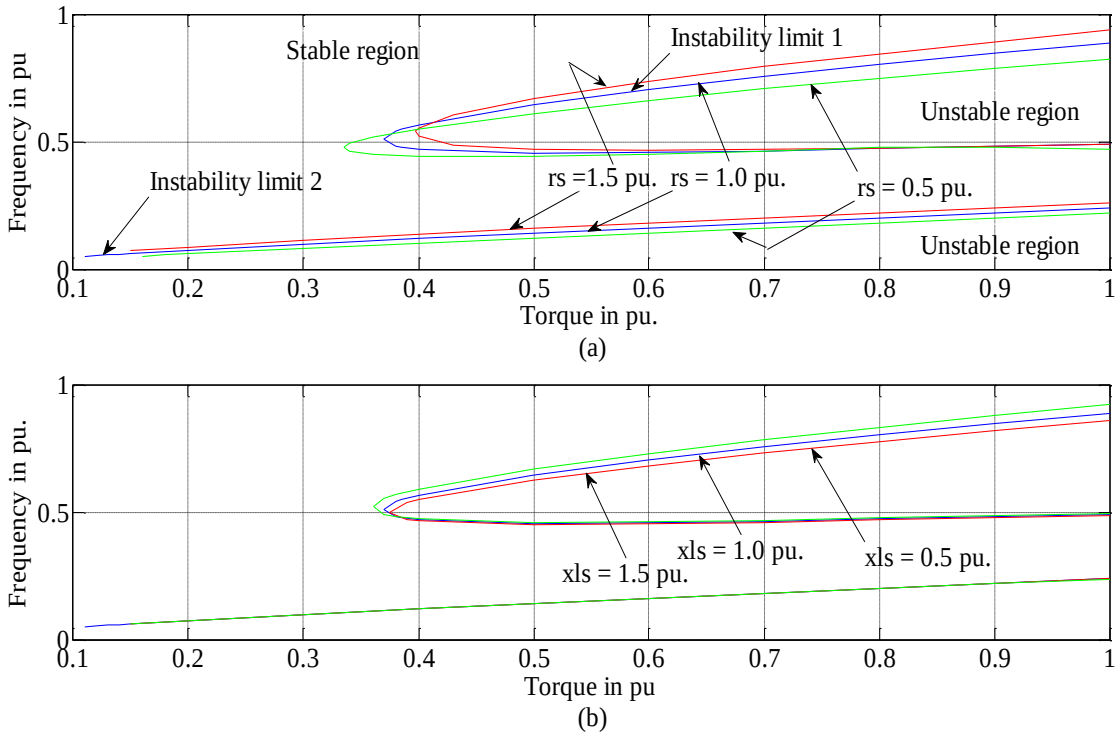

Fig. 5.3: Effect on instability boundary due to variation of (a) stator resistance r_s and (b) stator leakage reactance x_{ls}.

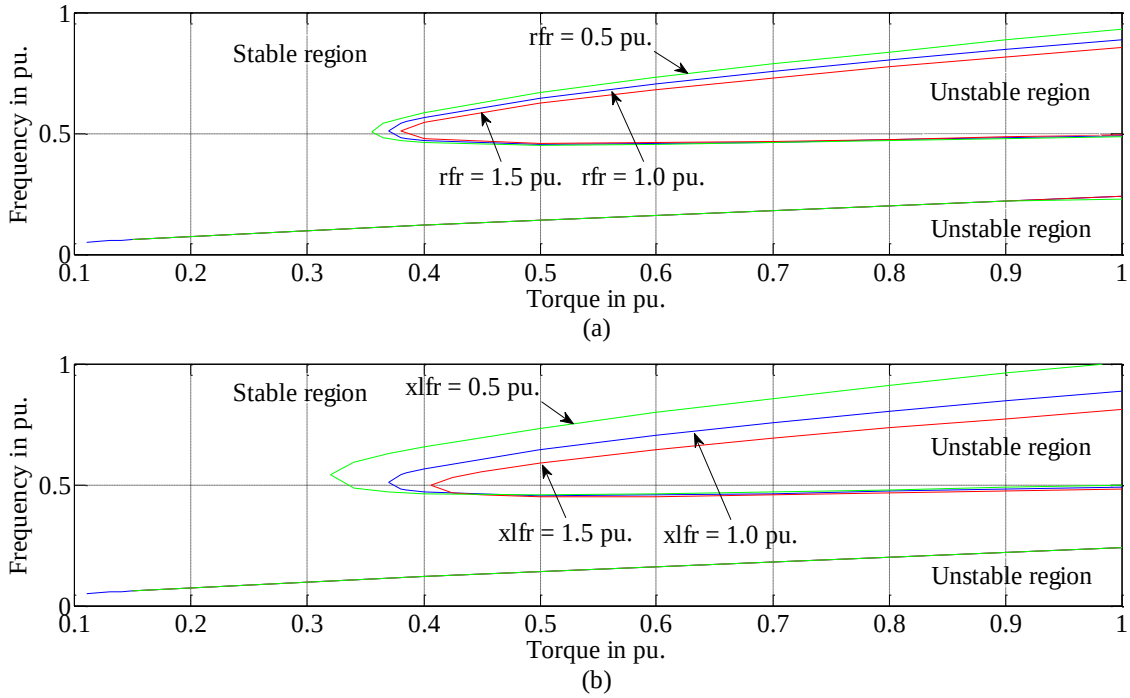

Fig. 5.4: Effect on instability boundary due to variation of field winding parameter (a) resistance r_{fr} and (b) leakage reactance x_{lfr}.

r_{fr} and field leakage reactance x_{lfr} , are shown in Fig. 5.4 (a) and Fig. 5.4 (b) respectively, where same effect can be observed on stability limit 1. The effect on instability limit 1 was more pronounced with the change in leakage reactance x_{lfr} . Therefore, the stability of motor at a particular operating point can be effectively increased by increasing the value of leakage reactance x_{lfr} i.e. increasing its time constant. But increasing the value of leakage reactance x_{lfr} will itself result in small decay of offset current in the field circuit. This is because the offset current in a particular circuit is associated with the inverse of effective time constant of circuit [20, 86]. Therefore, parameter of field circuit should be so selected which can ensure stable operation with acceptable decay of offset current in the field circuit. Effect on instability limit 2 was not observed for the variation of field resistance r_{fr} and field leakage reactance x_{lfr}.

5.4.3 Change in Damper winding parameters:

Effect of parameters variation of damper windings is shown in Fig 5.5. It was observed that the variation of resistance r_{Kq} of the damper winding along q axis has a pronounced effect on the motor stable operation. Increase in the value of r_{Kq} effectively increases the area of instability limit 1 in lower frequency and higher torque region both, as shown in Fig. 5.5 (a). Motor stability can be considerably enhanced by increasing the time constant of this winding by reducing the value of r_{Kq}. Effect of leakage reactance x_{lKq} was found to be negligible, as shown in Fig. 5.5 (b). For the analyzed motor parameter, effect of damper winding K_d on motor stability could not be observed as shown in Fig. 5.5 (c) and Fig. 5.5 (d). Effect on instability boundary 2 was not observed for parametric variation of damper windings.

5.4.4 Change in magnetizing reactance:

Magnetizing reactance along *d-q* axes (x_{md} and x_{mq}) are the important parameters, whose variation on motor stability has been depicted in Fig. 5.6. It has been found that the effect of magnetizing reactance along q axis, x_{mq} is more pronounced, when compared with magnetizing reactance along *d* axis, x_{md}. Region of instability limit 1 decreases with decrease in the value of x_{mq}. This limit vanishes, when it is decreased by 0.5 pu. Variation in the value of x_{md} results almost no change on motor instability limit 1. Only small change was noted on instability limit 2.

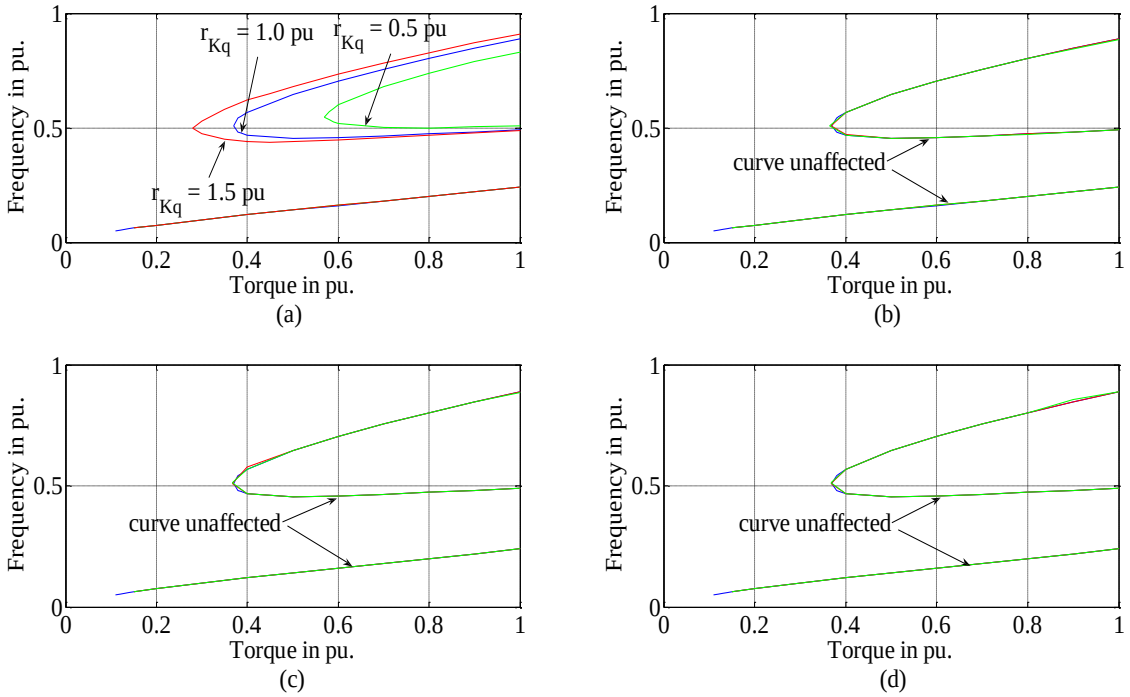

Fig. 5.5: Effect on instability boundary due to variation of damper winding parameters (a) resistance r_{Kq} (b) leakage reactance x_{lKq} (c) resistance r_{Kd} (d) leakage reactance x_{lKd}.

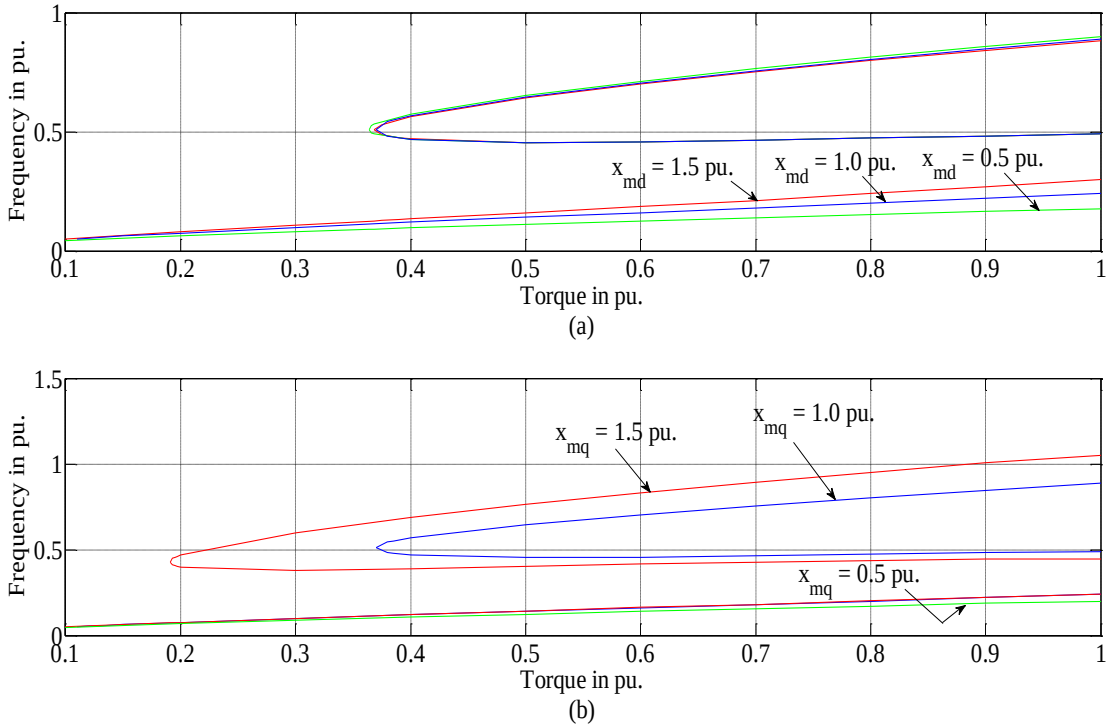

Fig.5.6: Effect on instability boundary due to variation of magnetizing reactance (a) x_{md} along d axis (b) x_{mq} along q axis.

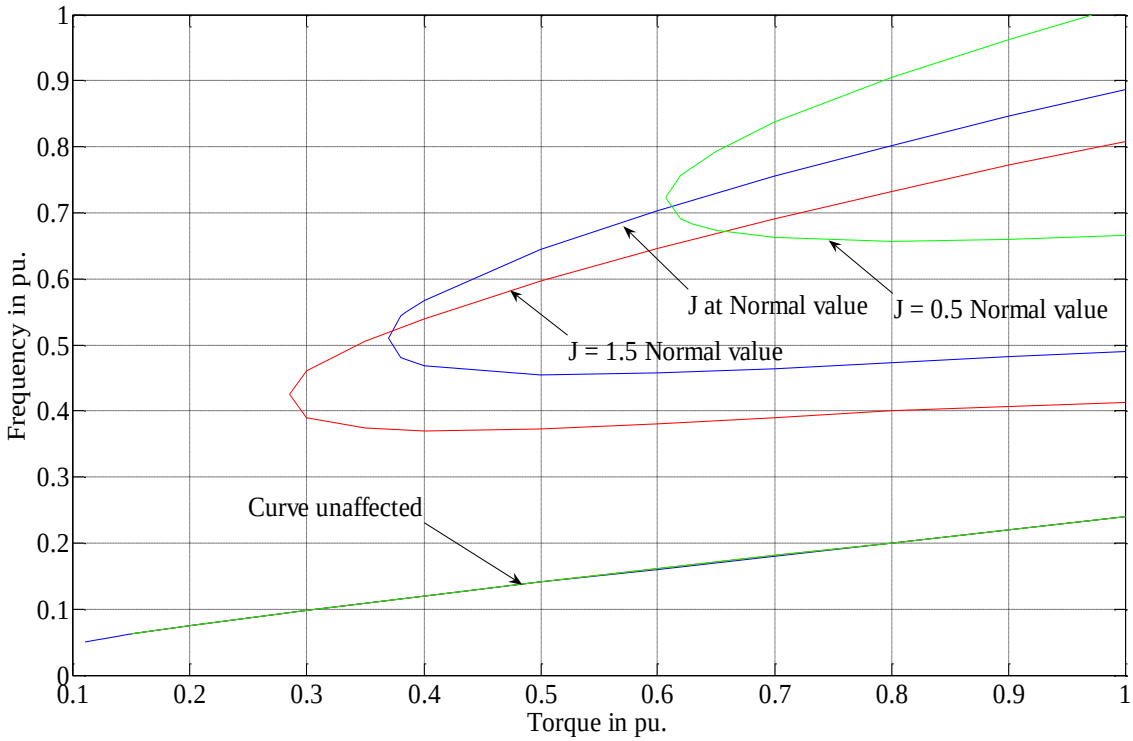

Fig. 5.7: Effect on instability boundary due to variation of moment of inertia *J*.

5.4.5 Change in Moment of Inertia:

Effect on motor stability due to the change in moment of inertia *J* i.e. motor-load combination is shown in Fig. 5.7. A shift in the region of instability limit 1 was noted for the variation in moment of inertia *J*. Increase in the value of *J* shifts the region of instability towards the region of lower torque and frequency. This region of instability becomes smaller, but shifts towards the rated frequency operation, when operating at lower value of *J*. Therefore, motor with a smaller value of *J* (low power rating machine) are more stable for the operation at lower frequency region. However, the motor with larger value of *J* (larger power rating machine) should be preferred for the operation near rated operating condition. Effect on instability limit 2 was not observed for variation of moment of inertia *J*.

Based on the effect of small signal stability of synchronous motor due to its parametric variation, some of the necessary measures can be incorporated during the design stage of motor to enhance its stability along with the consideration of other design factors. These measures have been listed in Table 5.7.

Table 5.7: Measures to improve the stability of motor

Motor Parameters		Action
Stator Parameters	Resistance r_s	Decrease
	Leakage reactance x_{ls}	Increase
Rotor Parameters	Field resistance r_{fr}	Increase
	Field leakage reactance x_{lfr}	Increase
	q axis magnetizing reactance x_{mq}	Decrease
	Damper resistance r_{Kq}	Decrease
	d axis magnetizing reactance x_{md}	No change
	Damper leakage reactance x_{lKq}	
	Damper resistance r_{Kd}	
	Damper leakage reactance x_{lKd}	
Moment of Inertia J		Application dependent

5.4.6 Change in Voltage and Frequency:

Effect on motor stability due to the change in voltage and frequency are illustrated in various characteristic curves in the preceding section at different load torque (operation shown at rated value of motor parameter). In order to have a complete instability boundary of motor operation, the curves shown in Fig. 5.8 are plotted at different operating loads for different Volt/Hertz ratio. This signifies the dependency of stability on operating voltage and frequency independently. Existence of motor instability can be noted at almost all operating frequency range at lower voltage level. A closed loop of instability limit was also found within intermediate frequency range. It can be inferred that increasing the operating voltage at a particular frequency or vice-versa tends the motor operation towards stable region. This has been illustrated by the motor operation at 50 percentage of rated torque operating at 60 V and 35 Hz, marked by point '*a*' in Fig. 5.8. Stability at this condition has been enhanced by increasing the input phase voltage to 80 V, marked by point '*b*'. Followed by the inclusion of impulse disturbance in load torque, unstable and stable modes of operation corresponding to these points are shown in Fig. 5.9 and Fig. 5.10, respectively.

5.4.7 Change in Load Torque:

Variation in motor stability limit due to the change in load torque has been already shown in the previous section, showing the operation at rated motor parameter. Complete instability boundary for the different motor load condition is shown in Fig. 5.8. It can be seen that under no-load condition, motor is almost stable at all range of operating voltages and frequencies

(14.4 Hz onwards). Area of instability region was found to be increased with the increase in motor load. Lower limit of frequency was found to vary a little for different load (except at no-load). But the upper limit of the closed loop instability boundary was found to vary at a larger scale (frequencies ranges are 9.25 – 32.6 Hz, 10.0 – 41.0 Hz and 10.4 – 51.9 Hz for operation at 0.25 pu, 0.5 pu and 1.0 pu of load torque, respectively). Similar variation was also found for voltage limit (voltages ranges 10.2 – 51.6 V, 13.2 – 78.0 V and 18.5 – 115.9 V for operation at 0.25 pu, 0.5 pu and 1.0 pu of load torque, respectively).

The maximum obtainable power for a stable operation was found to be dependent on input phase voltage. This is depicted in Fig. 5.11 (a), where operating frequency was kept constant at 50 Hz. However, to have a constant air gap flux (at constant Volt/Hz) at two voltage levels, 120 V and 140 V, are shown in Fig. 5.11 (b). Stability limit was found to be increased with the increase in input phase voltage. Variation of the stability limit on voltage level clearly indicates the effect of operating power factor, i.e. reactive power as shown in Fig. 5.11 (b). It is worthwhile to mention here that the maximum obtainable power is upto 1.76 times the rated power under safe current limit [16]. Output powers above this value are shown in Fig. 5.11 (a), as ideal operation of motor is considered (losses, winding insulation and other design factors are not considered).

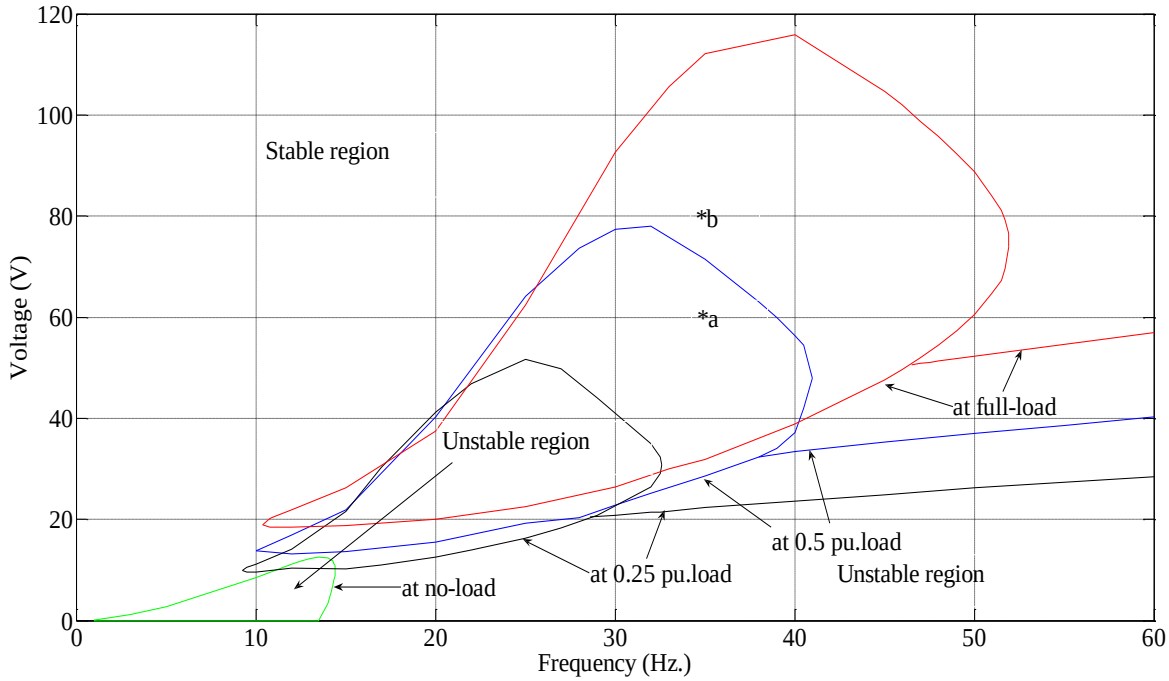

Fig. 5.8: Instability boundary under different voltage and frequency at different motor load.

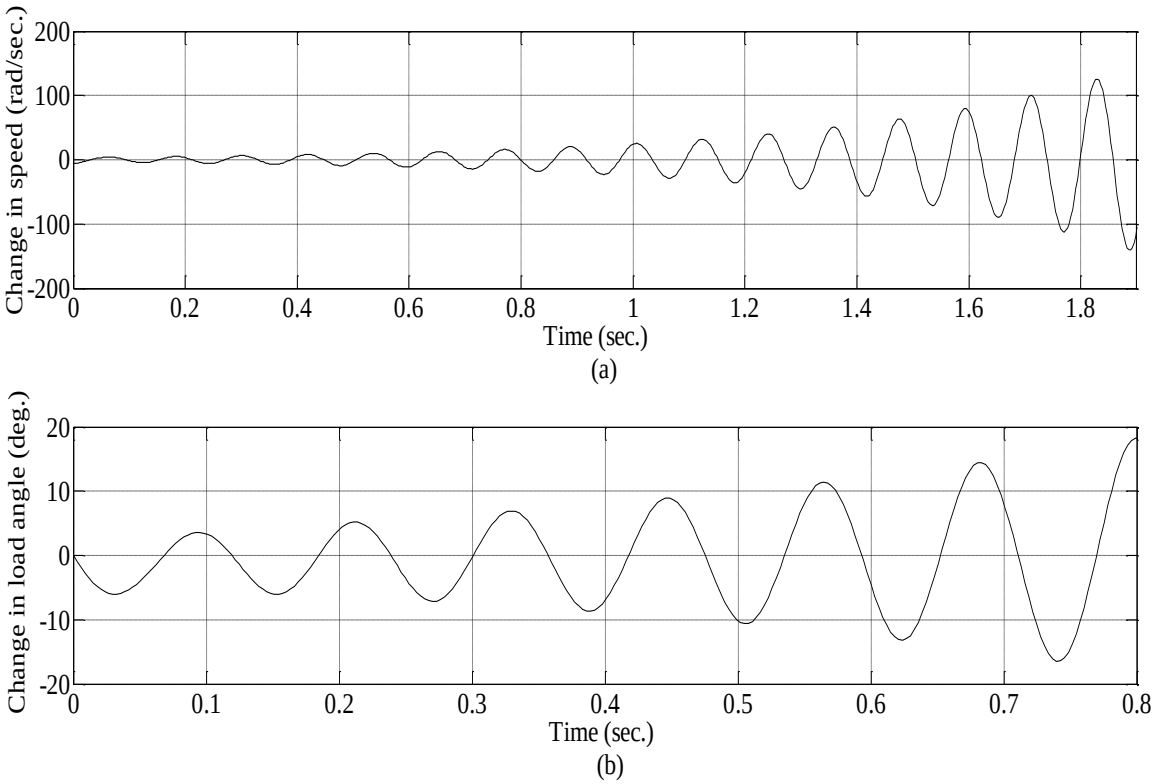

Fig. 5.9: Motor response at point marked '*a*'.

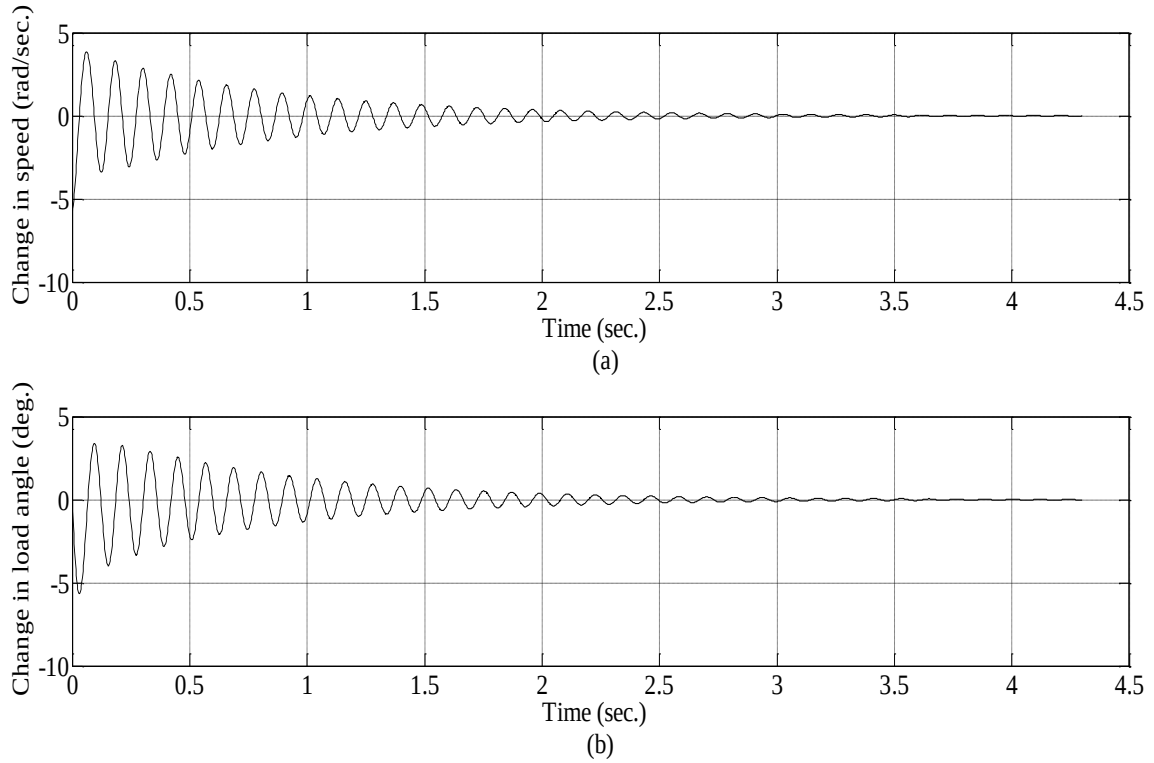

Fig. 5.10: Motor response at point marked '*b*'.

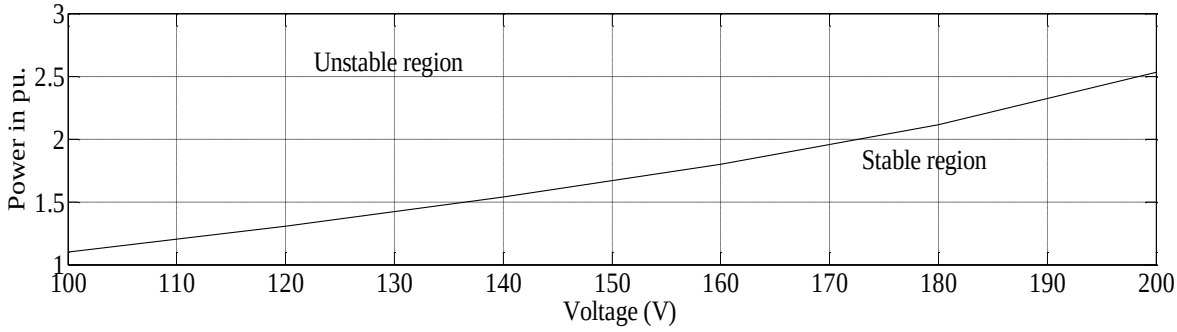

(a)

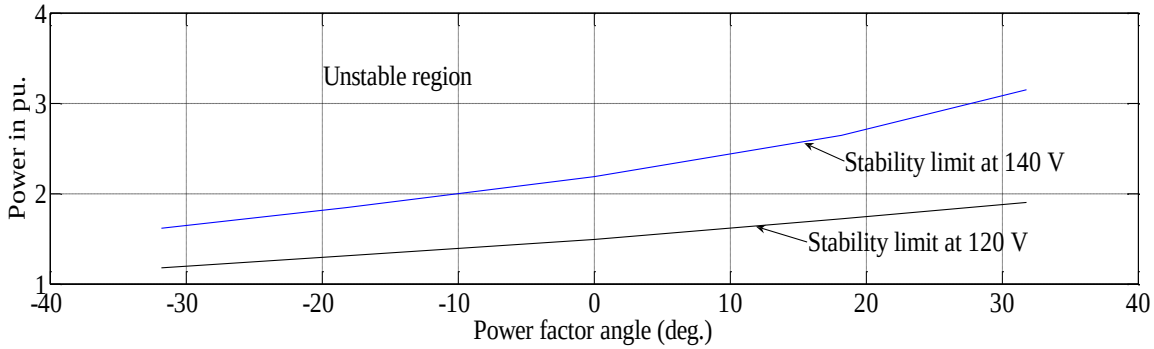

(b)

Fig. 5.11: Variation of stability limit with the variation of (a) input voltage (b) power factor angle.

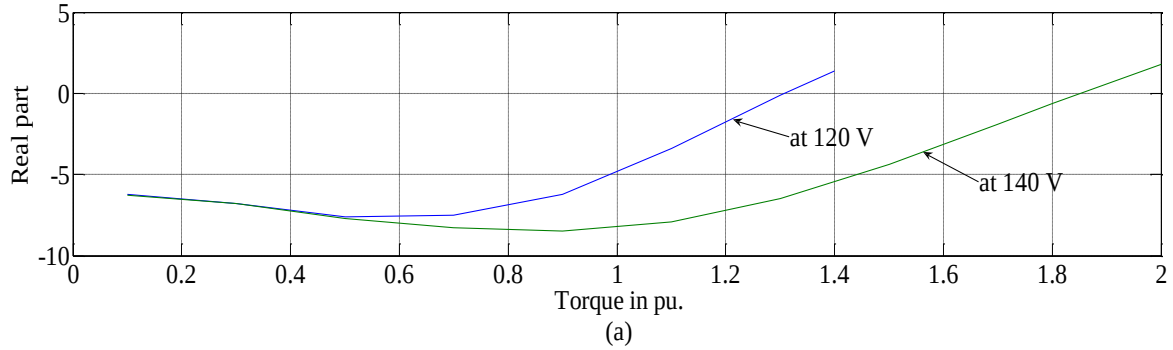

(a)

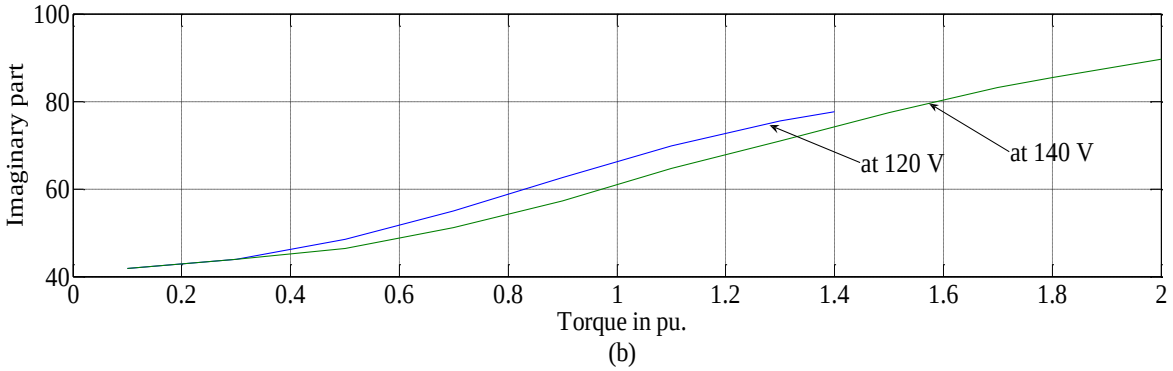

(b)

Fig. 5.12: Component variation of dominant eigenvalues with the variation of motor torque (a) real part (b) imaginary part.

Effect of motor load torque on dominant eigenvalues at two voltage level of 120 V and 140 V are depicted in Fig. 5.12. Stability of the motor operating at a higher voltage level was found to be increased (by increasing the magnitude of negative real component) followed by the increase in load torque upto a particular operating point (motor torque 0.52 pu and 0.90 pu at voltage level 120 V and 140 V, respectively), as shown in Fig. 5.12 (a). As far as the oscillatory behavior of the rotor is concerned (imaginary component of eigenvalues), quite a small variation was found, whose maximum variation was observed at rated operating load (66.2 rad/sec. and 60.9 rad/sec. at 120 V and 140 V, respectively), as shown in Fig. 5.12 (b).

5.5 Application of stabilization technique

Appropriate machine parameters will have to be incorporated at the design stage to ensure stable operation at a particular operating point, as suggested in Table 5.7, in the preceding section. Since, parametric variation of a machine is a difficult task from practical point of view which needs the application of stabilization technique in form of closed loop scheme, will have to be adopted to ensure a stable operation in all the operating regions (both stable and unstable region). Therefore, a simple but an effective scheme, known as state feedback technique or a linear optimal control (LOC) is employed and discussed below.

In order to design a linear optimal control, the linearized version of machine equations (derived in the preceding section) at a particular steady-state condition will be utilized (equation 5.39). For the present system (multiple input multiple output), performance index of the quadratic form is usually chosen

$$J = \frac{1}{2}\int_0^\infty (x^T Q x + u^T G u) dt \tag{5.43}$$

where, *Q* and *G* are the positive-semi definite and positive-definite constant coefficient weighting matrix of state variable deviation and that of control effort. Usually, both *Q* and *G* are diagonal matrices. The bracketed expression in the above equation is known as generalized energy function.

Hamiltonian function is now introduced which is given as

$$H\left(x, u, \frac{\partial V}{\partial x}\right) = \frac{1}{2}(x^T Q x + u^T G u) + \frac{\partial V}{\partial x}\frac{\partial x}{\partial t}$$

$$= \frac{1}{2}(x^T Q x + u^T G u) + \frac{\partial V}{\partial x}(Ax + Bu) \tag{5.44}$$

where, *V(x)* is a return function, given by

$$V(x) = \frac{1}{2}x^T Kx \tag{5.45}$$

where, $K \in R^{n\times n}$ is a symmetrical matrix. The known matrix K is calculated from the following non-linear differential equation (the so-called Riccati equation [89-91, 95-96, 100, 103])

$$\dot{K} = Q + A^T K + KA - KBG^{-1}B^T K \tag{5.46}$$

Minimization of Hamiltonian, i.e. making use of

$$\frac{\partial H}{\partial u}\left(x, u, \frac{\partial V}{\partial x}\right) = 0 \tag{5.47}$$

it is found that

$$u = -G^{-1}B\frac{\partial V}{\partial x}x$$

$$\text{or, } u = -K_f x \tag{5.48}$$

where,

$$K_f = G^{-1}BK \tag{5.49}$$

From equation 5.48, the closed loop state equation of the system can be written as

$$\dot{x} = Ax + Bu$$

$$= (A - K_f)x \tag{5.50}$$

Stability of the closed loop system can be checked by evaluating the eigenvalues of matrix $(A - K_f)$, where the required eigenvalues shift is obtained, to ensure the desire motor operation. In order to have an appropriate shift of dominant eigenvalues, all the diagonal elements of matrix Q will have to be updated. These elements can be calculated by using the concept of sensitivity as explained by the authors in ref. [89-90]. However, to get rid of these complicated computation procedure, an alternative means is adopted here. It includes the partitioning of diagonal matrix elements into three groups namely, Q_1, Q_2, and Q_3 as shown in equation 5.51.

$$Q = \begin{bmatrix} [Q_1]_{4\times4} & [0]_{4\times2} & [0]_{4\times3} \\ [0]_{2\times4} & [Q_2]_{2\times2} & [0]_{2\times3} \\ [0]_{3\times4} & [0]_{3\times2} & [Q_3]_{3\times3} \end{bmatrix} \tag{5.51}$$

Within each partitioned diagonal matrix, all diagonal elements are identical. These elements are q_1, q_2 and q_3, respectively. Q_1, Q_2 and Q_3 are partitioned diagonal matrices, corresponding to the state variable deviation associated with the stator side, rotor side and remaining variables, respectively. Complete steps of calculation in control scheme are shown in form of flow chart given in Fig. 5.13. Calculation of the eigenvalues, with and without the application of this technique for the motor operation at 50 percent of base torque, power factor of 0.95 (lagging), operating at 25 Hz (with constant Volt/Hz ratio), is depicted in Table 5.8. Elements of

Table 5.8: Motor eigenvalues without and with control scheme

Nomenclature	Eigenvalues (without control)	Eigenvalues (with control)
Stator eigenvalue I	-107.8 ± 52.4	-108.0 ± 52.4
Stator eigenvalue II	- 28.0 ± 65.6	- 28.5 ± 66.5
Rotor eigenvalue	0.8 ± 47.0	- 4.3 ± 46.3
Real eigenvalue	-9136.3, -712.5, -6.2	-9136.3, -712.5, -8.3

partitioned matrix *Q* was so adjusted to have a required shift of dominant eigenvalues, with quite a small effect on other eigenvalues. For this purpose, values were found to be $q_1 = q_2 = 1 \times 10^{-4}$ for a unity matrix *G*. Dominant eigenvalue shift was found to be almost unaffected on the value of q_3 variation. Motor transient response to an impulse disturbance input to load torque in open loop operation, for the change in rotor speed and load angle are shown in Fig. 5.14 (a) and Fig. 5.14 (b) respectively. This unstable operation can be easily avoided by applying a control scheme in closed loop, as depicted in Fig. 5.15. Effect of the variation of value of q_1, q_2 is shown in Fig. 5.16 (a) and Fig. 5.16 (b) for the transient response of change in rotor speed and load angle, respectively. Difference in transient response can be seen in Fig. 5.15 and Fig. 5.16. For, $q_1 = 10\, q_2$, i.e. increasing the matrix elements of *Q*, associated with rotor side, decreases the settling time of motor response, although it increases its peak overshoot. Hence, value of q_1 and q_2 can be adjusted for required response.

5.6 Formulation of Transfer Function

The linearized equations of a system are more offenly used for the analysis and design of controllers, like speed controller for variable speed drive system etc., which needs the formulation of transfer function. This is because the transfer function written from linearized system equations relates the output variable to be controlled to the controlling input variable. Moreover, it also facilitates the study of small displacement behavior of the system about a steady-state operating point rather than to use the detailed non-linear equations. Consequently, the different control theory approach can be applied like plotting of root locus, bode plot, nyquist plot etc. Hence, greatly simplifies the control analysis of a system, applicable for motor operation.

In this section, formulation of transfer function will be outlined, wherein the linearized equations of six-phase synchronous motor will be utilized. As an illustration, transfers function

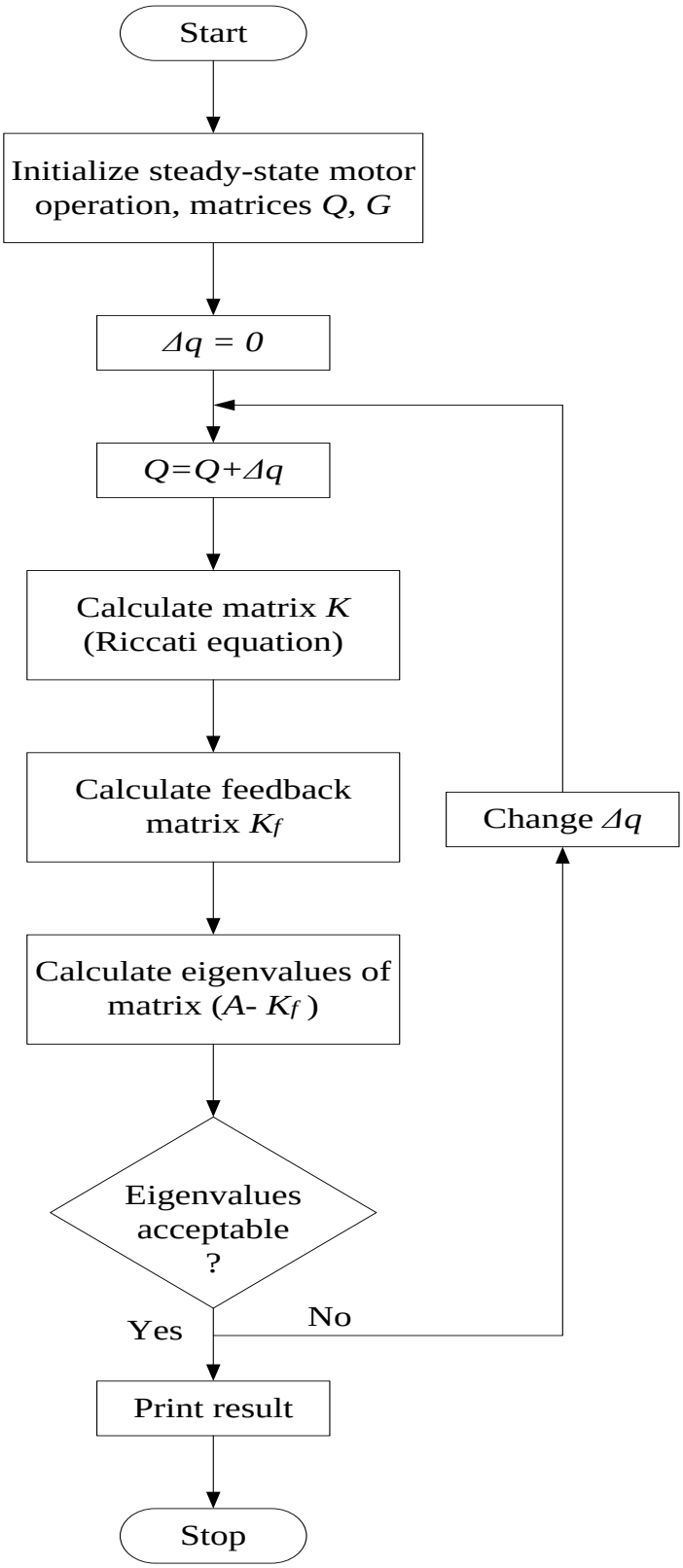

Fig. 5.13: Steps of calculation for the design of linear optimal control.

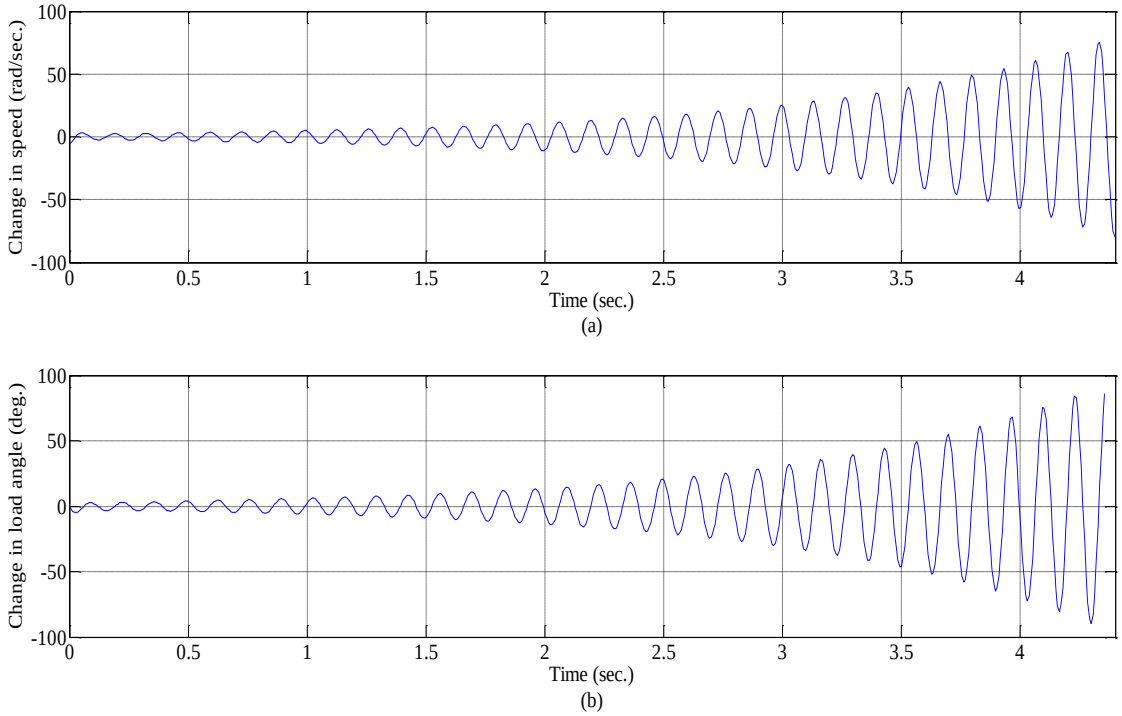

Fig. 5.14: Transient response of motor operation without control scheme showing change in (a) rotor speed and (b) load angle, *delta*.

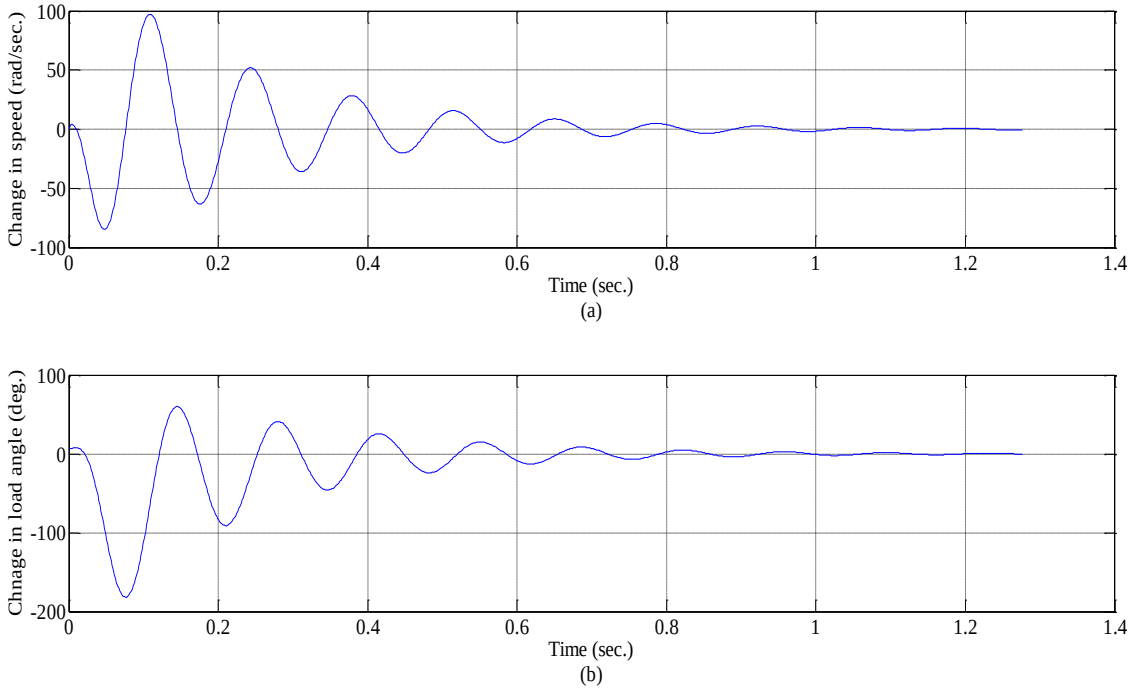

Fig. 5.15: Transient response of motor operation with control scheme (taking $q_1 = q_2$) showing change in (a) rotor speed and (b) load angle, *delta*.

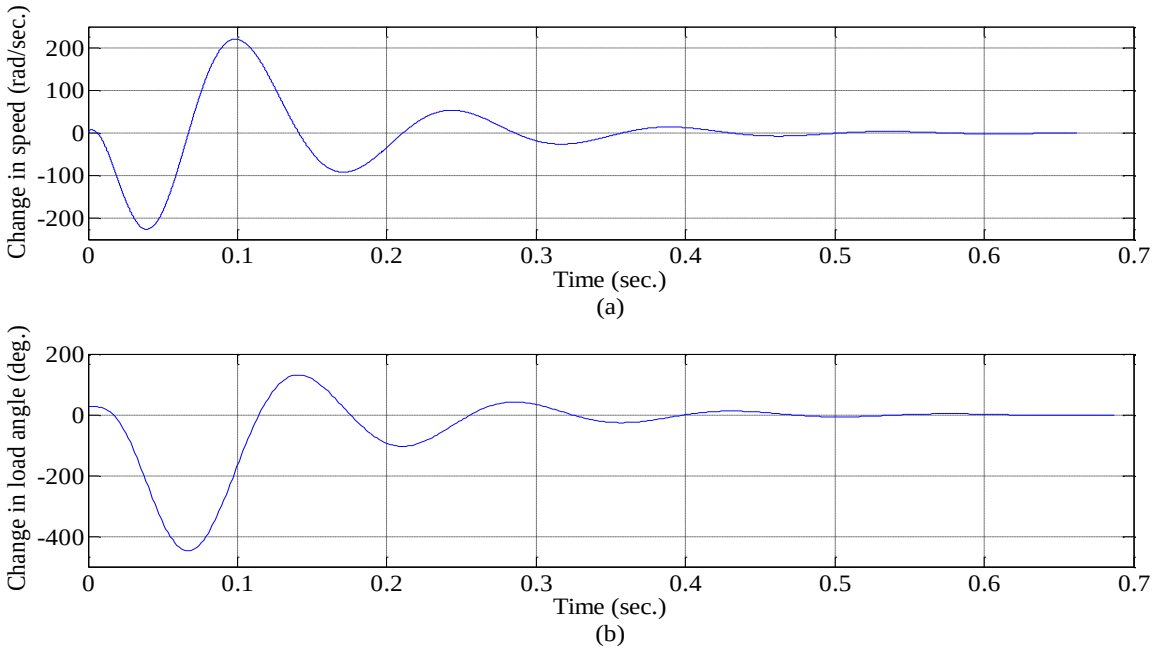

Fig. 5.16: Transient response of motor operation with control scheme (taking $q_1 = 10\ q_2$) showing change in (a) rotor speed and (b) load angle, *delta*.

of the change in reactive power w.r.t. the change in field excitation i.e. $\frac{\Delta Q(s)}{\Delta E_{fr}(s)}$ is derived in a simplified manner, followed by the plotting of root locus for stability analysis. The state equations of linear dynamic system are

$$\dot{x} = Ax + Bu \tag{5.39}$$

$$y = Cx + Du \tag{5.52}$$

where,

x is the state vector defined by equation 5.19

u is the input vector defined by equation 5.20

y is the output variable (or a set of output variables)

A is a matrix defined by equation 5.40

C and *D* matrices are defined below.

Solving the equation 5.39 for *x*, considering the initial condition to be zero and substituting the result in equation 5.52 yields

$$Y(s) = [C(sI - A)^{-1}B + D]U(s) \tag{5.53}$$

Therefore, transfer function is

$$G(s) = \frac{Y(s)}{U(s)} = [C(sI - A)^{-1}B + D] \tag{5.54}$$

Table 5.9: Zeros and poles of the transfer function $\frac{\Delta Q(s)}{\Delta E_{fr}(s)}$

Zeros	Poles
z_1 = -91.6 + j 104.7	p_1 = -91.6 + j 104.7
z_2 = -91.6 - j 104.7	p_2 = -91.6 - j 104.7
z_3 = -1.3 + j 103.5	p_3 = -14.3 + j 100.3
z_4 = -1.3 - j 103.5	p_4 = -14.3 - j 100.3
z_5 = -11.3 + j 54.7	p_5 = -11.5 + j 58.3
z_6 = -11.3 - j 54.7	p_6 = -11.5 - j 58.3
z_7 = -9508.4	p_7 = -9135.9
z_8 = -698.1	p_8 = -698.5
Gain K = 619.6	p_9 = -16.3

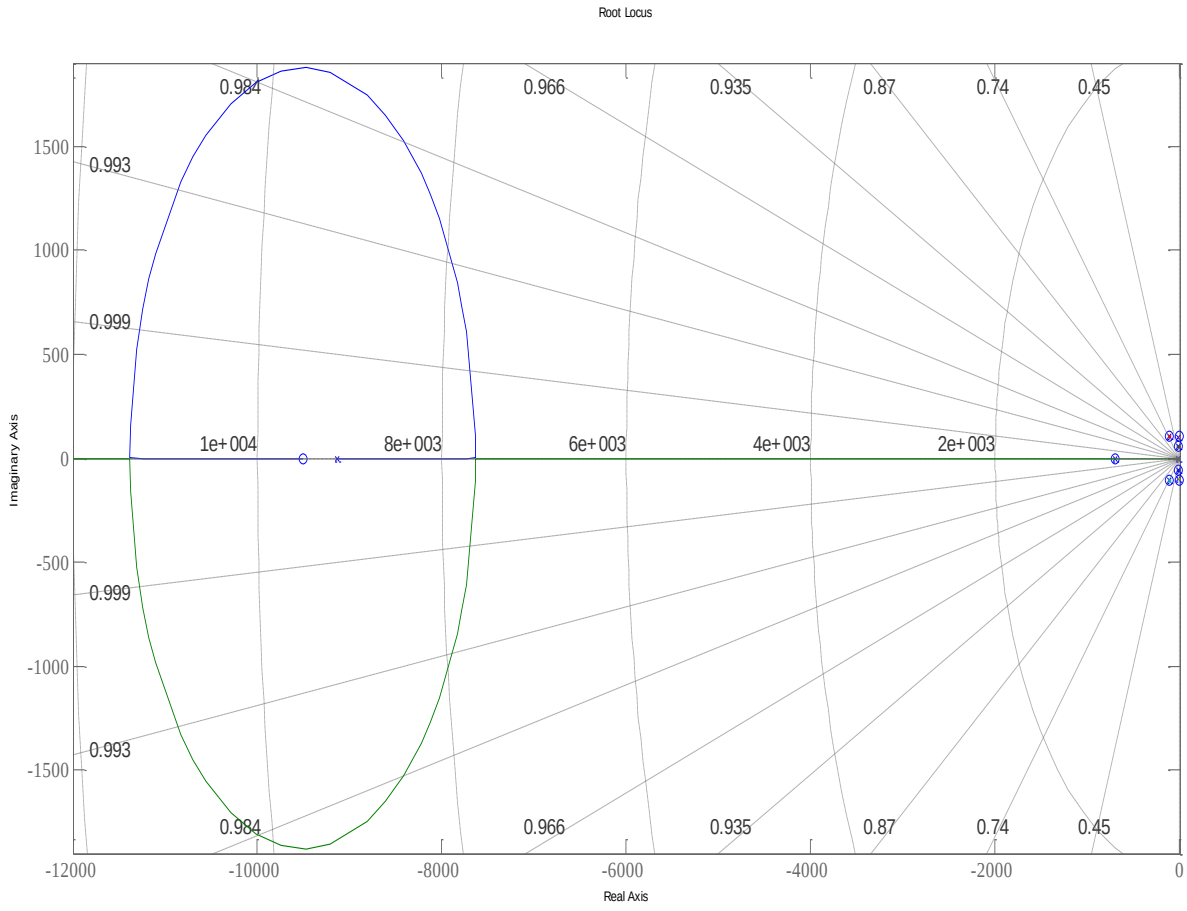

Fig. 5.17: Root locus for the transfer function $\Delta Q(s)/\Delta E_{fr}(s)$.

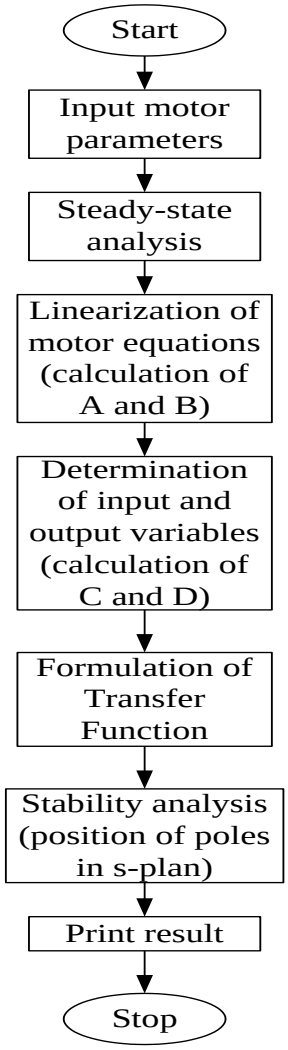

Fig. 5.18: Steps to perform stability analysis of six-phase synchronous motor.

For the purpose to drive the transfer function of $\frac{\Delta Q(s)}{\Delta E_{fr}(s)}$, the linearized expression for reactive power is given by

$$\Delta Q(s) = v_{q1}^e \Delta i_{d1}^e + i_{d1}^e \Delta v_{q1}^e - v_{d1}^e \Delta i_{q1}^e - i_{q1}^e \Delta v_{d1}^e + v_{q2}^e \Delta i_{d2}^e + i_{d2}^e \Delta v_{q2}^e - v_{d2}^e \Delta i_{q2}^e - i_{q2}^e \Delta v_{d2}^e$$
$$= Cx + Du \quad (5.55)$$

where,

$$C = \left[-v_{d1}^e, v_{q1}^e, -v_{d2}^e, v_{q2}^e, 0, 0, 0, 0, 0\right] \quad (5.56)$$

$$D = \left[i_{d1}^e, -i_{q1}^e, i_{d2}^e, -i_{q2}^e, 0, 0, 0, 0, 0\right] \quad (5.57)$$

Therefore, the transfer function will be in following form

$$\frac{\Delta Q(s)}{\Delta E_{fr}(s)} = K \frac{(s-z_1)(s-z_2)\ldots(s-z_m)}{(s-p_1)(s-p_2)\ldots(s-p_n)} \quad (5.58)$$

where, the value of gain *K*, zeros ($z_1, z_2, \ldots z_m$) and poles ($p_1, p_2, \ldots p_n$) have been calculated for the motor operation at 50 percent of rated load. These values are shown in Table 5.9. Root locus of the transfer function, given by equation 5.58 can be drawn by the well known procedure [88] and is shown in Fig. 5.17. It also shows that the system is stable for all the values of gain *K*, as all the poles are lying in negative half of *s*-plan. Necessary steps used to perform the small signal stability analysis of six-phase synchronous motor are shown in the form of flowchart in Fig. 5.18. Steps have to be followed for different combinations of input and output variables, while formulating the transfer function to study stability of a six-phase synchronous motor under small disturbance.

5.7 Conclusion

A linearized mathematical model of a six-phase synchronous motor has been developed, considering the mutual leakage coupling between both the stator winding sets *abc* and *xyz*, using *dq0* approach. This results in a set of linear differential equations, which describes the dynamic behavior of the motor under small displacement/excursion about a steady-state operating point, so that the basic linear control system theory can be applied to evaluate the eigenvalues. An eigenvalue criterion was used to study the stability of six-phase synchronous motor. Association between the eigenvalues and motor parameters has been established by calculating the eigenvalue at an operating point by changing the motor parameter. It was found that the two eigenvalues (stator eigenvalue I and II) are almost unaffected with the variation in rotor parameter and load. The other complex conjugate pair is affected by the variation in moment of inertia *J* and load. It actually indicates "settling out" rotor oscillation of synchronous motor during hunting or swing mode. The remaining three real eigenvalues indicate decay of the offset currents in rotor circuit and, therefore, associated with effective time constant of the circuit.

Based on the variation of dominant eigenvalues, stability of motor can be enhanced. As far as design stage is concerned, it can be carried out from stator as well as rotor side. From stator side, an effective way is to decrease the value of stator resistance, but alternatively, value of stator leakage reactance may be increased, if required. From the rotor side, it can be effectively carried out by increasing the value of leakage reactance of field circuit and /or by decreasing the value of resistance of damper winding along *q* axis.

Stability of motor was also found to be affected by the variation in operating conditions. It can be enhanced either by increasing the input voltage or operating frequency at a particular operating load. But increase in load torque upto a particular point increases the stability, but it tends towards instability for further motor loading, under constant Volt/Hz operation. From the field side, stability region was found to be increased by increasing the power factor angle (to interpret the effect of power factor).

A simple control scheme has also been introduced and analyzed, employing the state feedback technique. The applied control was found to be simple but effective, ensuring a stable operation of analyzed six-phase synchronous motor in all the operating region (both stable and unstable region). A way of selecting the elements of weighing matrix, associated with the motor state variable has also been addressed. Selection of these elements determines the required shift of dominant eigenvalues for a stable operation of motor.

Developed linearized model can be easily used to formulate the transfer function between input and output variables, where different stability plots (like root locus, nyquist plot, bode plot) can be easily drawn. Thus greatly simplifying the control analysis of a system applicable for six-phase synchronous motor.

Chapter 6

Load Commutated Inverter fed Six-phase Synchronous Motor Drive

6.1 General

The synchronous motor is preferred for the higher power (multi MW) applications, driven by either cycloconverter or load commutated inverter (LCI) [104-106]. Drive employing cycloconverter has been well explored in ref. [107-109]. But, it offers certain inherent disadvantages when compared with dc linked inverter (LCI drive) such as:

(i) Output frequency of cycloconverter is smaller than the fundamental line frequency (not more than one-third of fundamental).

(ii) Circuitry of cycloconverter is more complex, employing a larger number of power electronics switches (18 or 36 for three-phase cycloconverter).

These limitations can be easily eliminated by employing a topological circuitry using two stage conversion, inserting a dc link to decouple the line and machine converter [104]. Therefore, dynamic behavior of six-phase synchronous motor fed by LCI has been analyzed in this chapter for higher power applications. Such higher power applications are beyond the range of other motor drives, including dc motor and forced commutated induction motor drives. In LCI fed synchronous motor drive, commutation of inverter switches (low cost thyristor) is achieved by the motor induced emf during its operation at leading power factor, eliminating the use of complicated and expensive commutation circuit, making it more economical and structurally simple [106].

Large number of literatures are available for the analysis of LCI fed three-phase synchronous motor. The authors in [110] have discussed the detailed simulation steps of an inverter-fed self-controlled synchronous motor using *d-q* machine model. It was concluded that the presence of damper windings has pronounced effect for a current source inverter than voltage source inverter fed motor, by reducing the magnitude of voltage spikes during the commutation process. Simulation of a generalized machine/power electronics interface technique has been discussed in [111], by simulating the system of LCI fed synchronous motor

drive. Authors in [63, 112] have given an important state space analysis of LCI fed synchronous motor drive, both during conduction as well as commutation mode, by evaluating the state equation considering a constant dc-link current (i.e. infinite value of dc link inductance). But the selection of dc link inductor is an important factor and was considered in [113], wherein no iterative computation is required for evaluation of initial condition.

Closed loop operation of LCI fed synchronous motor in self-controlled mode has been developed and studied during steady-state in ref. [114-116]. But, as far as dynamic analysis of LCI fed synchronous motor drive is concerned, a very limited literature is available. Effect of various parameters on self-controlled synchronous motor drive was studied, while investigating the stability of system [117] by using its transfer function derived in [118]. Authors have further given a simple dynamic control strategy for a fast speed response without any overshoot in [119].

Analysis dealing with the LCI fed six-phase synchronous motor can be found in very few literature. The issue of starting a LCI fed six-phase synchronous motor has been addressed in [120], where load commutation was found to be superior over two-phase and source commutation schemes. Digital simulation of a LCI fed six-phase synchronous motor drive has been reported in [121-122] with some experimental validation in [121, 123-124]. A detailed analytical work describing commutation transients has been carried out in [122]. Authors have adopted the same analytical approach to simulate the drive system having five phase [125] and twelve phase synchronous motor [126]. In these works, the analytical results are presented for LCI fed synchronous motor during steady-state. But as far as the dynamic analysis of a LCI fed six-phase synchronous motor is concerned, it has not yet been reported.

In this chapter, LCI fed six-phase synchronous motor has been investigated together with the development of a closed loop scheme for the system operation in self-controlled mode. Further, steady-state response of this system is also presented.

6.2 Control scheme of LCI fed six-phase synchronous motor drive

The basic topology together with its control scheme of LCI-fed six-phase synchronous motor suitable for higher power application is shown in Fig. 6.1. It consists of two independent channels in the section of power converter. Hence, it has four identical six-pulse SCR bridges. These SCR bridges on supply side and machine side can either work as rectifier and inverter (in

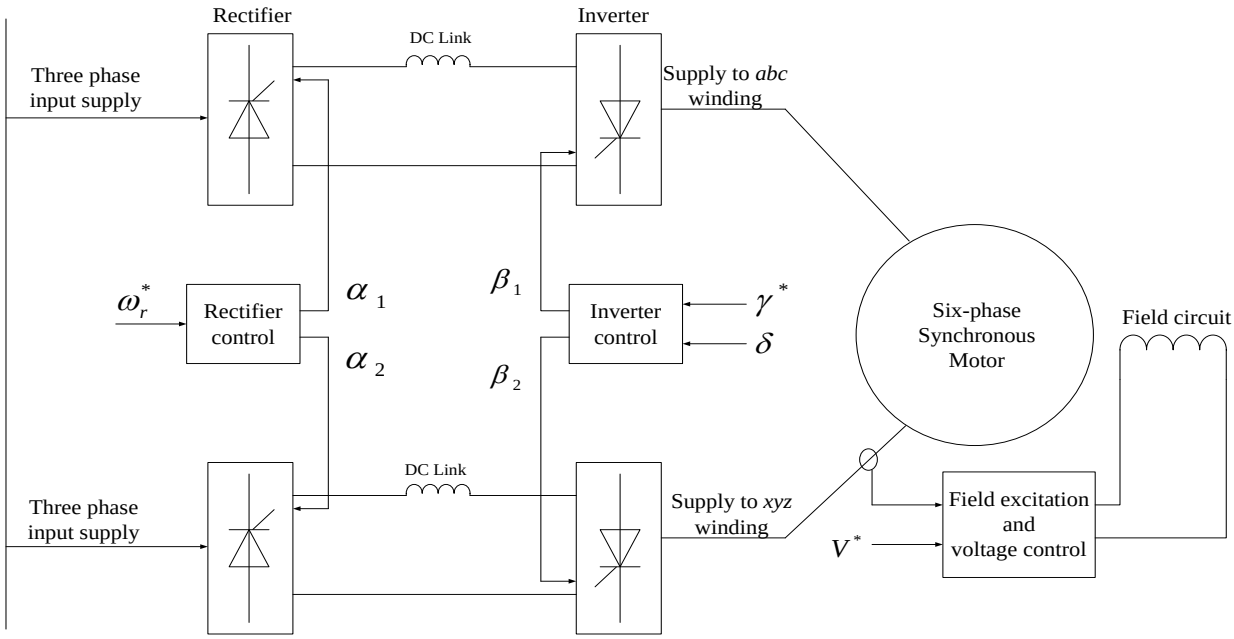

(a)

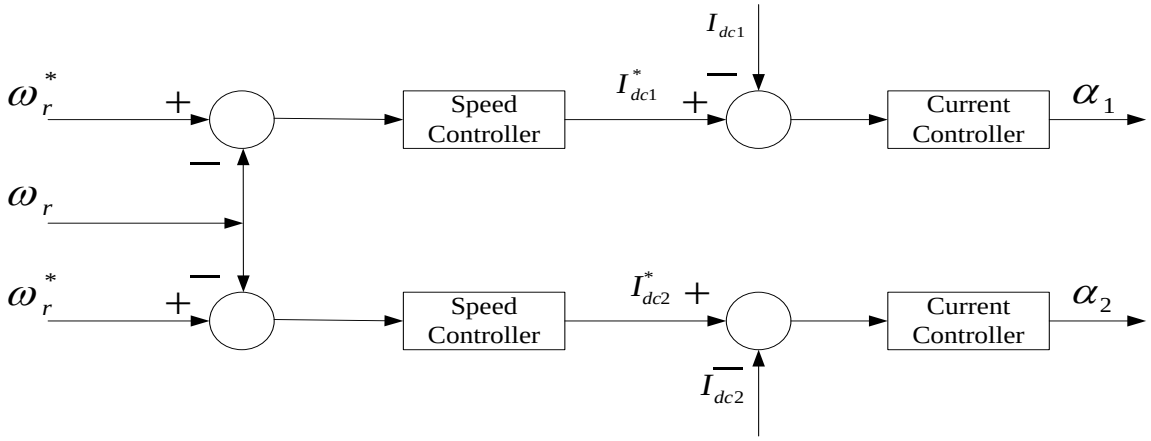

(b)

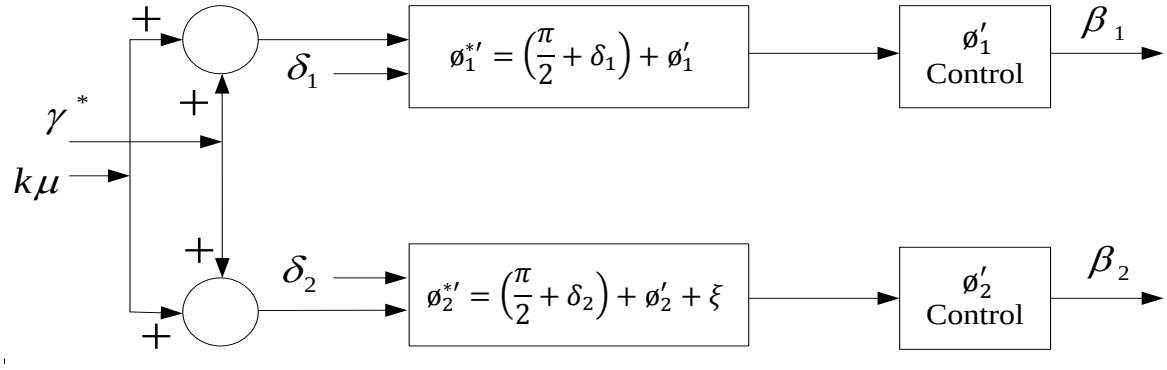

(c)

Fig. 6.1: Circuit diagram of LCI fed six-phase synchronous motor showing its (a) basic topology (b) rectifier control (c) inverter control.

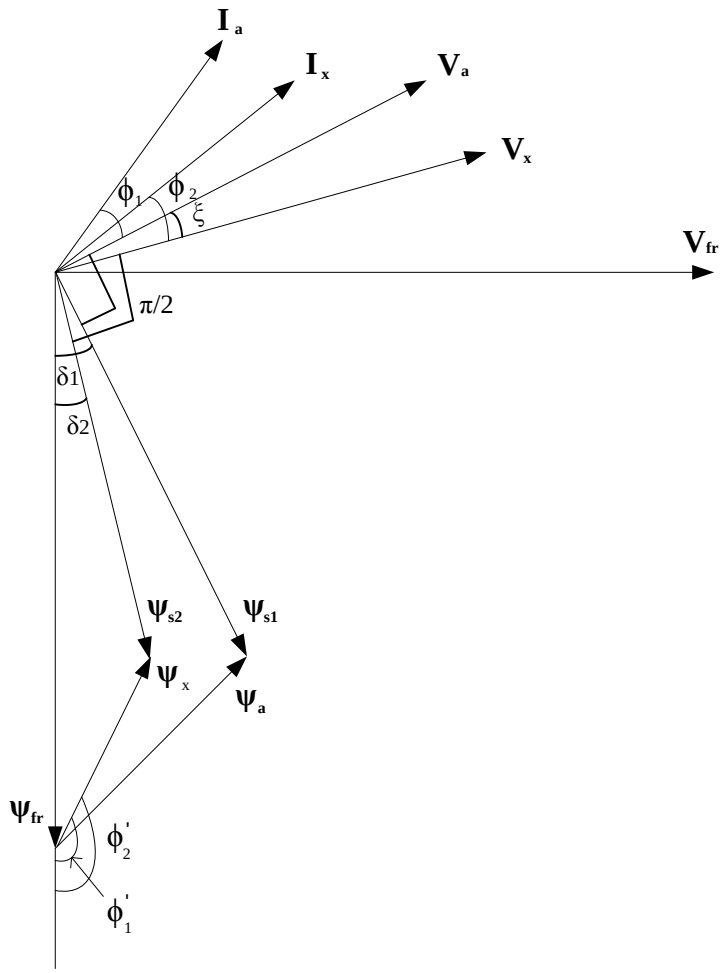

Fig. 6.2: Phasor diagram of LCI-fed six-phase synchronous motor.

motoring mode) or as inverter and rectifier (in regenerating mode). In the following section, only motoring mode is considered. In this topology, motor is ensured to operate at leading power factor (by maintaining its field excitation), as it assists the commutation of thyristor switches in inverter circuitry, without employing any commutation scheme [106, 111-114, 117]. A simplified phasor diagram showing the motor operation at leading power factor is depicted in Fig. 6.2. The flux $\boldsymbol{\psi_{fr}}$ determined by the field current is related to rotor position. The magnitude of stator current vectors $\boldsymbol{I_a}$ and $\boldsymbol{I_x}$ controlled by the rectifier circuits, resulting in armature fluxes $\boldsymbol{\psi_a}$ and $\boldsymbol{\psi_x}$, are positioned at required angle, as shown in phasor diagram. This requires the delay angle commands β_1 and β_2 (firing angles of inverters circuitry) associated with each winding sets *abc* and *xyz*. Delay angle command (β_k) is dependent on the angular position ϕ'_k (k =1 for winding set *abc* and is 2 for winding set *xyz*) and can be expressed as

$$\emptyset_1' = \delta_1 + \frac{\pi}{2} + \emptyset_1 \quad (6.1)$$

$$\emptyset_2' = \delta_2 + \frac{\pi}{2} + \emptyset_2 + \xi \quad (6.2)$$

where, δ (=$\delta_1 + \delta_2$) is the torque angle constituted by δ_1(due to load shared by the winding set *abc*) and δ_2 (due to load shared by the winding set *xyz*), which can either be measured or estimated as explained in [106].

Control scheme for drive operation, satisfying the phasor diagram consist of the following important elements: transformer

(i) Line-side converter (as rectifier)

(ii) Machine side converter (as inverter)

(iii) Control of field excitation

The first element i.e. line side rectifier is controlled by the speed and current control loop. Reference value of dc link currents (I_{dc1}^* and I_{dc2}^*) are obtained by comparing the reference speed ω_r^* with actual speed ω_r whose error signal is given as input to a speed controller (PI controller). The reference dc link currents I_{dc1}^* and I_{dc2}^* are independently compared with its actual values I_{dc1} and I_{dc2} , and error signals are separately given to a PI current controller. These current control loops give the required rectifier firing angles α_1 and α_2, associated with each winding sets *abc* and *xyz*.

Control of inverter circuitry is basically the determination of accurate position of armature reaction flux vectors $\boldsymbol{\psi_a}$ and $\boldsymbol{\psi_x}$ w.r.t. field flux $\boldsymbol{\psi_{fr}}$ (i.e. $\emptyset_1'$ and $\emptyset_2'$). It requires the determination of leading angle ϕ_1 and ϕ_2 associated with each winding set *abc* and *xyz*, and are given by

$$\phi_1 = \gamma + k\mu \quad (6.3)$$

$$\phi_2 = \phi_1 + \xi = \gamma + k\mu + \xi \quad (6.4)$$

where,

$\gamma =$ constant turn off angle

$\mu =$ commutation overlap angle

$k =$ is a fraction

The value of μ can be estimated by [106]

$$\mu = cos^{-1}\left[cos\,\gamma^* - \frac{2L_c I_{dc}^*}{\sqrt{6}\psi_s^*}\right] - \gamma^* \quad (6.5)$$

Reference value I_{dc}^{*} may either be I_{dc1}^{*} or I_{dc2}^{*} , as these are numerically same due to equal load being shared by each winding sets *abc* and *xyz*. Value of commutating inductance L_c is basically the subtransient inductance of motor and magnitude of reference flux vector $\boldsymbol{\psi}_{\boldsymbol{s}}^{*}$ (i.e. $\boldsymbol{\psi}_{\boldsymbol{s1}}^{*}$ or $\boldsymbol{\psi}_{\boldsymbol{s2}}^{*}$) is calculated by the steady-state analysis, as explained in chapter 3. With these calculations together with the calculated values of $\emptyset_1'$and $\emptyset_2'$ (given by equations 6.1 and 6.2) are used to determine the inverter firing angle [106], β_1 and β_2 for required drive operation.

It is necessary to keep the motor voltage at its reference V^{*}, by adjusting the feild excitation. It can be easily performed by comparing the sensed voltage magnitude with its reference and adjusting the field excitation through a PI controller, embedded in field excitation and voltage control block as shown in Fig. 6.1 (a). But, an alternative method includes the determination of reference field current I_{fr}^{*} by generating the field flux, as explained in [106].

6.3 Simulation Results

A six-phase synchronous motor of 3.7 kW (parameters given in Appendix II) has been employed in developed self-controlled LCI fed drive in Matlab/Simulink environment. A flexible drive operation has been obtained by having separate commutation process at rectifier and inverter ends. Synchronous motor can be easily made to operate at any required frequency, irrespective to that of the input supply at rectifier side. Motor has been simulated to operate at 220 V, 50 Hz with 240 V, 50 Hz input voltage at rectifier end. A detailed dynamic response of the system has been presented for a step change in motor load by 50 %. Initially, motor is operating at no-load condition, and load is applied at time, t = 3 sec. Following to the application of load, current increases not only in inverter circuits (shown in Fig. 6.3 (b) and Fig. 6.3 (d)) but also in rectifiers (shown in Fig. 6.4 (b) and Fig. 6.4 (d)) and dc links (shown in Fig. 6.5 (c) and Fig. 6.5 (d). Increase in q component of stator current (active component) i.e. i_{q1} and i_{q2} may be noted in Fig. 6.6 (a) and Fig. 6.6 (c), respectively. But, due to the armature reaction, decrease in *d* component of stator current, i_{d1} and i_{d2} (reactive component) was also noted (shown in Fig. 6.6 (b) and Fig. 6.6 (d), whose effect was neutralized by the increase in field current as shown in Fig. 6.6 (e). Further, the firing angle of both the rectifier circuit was found to be 25.06^0 electrical under no-load, and was noted to be decreased by 1.5^0 electrical, approximately during load condition. Firing angle of both inverter circuit was found to be 170^0 electrical under no-load with small variation under load condition (decreased by 1.4^0 electrical,

approximately). During the simulation, assumption of inherent phase shift (30^0 electrical) between input supplies to stator winding sets *abc* and *xyz* was made. Therefore, the numerical value of both inverter circuit firing angle are same, as shown in Fig. 6.7.

The waveform showing the operation of LCI fed six-phase synchronous motor during steady-state has been presented further. The three-phase input supply to both rectifiers is shown in Fig. 6.8. The output current of both inverters feeding the motor is shown in stationary reference frame (shown in Fig. 6.9) as well as rotor reference frame (shown in Fig. 6.10) both. A safe commutation was obtained in the simulated LCI drive, but the risk of simultaneous commutation may occur if $\xi \leq \mu$, as explained in ref. [122-123]. Also, the effect of mutual coupling between the winding sets (*abc* and *xyz*) results in the additional spikes in input voltages, having lower magnitude, as shown in Fig. 6.11. But, the reliability offered by such drive encourages the use of such drive system [125].

6.4 Conclusion

A simple and efficient control scheme for the operation of LCI fed six-phase synchronous motor in self-controlled mode has been developed and explored in detail via simulation of this system. Control scheme was developed in order to ensure the motor operation with leading power factor, satisfying the discussed phasor diagram for all operating conditions (no load and load condition). A detailed dynamic performance of the developed control scheme of drive system has been presented for a step increase in motor load (by 50 % of rated/rated). Also, steady-state response of the system was examined wherein the effect of mutual coupling between both the winding sets *abc* and *xyz* was noted, which results in increased number of spikes (of lower magnitude) of input supply voltage, received from the inverter. Safe commutation of inverter switches (low cost thyristor) was also achieved in the discussed system. Analytical results presented in this chapter for LCI fed six-phase synchronous motor could not be verified experimentally, due to the limitations in laboratory.

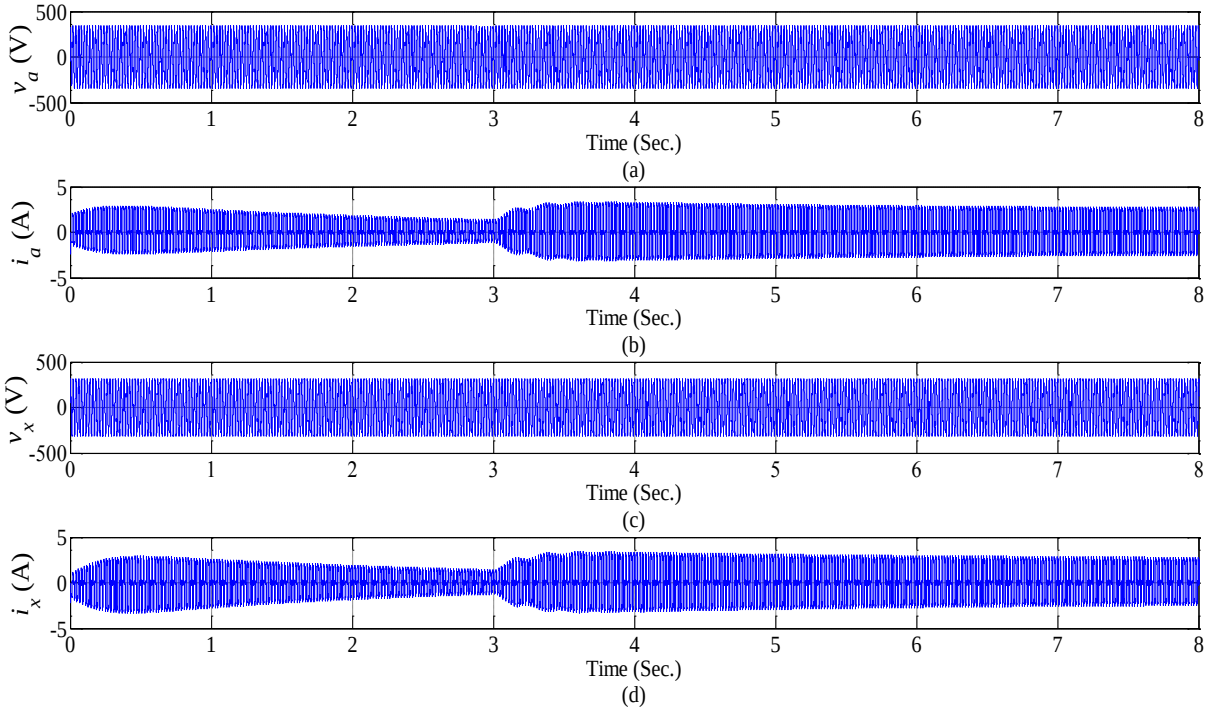

Fig. 6.3: Phase voltage and current waveforms of inverter feeding the motor showing (a) v_a (b) i_a (c) v_x (d) i_x.

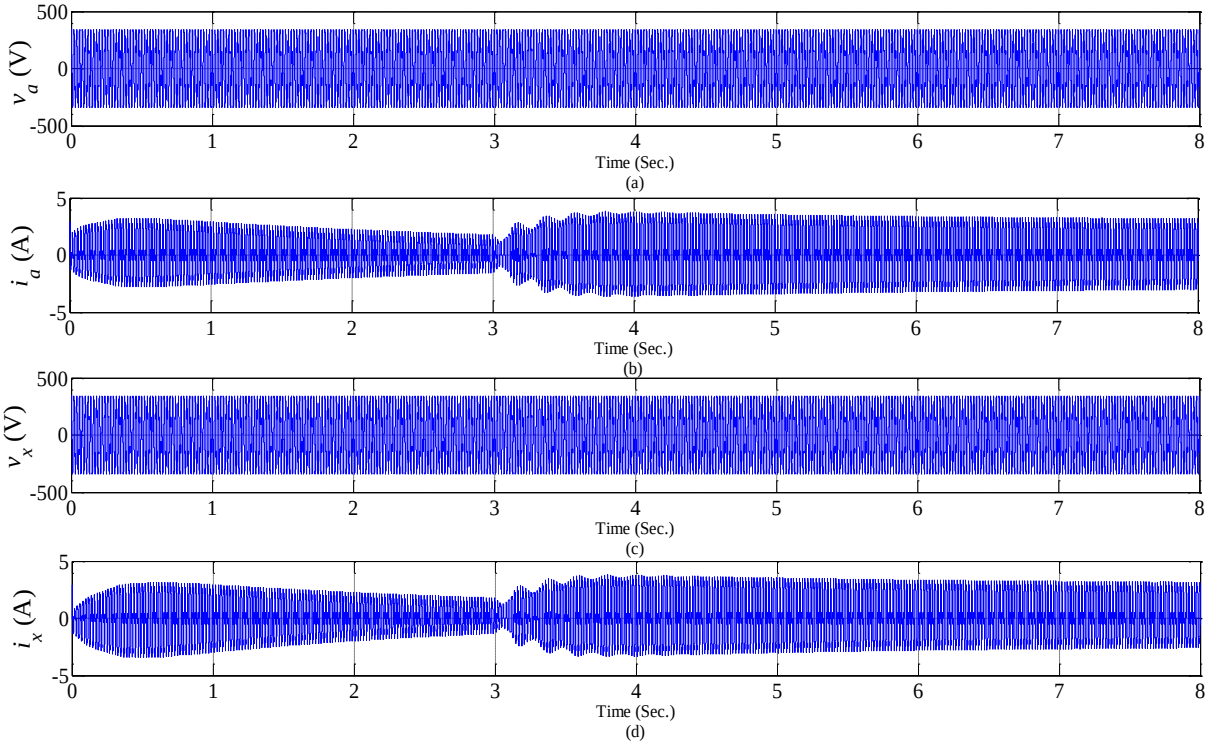

Fig. 6.4: Phase voltage and current waveforms of input supply feeding the rectifiers showing (a) v_a (b) i_a (c) v_x (d) i_x.

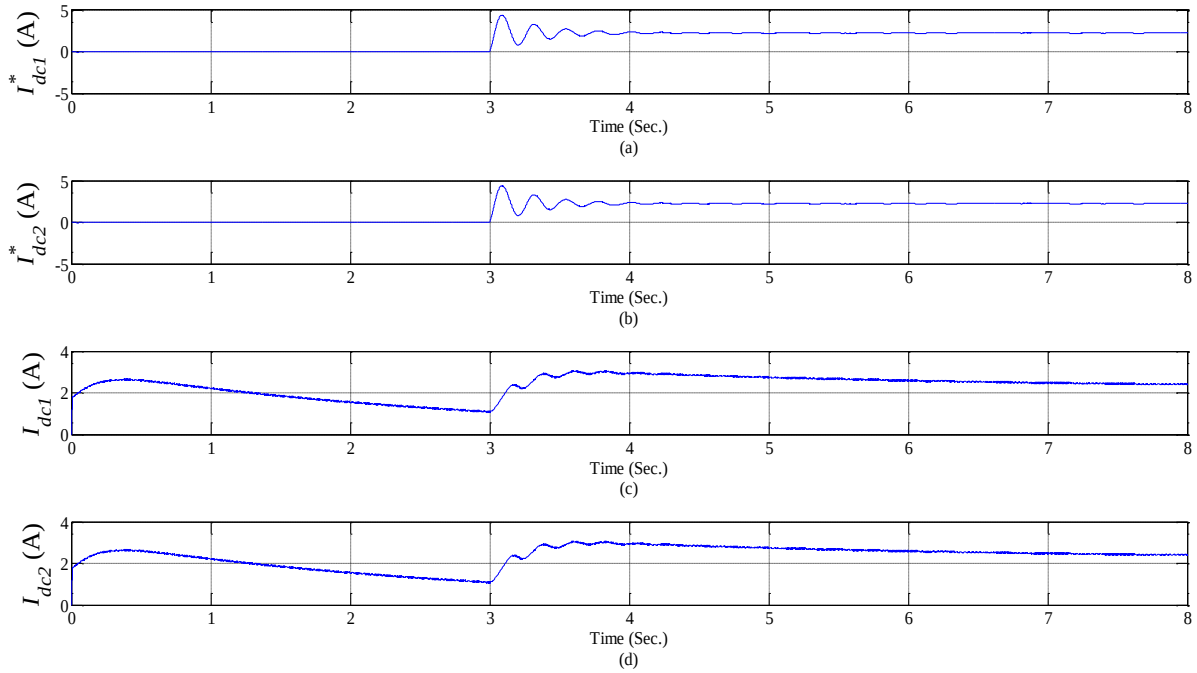

Fig. 6.5: Dynamic response of DC link current showing both the generated reference (a) I^*_{dc1} (b) I^*_{dc2} and actual (c) I_{dc1} (d) I_{dc2}.

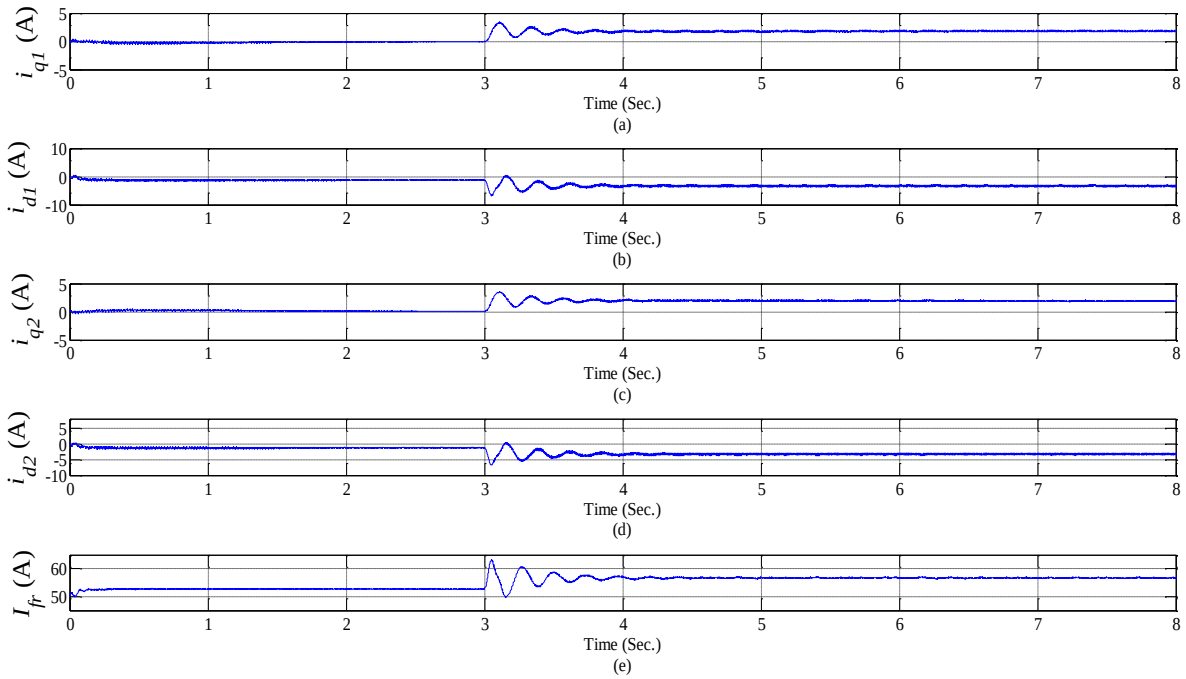

Fig. 6.6: Motor currents in rotor reference frame showing (a) i_{q1} (c) i_{d1} (c) i_{q2} (d) i_{d2} (e) I_{fr}.

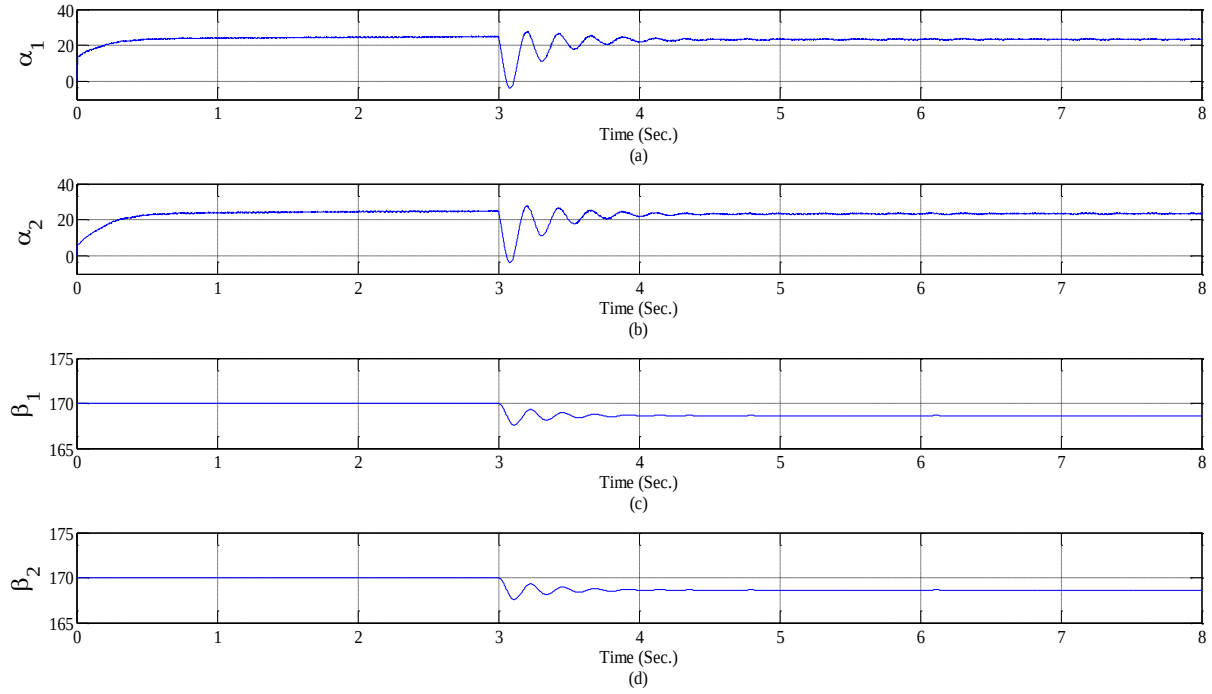

Fig. 6.7: Firing angles of both sets of rectifier-inverter circuitry showing (a) α_1 (b) α_2 (c) β_1 (d) β_2, in electrical degree

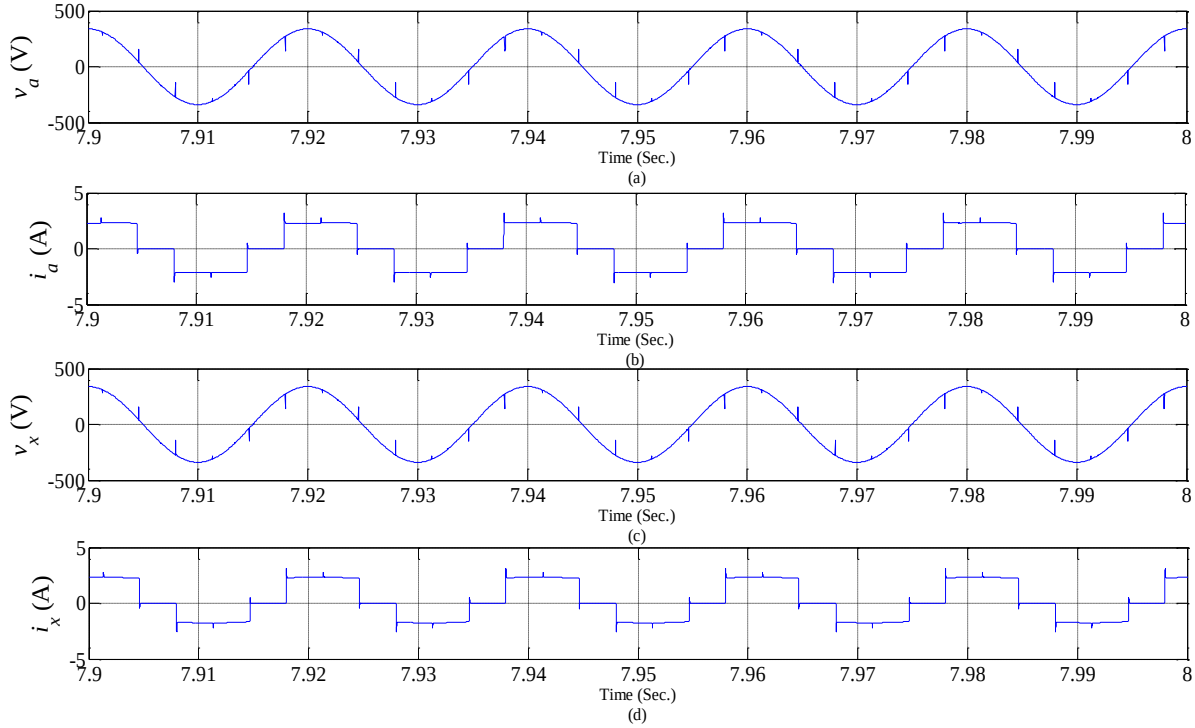

Fig. 6.8: Steady-state phase voltage and current waveforms of input supply feeding the rectifiers showing (a) v_a (b) i_a (c) v_x (d) i_x

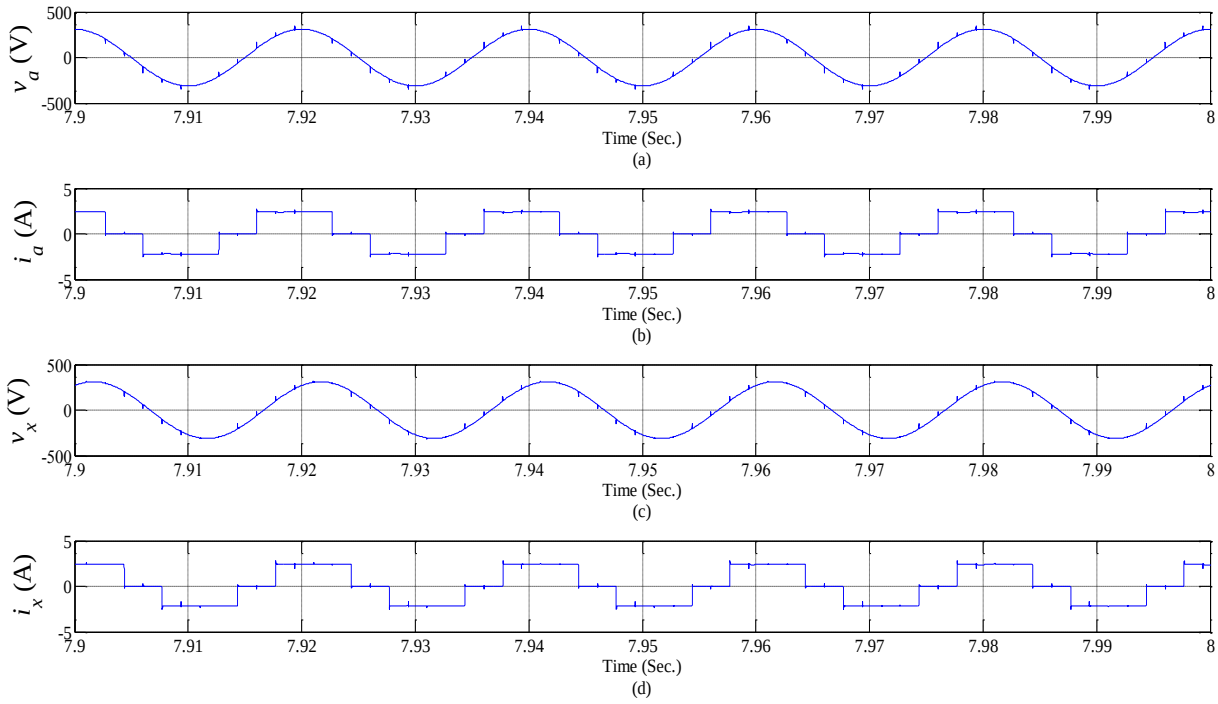

Fig. 6.9: Steady-state phase voltage and current waveforms of inverter feeding the motor showing (a) v_a (b) i_a (c) v_x (d) i_x.

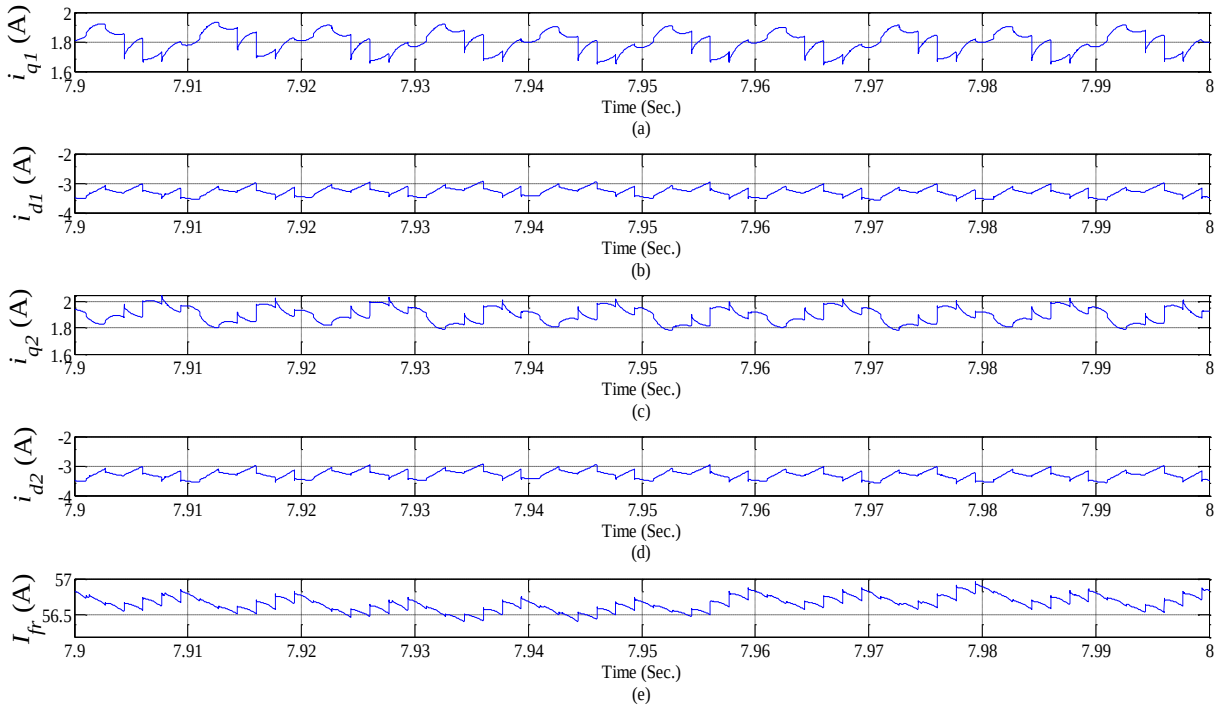

Fig. 6.10: Motor current during steady-state showing (a) i_{q1} (c) i_{d1} (c) i_{q2} (d) i_{d2} (e) i_{fr}.

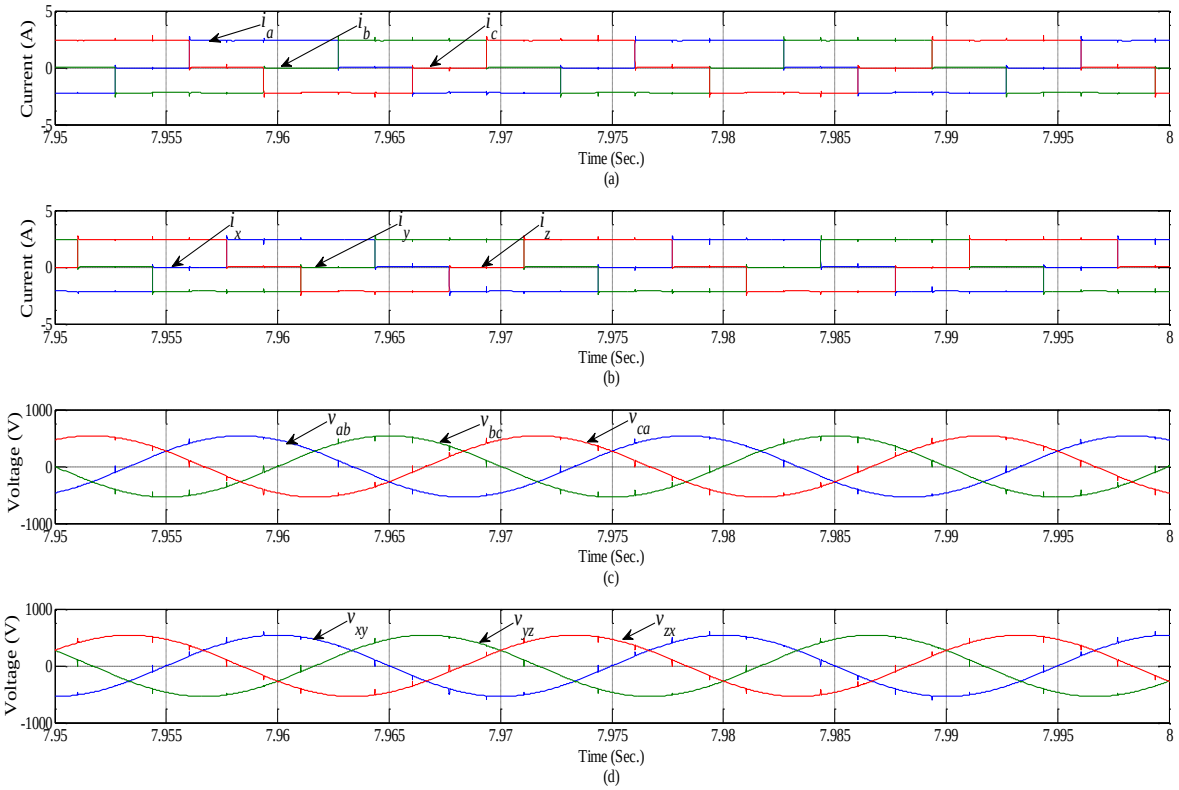

Fig. 6.11: Line voltage and current of inverter feeding the motor.

Chapter 7

Experimental investigation of six-phase synchronous motor

7.1 Introduction

This chapter presents a detailed steady-state performance analysis of a six-phase synchronous motor under different operating conditions. Initially, motor was operated under different load and input voltage levels, followed by its operation under different cases of open circuit fault created at input terminals.

Performance of any electrical machine, whether it is dc or ac (single phase, three-phase or more than three-phase) is directly affected by the inherent presence of different losses. In order to determine the accurate performance of electrical machine, determination of different losses is extremely important. A number of literatures can be found for the evaluation of different losses of three phase machine (both induction and synchronous), with standard test procedure [127-128]. Works embodied in references [102, 129-130] deal with the losses in six-phase induction machine and its comparison with its three-phase counterpart. However, no reference related to the detection of losses in six-phase synchronous machine is available. Therefore, this chapter also presents an experimental investigation for the determination of various losses under no load condition in a six-phase synchronous machine. A comparative study of losses for six and three-phase synchronous machine has also been made. Experimental results are presented in the following sections, obtained by utilizing the available facilities in machine laboratory.

7.2 Description of Experimental setup

In order to evaluate the performance of six-phase synchronous motor, a 3.7 kW, 36 slots, 6 poles, 3-phase synchronous machine was used (parameters given in Appendix II). On its terminal box, all the 72 end terminals of stator winding coils were connected to realize the different winding scheme for different number of phase and poles. Six-phase winding was obtained by using the technique of phase belt split [6-7], in a three-phase synchronous machine. Winding configuration of six phase is asymmetrical in nature, because of the existence of 30^0

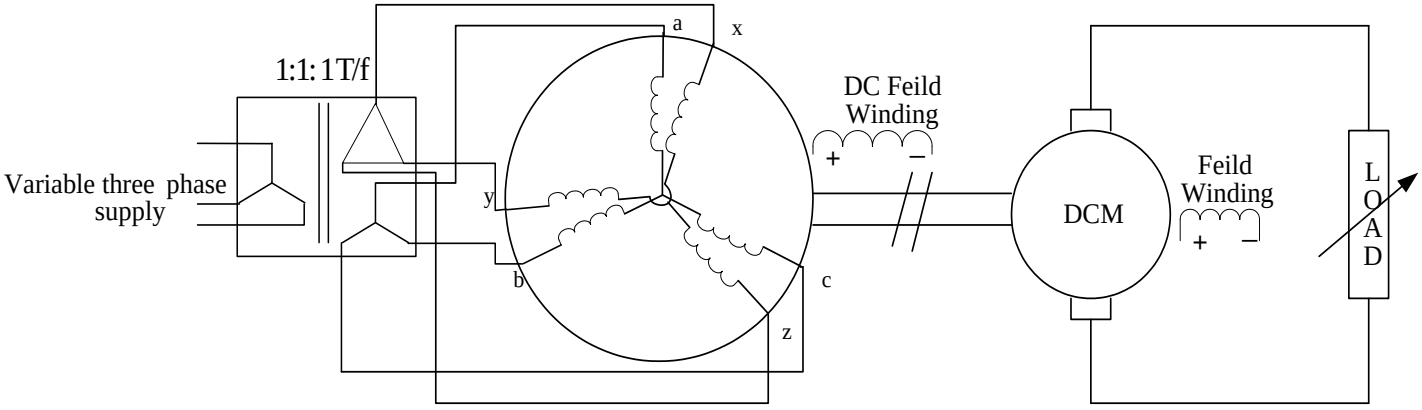

(a)

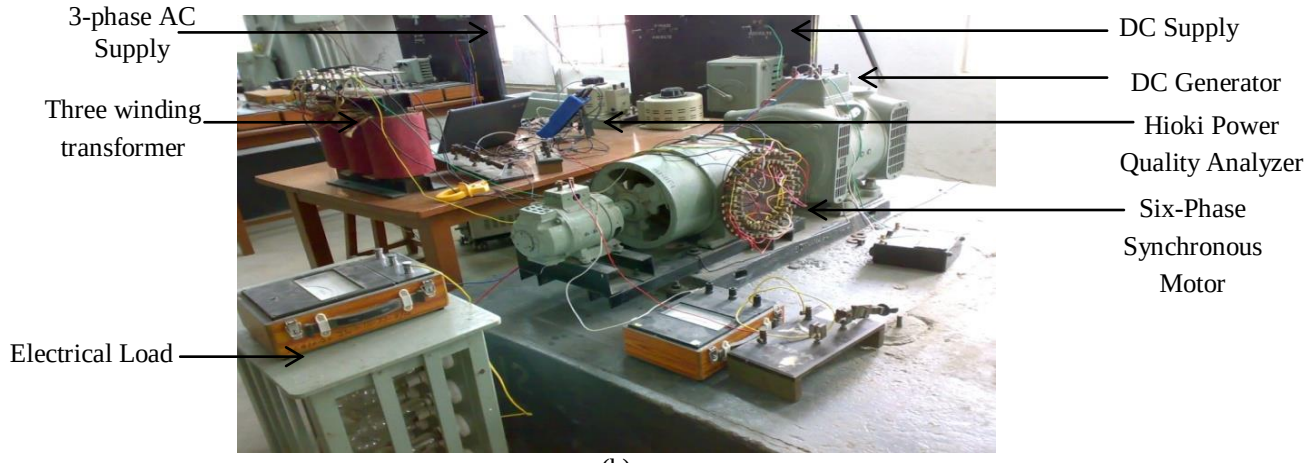

(b)

(c)

(d)

Fig. 7.1: Experimental set up showing (a) schematic diagram (b) general view (c) decoupled and (b) coupled test synchronous machine and DC machine.

electrical phase shift between the winding sets *abc* and *xyz*, having separate neutral points. Hence, physical fault propagation between the winding sets *abc* and *xyz* is prevented together with the prevention of flow of third and its multiple harmonic current.

As shown in Fig. 7.1 (a), the variable six-phase ac supply was obtained by using an inverter and three winding transformer. This enables to obtain the variable six-phase ac supply of different magnitude (and frequency). In order to obtain the two three-phase supplies, having a phase shift of 30^0 electrical, 10 kVA, 415/415-415 V, Y/Y-Δ, three to six-phase, three winding transformer has been employed in the experimental setup. Three winding transformer was locally manufactured. The magnitude of phase voltages at both the secondary were slightly different due to manufacturing defect. In this experimental setup, synchronous motor was mechanically coupled to a DC machine of 5 kW, 250 V, 21.6 A, 1300/1750 rpm, which is acting as a dc generator. DC machine was separately calibrated previously. An electrical load in form of lamp load was connected to the output of dc generator. Experimental scheme is shown in Fig. 7.1 (a), while the general view of the test rig is shown in Fig. 7.1 (b).

Measurement and recording of various waveforms and performance indices were carried out by using a Power Quality Analyzer (Hioki 3197) together with several analog ammeters and voltmeters. It is important to state that a small variation in the data of various experimental waveforms for the same operating condition was observed. This is due to the time lag in manual recording of the waveform and data.

7.3 Operation during steady-state

Experimental investigation of six-phase synchronous motor was initiated by feeding it with the two sets of three-phase input supply through a three winding transformer. Starting of synchronous motor was achieved by its operation as an induction motor. After it picks up the sufficient speed (say, 900 rpm approximately), the dc excitation was initiated by using a single pole single throw switch connected to its field circuit. At this condition, motor starts to run at synchronous speed, due to the interlocking of magnetic field produced by rotor as well as armature circuit.

Since, a dc machine (acting as a generator) is also coupled to the synchronous motor. Therefore, generator output voltage was used to supply an electrical load in form of lamp load. Variation in electrical load was used to create the different load conditions of test synchronous motor though dc generator. Following to the switching ON of some lamps, the steady-state

value of voltage and current was noted at different phases of synchronous motor. The steady-state value of input phase current of winding sets *abc* and *xyz* was found be 3.23 A (at 160.1 V), 3.32 A (at 162.3 V), 2.81 A (at 163.1 V) and 2.78 A (at 154.9 V), 2.36 A (at 156.3 V), 2.45 A (at 157.3 V) respectively, as shown in Fig. 7.2. Supply asymmetries was found to be contributed by the difference in magnitude of the output secondary voltage by the three winding transformer and continuous change of supply voltage and current due to the variation of other loads connected to supply line.

Motor behavior can further be explored for different operating conditions such as operation at different loads, operating voltages or frequencies. Two such operations at different loads and different voltage levels (at 50 percent of motor base/rated torque) have been tabulated in Table 7.1 and Table 7.2, respectively.

7.3.1 Motor operation with excitation in one set of winding

This operating condition was experimentally examined for a complete outage of three phase input supply of one winding set of the motor. The input phase voltage was maintained at 160 V. Small voltage was selected to safeguard the conductor insulation as the six-phase connection was realized from three-phase stator winding through split-phase. In this mode of operation, the input supply was given to only one set of winding (winding set *abc*). Therefore, the voltage will be generated on the other winding set (winding set *xyz*) due to the generator action which was found to be 145 V, 148 V, 147 V for phases *x*, *y*, *z* respectively. Low voltage generation at other winding set is due to the fact that the power flow in other winding is reversed. Hence, synchronous machine in this mode, will operate as motor as well as generator both. In this mode of operation, the machine mechanical output power needs to be constant which is supplied by only one winding set *abc*. Currents of this winding set were found to be 5.43 A, 5.23 A, and 5.08 A for phase *a*, phase *b* and phase *c*, respectively. Flow of current was found to be more balanced as compared to above case. This is because of its reduced sensitivity towards supply asymmetry when working with three phase winding configuration. The steady state phase voltage and current of phase *a* (winding set *abc*) along with the generated voltage of phase *x* (winding set *xyz*) are shown in Fig. 7.3. Furthermore, a variation of generated voltage in winding set *xyz* was observed with the variation of load torque and the input voltage of winding set *abc* at constant output load torque (50 percent of rated/base torque). The generated voltage was found to decrease proportionately with the increase in load torque whereas it

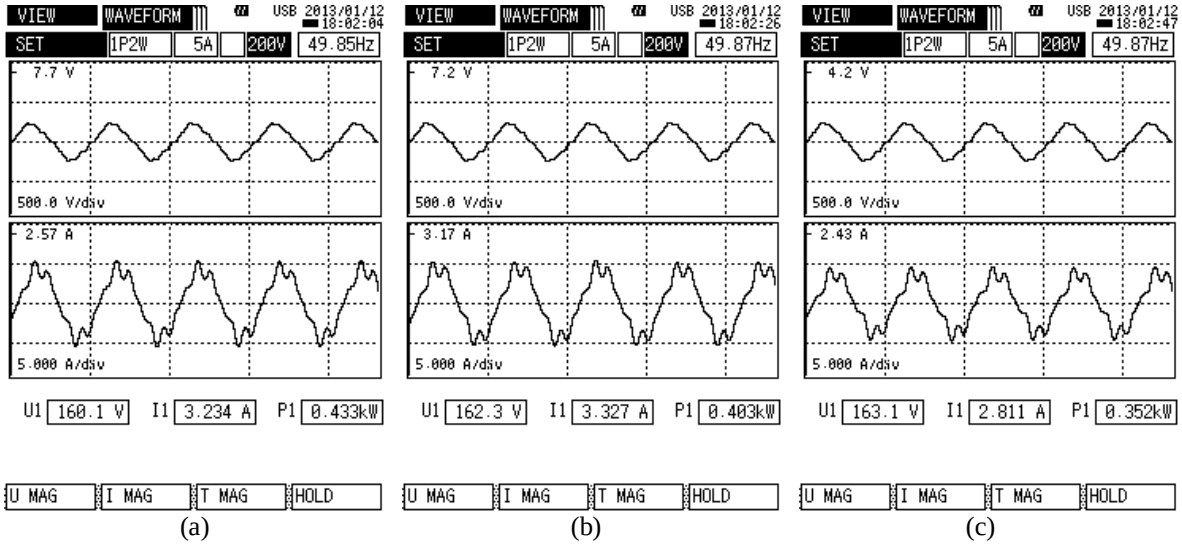

Fig. 7.2: Terminal voltage and current of winding set *abc* and *xyz* (a) phase *a* (b) phase *b* (c) phase *c* (d) phase *x* (e) phase *y* (f) phase *z*.

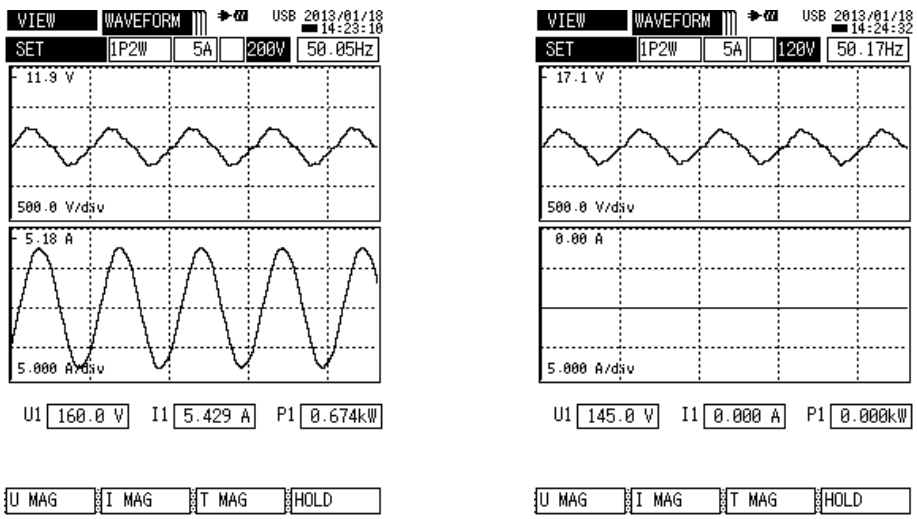

(a) (b)

Fig. 7.3: Steady state voltage and current of (a) phase *a* and (b) generated voltage of phase *x*.

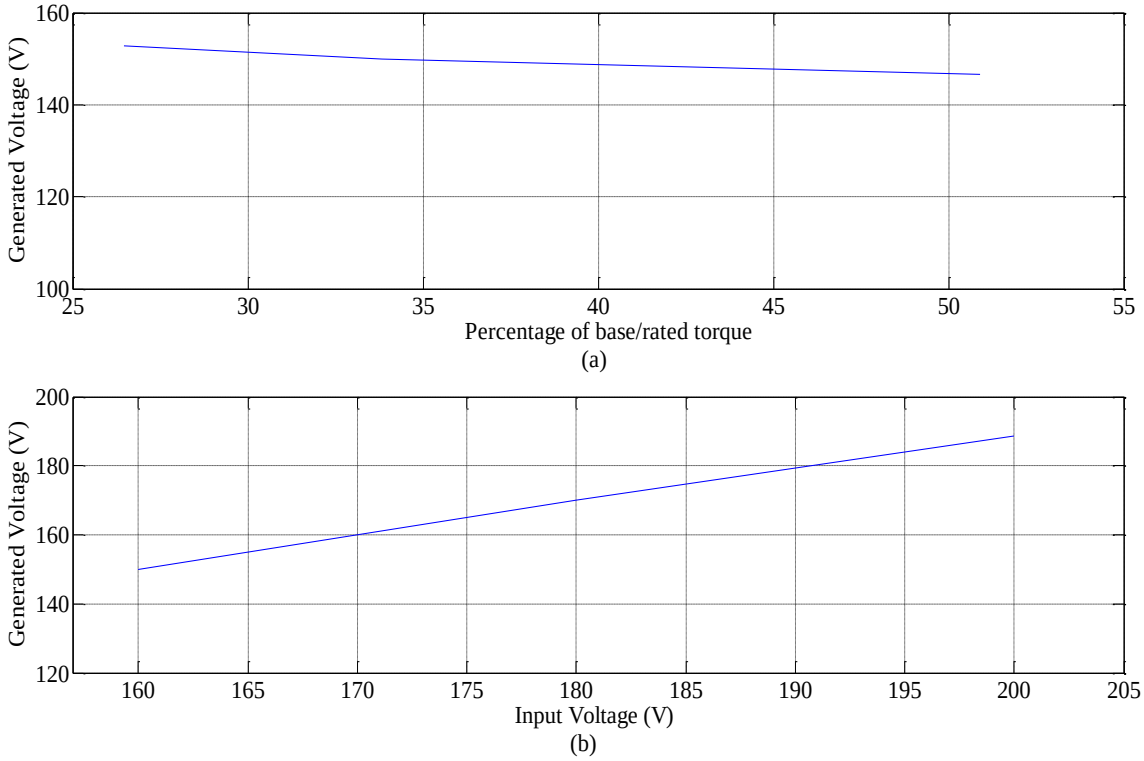

Fig. 7.4: Plot of generated voltage (of winding set *xyz*.) with the variation in (a) load torque and (b) input voltage.

increases proportionately with the increase in magnitude of input voltage of winding set *abc*, as depicted in Fig. 7.4. It is worthwhile to mention here that the experimental results are presented for upto 50 percent of mechanical load on motor. This is because the phase current approaches to rated value, when machine is delivering the power with input supply given to only one winding set *abc* (only half of the armature is being utilized). Therefore, the motor was derated by 50 percent approximately, to ensure a reliable operation of system under safe current limit. Further, it has to be noted that the flow of unbalance current in motor due to supply asymmetry also results in the performance degradation. Calculation of derating of multiphase motor due to supply asymmetry has been reported in [18].

7.4 Operation during open-circuit fault

7.4.1 One phase opened

Prior to the analysis of phase redundancy, the steady state pre-fault current of winding sets *abc* and *xyz* was found to be 3.23 A (at 160.1 V), 3.32 A (at 162.3 V), 2.81 A (at 163.1 V) and 2.78 A (at 154.9 V), 2.36 A (at 156.3 V), 2.45 A (at 157.3 V) respectively. Phase redundancy property was experimentally analyzed by creating an open circuit at one of the motor input terminal. This condition is sometime referred as 'open conductor fault' at the terminal. An open conductor fault of a particular phase is most common fault, which often occurs in any of the multiphase ac drive system. Therefore, motor behavior is examined after the occurrence of such condition on any of the input supply phase of motor terminal. This condition was manually created on phase *a* of synchronous motor using a single pole single throw switch. The steady state post-fault phase current of phases *x*, *y* and *z* was found to be 4.26 A (53.80% higher), 4.75 A, i.e. almost double (101.27% higher) and 2.71 A (11.06% higher) respectively, indicating larger power shared by the winding set *xyz*. Current in remaining healthy phases *b* and *c* of the winding set *abc* was found to be decreased by 2.78 A (16.27% decreased) and 2.77 A (1.80% decreased) respectively, indicating a decreased power sharing. Steady state phase voltage and current of remaining healthy phases of both the winding sets *abc* and *xyz* are shown in Fig. 7.5. Unequal flow of current in individual phase winding is due to minor magnitude unbalance of voltage.

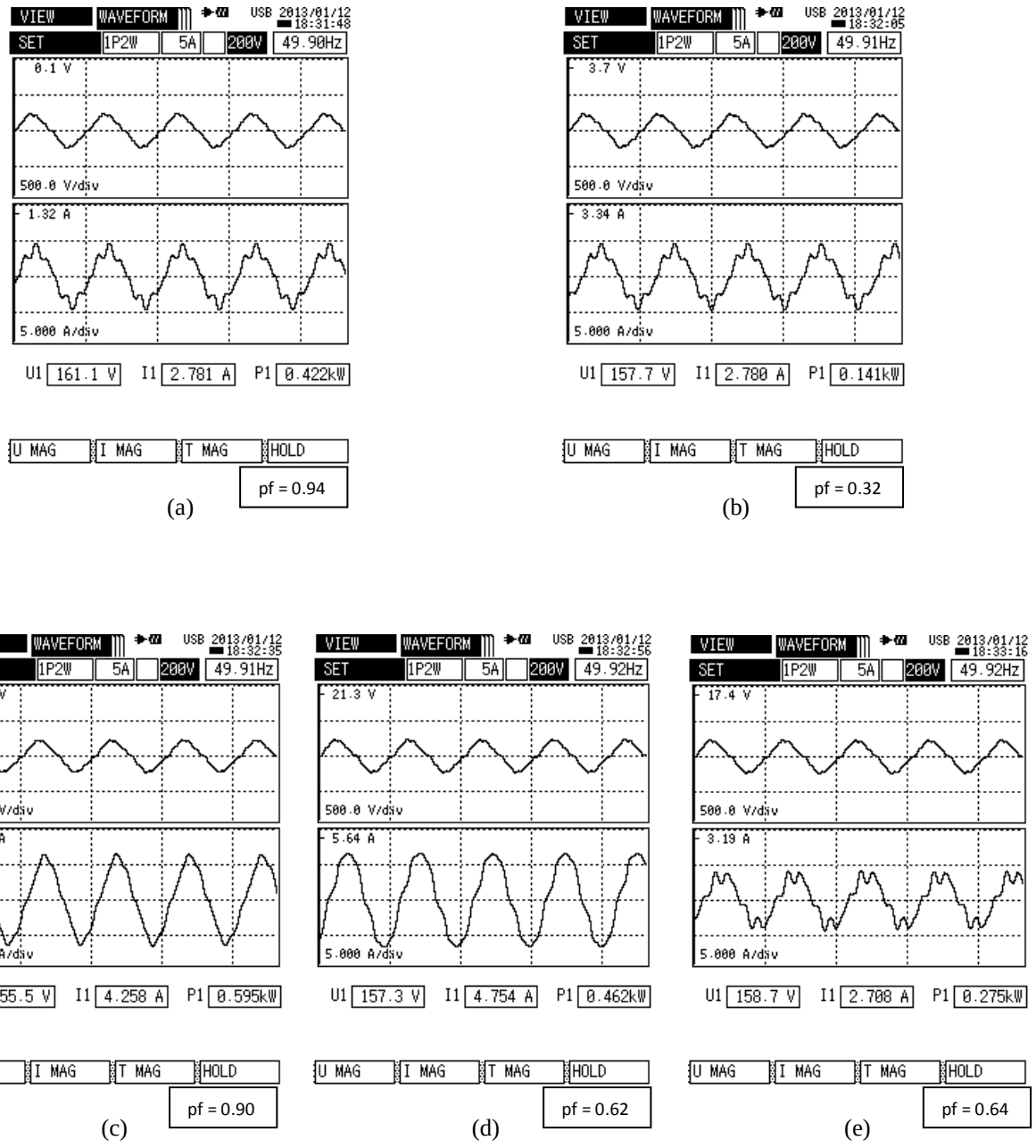

Fig. 7.5: Steady state phase voltage and current of healthy phases of winding set *abc*, (a) phase *b* (b) phase *c* and winding set *xyz* (c) phase *x* (d) phase *y* (e) phase *z* after the occurrence of single phase open circuit.

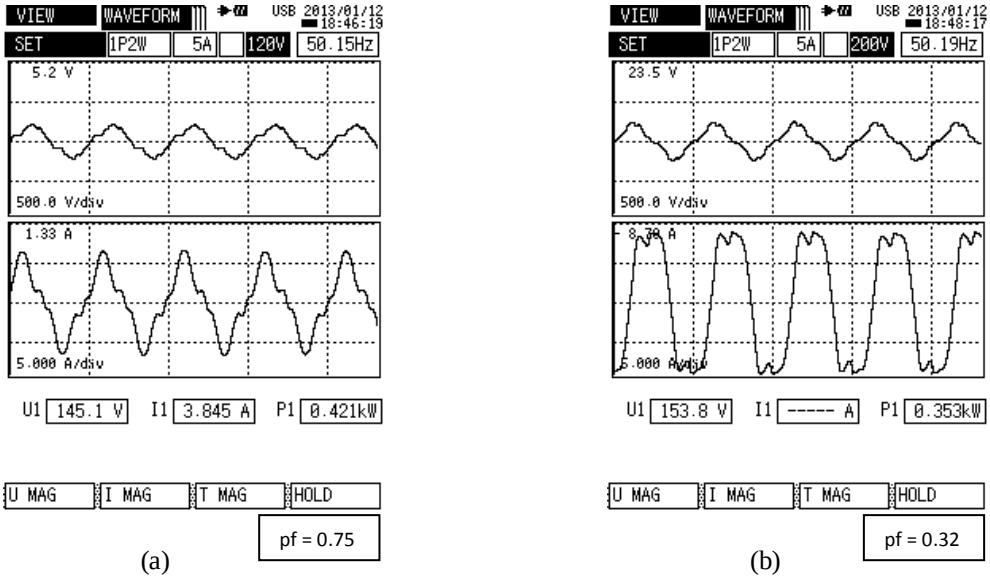

Fig. 7.6: Steady state phase voltage and current of healthy phases of winding set *abc* (a) current i_b and winding set *xyz* (b) current i_y , after the occurrence of double phase open circuit.

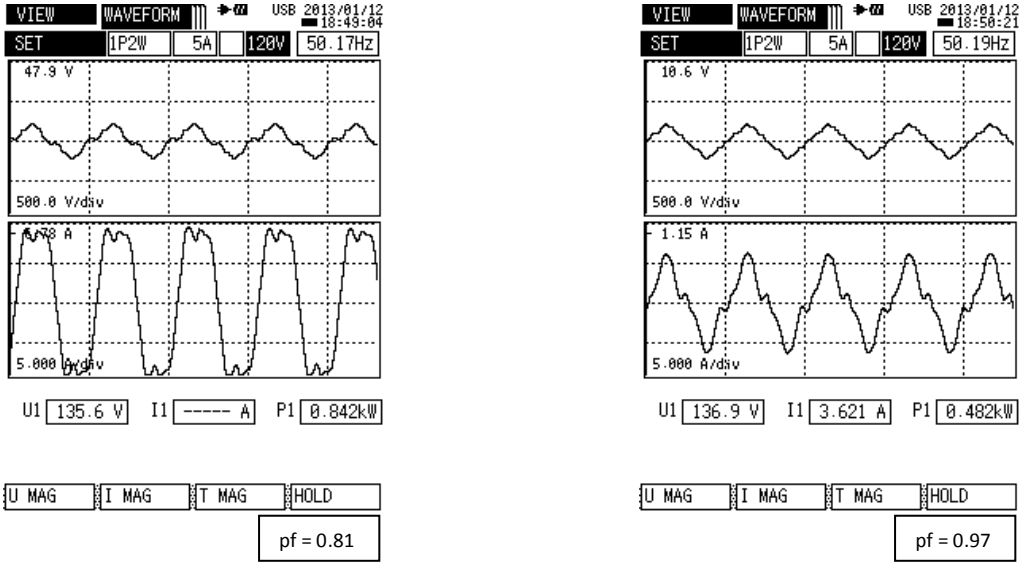

Fig. 7.7: Steady state phase voltage and current of healthy phases of winding set *abc* (a) current i_b and winding set *xyz* (b) current i_x, after the occurrence of double phase open circuit.

7.4.2 Two phase opened

Performance of six-phase synchronous motor has also been experimentally analyzed for the outage of two phases of input supply of the motor at a time. Opening of two phase at a time was manually created by using a double pole single throw switch, such that current of phase *a* and phase *x* ceases to zero. After the occurrence of this fault, the steady-state phase voltage and current of one healthy phase of winding sets *abc* and *xyz* are shown in Fig. 7.6 (a) and Fig. 7.6 (b), respectively. The post-fault steady state phase current of healthy phases *b* and *c* was found to be 3.85 A (15.96% higher) and 3.83 A (35.18% higher) respectively. Similarly, the phase current for healthy phase of *y* and *z* was found to be 7.28 A, i.e. almost three times (208.47% higher) and 7.20 A (213.04% higher) respectively, under safe current limit. As already mentioned that there might be the different combination of such condition. One more combination was explored, i.e. by opening the phase *a* and *y*. It was observed that the nature of variation of remaining healthy phase current was found to be similar. Phase currents of phase *b* and *c* was found to be 7.61 A. (129.21% higher) and 7.60 A (230.30% higher) respectively. Similarly for phase current of phases *x* and *z* was found to be 3.63 A (31.05% higher) and 3.61 A (34.32% higher) respectively. It is worthwhile to mention that the recording of waveforms have been done on per phase basis, and there was continuous a small fluctuation of supply (magnitude/frequency). So the magnitude of current in remaining healthy phases of a particular winding set was found to have a small variation. Variation in the current magnitude can be noted for healthy phase *b* and *c* and phase *y* and *z* (phase *a* and *x* opened), similarly for healthy phase *b* and *c* and phase *a* and *z* (phase *a* and *y* opened) in Fig. 7.7.

Redundancy characteristic of the motor can be explored for different operating conditions. Conditions include the operation at different loads, operating voltages or frequencies. Two such operations at different loads and different voltage levels (at 50% load torque) have been tabulated in Table 7.3 and Table 7.4, respectively. It includes both the pre-fault as well as post- fault current of each phase of the motor. Both the experimental and simulation results have been included. A small variation of remaining healthy phases of a particular winding set can be accounted by the time lag during recording of wave forms of different phases (due to manual recording), as already mentioned. This can be noted in double phase opened case. It has been observed that the change of phase current of phase *b* and *c* was found to be small (not more than 20%) for both single phase and double phase open circuit.

Change in the phase current of winding set *xyz* was found to be irregular. Current variation of phase *y* was found to be maximum for single phase (about double) and double phase (about three times) open circuit, under safe current limit. The large increase in the phase current of winding set *xyz* can be accounted for the existence of supply asymmetries resulting in the decrease in power factor of winding set *xyz*, as same output power has to be shared by the healthy phases, working under unhealthy condition. Difference in the magnitude of output secondary voltage of three winding transformer was found to be a major reason for the presence of supply asymmetries, followed by the continuous change of supply voltage due to the variation of other load connected to supply line. Moreover, the presence of highly inductive element in the form of three winding transformer further affects the motor current during experimentation. It is worthwhile to mention here that in developed analytical model (Chapter 3), saturation, space harmonics, parameter sensitivity have been neglected. Saturation effect introduces the synchronous, asynchronous and parasitic losses; space harmonic results in non-sinusoidal waveshape of current and parameter sensitivity introduces the inaccuracy in results. These factors together with the supply asymmetry are the main reason for small mismatch of current waveform in the analytical and experimental results.

Effect of supply asymmetry can be reduced by carefully selecting the components in the electrical circuit. However, it can be effectively reduced by employing a closed loop current control scheme, as illustrated in [18, 50-51].

7.5 Some Observation on No-load Losses of Asymmetrical Six-Phase Synchronous Machine

7.5.1 Evaluation of fixed losses of DC Machine

Evaluvation of different no-load losses has been carried out by treating the test synchronous machine as an alternator with the coupled dc machine as its prime mover (dc motor). Initially, both the machines (synchronous machine and dc machine) were mechanically uncoupled as shown in Fig. 7.1 (c) The dc motor was run at synchronous speed of the test machine, and current and voltage was recorded. Power input minus copper loss will give the iron loss, friction and windage loss of dc machine as given by

$$L_1 = V_a I_a - I_a^2 R_a \tag{7.1}$$

where, V_a and I_a are the input dc voltage and current fed to dc motor, having its armature resistance R_a.

It is worthwhile to note here that the iron-loss of dc machine is dependent on both rotor speed as well as field current. At a constant speed, it becomes dependent on the flow of field current only. Therefore, at constant rotor speed, fixed losses, L_1 can be plotted as the function of motor field current, I_f. Results have been presented in Fig. 7.8, wherein, effect of both field current and rotor speed are shown. A series of experimental recording has been made at different speeds, i.e. at 600, 700, 800, 900, 1000, 1100 rpm (synchronous speed of 30, 35, 40, 45, 50, 55 Hz.). Almost linear dependency of fixed losses may be noted not only on the motor field current but also on its rotor speed.

7.5.2 Determination of friction and windage losses

The test synchronous machine (acting as alternator) and its prime mover (i.e. dc motor) are mechanically coupled as shown in Fig. 7.1 (d). The coupled machines are run at the synchronous speed with field circuit of test synchronous alternator remain unexcited. During this condition, power taken by dc motor will be equal to its losses (L_1+ armature copper loss) and windage and friction losses of synchronous alternator (L_{fw}). Mathematically,

$$L_{fw} = V_a I_a - I_a^2 R_a - L_1 \qquad (7.2)$$

where, value of L_1 (iron and, friction and windage losses of dc motor) is evaluated in earlier section. This test was repeated for different rotor speed, corresponding to different operating frequency of test synchronous alternator. An approximately linear dependency of friction and windage losses on rotor speed was noted, as depicted in Fig. 7.9 by green bar graph.

7.5.3 No load losses in Synchronous machine

DC supply is fed to the prime mover (dc motor) so as to run the alternator at synchronous speed. Field circuit of alternator is excited with its armature open circuited. A series of reading was recorded for alternator generated voltage V_{oc}, dc motor field current I_f, input voltage V_a and current I_a of prime mover armature circuit, associated with different values of alternator field current I_{fr}. In this test, the input power to dc motor ($V_a I_a$) basically accounts for different losses. These losses include the copper loss of motor armature $I_a^2 R_a$, fixed losses of dc motor L_1, alternator friction and windage losses L_{fw} and its core-losses L_c. Mathematically, it can be

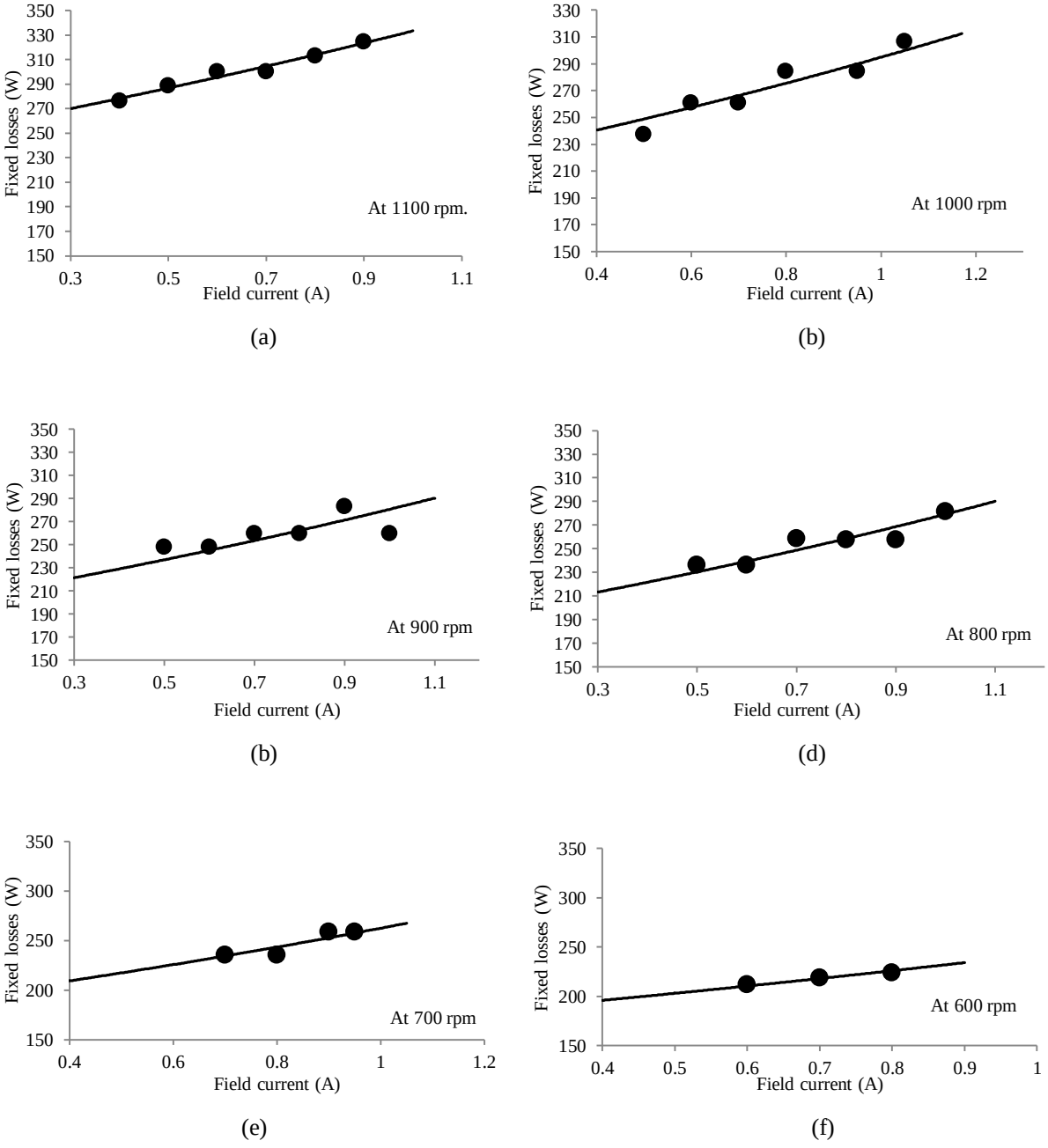

Fig. 7.8: Fixed losses of dc motor at different rotor speed associated with the synchronous speed of (a) 1100 rpm (b) 1000 rpm (c) 900 rpm (d) 800 rpm (e) 700 rpm (f) 600 rpm.

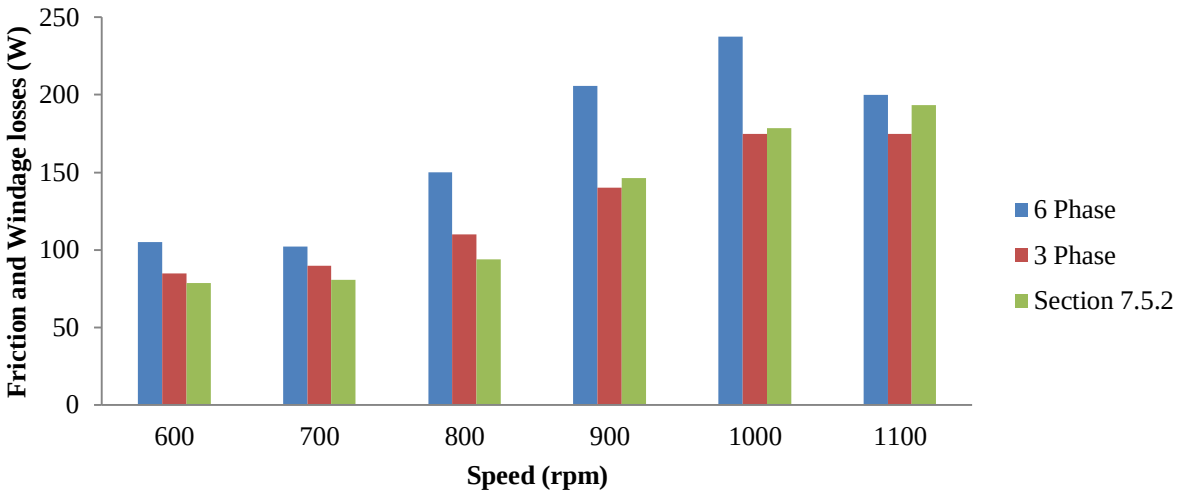

Fig. 7.9: Friction and windage losses of synchronous machine by experiment in section 7.5.2 (green bar) and by experiment in section 7.5.3 for 6 phase (blue bar) and 3 phase (red bar).

expressed as

$$L_{fw} + L_c = V_a I_a - (L_1 + I_a^2 R_a) \tag{7.3}$$

It will be convenient to determine the value of $(L_{fw} + L_c)$ graphically, with the variation of alternator generated voltage/field current. A series of experimental test has been carried out on test synchronous alternator having its winding configuration of both six phase as well as three phase, whose results are depicted in Fig. 7.10. In general, the magnitude of no load losses increases with the increase in generated open circuit voltage or field excitation current of synchronous alternator, at a particular rotor speed. Further, the magnitude of no load losses increases with the increase in rotor speed, showing its dependency on the operating frequency. Comparatively, this magnitude was found to be higher for the test synchronous alternator with its six phases winding configuration. It is worthwhile to mention here that the *y*-intercept in Fig. 7.10 determines the magnitude of friction and windage losses (L_{fw}) of test synchronous alternator, which are also shown in Fig. 7.9. Friction and windage losses were found to be dependent not only on its operating rotor speed but also on the type of armature winding configuration (six or three phase stator winding of test machine). In general, the value of L_{fw} is higher for six phase winding configuration when compared with its three phase winding configuration of the test alternator. In addition to friction and windage losses, the major component of no load losses is constituted by the core loss. This loss is inherently present in all

the electrical machine, which is dependent on type of core material used, operating frequency and flux level. The core loss consists of eddy current loss and hysteresis loss. A convenient way for the evaluation of these losses has been discussed in following section.

7.5.3.1 Separate evaluation of eddy and hysteresis losses

The component of machine core loss, i.e. eddy current loss (L_{ce}) and hysteresis loss (L_{ch}) are expressed as

$$L_c = L_{ce} + L_{ch} \tag{7.4}$$

$$\left.\begin{aligned} L_{ce} &= K_e f^2 B_m^2 \\ L_{ch} &= K_h f B_m^n \end{aligned}\right\} \tag{7.5}$$

where, K_e = a constant, whose value depends on the type of ferromagnetic material used, lamination thickness and volume of core material.

K_h = a constant, whose value depends on core weight.

B_m = maximum value of flux density. *n* denotes the Steinmetz constant, whose value varies from 1.5 to 2.5, depending on the magnetic properties of the core material.

Hence, eddy current loss varies with the squared value of frequency and hysteresis loss becomes proportional to the operating frequency, at a fixed value of flux density (i.e. flux linkage of synchronous machine).

Therefore, it will be convenient to rewrite equation (7.5) as

$$\left.\begin{aligned} L_{ce} &= C_e f^2 \text{ (eddy current loss)} \\ L_{ch} &= C_h f \text{ (hysteresis loss)} \end{aligned}\right\} \tag{7.6}$$

Value of constants, C_e and C_h is determined experimentally, for a fixed flux density. In this experiment, the magnitude of test machine flux linkage is kept constant by just keeping the value of field excitation current at a fixed value. This is because, machine is operating at no load condition with no armature reaction, and flux linkage is determined by the field circuit only. Therefore, field current of the alternator is kept constant at some suitable value of 0.6 ampere, and a series of experimental data was recorded for different rotor speed (synchronous speed corresponding to 30, 35, 40, 45, 50, 55 Hz.) Results obtained are depicted in Fig. 7.11, for both six phase and three phase winding configuration. In this figure, the expression for

losses has been determined by curve fitting. The constant term indicates the friction and windage losses, the first order term indicates the hysteresis loss, whereas the second order term indicates the eddy current loss. The hysteresis and eddy current losses are plotted for different operating rotor speed/frequency for both six phase and three phase winding configuration, in Fig. 7.12 (a) and Fig. 7.12 (b), respectively. Clearly, both hysteresis and eddy current losses are greater in magnitude for six phase synchronous alternator than its three phase counterpart, resulting in the increased no load losses in six-phase synchronous machine. The reason behind this is explained below:

In case of three-phase synchronous machine operation, their exist a magnetic interlocking between the stator and rotor field. Moreover, the salient structure of rotor will align itself along the path of least reluctance. Therefore, during steady-state, a small airgap *x*, exists between rotor and stator field, as shown in Fig. 2.38 (a) in chapter 2 for symmetrical winding configuration. But, during the machine operation with asymmetrical six-phase winding configuration, voltage is independently induced in both the winding sets *abc* and *xyz* of constant magnitude, while maintaining the phase shift of 30^0 electrical between the phase *a* and phase *x*. In this case, rotor aligns itself along the resultant stator field as depicted in Fig. 2.38 (b). Rotor axis in this position will have the airgap x', w.r.t. magnetic axis of the individual winding sets *abc* and *xyz.* The airgap x' (for six-phase operation) is clearly greater than *x* (for three-phase operation). Therefore, to establish the required flux level in airgap, magnetizing current (i.e. field current I_{fr} in present case) is increased, resulting in increased no-load losses in the test machine having asymmetrical six-phase winding configuration. Furthermore, the machine with constant field excitation at no-load, flux linkage to stator winding with three-phase configuration will be greater than its operation with six-phase winding configuration,

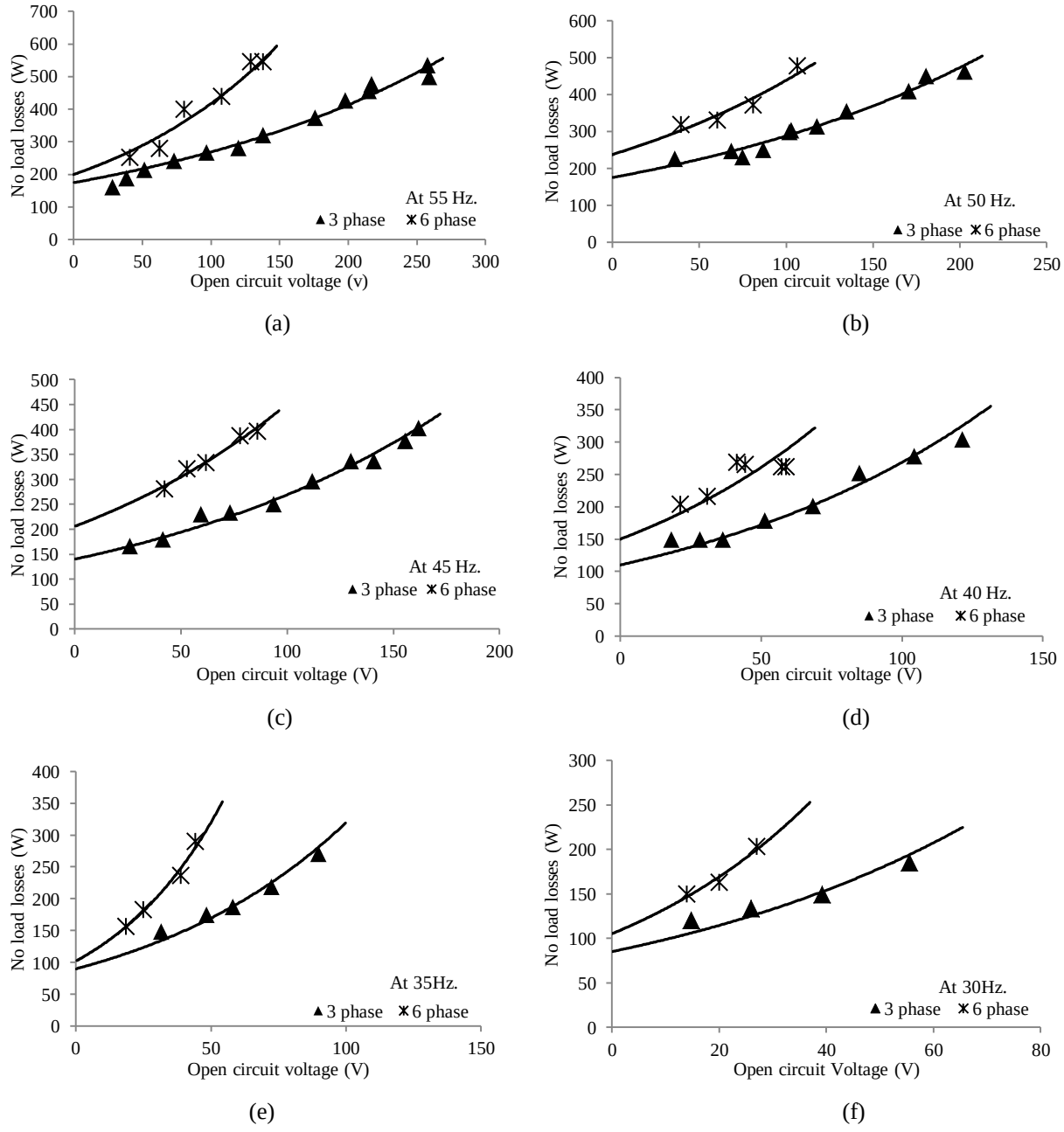

Fig. 7.10: Experimental results of no load loss of synchronous machine in 3 phase and 6 phase winding configuration at different synchronous speed (a) 55 Hz. (b) 50 Hz. (c) 45 Hz. (d) 40 Hz. (e) 35 Hz. (f) 30 Hz.

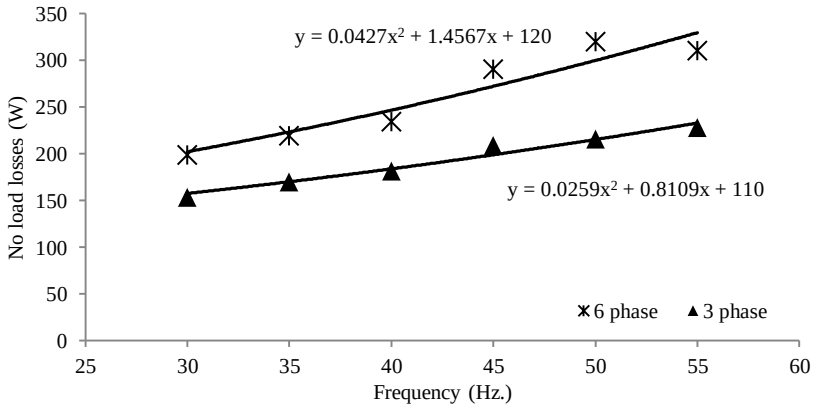

Fig. 7.11: No load losses at constant flux density (field current at 0.6 A) of test machine under its different synchronous speed.

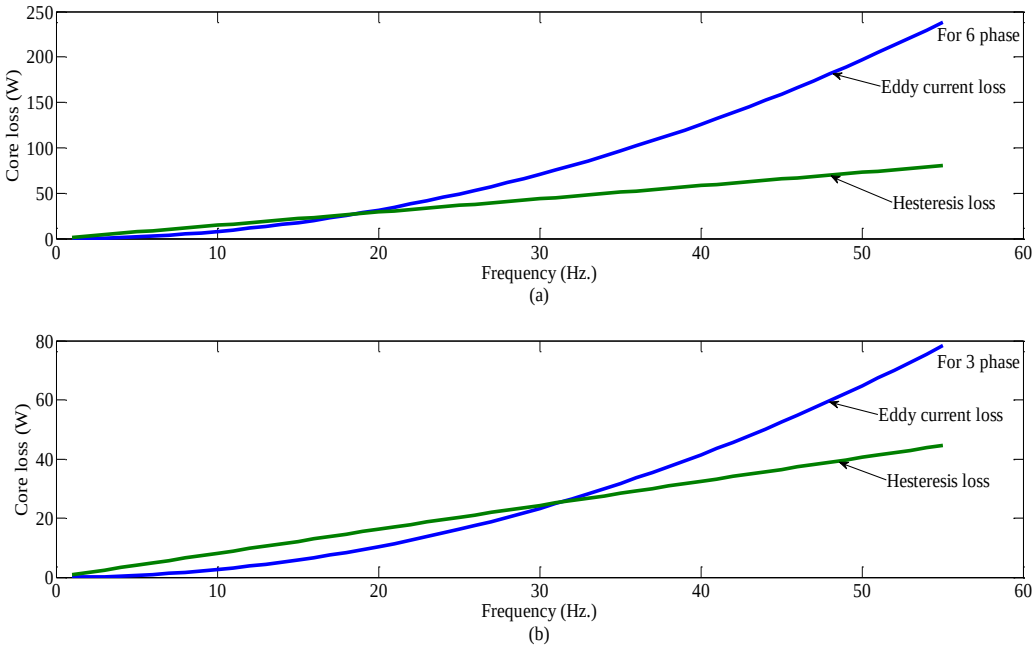

Fig. 7.12: Separate evaluation of hysteresis loss and eddy current loss of test machine with its winding configuration of (a) six phase (b) three phase.

because $x' > x$. Hence, voltage generation in six-phase machine will be somewhat lesser than half the generated voltage (theoretically it should be exactly half) in armature winding in three-phase configuration with increased no-load losses with six-phase winding configuration.

7.5.4 Determination of Short circuit (SC) load test

The rotor speed was maintained constant at synchronous speed from prime mover side and the end terminals of alternator stator winding is shorted (symmetrical SC). It should be noted that in case of alternator with six phase winding configuration, each three phase set (*abc* and *xyz*) is shorted separately. The power consumed by dc motor ($V_a I_a$) will be equal to the sum of losses $L_1 + I_a^2 R_a + L_{fw}$, together with the alternator load losses corresponding to the stator SC current. Hence, SC load loss can be easily evaluated by knowing the value of other losses from the experimental procedure explained in above sections. Mathematically,

SC load loss = $V_a I_a - (L_1 + I_a^2 R_a + L_{fw})$ (7.7)

Further, stray load loss may be evaluated if the dc resistance of alternator stator winding r_1 (and r_2) is known, by using equation 7.8.

Stray load loss = (SC load loss) $-$ (armature dc copper loss $I_{s1}^2 r_1 + I_{s2}^2 r_2$) (7.8)

where, I_{s1}, I_{s2} and r_1, r_2 are the stator phase current and dc resistance of both winding set *abc* and *xyz*, respectively.

These experimental steps have been carried out for both six phase and three phase machine, at different rotor speed. The SC loss magnitude was found to be dependent on the flow of stator current only, not much effected on rotor speed, for particular field excitation. This has been depicted in Fig. 7.13 wherein, the dependency of SC loss on squared value of stator current has been signified by the straight line. The SC load loss comprises of the armature copper loss, core loss due to armature leakage flux together with a small core loss due to resultant flux. Magnitude of stator current is much larger in six phase winding configuration than its three phase counterpart. Although, the magnitude of total armature copper is almost same, for both six phase and three phase machine. But in the case of six phase operation, magnitude of leakage flux and also the resultant flux is increased. The increased magnitude of flux linkage results in higher magnitude of core loss. Therefore, the magnitude of SC loss was found to be higher in six phase machine configuration than its three phase counterpart. By utilizing the evaluated values of SC loss, equation 7.8 was used to find the alternator stray loss.

This has been expressed for stator current of 2 A, at different rotor speed, for both six phase and three phase machine, as shown in Fig. 7.14. Stray loss was also found to be greater for six phase than its three phase counterpart.

During the process of loss determination, supply voltage was found to be fluctuating due to other load connected to the supply system, resulting in the change of input (dc through rectifier) voltage. During the experiment, rotor speed was also controlled manually by using rheostat in armature and field circuit of prime mover. It was practically difficult to maintain the rotor speed exactly constant. These factors, together with the manual recording of a larger number of measuring devices may result in some error.

7.5.5 Determination of Field circuit losses (copper loss)

Determination of field copper loss requires the accurate value of field circuit resistance. Since, value of resistance is dependent on the operating temperature, therefore, the corrected value of resistance may be obtained by using following equation:

$$R_1 = R_2 \frac{(k+t_1)}{(k+t_2)} \tag{7.9}$$

where, R_1 and R_2 are the resistance at cold standard temperature t_1 such as 25^0C and at operating condition temperature t_2. K is a constant, whose value depends on type of material used. Furthermore, value of brush resistance loss will also have to be taken into consideration. This value at individual slip ring is equal to the product of (field current × 1 volt drop) watts. Alternatively, the field circuit copper loss may be evaluated if the magnitude of brush voltage V_{fr} is known for a given value of field current I_{fr}. Value of field current should be regulated to maintain the rated terminal voltage of synchronous alternator at a particular operating condition.

In the experimental setup, a small exciter generator is mounted to feed the field circuit through slip ring and brush arrangement. The magnitude of generated voltage is proportional to the shaft speed. The generated voltage together with the above discussed experimental steps, copper loss of field circuit may be determined at different excitation current (I_{fr}), as shown in Fig. 7.15.

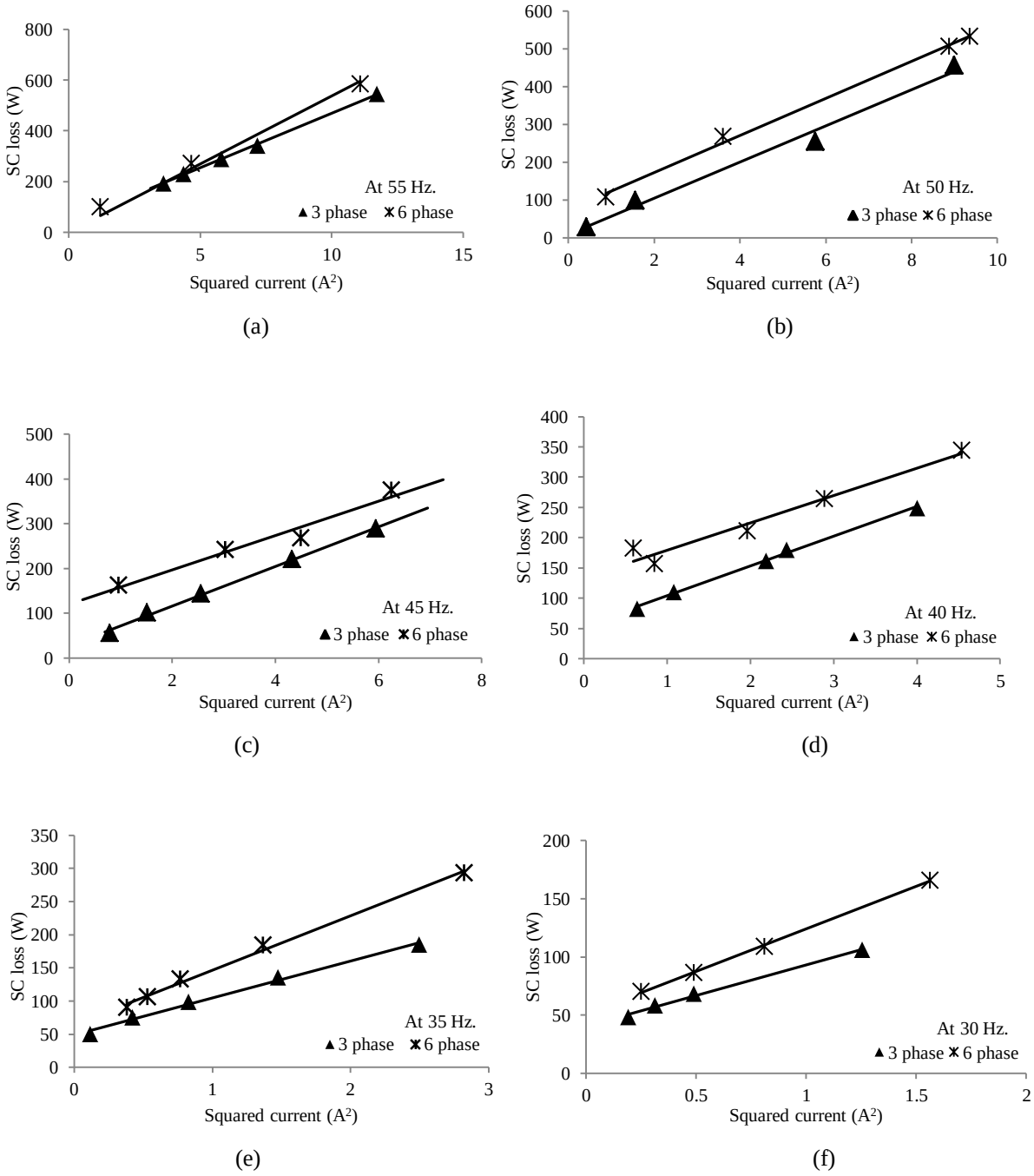

Fig. 7.13: Short circuit loss of test synchronous machine at different rotor speed.

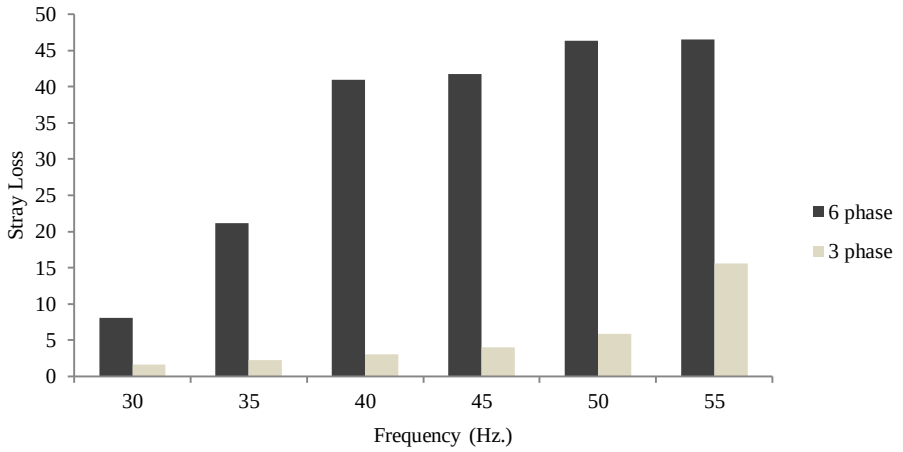

Fig. 7.14: Stray loss at different synchronous speed.

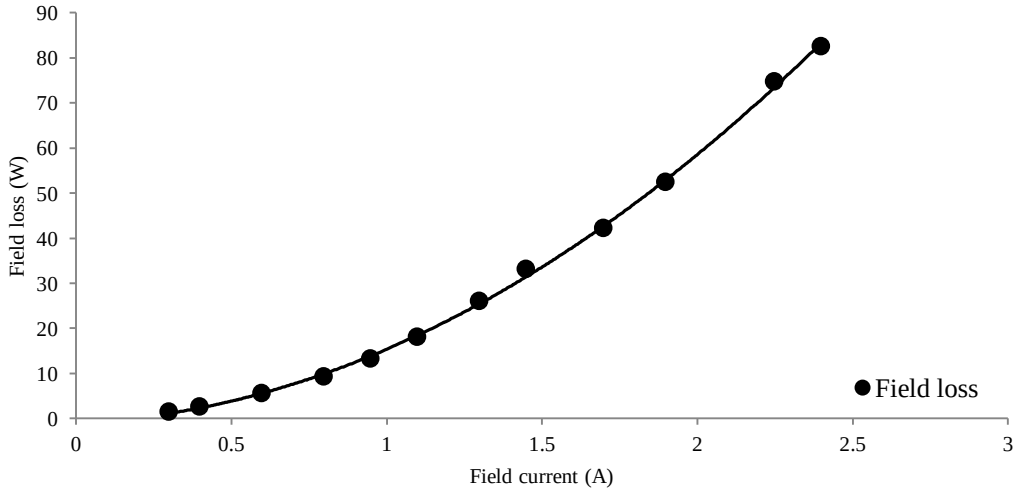

Fig. 7.15: Field loss in excitation circuit.

7.6 Efficiency evaluation

Performance evaluation of the six-phase synchronous motor has been carried out at different load condition, followed by the comparison with its three-phase counterpart. Evaluation of efficiency of six-phase synchronous motor may be determined in following two aspects:

(a) Consideration of enhanced power handling capability of six-phase synchronous motor when compared with its three-phase counterpart [7, 12 – 14, 16].

(b) Power rating of the test machine is assumed to be constant (rated power), irrespective of the type of stator winding configuration (six-phase or three-phase) [102, 129 – 130].

In above first aspect, efficiency has been evaluated at different load with constant input terminal voltage for both six-phase and three-phase stator winding configuration. Fig. 7.16 and Fig. 7.17 shows the evaluated efficiency curve with input phase voltage maintained at 200 V, for six-phase and three-phase synchronous motor, respectively. Experimentally, maximum efficiency of six-phase synchronous motor was found to be 75.1 % at input power of 3.6 kW; whereas it is 70.5 % at input power of 2.1 kW for three-phase winding configuration. Maximum efficiency of six-phase motor was found to be higher than its three-phase counterpart, by 4.6 % approximately.

Furthermore, it is a usual practice to compare the motor performance with different number of phases, under same magnetic condition in motor core. In this condition, above second aspect will be fulfilled [102, 129] such that the input voltage in six-phase winding configuration will be about half the voltage of motor with three-phase winding. Keeping in view of this fact, the efficiency of the motor has been evaluated for both six-phase (with input phase voltage at 120 V) and three-phase (with input phase voltage at 240 V) stator winding configuration in Fig. 7.18 and Fig. 7.19, respectively. Efficiency curve of motor was found to be similar for both six-phase and three-phase motor operation. Maximum efficiency of six-phase synchronous motor was found to be 73 % at input power of 2.12 kW; whereas it is 72 % for three-phase motor with 2.09 kW input power. In present aspect, efficiency of six-phase synchronous motor was also found to be greater than three-phase motor operation, but by small value i.e. 1 % approximately.

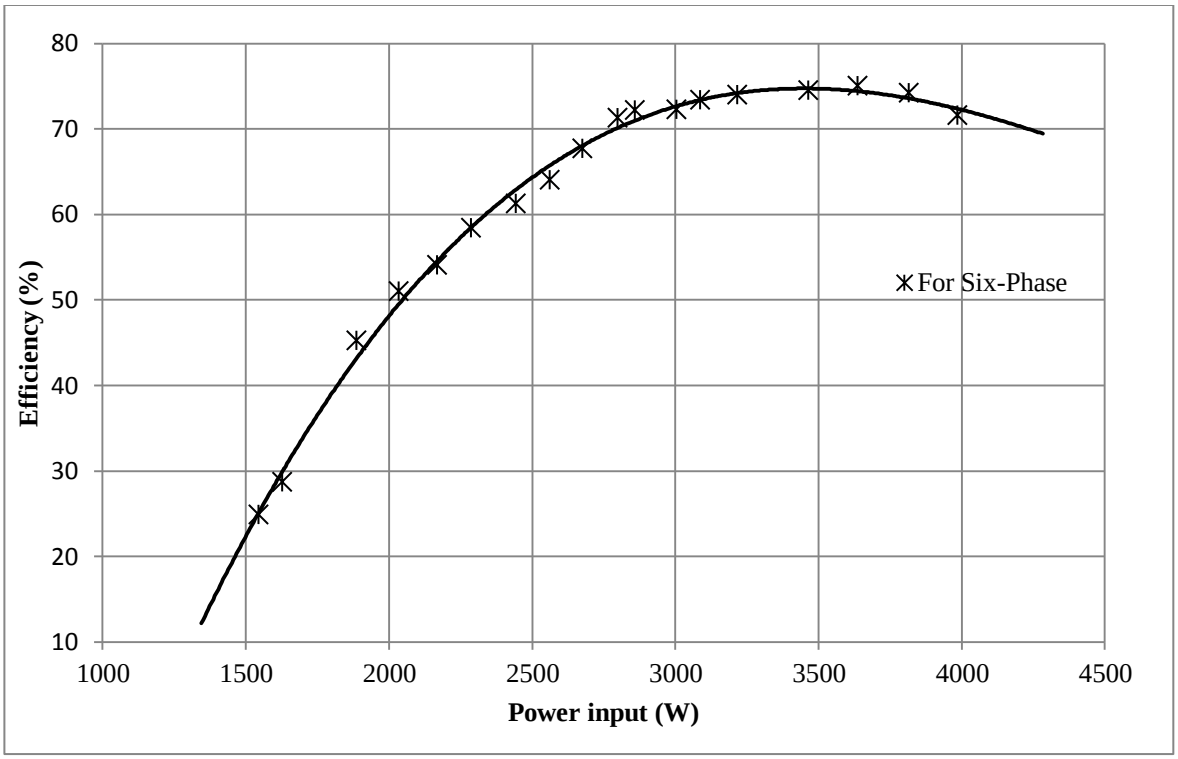

Fig. 7.16: Efficiency curve of six-phase synchronous motor operation with input phase at 200 V.

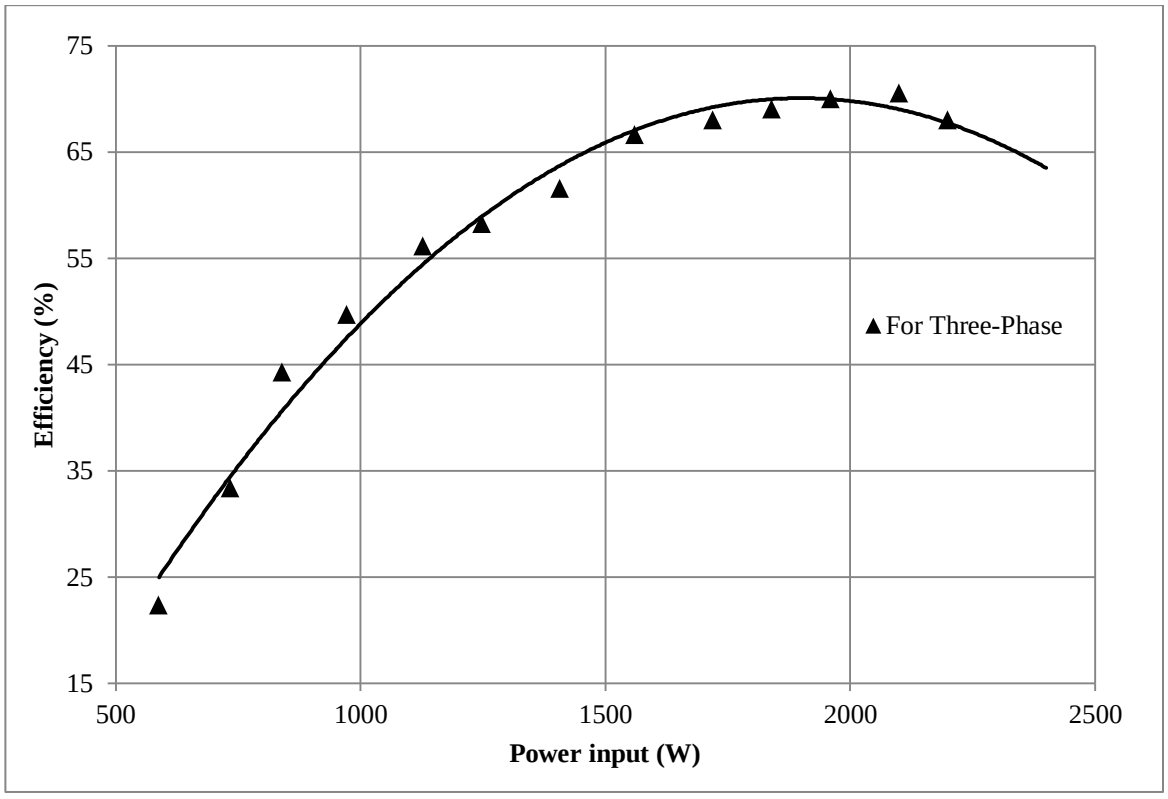

Fig. 7.17: Efficiency curve of three-phase synchronous motor with input phase at 200 V.

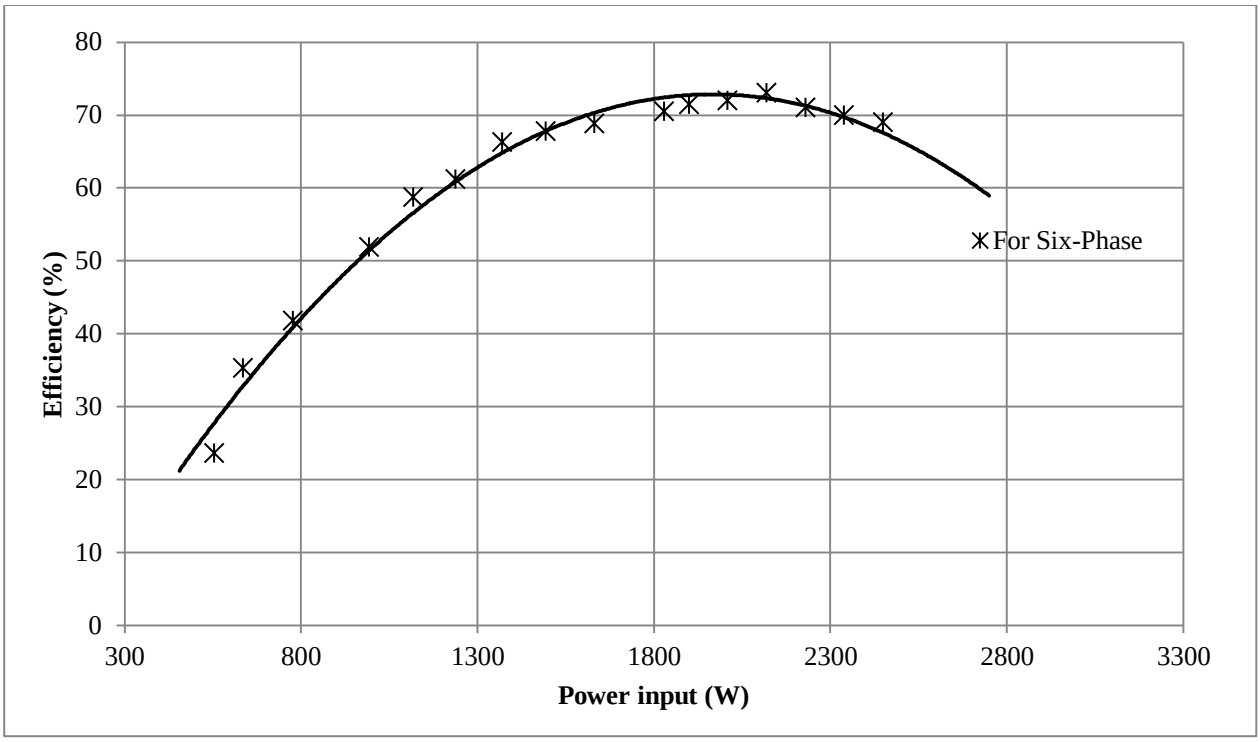

Fig. 7.18: Efficiency curve of six-phase synchronous motor operation with input phase at 120 V.

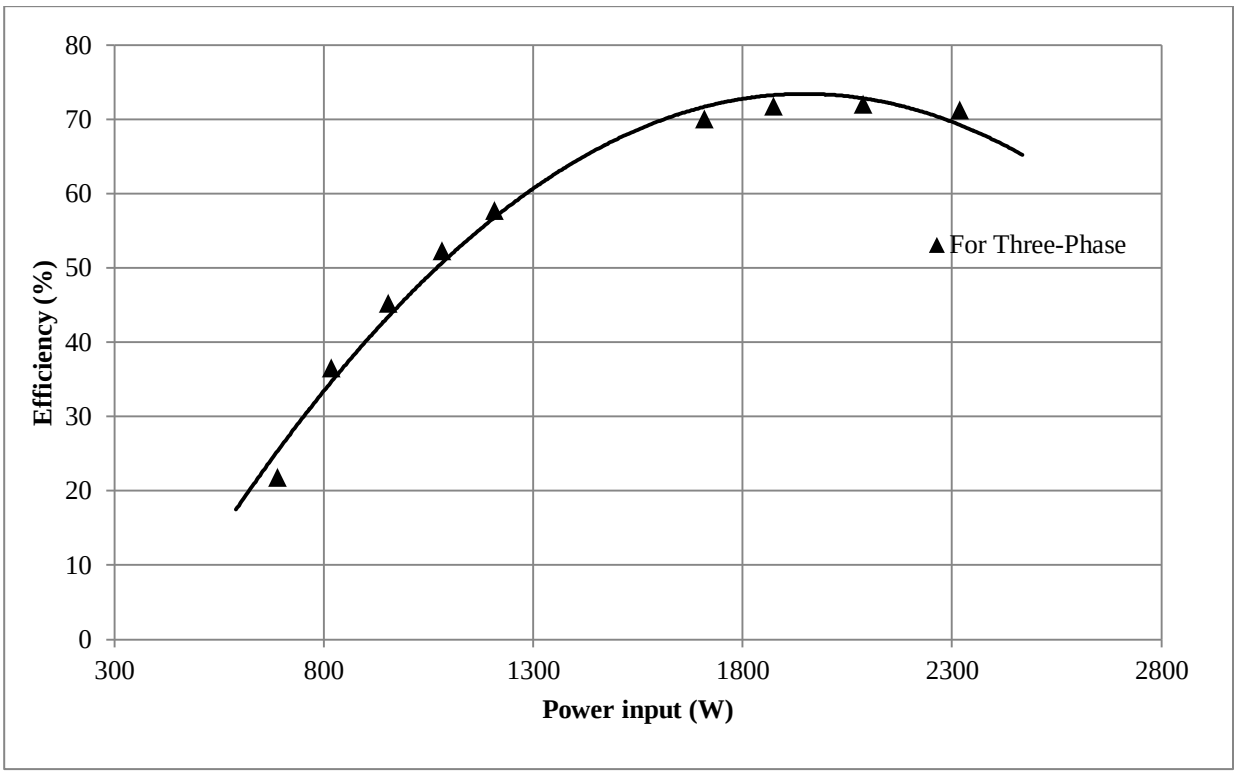

Fig. 7.19: Efficiency curve of three-phase synchronous motor with input phase at 240 V.

7.7 Conclusion

A detailed performance evaluation of a six-phase synchronous motor has been carried out under different operating conditions during steady state. Operation during steady state with input supply to both winding sets *abc* and *xyz*, and input supply to only one winding set *abc* have been presented. Experimentally, reduced sensitivity of motor operation towards supply asymmetry was noted when operating with input supply to one winding set only (i.e. motor generator mode).

Redundancy characteristic was further investigated by the inclusion of open circuit fault at input terminals of motor. It was experimentally found that the current magnitude in remaining healthy phases increases with the increase in number of open circuit faults at motor terminals (including the operation in motor-generator mode), for constant output power. Infact, above faults can even be sustained and still motor gives a satisfactory performance, showing its redundancy characteristic. This feature encourages the use of six-phase (multiphase in general) synchronous motor for the operation where reliability is of prime importance.

Further, a detailed experimental evaluation of different losses of six phase synchronous machine have also been presented. Results have been presented for different rotor synchronous speed (at frequency of 30, 35, 40, 45, 50, 55 Hz.). In general, the different no load losses of synchronous machine with six phase winding configuration were found to be greater than its three phase counterpart. Some of the important concluding remarks may be listed:

(a) Friction and windage losses were found to be a linear function of rotor speed.

(b) No load losses of the test synchronous machine were found to be dependent on both field voltage/current and rotor speed. At a particular excitation, difference in no load losses for machine with six phase and three phase winding configuration, increases linearly with rotor synchronous speed. The increased core loss for six phase machine is due to the increased magnetic coupling of two sets of three phase winding (*abc* and *xyz*), occupying the same stator slots (local core loss).

(c) In six phase test machine, the magnitude of short circuit loss was found to be higher than its three-phase counterpart. This is mainly because of the increased magnitude of resultant flux, thereby increasing the value of local core losses.

(d) Losses in field circuit are dependent on the magnitude of its excitation current. These losses are independent of the rotor speed for a particular excitation current. Losses in field circuit were found to be proportional to the squared value of excitation current.

Although the different no-load loss components of synchronous machine with six phase winding configuration were found to be greater than its three phase counterpart, but during load condition, the per phase current in six-phase winding configuration is substantially reduced for a given load. Further, asymmetrical six-phase winding configuration with displacement angle of 30^0 electrical results in the elimination of all the airgap flux harmonics of order ($6x \pm 1; x = 1,3,5 \ldots$). This leads to substantial decrease in losses (particularly stray loss), and overall improved performance of the six-phase synchronous machine as compared to its three-phase counterpart.

Table 7.1: Steady-state performance calculation under different load.

Phase	**A**		**B**		**C**		**X**		**Y**		**Z**	
Load Torque	**Exp.**	**Sim.**	**Exp.**	**Sim.**	**Exp.**	**Sim.**	**Exp.**	**Sim.**	**Exp.**	**Sim.**	**Exp.**	**Sim.**
33.83%	2.58	2.53	2.73	2.70	2.19	2.21	2.38	2.34	1.94	1.85	1.96	2.05
26.46%	2.32	2.36	2.51	2.56	1.97	2.07	1.87	1.90	1.44	1.42	1.52	1.59

Table 7.2: Steady-state performance calculation under different voltage.

Phase	**A**		**B**		**C**		**X**		**Y**		**Z**	
Voltage level	**Exp.**	**Sim.**	**Exp.**	**Sim.**	**Exp.**	**Sim.**	**Exp.**	**Sim.**	**Exp.**	**Sim.**	**Exp.**	**Sim.**
180	3.55	3.52	3.74	3.70	3.11	3.19	3.27	3.22	2.89	2.80	2.83	2.85
200	3.87	3.86	4.24	4.28	3.61	3.68	3.82	3.82	3.32	3.25	3.24	3.20

Table 7.3: Pre and post fault current data of winding sets *abc* and *xyz* at different load torque.

Phase		**A**		**B**		**C**		**X**		**Y**		**Z**	
Load Torque	**Operational mode**	**Exp.**	**Sim.**	**Exp.**	**Sim.**	**Exp.**	**Sim.**	**Exp.**	**Sim.**	**Exp.**	**Sim.**	**Exp.**	**Sim.**
33.83%	Normal	2.58	2.50	2.73	2.75	2.19	2.22	2.38	2.30	1.94	1.80	1.96	2.07
	Single phase opened	0	0	2.19	2.10	2.21	2.10	3.23	3.31	3.70	3.72	2.21	2.10
	Double phase opened	0	0	2.77	2.73	2.77	2.73	0	0	4.99	5.07	4.97	5.07
26.46%	Normal	2.32	2.22	2.51	2.50	1.97	1.98	1.87	1.83	1.44	1.34	1.52	1.52
	Single phase opened	0	0	1.99	2.00	1.99	2.00	2.75	2.88	3.11	3.21	1.63	1.61
	Double phase opened	0	0	2.17	2.20	2.16	2.20	0	0	3.72	3.70	3.77	3.70

Table 7.4: Pre and post fault current data of winding sets *abc* and *xyz* at different voltage levels (phase voltage).

Phase		**A**		**B**		**C**		**X**		**Y**		**Z**	
Voltage level	**Operational mode**	**Exp.**	**Sim.**	**Exp.**	**Sim.**	**Exp.**	**Sim.**	**Exp.**	**Sim.**	**Exp.**	**Sim.**	**Exp.**	**Sim.**
180	Normal	3.55	3.50	3.74	3.77	3.11	3.17	3.27	3.31	2.89	2.80	2.83	2.80
	Single phase opened	0	0	2.99	2.97	3.01	2.99	4.80	4.91	5.40	5.44	3.06	2.90
	Double phase opened	0	0	3.58	3.55	3.59	3.55	0	0	6.59	6.61	6.60	6.61
200	Normal	3.87	3.86	4.24	4.28	3.61	3.68	3.82	3.82	3.32	3.25	3.24	3.20
	Single phase opened	0	0	3.42	3.43	3.43	3.43	5.12	5.24	5.93	6.01	3.39	3.30
	Double phase opened	0	0	3.83	3.90	3.82	3.90	0	0	7.02	7.08	7.04	7.08

Chapter 8

Conclusions and future works

8.1 Main Conclusions

This thesis presents a comprehensive analysis of six-phase synchronous motor having two sets of three phase stator windings *abc* and *xyz*, with asymmetrical winding structure (30^o displacement between both the winding sets). Initially a simple but effective mathematical model has been developed considering the effect of mutual leakage reactance between the two stator winding sets *abc* and *xyz* in rotor reference frame. The developed model was employed to evaluate the dynamic performance of six-phase synchronous motor under step change in load torque, field excitation and input voltage. A satisfactory performance was noted with less swing in stator current and rotor speed, resulting in its stable operation. Further, the effect of displacement angle (between both stator winding sets *abc* and *xyz*) was also investigated. It was found that for 30^o phase displacement between both stator winding sets, when supplied by independent three phase source (six-step VSI) results in a substantial decrease in harmonic torque and less rotor current harmonics, leading to a smooth motor operation with less mechanical noise and vibration in machine. Increased harmonics in stator current was also recorded, leading to heating of stator. But the increased heating of stator can be easily taken care of by providing better cooling arrangement.

An exclusive investigation of six phase synchronous motor during steady state has also been reported in this work. Steady state analysis has been carried out for two different operating conditions at input terminals, i.e. the input supply to both stator winding sets as well as at only one set of three phase stator winding (motor-generator mode). This includes the mathematical modeling of synchronous motor during steady state, followed by the development of its phasor diagram at a particular operating condition (both at lagging and leading power factor).

Fault analysis of motor drive system is extremely important to design its suitable protective scheme. Most frequent faults, which are usually encountered are open-circuit and short-circuit at the input terminals of machine. Analysis of six-phase synchronous motor during

open-circuit and short-circuit fault conditions (both asymmetrical and symmetrical) have been carried out in detail, and following important conclusions can be listed:

(i) During open-circuit fault, the magnitude of stator current is increased in remaining healthy winding set due to higher power shared by it. Flow of stator current was found to be unequal in magnitude of each phase due to asymmetrical condition. Non-uniformity in current flow diminishes with increase in supply outage to more phases and it finally becomes balanced in nature for a complete outage of a supply to a particular winding set, but with increased magnitude.

(ii) The output of the three winding transformer used in experimentation had an inherent supply magnitude asymmetry and this was reflected in the test results. Supply asymmetry results in unbalanced flow of current in motor. Six-phase synchronous motor was found to be more sensitive towards supply asymmetry as compared to its operation as a three phase motor with supply in only one winding set (three phase winding configuration).

(iii) Machine was found to operate simultaneously both as a motor as well as generator when three phase input supply was fed to only one winding set. This operating mode makes the machine suitable for special application (like air conditioner in electric railway etc.).

(iv) Current during short circuit increases abruptly irrespective to the type of fault. Magnitude of current was found to be dependent on the type of fault and becomes maximum during symmetrical short circuit.

(v) During asymmetrical short circuit, motor operation was found to remain stable whereas instability was noted if symmetrical short circuit is not cleared within few cycles (not more than three cycles).

(vi) During short circuit, variation in the ripple magnitude of motor torque T_e was found to be dependent on input voltage. A small variation in ripple magnitude was also noted with the change in motor load.

Stability of an electrical machine is extremely important when small disturbance is encountered during steady-state. A detailed small-signal stability analysis of a six-phase synchronous motor has been carried out by developing a linearized mathematical model wherein the mutual leakage between both the stator winding sets *abc* and *xyz* is considered, using *dqo* approach. The developed linearized model is capable of describing the dynamic behavior of small displacement/excursion about a steady-state operating point, so that the basic linear control system theory can be applied to evaluate the eigenvalues. Association of eigenvlaues and motor parameter has been established by evaluating the eigenvalue at an operating point by changing the motor parameter within a particular range. It was found that the two eigenvalues named as "Stator eigenvalue I and II", are almost unaffected by the variation in rotor parameter and load. The other complex conjugate pair is affected by the variation in moment of inertia *J* and load, which actually indicates "settling out" of rotor oscillation of synchronous motor during hunting or swing mode. The remaining three real eigenvalues indicate decay of the offset currents in rotor circuit and, therefore, are associated with the effective time constant of the circuit.

Based on the variation of dominant eigenvalues, some important steps have been suggested to enhance the stability of motor during steady-state. At design stage, stability enhancement can be carried out from both stator and rotor side. From stator side, an effective way is to decrease the value of stator resistance, but alternatively, value of stator leakage reactance may be increased, if required. From the rotor side, it can be effectively carried out by increasing the value of leakage reactance of the field circuit and /or by decreasing the value of resistance of damper winding along *q*-axis. Further, stability of motor was also found to be dependent on operating conditions. It can be enhanced either by increasing the input voltage or operating frequency at a particular load. Increase in load torque upto a particular point increases the stability, but it tends towards instability for further motor loading, under constant Volt/Hz operation. Moreover, from field side, stability can also be increased by increasing the power factor angle.

At a particular motor operation, stability can be enhanced by varying its parameters. Since, parametric variation of a machine is a difficult task from practical point of view; therefore, a simple closed-loop control scheme has been developed and analyzed, employing

state-feedback technique. The developed control scheme is simple but effective which ensures a stable operation of the six-phase synchronous motor in all the operating regions.

A way of selecting the elements of weighing matrix, associated with the motor state variable has also been addressed. Selection of these elements determines the required shift of dominant eigenvalues for stable operation of the motor.

The developed linearized model can be easily used to formulate transfer function between input and output variables, where different stability plots (like root locus, nyquist plot, bode plot) can be easily drawn. Thus greatly simplifying the control analysis of a system applicable for six-phase synchronous motor.

Finally, a simple and effective closed loop scheme has been developed for load-commutated inverter fed six-phase synchronous motor, operating in self-controlled mode. The control scheme ensures the motor operation at leading power factor at all load conditions (no load and load condition). Control of rectifier as well as inverter circuits have been explained in detail, followed by the dynamic analysis for a step change in load torque (increased by 50 % of rated/base value). Further, motor drive operation during steady-state was also examined. The number of spikes was observed in the six-phase case, though commutation of inverter switches (low cost thyristor) was found to be safe.

Further, a detailed experimental evaluation of various losses of six phase synchronous machine has also been presented, for different rotor synchronous speed (at frequency of 30, 35, 40, 45, 50, 55 Hz.). The different losses (eddy current and hysteresis losses, short circuit loss, losses in field circuit and, friction and windage losses) of the test machine were found to be larger than its three-phase counterpart. This is because of the increased effective airgap with asymmetrical six-phase stator winding in comparison with its three-phase counterpart ($x' > x$).

8.2 Future Works

In this chapter, important conclusions have been drawn through a comprehensive analysis of six-phase synchronous motor. In this view, following aspects can be taken as the subject of future investigation as the extension of present work, applicable for a six-phase synchronous motor (multiphase motor in general):

(i) Mathematical modeling and analysis, which has been carried out so far, considered the motor parameters as a constant value. In actual motor operation, its parameter also varies. This is because of its dependency on temperature and saturation effect. Temperature changes the value of system resistances whereas, the saturation effect changes the value of magnetizing inductances. These factors (particularly saturation effect) can be incorporated while developing the mathematical model of synchronous motor.

(ii) Mathematical modeling of six-phase synchronous motor has been carried out by ignoring the presence of harmonics in input supply. Effect of harmonics can be incorporated in the modelling of synchronous motor.

(iii) Mathematical modeling together with the investigation of motor behavior during fault conditions (open circuit and short circuit) has been carried out in detail. As an extension of this work, suitable fault tolerant/protective scheme can be developed for abnormal working situations created by the open circuit/short circuit fault. Further, occurrence of fault conditions has been assumed and analyzed at input terminals of motor. But fault occurrence within the machine, i.e. in the windings of stator or rotor, may also be investigated with suitable fault detection technique together with the development of suitable protective schemes.

(iv) The present work can also be extended to the development and analysis of drive system using different power electronics converters for closed operation.

(v) In the discussion of LCI fed synchronous motor, machine was considered to operate in motoring mode only. But, analysis may also be extended for the machine operation in regenerative mode too.

References

[1] T. F. Barton, "The double winding generator", General Electric Review, 302-308, 1929.

[2] P.L. Alger, E.H. Freiburghouse and D.D. Chase, "Double windings for turbine alternators", AIEE Tansactions, 49 (1) 226-244, 1930.

[3] P.E. Power and L.A. Kilgore, "Developement in generators and systems as they affect system reliability", Electic Journal, 480-487,1929.

[4] E.E. Ward, and H. Harer, "Preliminary investigation of an invertor-fed 5-phase induction motor", Proceedings IEE, 116 (6), 980-984, 1969.

[5] R.H. Nelson, and P.C. Krause, "Induction machine analysis for arbitrary displacement between multiple winding sets", IEEE Transactions on Power Apparatus and System, 93 (3), 841-848, 1974.

[6] E.A. Klingshrin, "High phase order induction motor-Part-I: Description and theoretical consideration", IEEE Transactions on Power Apparatus and System, 102 (1), 47-53, 1983.

[7] G.K. Singh, "Multiphase induction machine drive research-A survey", Electric Power System Research, 61 (2), 139-147, 2002.

[8] Umesh Dikshit and R. K. Tripathi, "Direct Torque Control for Dual Three-Phase Induction Motor Drives" Proc, IEEE Students' Conference on Engineering & Systems (SCES 2012), pp. 1-6, March 17-19, 2012, MNNIT Allahabad, India.

[9] Marguerite Touma-Holmberg, and Kailash Srivastava, "Double Winding, High-Voltage Cable Wound Generator: Steady-State and Fault Analysis", IEEE Transactions on Energy Conversion, 19 (2), pp. 245-250, 2004.

[10] M.A. Abbas, R. Cheisten and T.M. Jahns, "Six-phase voltage source inverter driven induction motor", IEEE Transactions on Industrial Applications, 20 (5), 1251-1259, 1984.

[11] T.A. Lipo, "A d-q model for six phase induction machine", International conference, Electric machines, Athens, Greece, 860-867, Sept. 15-17, 1980.

[12] G.K. Singh, V. Pant and Y.P. Singh, "Voltage source inverter driven multi-phase induction machine", Computer and Electrical Engineering, 29, 813-834, 2003.

[13] E. Levi, R. Bojoi, F. Profumo, H.A. Toliyat and S. Williamson, "Multiphase induction motor drives-a technology status review", IET Electric Power Applications, 1 (4), 489-

516, 2007.

[14] E. Levi, "Multiphase electric machines for variable-speed applications", IEEE Transactions on Industrial Applications, 38 (5), 1893-1909, 2008.

[15] Kaiyuan Lu and Ewen Ritchie, "Preliminary Comparison Study of Drive Motor for Electric Vehicle Application", Proceedings of the Fifth International Conference on Electrical Machines and Systems, 2001. ICEMS 2001, vol-2, pp. 995-998, Aug 2001, Shenyang.

[16] G.K. Singh, "A six-phase synchronous generator for stand-alone renewable energy generation: Experimental analysis", Energy, 36 (3), 1768-1775, 2011.

[17] T.M. Jahns, "Improved reliability in solid-state ac drives by means of multiple independent phase drive units", IEEE Transactions on Industrial Applications, 16, (3), 321-331, 1980.

[18] J.M. Apsley, "Derating of multiphase induction machines due to supply imbalance", IEEE Transactions on Industrial Applications, 46, (2), 798-805, 2010.

[19] D.C. White and H.H. Woodson, "Electromechanical energy conversion", Wiley, New York, 1959.

[20] PC Krause, O Wasynczuk and SD Sudhoff , "Analysis of electrical machinery and drive Systems", IEEE Press, A John Wiley & Sons, Inc. Publication, 2004.

[21] E.F. Fuch and LT Rosenberg, "Analysis of an alternator with two displaced stator windings", IEEE Transactions on Power Apparatus and System, 93 (6), 1776-1786, 1974.

[22] R.F. Schiferl and C.M. Ong, "Six phase synchronous machine with ac and dc stator connection, Part-I", IEEE Transactions on Power Apparatus and System, 102 (8), 2685-2693, 1983.

[23] R.F. Schiferl and C.M. Ong, "Harmonic studies and a proposed uninterruptible power supply scheme, Part-II", IEEE Transactions on Power Apparatus and System, 102 (8), 2694-2701, 1983.

[24] T. Kataoka and E.H. Watanebe, "Steady-state characteristic of a current-source inverter/double-wound synchronous machine system for AC power supply", IEEE Transactions on Industrial Applications, 16 (2), 1980.

[25] G.K. Singh, "Modeling and analysis of six-phase synchronous generator for stand-alone

renewable energy generation", Energy, 36 (9), 5621-5631, 2011.

[26] Y. Zhao and T.A. Lipo, "Space vector PWM control of dual three-phase induction machine using vector space decomposition", IEEE Transactions on Industrial Applications, 31 (5), 1100-1109, 1995.

[27] Y. Zhao and T.A. Lipo, "Modeling and control of a multiphase induction machine with structural unbalance. Part I: Machine modeling and multi-dimensional current regulation", IEEE Transactions on Energy Conversion, 11 (3), 570-577, 1996.

[28] F. Jen-Ren and T.A. Lipo, "Disturbance-free operation of a multiphase current-regulated motor drive with an opened phase", IEEE Transactions on Power Apparatus and Systems, 30 (5), 1267-1274, 1994.

[29] G.K Singh, V. Pant, "Analysis of a multiphase induction machine under fault condition in a phase-redundant A.C. drive system", Electric. Machines and Power Systems, 28 (6), 577-590, 2000.

[30] L. Alberti, N. Bianchi, "Experimental test of dual three-phase induction motor under fault operating condition", IEEE Transactions on Power Electronics, 59 (5), 2041-2048, 2012.

[31] R. Kioniezhad, B. Nahid-Mobarakeh, L. Baghli, F. Betin and G. Capolino, "Modeling and control of six-phase symmetrical induction machine under fault condition due to open phases", IEEE Transactions on Industrial Electronics, 55 (5), 1966-1977, 2008.

[32] A. Tani, M. Mengoni, L. Zarri, G. Serra and D. Casadei, "Control of multiphase induction motors with an odd number of phases under open circuit phase faults", IEEE Transactions on Power Electronics, 27 (2), 565-577, 2012.

[33] X. Kestelyn, F. Locment, Y. Crevits and E. Semail, "Easy-to-Implement Integral Numerical Simulation of Multi-phase Drives under Fault Supply Condition", IEEE International Electric Machines & Drives Conference IEMDC '07; 3-5 May 2007, Antalya, Terkey.

[34] F. Terrien and M.F. Benkhoris, "Analysis of double star motor drives for electric propulsion", IEE, 9th International coference on Electric Machines and drives, Conference publication no.468; 1-3 September, 1999; Canterbury, France.

[35] I. Abuismais, W.M. Arshad, S. Kanerva, "Analysis of VSI-DTC fed six phase synchronous machines", In: IEEE 2008 Power Electronics and Motor control

conference (EPE-PEMC); 1-3 September 2008; Poznan, Poland.

[36] K Srivastava and B Berggren, "Simulation of synchronous machines in phase coordinates including magnetic saturation", Electric Power Systems Research 56 (3), 177-183, 2000.

[37] P.L. Alger, "Induction machines", New York, Gorden and Breach, 1970.

[38] M.R. Aghamohammadi and M. Pourgholi, "Experience with SSSFR test for synchronous generator model identification using Hook-Jeeves optimization method", International Journal of System Applications, Engineering & Development, 2, 122-127, 2008.

[39] C.V. Jones, "The unified theory of electric machine", London, Butterworths, 1967.

[40] Kaiyuan Lu, Mario Vetuschi, Peter Omand Rasmussen and Andrew Ewen Ritchie, "Determination of High-Frequency d- and q-axis Inductances for Surface-Mounted Permanent-Magnet Synchronous Machines", IEEE Transactions on Instrumentation and Measurement, 59 (9), 2376-2382, 2010.

[41] Kaiyuan Lu, Peter O. Rasmussen, and Ewen Ritchie, "A Simple and General Approach to Determination of Self and Mutual Inductances for AC machines", International Conference on Electrical Machines and Systems (ICEMS), pp. 1-4, August 20-23, 2011, Beijing.

[42] H. Bulent Ertan, Ertan Murat and Baris Colak, "A Novel Approach to Detection of Some Parameters of Induction Motors", IEEE International Electrical Machines and Drives Conference IEMDC 2007 3-5 May 2007, Antalya, Turkey pp. 1626-1631.

[43] H. Bülent Ertan, Volkan Sezgin and Baris Colak, "Detection of Some Parameters of Induction Motors a Proposal and Its Verification", The Seventh International Conference on Power Electronics and Systems PEDS'07, pp. 1337-1343, November 27-30, 2007, Bangkok, Thailand.

[44] H. Bülent Ertan and Çağlar H. Özyurt; "Prediction of Induction motor Parameters From Manufacturer's Data", International Symposium on Electrical Apparatus and Technologies CD Proceedings (SIELA 2005) , 1, pp.1, 2-3 June 2005, Plovdiv, Bulgaria.

[45] Cheng Ming, K.T. Chau and Chan C.C., "Design and analysis of a new doubly salient permanent magnet motor", IEEE Transactions on Magnetics, 37 (4) , 3012-3020, 2001.

[46] Cheng Ming, Sun Qiang, E. Zhou and K.T. Chau, "New methods of measuring inductance of doubly salient permanent magnet motors", Electric Power Components and Systems, 30 (11) , 1127-1135, 2002.

[47] Cheng Ming, Li Guangfu and E. Zhou, "Magnetic circuit analysis and parameter calculation of the hybrid PM synchronous motors with rare earth magnets", Journal of Southeast University, 21 (6), 8-15, 1991.

[48] Cheng Ming, K.T. Chau, Sun Qiang and E. Zhou, "Inductance measurement of doubly salient permanent magnet motors", Proceedings of International Conference on Electrical Machines and Systems, pp. 842-845, August 18-20, 2001 Shenyang, China.

[49] R. Bojoi, F. Farina, M. Lazzari, F. Profumo and A. Tenconi, "Analysis of the asymmetrical operation of dual three-phase induction machines", Proceedings of the IEEE International Electric Machine and Drives Conference IEMDC, Madsion, WI, pp. 429-435, 2003,

[50] R. Bojoi, M. Lazzari, F. Profumo and A. Tenconi, "Digital field-oriented control of dual three-phase induction motor drives", IEEE Transactions on Industrial Applications, 39 (3), 752-760, 2003.

[51] R.O.C. Lyra and T.A. Lipo, "Torque density improvement in a six-phase induction motor with third harmonic current injection", IEEE Transactions on Industrial Applications, 38 (5), 1351-1360, 2003.

[52] D.D. Robb and P.C. Krause, "Dynamic simulation of generator fault using combined *abc* and *0dq* variables", IEEE Transactions on Power Apparatus and Systems, 94 (6), 2084-2091, 1975.

[53] R.J. Kerkman, P.C. Krause,and T.A. Lipo, "Simulation of a synchronous machine with an open phase", Electric Machine and Electromechanics, 1 (3), 245-254, 1977.

[54] B.A. Welchko, T.M. Jahns, S. Hiti, "IPM synchronous machine drive response to a single-phase open circuit fault", IEEE Transactions on Power Electronics, 17 (5), 764-771, 2002.

[55] H. H. Hwang, "Transient analysis of unbalanced short circuit of synchronous machines", IEEE Transactions on Power Apparatus and System, 88 (1), 67–72, 1969.

[56] G. Reddy and C. V. Jones, "Line-line short circuit of synchronous machine: Illustration of computer-aided machine analysis", Proc. IEE, 118 (1), 161–168, 1971.

[57] J.C. Das, “Power System Analysis”, Marcel Dekker, Inc., USA, 2002

[58] N. Tleis, “Power System Modelling and Fault Analysis”, Elsevier Ltd., 2008.

[59] P.S.R. Murty, “Power System Analysis”, BS Publication, Hydrabad, India, 2007.

[60] B. Adkins and R.G. Harley, “The General Theory of Alternating Current Machines”, Chapman and Hall, London, 1975.

[61] B.A. Welchko, T.M. Jahns, W.L. Soong and J.M. Nafashima, “IPM Synchronous Machine Drive Response to Symmetrical and Asymmetrical Short Circuit Faults”, IEEE Transaction on Energy Conversion, 18 (2), 291-298, 2003.

[62] S.S. Kalsi and T.A. Lipo, “A Modal Approach to the Transient Analysis of Synchronous machine”, Electric Machines & Power Systems, 1 (4), 1977.

[63] T.A. Lipo, “Analysis of Synchronous Machines”, Second edition, CRC Press, New York, 2012.

[64] H. Saadat, “Power System Analysis”, WCB/McGraw-Hill, 1999.

[65] H.M. Ryu, J.W. Kin, S.K. Sul, “Synchronous-frame current control of multiphase synchronous motor under asymmetric fault condition due to open phases”, IEEE Transactions on Industrial Applications", 42 (4), 1062-1070, 2006.

[66] O. Jasim, M. Sumner, C. Gerada and J.A. Padilla, “Development of a new fault-tolerant induction motor control strategy using an enhanced equivalent circuit model”, IET Electric Power Applications, 5 (8), 618-627, 2011.

[67] G.J. Rogers, “Linearized analysis of induction motor transients”, IEE Proc., 112 (10), 1917-1926, 1965.

[68] F.I. Fallside and A.T. Wortley, “Steady-state oscillation and stabilization of variable frequency inverter fed induction motor drives”, IEE Proc., 116 (6), 991-999, 1969.

[69] T.A. Lipo and P.C. Krause, “Stability analysis of a rectifier-inverter induction motor drive”, IEEE Transactions on Power Apparatus and Systems, 88 (1), 55-66, 1969.

[70] R.H. Nelson, T.A. Lipo and P.C. Krause, “Stability analysis of a symmetrical induction machine”, IEEE Transactions on Power Apparatus and Systems, 88 (11), 1710-1717, 1969.

[71] E.P. Cornell and T.A. Lipo, “Modeling and design of controlled current induction motor drive systems”, IEEE Transactions on Power Apparatus and Systems, 13 (4), 321-330, 1977.

[72] M.L. Macdonald and P.C. Sen, "Control loop study of induction motor drives using DQ model", IEEE Transactions on Industrial Electronics and Control Instumentation, 26 (4), 237-243, 1979.

[73] O.T. Tan and G.G. Richards, "Decoupled boundary layer model of induction machines", IEE Proceedings., 133 (4), 255-262, 1986.

[74] M.M. Ahmed, J.A. Tanfig, C.J. Goodman and M. Lockwood, "Electrical instability in a voltage source inverter fed induction motor drive", IEE Proceedings, 133 (4), 299-307, 1986.

[75] T.A. Lipo and P.C.Krause, "Stability analysis of a reluctance-synchronous machine", IEEE Transaction on Power Apparatus and Systems, 86 (7), 825-834, 1967.

[76] T.A. Lipo and P.C. Krause, "Stability analysis for variable frequency operation of synchronous machines", IEEE Transactions on Power Apparatus and Systems, 87 (1), 227-234, 1968.

[77] C.A. Stapleton, "Root-locus study of synchronous-machine regulation", IEE Proceedings, 111 (4), 761- 768, 1964.

[78] M. Moghavvemi and NorAzlan, "Predictive Power System Small Signal Stability Analysis Using Eigenvalues", International Journal of Emerging Electric Power Systems, IJEEPS, P. Berkeley publication, 2007.

[79] M. Moghavvemi and H. Norazlan, "The Eigenvalue Analysis for Power System Small Signal Stability", International Power Engineering and Optimization Conference (IPEOCO2007), pp 22, June 2007.

[80] Haider A. F. Mohamed, Lokman H. Hassan and M. Moghavvemi, and S. S. Yang, "The Eigen-solution Model Analysis for Iraqi National Super Grid System Small Signal Stability", IEEE sponsored International Colloquium on Signal Processing and its Application (CSPA 2008), Paper CSPA0987, 7-9 March, 2008, Kuala Lumpur .

[81] R.J. Abraham, D. Das and Amit Patra, "Damping Oscillations in Tie-power and Area Frequencies in a Thermal Power System with SMES-TCPS Combination", International Journal of Electrical Systems, 7 (1), 71-80, 2011.

[82] Lokman H. Hassan, M. Moghavvemi and Haider A.F. Mohamed, "Dynamic Stability Assessment of the Iraqi Power System Network", International Conference for Technical Postgraduates (TECHPOS 2009), pp. 1-5, 14-15 Dec. 2009, Kuala Lumpur.

[83] K.N. Srivastava and SC Srivastava, "Application of Hopf bifurcation theory for determining critical value of a generator control or load parameter", International Journal of Electrical Power & Energy Systems, 17 (5), 347-354, 1995.

[84] P. K. Satpathy, D. Das and P.B. Duttagupta, "A fuzzy approach to handle parameter uncertainties in Hopf bifurcation analysis of electric power system", International Journal of Electric Power and Energy Systems, 26 (7), 23-31, 2004.

[85] P. K. Satpathy and D. Das, "Impact of various load models in power system bifurcation analysis", Electric Power Components and Systems, 31 (7), 653-669 (2003).

[86] G.K. Singh, V. Pant and Y.P. Singh, "Stability analysis of a multiphase (six-phase) induction machine", Computer & Electrical Engineering, 29 (7), 727-756, 2003.

[87] M.J. Duran, F. Salas, and M.R. Arahal, "Bifurcation analysis of five-phase induction motor drives with third harmonic injection", IEEE Transactions on Industrial Electronics, 55 (5), 2006-2014, 2008.

[88] J.J. D'Azzo, C. Houpis, "Linear control system analysis and design with matlab", McGraw-Hill, New York, 1995.

[89] H.A. Moussa and Y.N. Yu, "Optimal power system stabilization through excitation and/or governor control", IEEE Transactions on Power Apparatus and Systems, 91 (3), 166-1174, 1972.

[90] Y.N. Yu, "Electric power system dynamics", New York, Acadamic press, 1983.

[91] J.H. Anderson, "The control of a synchronous machine using optimal control theory", Proceedings of the IEEE, 59 (1), 25-35, 1971.

[92] Sandeep Gupta, and R. K. Tripathi, "A Pole Placement Controller for CSC Based STATCOM with GA", 3rd IEEE Advance Computing Conference (IACC-2013), pp. 931-936, Feb 22-23, 2013, Ghaziabad, India.

[93] Sandeep Gupta, and R. K. Tripathi, "An LQR and Pole Placement Controller for CSC Based STATCOM", IEEE International Conference on Power, Energy and Control (ICPEC '13), pp. 115-119, Feb. 6-8, 2013, PSNA College of Engg. Dindigul, Tamilnadu, India.

[94] K. Ramar and S. Velusami, "Design of decentralized load-frequency controllers using pole placement technique," Electric Machines and Power Systems, 16 (3), 193–207, 1989.

[95] J.D. Edward and S.R. Narayan, "The optimal output feedback control of a synchronous machine", IEEE Transaction on Power Apparatus and Systems, 90 (5), 2123-2134, 1970.

[96] V.H. Quintana, M.A. Zohdy and J.H. Anderson, "On the design of output feedback excitation controller of synchronous machine", IEEE Transactions on Power Apparatus and Systems, 95 (1), 954-961, 1976.

[97] S. Velusami, I.A. Chidambaram, "Design of Decentralized Biased Dual Mode Controllers for Load–Frequency Control of Interconnected Power Systems", Electric Power Components and Systems, 34 (10), 1057-1075, 2007.

[98] I. A. Chidambaraml and S. Velusami, "Decentralized Biased Controllers for Load - Frequency Control of Interconnected Power Systems Considering Governor Dead Band Non-Linearity", IEEE Indicon 2005 Conference, Chennai, India, pp. 521-525, 11-13 Dec. 2005.

[99] I. A. Chidambaraml and S. Velusami, "Design of Decentralized Biased Controllers for Load-Frequency Control of Interconnected Power Systems", Electric Power Components and Systems, 33 (12), 1313-1331, 2005.

[100] J. Faiz and A. Azami, "Closed-loop control stability for permanent magnet synchronous motor", International Journal of Electrical Power & Energy Systems, 19 (5), 331-337, 1997.

[101] M. Ilic'-Spong, R. Marino, S.M. Peresada and D.G. Taylor, "Feedback linearizing control of switched reluctance motors", IEEE Transactions on Automatic Control, 32 (5), 371-379, 1987.

[102] A. Boglietti, R. Bojoi, A. Cavagnino, and A. Tenconi, "Efficiency analysis of PWM Inverter fed three-phase and dual three-phase high frequency induction machines for low/medium power applications," IEEE Transactions on Industrial Electronics, 55 (5), 2015-2023, 2008.

[103] S.E. Lyshevski, "Control system theory with engineering applications", New York, Springer Science, 2001.

[104] W. Leonhard, "Control of electric drives", New York, Third edition, Springer, 2001.

[105] H. Bülent Ertan, M. Ylldlnm, Ron Colyer and Alfio Consoli, "Modern Electrical Drives", Springer- Science, 1st edition 2000.

[106] B.K. Bose, "Mordern power electronics and AC drives", Prentice Hall PTR, Upper Saddle River, NJ, 2002.

[107] S. P. Das and A. K. Chattopadhyay, “Observer Based Stator Flux Oriented Vector Control of Cycloconverter-fed Synchronous Motor Drive”, IEEE Transaction on Industry Applications, 33 (4) , 943-955, 1997.

[108] S. P. Das and A. K. Chattopadhyay, “Simulation and test results for a cycloconverter-fed AC commutator-less motor drive with a modified machine model”, IEE Proceedings on Electric Power Applications, 51 (5), 622-627, 2004.

[109] S. P. Das and A. K. Chattopadhyay, “Modelling of a cycloconverter-fed synchronous motor drive under field co-ordinate control”, Third International Seminar on Industrial Electronics, Drives & Automation System (INTRONICS-94), pp. 1-7, Nov 24-25, 1994, Bangalore, India.

[110] C. Namuduri and P.C. Sen, “Digital simulation of an inverter-fed self-controlled synchronous motor”, IEEE Transactions on Industrial Electronics, 34 (2), 205-215, 1987.

[111] M.D. Otto and D.V. Otto, “Computer simulation of elctric motor drive system including the power electronic network”, IEEE Transactions on Industry Applications, 28 (5), 1072-1080, 1992.

[112] R.S. Colby, T.A. Lipo and D.W. Novotny, “A state space analysis of LCI fed synchronous motor drives in the steady state”, IEEE Transactions on Industry Applications, 21 (4), 1016-1022, 1985.

[113] R.S. Colby, M.D. Otto and J.T. Boys, “Analysis of LCI synchronous motor drives with finite DC link inductance”, IEE Proceedings, 140 (6), 379-386, 1993.

[114] S.P. Srivastava, V.K. Verma and B. Singh, “Steady-state analysis of a self-controlled synchronous motor” Electric Power Systems Research, 36 (3), 211-216, 1996.

[115] S.P. Srivastava, V.K. Verma and B. Singh, “Performance Analysis of Load Commutated Inverter-Fed Synchronous Motor Drive”, Institution of Engineers India Part El Electrical Engineering Division, 73, 289-289, 1993.

[116] C.L. Puttaswamy, V.K. Verma and Bhim Singh, “Development and performance of microprocessor based self-controlled synchronous motor drive”, Institution of Engineers India Part El Electrical Engineering Division, 71 (1), 13-19, 1990.

[117] S. Nishikata, S. Muto and T. Kataoka, “Dynamic performance analysis of self-controlled synchronous motor speed control system”, IEEE Transactions on Industry Applications, 18 (3), 205-212, 1982.

[118] T. Kataoka and S Nishikata, “A transient analysis of dc commutatorless motor”, Transaction of Institute of electrical engineering in Japan, 98 (3), 527-534, 1978.

[119] S. Nishikata and T. Kataoka, “Dynamic control of a self-controlled synchronous motor drive system”, IEEE Transactions on Industry Applications, 20 (3), 598-604, 1984.

[120] S.D. Sudhoff, E.L. Zivi, T.D. Collins, “Start up performance of load-commutated inverter fed synchronous machine drives”, IEEE Transactions on Energy Conversion, 10 (2), 268-274, 1995.

[121] J.J. Simond, A. Sapin, M.T. Xuan, R. Wetter and P. Burmeister, “12-pulse LCI synchronous drive for a 20 MW compressor modeling, simulation and measurements”, Industrial applications conference, vol. 4, 2302-2308, 2005.

[122] A. Tessarolo and S. Castellan, “Analytical and circuital modeling of commutation transients in phase-split synchronous motors supplied in multiple load commutated inverters”, 18th International conference on electrical machines, 1-8, 2008, Vilamoura.

[123] A. Tessarolo, S. Castellan, R. Menis and G. Ferrari, “On the modeling of commutation transients in split-phase synchronous motors supplied by multiple load-commutated inverters”, IEEE Transactions on Industrial Electronics, 57 (1), 35-42, 2010.

[124] A. Tessarolo, C. Bassi, G. Ferrari, D. Giulivom, R. Macuglia and R. Menis, “Investigation into the high-frequency limits and performance of load commutated inverters for high-speed synchronous motor drives”, IEEE Transactions on Industrial Electronics, 60 (6), 2147-2157, 2013.

[125] A. Tessarolo, “Analysis and simulation of a novel load-commutated inverter drive based on a symmetrical five-phase synchronous motor”, 13th European conference on Power Electronics & Applications, EPE'09, pp 1-11, Barcelona, 8-10 Sept. 2009.

[126] A. Tessarolo, S. Castellan and R. Menis, “Feasibility and performance analysis of a high power drive based on four synchro-converters supplying a twelve-phase synchonous motor”, IEEE Power Electronics Specialist Conference, pp 2352–2357, 2008.

[127] D.R. Kohli, S.K. Jain, “A laboratory course in electrical machines”, JBA Publisher, 2nd edition, 2000, pp. 300-307.

[128] The Institute of Electrical and Electronics Engineers Inc. 1995 *IEEE Guide: Test Procedures forSynchronous Machines (IEEE Std 115-1995).*

[129] E.A. Klingshrin, “High phase order induction motor-Part-II: Experimental results”, 1983, 102 (1), pp. 54-59.

[130] D.G. Dorrell, C.Y. Leong, R.A. McMahon, “Performance assessment of six-pulse inverter-fed three phase and six phase induction machine”, IEEE Transactions on Industrial Applications, 2006, 42 (6), pp. 1487-1495.

Appendix I

Stator self and mutual inductances:

$L_{aa} = L_{A1} - L_{A2}\cos(2\theta_r)$

$L_{bb} = L_{A1} - L_{A2}\cos 2(\theta_r - \frac{2\pi}{3})$

$L_{cc} = L_{A1} - L_{A2}\cos 2(\theta_r + \frac{2\pi}{3})$

$L_{ab} = L_{ba} = -\frac{1}{2}L_{A1} - L_{A2}\cos(2\theta_r - \frac{2\pi}{3})$

$L_{bc} = L_{cb} = -\frac{1}{2}L_{A1} - L_{A2}\cos(2\theta_r)$

$L_{ac} = L_{ca} = -\frac{1}{2}L_{A1} - L_{A2}\cos\left(2\theta_r + \frac{2\pi}{3}\right)$

$L_{xx} = L_{X1} - L_{X2}\cos 2(\theta_r - \xi)$

$L_{yy} = L_{X1} - L_{X2}\cos 2(\theta_r - \xi - \frac{2\pi}{3})$

$L_{zz} = L_{X1} - L_{X2}\cos 2(\theta_r - \xi + \frac{2\pi}{3})$

$L_{xy} = L_{yx} = -\frac{1}{2}L_{X1} - L_{X2}\cos(2\theta_r - 2\xi - \frac{2\pi}{3})$

$L_{yz} = L_{zy} = -\frac{1}{2}L_{X1} - L_{X2}\cos(2\theta_r - 2\xi)$

$L_{xz} = L_{zx} = -\frac{1}{2}L_{X1} - L_{X2}\cos(2\theta_r - 2\xi + \frac{2\pi}{3})$

$L_{ax} = L_{xa} = L_{AX1}cos\xi - L_{AX2}\cos(2\theta_r - \xi)$

$L_{ay} = L_{ya} = L_{AX1}cos(\xi + \frac{2\pi}{3}) - L_{AX2}\cos(2\theta_r - \xi - \frac{2\pi}{3})$

$L_{az} = L_{za} = L_{AX1}cos(\xi - \frac{2\pi}{3}) - L_{AX2}\cos(2\theta_r - \xi + \frac{2\pi}{3})$

$L_{bx} = L_{xb} = L_{AX1}cos(\xi - \frac{2\pi}{3}) - L_{AX2}\cos(2\theta_r - \xi - \frac{2\pi}{3})$

$L_{by} = L_{yb} = L_{AX1}cos(\xi) - L_{AX2}\cos(2\theta_r - \xi + \frac{2\pi}{3})$

$L_{bz} = L_{zb} = L_{AX1}cos(\xi + \frac{2\pi}{3}) - L_{AX2}\cos(2\theta_r - \xi)$

$L_{cx} = L_{xc} = L_{AX1}cos(\xi + \frac{2\pi}{3}) - L_{AX2}\cos(2\theta_r - \xi + \frac{2\pi}{3})$

$$L_{cy} = L_{yc} = L_{AX1}cos(\xi - \frac{2\pi}{3}) - L_{AX2}\cos(2\theta_r - \xi)$$

$$L_{cz} = L_{zc} = L_{AX1}cos(\xi) - L_{AX2}\cos(2\theta_r - \xi - \frac{2\pi}{3})$$

Mutual inductances between stator and rotor:

$$L_{aKq} = L_{q1}cos(\theta_r)$$

$$L_{bKq} = L_{q1}cos\left(\theta_r - \frac{2\pi}{3}\right)$$

$$L_{cKq} = L_{q1}cos\left(\theta_r + \frac{2\pi}{3}\right)$$

$$L_{aKd} = L_{q1}sin(\theta_r)$$

$$L_{bKd} = L_{q1}sin\left(\theta_r - \frac{2\pi}{3}\right)$$

$$L_{cKd} = L_{q1}sin\left(\theta_r + \frac{2\pi}{3}\right)$$

$$L_{afr} = L_{f1}sin(\theta_r)$$

$$L_{bfr} = L_{f1}sin\left(\theta_r - \frac{2\pi}{3}\right)$$

$$L_{cfr} = L_{f1}sin\left(\theta_r + \frac{2\pi}{3}\right)$$

$$L_{xKq} = L_{q2}cos(\theta_r - \xi)$$

$$L_{yKq} = L_{q2}cos\left(\theta_r - \xi - \frac{2\pi}{3}\right)$$

$$L_{zKq} = L_{q2}cos\left(\theta_r - \xi + \frac{2\pi}{3}\right)$$

$$L_{xKd} = L_{q2}sin(\theta_r - \xi)$$

$$L_{yKd} = L_{q2}sin\left(\theta_r - \xi - \frac{2\pi}{3}\right)$$

$$L_{zKd} = L_{q2}sin\left(\theta_r - \xi + \frac{2\pi}{3}\right)$$

$$L_{xfr} = L_{f2}sin(\theta_r - \xi)$$

$$L_{yfr} = L_{f2}sin\left(\theta_r - \xi - \frac{2\pi}{3}\right)$$

$$L_{zfr} = L_{f2}sin\left(\theta_r - \xi + \frac{2\pi}{3}\right)$$

Appendix II

Parameter of 3.7 kW, 6-poles, 50Hz, six-phase synchronous motor is given below:

$x_{mq} = 3.9112\ \Omega$	$x_{l1} = x_{l2} = 0.1758\ \Omega$	$r_1 = 0.210\ \Omega$
$x_{md} = 6.1732\ \Omega$	$x_{ldq} = 0\ \Omega$	$r_2 = 0.210\ \Omega$
$x_{lKq} = 0.66097\ \Omega$	$x_{lm} = 0.001652\ \Omega$	$r_{Kq} = 2.535\ \Omega$
$x_{lKd} = 1.550\ \Omega$	$r_{fr} = 0.056\ \Omega$	$r_{Kd} = 140.0\ \Omega$
$x_{lfr} = 0.2402\ \Omega$	$J = 0.528$ kg-m^2	

Appendix III

Stator winding coil arrangement of six-phase synchronous motor having 6-poles, 36 slots with two 3-phase sets (*abc* and *xyz*), physically displaced by 30 degree.